Spring 5-15-2017

Functional Brain Organization in Space and Time

Timothy Laumann
Washington University in St. Louis

WASHINGTON UNIVERSITY IN ST. LOUIS

Division of Biology and Biomedical Sciences
Neurosciences

Dissertation Examination Committee:
Steven Petersen, Chair
Marcus Raichle
Bradley Schlaggar
Olaf Sporns
David Van Essen

Functional Brain Organization in Space and Time

by
Timothy Otto Laumann

A dissertation presented to
The Graduate School
of Washington University in
partial fulfillment of the
requirements for the degree
of Doctor of Philosophy

May 2017
St. Louis, Missouri

Table of Contents

List of Figures

List of Tables

Acknowledgments

To the extent that there were any successes achieved over the years of my PhD, I attribute it to the exceptional people I have had the opportunity to work and play with during this time. Certainly, without the large cast of characters acknowledged here (and others not here named) this dissertation would not have been possible. I am grateful to all of them.

First, and foremost, I'd like to thank my thesis advisor Steve Petersen. Steve is an insightful, careful, and provocative mentor. He has a well-honed capacity to allow students to explore new ideas while maintaining a guiding hand that protects against garden paths paved by navel-gazing and headed into hyperspace. We don't always see things the same way, at first, but it is always for a good reason. He forces clarity of thought and has always pushed me to take a broader view of the question at hand. I also could not have asked for a better role model for how to be a successful scientist. His skepticism is honest and precise, even when directed at himself. He is also motivated to understand the questions that fascinate him, not to chase after the hottest story of the moment. His approach to science has set guiding principles for my future endeavors.

I would also like to thank the other members of my thesis committee. Bradley Schlaggar, a close collaborator with Steve, has been a key mentor in my scientific and career development. Brad defies the notion that no man can do everything, and he accomplishes this feat with élan. Despite the many demands on his time, he has always been available with worldly advice (or sidelong perspective) that has been invaluable to my career development over the years. Marcus Raichle has been a keen observer and

sounding board over the years and has consistently helped me connect to broader themes in neuroscience that have critically reoriented my thinking on more than one occasion. Olaf Sporns has provided a thoughtful alternate perspective throughout my PhD including a willingness to get into the methodological weeds that several times has clarified the appropriate analytic approach. I only wish that he were closer to home, so that we could talk neuroscience (over a beer or two) more often than just at meetings and conferences. Finally, David Van Essen was the first person to take me on as a rotation student and he has been a central figure in my PhD career ever since. I will always remember with great fondness the heady early days of collaboration in developing the Human Connectome Project for which his leadership provided the opportunity. My 'rotation' grew into a much richer extended experience as a result and it has been a great privilege to work with him in this capacity over the years. I have tremendous admiration for his methodical approach to scientific inquiry, which has also translated to an exceptional talent for flip cup (if not the accompanying trash-talk).

There are several scientific collaborators that have been particularly critical in helping to produce the work contained in this document. First, I must acknowledge Avi Snyder. He is an essential pillar of the Neuroimaging Laboratories, having developed many of the approaches and tools used by the entire community. To me, however, he is both a scientific collaborator and a close friend. He always listens carefully and will take as long as it takes to resolve an inquiry or pursue a line of reasoning to its conclusion. As a collaborator, his intellectual and temporal generosity is unsurpassed. I know that I can't ever repay him fully for his help, but, as a friend, I can advise that late-night YouTube viewing is a dangerous habit. Viola!

Gagan Wig was a post-doc with Steve for the first two years I was in the lab. Gagan and I became fast friends, as I was drawn to his disputatious, but warm-hearted style and because of the many interests we shared in common. We pursued different means of brain parcellation in parallel but eventually closely cooperated on several projects together (one of which is reported in full here). Evan Gordon joined as a post-doc just as Gagan left and again, we became fast friends. I was drawn to his disputatious, but cold-hearted style, and because of the many clothes we shared in common. We pursued several brain parcellation related projects together (two of which are reported here). I learned a lot about science, science presentation, and science writing from Gagan and Evan, and especially learned that the best work is created through honest and unfiltered collaborative disputation. I thank them both for engaging so whole-heartedly with me.

Caterina Gratton is the newest post-doc with whom I have quickly become a collaborator. I'm excited by how she has pushed forward our understanding of task-related changes in functional connectivity, one of the original aims of my thesis proposal. I look forward to continuing our collaboration.

Nico Dosenbach, with Adrian Gilmore and Steve Nelson, led the effort to collect datasets following the new approach suggested by Chapter 4, i.e., extensive data collection on single subjects. These datasets form the basis for the analyses in Chapter 5. Nico's enthusiasm and persistence in pursuing this project has helped to solidify the validity of the approach and has inspired many new directions of inquiry that we are only beginning to exploit.

Much of the work presented here would not have been possible without the foundational work laid out by previous students. Alex Cohen was a former grad student upon whose code I first cut my teeth on the enterprise of brain parcellation. Steve Nelson was a former grad student who helped develop a strategy for connecting task, correlation-based, and network-level dissociations in brain organization. Jonathan Power was a former grad student with whom I shared a dark cave for a couple of years. He helped to clarify the importance of scrutinizing data quality and helped shepherd me into graph-based approaches of data analysis.

I have to acknowledge all the other hard-working and fun people Steve and Brad have drawn to their laboratories and make them such a great place to be. In particular, all of the administrators and coordinators of the McDonnell Center, past and present, including Lydia Counts, Laura Williams, Stephanie McManus, Amy Toenjes, Mary Downey-Jones and Melissa O'Sullivan. I particularly appreciate the effort Mary and Melissa put into scheduling the impossible, namely my committee meetings. This crew doesn't just make the trains run on the time, they make the lab a positive and fun place to be. I am also in close proximity to exceptional technical staff, including Becky Coalson, Fran Miezin, Annie Nguyen, Rashina Seabury, and Babatunde Adeyemo. Babatunde, in particular, has been a steady source of support including practical and scientific feedback over the years for most of the projects on which I have worked. I thank him for his brotherly attention and apologize to anyone who has ever had to listen to us argue about the meaning of a word. Finally, there are several past and present graduate students and post-docs who have positively shaped my experience in big and

small ways, including Maital Neta, Deanna Greene, Mario Ortega, Joe Dubis, Binyam Nardos, Haoxin Sun, and Benjamin Seitzman.

I'd also like to thank all of the amazing people who run the MSTP office, and, in every way, have made my life much more pleasant during the PhD. These include Wayne Yokoyama, the director of the MSTP program, and Brian Sullivan, Christy Durbin, Liz Bayer, and Linda Perniciaro, the executive director and administrators of the MSTP program. They have anticipated all of the necessary demands at each stage of the process and, consequently, make every transition that much easier. I'd also like to thank the Neuroscience program coordinators Sally Vogt and Shirley McTigue who have been a great help over the years and, among other things, have made sure that my grant funding was properly submitted and implemented.

I want to acknowledge all of the exceptional MSTP students with which I have been fortunate enough to overlap. Many individuals in this cohort are comrades-in-arms and have become repeated scientific collaborators. In particular, Matthew Glasser, Carl Hacker, Anish Mitra, Matthew Brier, Nick Szrama, and Joshua Siegel. I am constantly impressed by their originality, persistence, and diligence and have been inspired, from the start, to do better and be better because of them. I have also just enjoyed all the good times we've been able to have together.

Jenny Enright has been the best romantic partner, and best partner in crime, I could have asked for over the past six years. Despite trundling down her own MSTP track, on which she beat me quite handily to the next station (having already completed her PhD months ago), she has shown me incredible patience and forbearance (including endless late nights and late dinners with only the rarest grumble). More

importantly, she has made this journey a lot more fun, sharing scientific excitement, worldly adventures, and daily achievements without restraint. I know the next set of challenges we take on together will be just as fun with her by my side.

Finally, I want to thank my parents, Anne and Ed Laumann. They provided me with all of the educational opportunities that have brought me to this point and have supported each decision I have made along the way. They never made a demand one way or the other, but it is perhaps not a surprise that I have pursued a path that attempts to synthesize both of their views on the world. I am grateful for their examples.

Funding: This work was supported by an institutional IGERT grant for the Cognitive, Computational and Systems Neuroscience (CCSN) program, and an NIMH F30 grant, MH100872.

Timothy Laumann

Washington University in St. Louis

May 2017

ABSTRACT OF THE DISSERTATION

Functional Brain Organization in Space and Time

by

Timothy Otto Laumann

Doctor of Philosophy in Biology and Biomedical Sciences

Neurosciences

Washington University in St. Louis, 2017

Professor Steven Petersen, Chairperson

The brain is a network functionally organized at many spatial and temporal scales. To understand how the brain processes information, controls behavior and dynamically adapts to an ever-changing environment, it is critical to have a comprehensive description of the constituent elements of this network and how relationships between these elements may change over time. Decades of lesion studies, anatomical tract-tracing, and electrophysiological recording have given insight into this functional organization. Recently, however, resting state functional magnetic resonance imaging (fMRI) has emerged as a powerful tool for whole-brain non-invasive measurement of spontaneous neural activity in humans, giving ready access to macroscopic scales of functional organization previously much more difficult to obtain. This thesis aims to harness the unique combination of spatial and temporal resolution provided by functional MRI to explore the spatial and temporal properties of the functional organization of the brain. First, we establish an approach for defining cortical areas

using transitions in correlated patterns of spontaneous BOLD activity (Chapter 2). We then propose and apply measures of internal and external validity to evaluate the credibility of the areal parcellation generated by this technique (Chapter 3). In chapter 4, we extend the study of functional brain organization to a highly sampled individual. We describe the idiosyncratic areal and systems-level organization of the individual relative to a standard group-average description. Further, we develop a model describing the reliability of BOLD correlation estimates across days that accounts for relevant sources of variability. Finally, in Chapter 5, we examine whether BOLD correlations meaningfully vary over the course of single resting-state scans.

Chapter 1: Introduction

1.1 Spontaneous neural activity reflects the underlying functional architecture of the brain

Spontaneous neural activity has been observed for as long as neuroscientists have been recording neural activity. Most research aimed at understanding brain function and organization, however, has focused on probing the fraction of activity that can be directly elicited by externally imposed tasks. For such study, the brain is implicitly viewed as a black box, with controlled inputs and experimentally exposed outputs. The variability encountered in trial-to-trial measurement is 'noise' in the system to be averaged out and spontaneous activity in the absence of a task can be ignored. While this strategy has led to a detailed and continuously developing understanding of the brain's functional organization, it sidesteps the fact that the bulk of brain activity is not necessarily contingent on immediate stimulus demands (M. D. Fox et al., 2007a).

In recent decades, however, the role of spontaneous activity as an essential organizing property of the brain has been increasingly recognized. Spontaneous activity is known to be critical for appropriate segregation and maturation of eye-specific layers in the LGN and ocular dominance columns in the cortex, and is believed to play a similar role sculpting synaptic relationships during development throughout the brain (Katz et al., 1996; Penn et al., 1999; Shatz, 1990). Spontaneous activity subsequent to learning has also been hypothesized as a key mechanism reflecting memory consolidation at the level of the synapse (Wilson et al., 1994). One of the most salient properties of spontaneous activity for our purposes, however, is that it appears to reflect the spatiotemporal functional organization of the brain. Arieli and colleagues have

vividly demonstrated this phenomenon in a series of studies using optical imaging of the visual cortex of anesthetized cats (Arieli et al., 1996; Kenet et al., 2003). They found that, in total darkness, columns in the visual cortex of the cat exhibits spontaneous repeating transient (~10's of ms) patterns of coordinated activity that in their spatial profile precisely replicate patterns of activity displayed when the cat is actually viewing moving gratings of specific orientations. They show further that particular orientation profiles (0 and 90 degrees) appear more frequently than others, perhaps reflecting the relative frequency of these stimuli in the cat's natural environment. Viewed over long stretches of time one could use the aggregate synchrony of different cortical areas in anesthetized cats to map out of the organization of orientation columns across the visual cortex.

At a broader spatial and temporal scale, spontaneous neural activity can be measured in humans across the entire brain by recording the blood oxygen level depending (BOLD) signal with fMRI while subjects 'rest' in a scanner, i.e. they are given no explicit task instructions other than to fixate on a crosshair. Although not all environmental stimuli can be eliminated during an fMRI scan, this undirected passive resting state is as close to generating unconstrained neural activity in humans as we are likely to achieve. Remarkably, as first observed by Biswal and colleagues in 1995, in the context of this 'resting state,' robust and specific correlations in spontaneous BOLD activity can be found between the two hemispheres of the motor cortex (B. Biswal et al., 1995), even though subjects are not performing any motor-related task. Since then, spontaneous correlation in low frequency (<0.1 Hz) BOLD activity between spatially distributed but functionally related regions, known as resting state functional

connectivity (RSFC), has been observed throughout the brain including the visual cortex (Lowe et al., 1998), the auditory cortex (Cordes et al., 2000), the default mode network (Greicius et al., 2003), and attention and control networks (Dosenbach et al., 2007; Vincent et al., 2008) Indeed, there is an emerging consensus that RSFC readily reveals a reasonably small number of sub-networks that correspond to major functional systems describing most of the gray matter in the brain (Doucet et al., 2011; Power et al., 2011; Smith et al., 2009; Yeo et al., 2011).

One explanation for the presence of these coherent patterns of RSFC hidden in the neural 'noise' is that they reflect a history of co-activation. In this view, relationships in spontaneous neural activity are generated by a 'Hebbian-like' mechanism of common recruitment during evoked activity (Dosenbach et al., 2007; Nelson et al., 2010a; Wig et al., 2011b). That is, brain areas recruited for a common purpose during many tasks will change their synaptic efficiency with respect to each other as a result of that co-activation, resulting in synchronous activity even when they are no longer explicitly being recruited for that purpose. Broad evidence for this view exists in that the dominant spatial patterns of resting state correlation are consistent with the convergent cross-study patterns of task-evoked co-activation (Smith et al., 2009). Further evidence for and caveats to this view will be discussed below in the context of temporal scales of spontaneous BOLD activity.

In any case, the observation of coherent functionally-relevant organization in spontaneous BOLD activity and the apparent ease with which such data can be acquired has motivated a vast literature exploring the properties and details of this organization and how these correlational relationships may differ under different

conditions, between different populations, and over the lifespan. In our view, this enterprise cannot successfully proceed without a clear accounting of the spatial and temporal scales of functional organization spontaneous BOLD activity represents. In the following sections, we will introduce the possibility that, in addition to systems-level organization, spontaneous BOLD activity may also be able to capture the areal-level organization of the brain; we will, however, posit the need to account for individual variability in spatial organization; and finally, we will ask whether spontaneous BOLD activity meaningfully varies over short time scales, the answer to which should give insight into its physiological relevance.

1.2 Using spontaneous BOLD activity to study spatial functional organization

Brain parcellation

The cortex of the human brain contains a large set of discrete interacting functional areas that form a level of organization, at about a centimeter scale, essential for processing information related to perception, cognition, and behavior (Churchland et al., 1988). The identification and mapping of the relative positions of these functional areas on the cortex, known as brain 'parcellation', is one of the grand unfinished projects of neuroscience, despite aggressive pursuit for over 100 years (since, at least, e.g. (Brodmann, 1909)). An accurate map of cortical areas is critical for defining the constituent parts of the 'wiring diagram' that describes the flow of information through the brain's various processing systems. Further, the global study of the brain as a complex network, a rapidly growing field known as 'connectomics' (Sporns et al., 2005),

demands measurement of relationships between cortical areas, or network ‘nodes’, and is thus necessarily constrained by the specific properties of the parcellation, including the number, size, and position of the identified areas.

Classically, identification of distinct cortical areas is performed by finding spatial discontinuities in one or more underlying brain properties, including functional responses, architectonics (cyto-, myelo-, and chemo-), anatomic connectivity, and, where possible (e.g. V1/V2), topographic maps (D. J. Felleman et al., 1991a). Relatively comprehensive areal parcellations have been developed and refined in the macaque using this strategy (Van Essen, 2013). Unfortunately, the need for invasive procedures to measure several of these brain features has historically limited the extent of areal parcellation in the human brain. As noted above, however, measurement of RSFC offers the possibility of comprehensive non-invasive whole-brain functional mapping in living humans. Indeed, RSFC allows for measurement of the functional associations of every location in the brain, limited only by the spatial resolution of BOLD imaging (~2-4 millimeters). Thus, just as it has successfully revealed the systems-level functional organization of the brain, RSFC may be able to delineate functional organization at the mesoscale of cortical areas.

Transitions in RSFC can be used to define cortical areas

By analogy with the classical methods mentioned above, RSFC is presumed to be relatively uniform within the extent of a cortical area and distinct from the RSFC of adjacent cortical areas. Thus, it may be hypothesized that as one measures RSFC along the cortex, abrupt transitions in the pattern of RSFC may correspond to putative boundaries between cortical areas. Cohen et al. first demonstrated the proof-of-concept

for this strategy of cortical area definition on a small patch of cortex in 2008 (Cohen et al., 2008a). Subsequently, the approach was successfully extended to areal delineation of the parietal cortex (Barnes et al., 2012; Nelson et al., 2010a) and preliminarily to areal centers throughout the rest of the brain (i.e., 264 spherical regions of interest reported in (Power et al., 2011)).

In Chapters 2 and 3, we present our efforts to refine this technique and expand its use to the entire cortex, developing a complete functional areal parcellation of the cortex. Critically, we also propose and demonstrate measures for internal and external validation of the putative cortical areas identified by RSFC. Specifically, RSFC-based parcellation should produce a reliable topology across cohorts of subjects; putative cortical areas should demonstrate homogenous patterns of correlation, even when applied to distinct datasets; and RSFC-based cortical areas should correspond with areal distinctions defined by other brain properties such as architectonics and functional responses.

Defining functional organization accounting for sources of individual variability

The proposed areal parcellation discussed above represents functional brain organization inferred from group-average data. Ideally, however, we would like to generate individual-level descriptions of functional organization. Anatomic and functional variability across individuals is well-known (Devlin et al., 2007; Frost et al., 2012; Mueller et al., 2013; Van Essen et al., 2007). Consequently, a group-average parcellation will never exactly reflect each individual's idiosyncratic brain organization,

ultimately limiting our ability to correctly connect brain features with individual differences in behavior and cognition.

Our early attempts to apply an RSFC-based boundary detection procedure to individuals showed provisional utility (e.g., Wig et al., 2014a), but was limited by insufficient data available in each subject. It remained unclear how much data was needed to provide reliable and accurate estimates of functional organization in individual subjects based on spontaneous BOLD activity. Fortunately, we were able to address this limitation by using a massive fMRI dataset collected on a single subject over more than 100 scanning sessions, including resting state and task data. In chapter 4, we describe our efforts to generate an individual-level parcellation with this dataset, subjecting it to the same tests of internal and external validity applied to the group data. This dataset allows us to account for relevant sources of sampling variability and points the way to a new approach for studying brain organization using fMRI that focuses on detailed evaluation of individuals.

1.3 Temporal scales of spontaneous BOLD activity

What is the physiological relevance of spontaneous BOLD activity?

Empirically, as described in the first chapters of this thesis, spontaneous BOLD activity provides valuable information about the spatial organization of functional systems in the brain. However, since its emergence as a widely applied tool for studying brain organization, there has been considerable debate about the specific physiological relevance of spontaneous BOLD activity itself (e.g. (Morcom et al., 2007)). In particular, what underlying brain processes do the observed coherent BOLD fluctuations represent? Do they relate to online moment-to-moment changes in cognition? Or are

they a natural result of spontaneous neural activity playing out in a specific structural topology of connections (C. J. Honey et al., 2010)? Or does spontaneous BOLD activity relate to off-line processes including synaptic homeostasis (Maffei et al., 2009) and/or plasticity related to consolidation of past events (Miall et al., 2006)? Answers to these questions are not necessarily mutually exclusive, but we believe that study of the temporal features of spontaneous BOLD activity may provide some direction in sorting them out. To start, we would like to provide some key observations that may help constrain possible interpretations of the spontaneous BOLD phenomenon, including how spontaneous BOLD activity changes over various time-scales. Finally, we will ask whether spontaneous BOLD activity meaningfully varies over very short time-scales.

Spectral content of spontaneous BOLD activity

Since Biswal et al.'s first observation of the phenomenon, it has been noted that correlations in resting-state BOLD activity are most prominent at low frequencies (i.e., <0.1 Hz). Higher frequency content is also present in raw BOLD timeseries related to scanner noise, cardiac pulsation (B. Biswal et al., 1996), and respiratory motion (Birn et al., 2006), though these latter physiological artifacts are frequently not directly measurable at the sampling frequency used in most resting state studies (the typical Nyquist frequency is usually less than 0.2-0.3 Hz). Fluctuations in the partial pressure of end-tidal CO_2 in blood related to variable respiration depth may contribute to BOLD signal variability at lower frequencies (i.e., <0.05 Hz; Wise et al., 2004). However, this potential confound is likely well-controlled by the commonly used processing step of global signal regression (Birn et al., 2006). Setting aside these artifactual sources of variability, BOLD signal fluctuations essentially appear to demonstrate a $1/f^2$ power-law

distribution in the spectral domain. The presence of this aperiodic, so-called ‘scale-free’, behavior in spontaneous BOLD activity likens it to many dynamic natural phenomena (e.g., earthquakes, stock market), but distinguishes it from the high-frequency periodic oscillations (e.g. theta (4-8 Hz); alpha (9-12 Hz); gamma (>30 Hz)) that are so prominent in studies of electrical brain activity (He et al., 2010).

Spontaneous BOLD activity relates to structural connectivity

RSFC between cortical areas appear to at least partially respect the structural connections, i.e. axonal tracts, between them. Indeed, there is evidence that patterns of RSFC can be predicted, in a limited way, by the known structural organization of the brain (Behrens et al., 2012; C. J. Honey et al., 2009b). Thus, RSFC may be expected to reflect, in part, the temporal stability of anatomic relationships. It is important to note, however, that while some correlations in BOLD activity may be caused by direct monosynaptic connections between cortical areas, there is evidence that the bulk of the correlations are generated by a common input to each area or by indirect two or three-step connections. This latter kind of relationship has been clearly demonstrated by the strong correlation in spontaneous BOLD activity observed in anesthetized macaques between left and right peripheral V1, which are known to have no monosynaptic axonal connection (Vincent et al., 2007a). Further, inter-hemispheric RSFC relationships in a macaque have been found to be largely retained following corpus callosotomy if the anterior commissure alone was left intact, suggesting that indirect structural connections are sufficient to maintain RSFC between regions that have lost their direct structural connection (O'Reilly et al., 2013). While the long-term stability of indirect functional relationships is unclear, we can safely conclude that the functional architecture of the

brain reflected by RSFC is a remarkably robust feature of brain organization not wholly dependent on direct structural connections.

Correlations in BOLD activity are relatively stable

The topographic organization of RSFC appears to demonstrate considerable consistency in several dimensions. Identifiable patterns of RSFC persist, albeit with significant signal attenuations, during sleep (Larson-Prior et al., 2009) and anesthesia (Palanca et al., 2015), and even appear to have similar homologues in anesthetized monkeys (Vincent et al., 2007a). Patterns of RSFC are also highly reproducible across cohorts of subjects (Damoiseaux et al., 2006; Shehzad et al., 2009), and, as we show in chapter 4, have relatively high reproducibility within a single individual across scanning sessions. These observations seriously challenge the notion that spontaneous BOLD activity relates directly to unconstrained cognition. While the content, or even presence of cognition, may be expected to vary dramatically across days within a subject, across subjects, across states of consciousness, and between species, coherent patterns of RSFC are evident under all of these conditions.

But correlations are not static

While patterns of RSFC demonstrate considerable stability, there are several important contexts in which significant changes in RSFC have been observed. In the following sections, we highlight evidence for changes in RSFC over various temporal scales, including the years of early-life development, in the hours and days following task training, and in the context of particular behavioral states.

RSFC changes during development

A considerable literature has developed studying patterns of RSFC over the course of early life, including infancy (e.g., (Fransson et al., 2011; Smyser et al., 2010) and early adolescence (e.g., (Dosenbach et al., 2010; Fair et al., 2009; Power et al., 2010; Vogel et al., 2010). One relevant observation is that term and pre-term infants exhibit coherent bilateral spontaneous BOLD activity within recognizable functional systems (e.g. somatomotor, visual and auditory cortex; Lin et al., 2008; Redcay et al., 2007; Smyser et al., 2010) suggesting that at least some RSFC may be instantiated prior to any history of task-related co-activation (in contrast to a purely 'Hebbian' hypothesis of RSFC). There are also clear distinctions in patterns of RSFC relative to adults. Unfortunately, many of these studies are confounded, in the first instance, by the fact that infants can only be studied while asleep, and, in the second instance, by the fact that children exhibit substantially more head motion than adults, artifactually biasing the observed patterns of RSFC towards short-distance correlations (Power et al., 2012; Satterthwaite et al., 2012). More recent studies carefully controlling head motion (Power et al., 2014), however, have been able to identify developmental changes in RSFC between children and adults (Greene et al., 2014) and between 6 and 12-month old infants (Pruett et al., 2015). Thus, RSFC is reasonably supposed to reflect relevant changes in cortical and subcortical organization during maturation.

Experience-dependent changes in RSFC

According to the co-activation hypothesis, the strength of correlation in BOLD activity between different areas of the brain should be modifiable by controlled exposure to tasks that encourage coordinated activity between them. Lewis et al. demonstrated

this predicted effect by making subjects undergo several days of intense training on a visual perception task (Lewis et al., 2009). Furthermore, the degree of change in resting correlations between the regions involved in the task was related to behavioral performance. Tambini et al. reported a related finding showing that the increase in correlation in resting BOLD activity between hippocampus and lateral occipital complex immediately following a memory-encoding task was associated with subsequent memory performance (Tambini et al., 2010). Post-training changes in RSFC have been reported in various functional systems (for review, (Kelly et al., 2014)), with effects observed with as little as 11 minutes (Albert et al., 2009) or as much as 70 hours of training (Mackey et al., 2013). However, it remains unknown whether these changes are transient or become permanent features of brain organization. Regardless, it is already reasonable to conclude that spontaneous BOLD correlations are experimentally modifiable over hours or days.

State-dependent changes in spontaneous BOLD activity

Many investigators have attempted to measure spontaneous BOLD activity in the context of different behavioral and environmental states, as opposed to the typical, eyes-open, passive fixation resting condition. Most simply, eyes-open rest has been compared to eyes-closed rest. In this case, spontaneous BOLD activity is decreased particularly in visual and ventral somatomotor regions when the eyes are open (McAvoy et al., 2008), although large-scale system organization is mostly preserved (see Chapter 4, supplemental Figure 5). RSFC has also been observed to subtly change from the morning to the evening particularly between medial temporal regions and regions in the posterior cingulate and dorsolateral prefrontal cortex (Shannon et al., 2013). Less

controlled, but no less revealing is the measurement of spontaneous BOLD activity during stages of sleep. As mentioned before, BOLD activity during sleep reveals recognizable RSNs, but significant differences from the waking resting state are also observed, including increased modular segregation during deeper sleep stages (Tagliazucchi et al., 2013). Critically, sleep staging based on spontaneous BOLD activity has revealed that many extant 'awake' resting-state datasets are contaminated by sleep (Tagliazucchi et al., 2014). This observation is relevant for understanding the causes of 'dynamic' RSFC discussed below.

Subtler task manipulations have also revealed changes in RSFC. For example, manipulation of visual attention has been able to elicit changes in background BOLD correlation between low-level visual areas (e.g. V3, V4) and higher-level visual processing areas (i.e. PPA, FFA) during a task (Al-Aidroos et al., 2012). Crucially, these effects were observed after accounting for task-related evoked activity. More generally, distinct tasks appear to generate mild task-specific changes in background BOLD correlations, while preserving a common underlying functional organization (Cole et al., 2014; Krienen et al., 2014). Thus, subtle changes in RSFC may be observable when shifting between different task states or behavioral conditions, but wholesale changes in functional organization have so far not been observed.

Do BOLD correlations meaningfully vary over shorter time scales?

Spontaneous BOLD activity may change over the lifespan, may be induced to change following training, and may even subtly change in the context of different states, but does spontaneous BOLD activity meaningfully change from moment-to-moment over the course of a resting state scan? It is reasonable to hypothesize that there may

be considerable variability in the correlation between regions over the course of a resting state scan, especially if it is assumed that spontaneous BOLD activity actually reflects moment-to-moment cognition. Indeed, this hypothesis is supported by the observation that spontaneous BOLD correlations, when measured over short time windows (e.g. 1-2 minutes), exhibit large fluctuations over the course of a single resting state scan (see Figure 1). Chang and Glover first reported this type of 'dynamic' relationship between an ROI in the posterior cingulate cortex and several other ROIs in the brain (Chang et al., 2010). Others have claimed that sliding window analysis of RSFC reveals a series of distinct states that meaningfully capture the unfolding dynamics of spontaneous BOLD activity over the course of a scan (Allen et al., 2012). A large literature has developed around these observations hoping that short time-scale variability in spontaneous BOLD correlation will reveal previously inaccessible features of brain organization (Calhoun et al., 2014; Hutchison et al., 2013; Kopell et al., 2014).

We believe, however, that the initial excitement over the observation of RSFC 'dynamics' may be, at least partially, misguided (we include ourselves in this assessment). There are two major problems with the current evaluation of RSFC 'dynamics'. Firstly, perfectly stationary timeseries, i.e. timeseries whose statistics do not change over time, will exhibit large, but meaningless, sampling variability if statistics are computed on small quantities of data (e.g. short windows). Defining and analyzing a stationary simulation of BOLD data will help to illustrate this problem. Second, and more insidious, artifactual and uninteresting sources of non-stationary changes in BOLD activity, e.g. head motion and drowsiness, must be accounted for when interpreting RSFC 'dynamics'. In Chapter 5, we attempt to evaluate RSFC 'dynamics' with these

issues in mind, and speculate on how the observation of stationary spontaneous BOLD activity may inform our understanding of its physiological relevance.

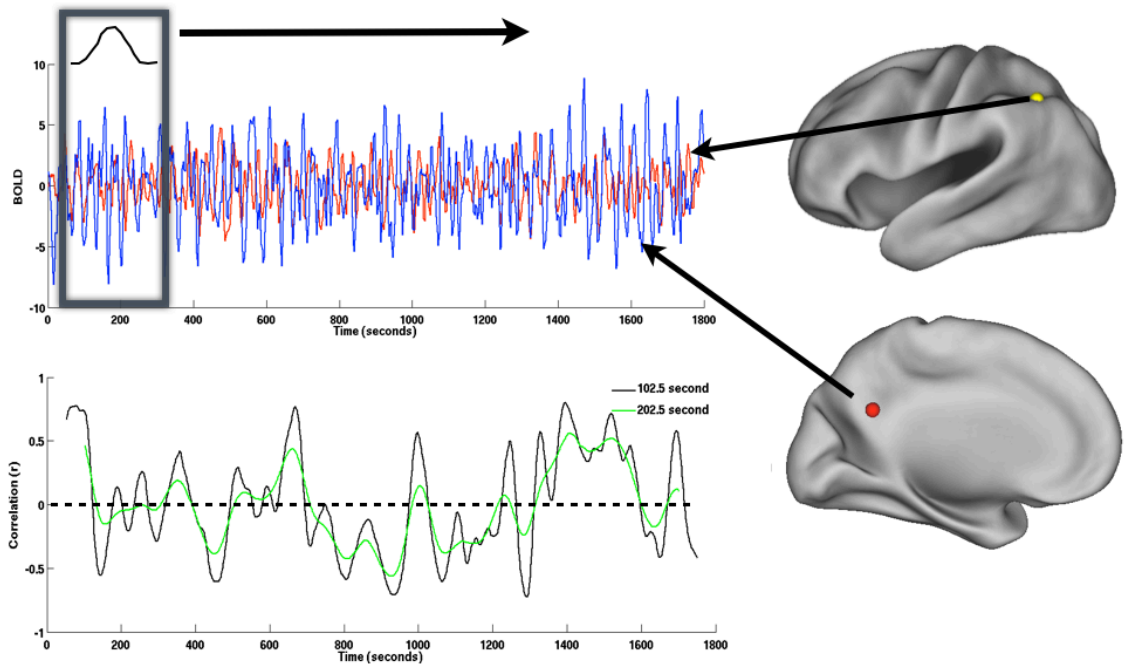

Figure 1-1. Illustration of sliding window correlation procedure. Top graph depicts BOLD signal from two ROIs over a 30-minute resting state scan. Bottom graph depicts variability of correlation between ROIs over time for two different window sizes.

References

Al-Aidroos, N., Said, C. P., & Turk-Browne, N. B. (2012). Top-down attention switches coupling between low-level and high-level areas of human visual cortex. Proc Natl Acad Sci U S A, 109(36), 14675-14680.

Albert, N. B., Robertson, E. M., & Miall, R. C. (2009). The resting human brain and motor learning. Curr Biol, 19(12), 1023-1027.

Allen, E. A., Damaraju, E., Plis, S. M., Erhardt, E. B., Eichele, T., & Calhoun, V. D. (2012). Tracking Whole-Brain Connectivity Dynamics in the Resting State. Cereb Cortex.

Arieli, A., Sterkin, A., Grinvald, A., & Aertsen, A. (1996). Dynamics of ongoing activity: explanation of the large variability in evoked cortical responses. Science, 273(5283), 1868-1871.

Barnes, K. A., Nelson, S. M., Cohen, A. L., Power, J. D., Coalson, R. S., Miezin, F. M., Vogel, A. C., Dubis, J. W., Church, J. A., Petersen, S. E., et al. (2012). Parcellation in left lateral parietal cortex is similar in adults and children. Cereb Cortex, 22(5), 1148-1158.

Behrens, T. E., & Sporns, O. (2012). Human connectomics. Curr Opin Neurobiol, 22(1), 144-153.

Birn, R. M., Diamond, J. B., Smith, M. A., & Bandettini, P. A. (2006). Separating respiratory-variation-related fluctuations from neuronal-activity-related fluctuations in fMRI. Neuroimage, 31(4), 1536-1548.

Biswal, B., DeYoe, E. A., & Hyde, J. S. (1996). Reduction of physiological fluctuations in fMRI using digital filters. Magn Reson Med, 35(1), 107-113.

Biswal, B., Yetkin, F. Z., Haughton, V. M., & Hyde, J. S. (1995). Functional connectivity in the motor cortex of resting human brain using echo-planar MRI. Magn Reson Med, 34(4), 537-541.

Brodmann, K. (1909). *Vergleichende lokalisationslehre der grosshirnrinde in ihren prinzipien dargestellt auf grund des zellenbaues*. Leipzig: J. A. Barth.

Calhoun, V. D., Miller, R., Pearlson, G., & Adali, T. (2014). The chronnectome: time-varying connectivity networks as the next frontier in fMRI data discovery. Neuron, 84(2), 262-274.

Chang, C., & Glover, G. H. (2010). Time-frequency dynamics of resting-state brain connectivity measured with fMRI. Neuroimage, 50(1), 81-98.

Churchland, P. S., & Sejnowski, T. J. (1988). Perspectives on cognitive neuroscience. Science, 242(4879), 741-745.

Cohen, A. L., Fair, D. A., Dosenbach, N. U., Miezin, F. M., Dierker, D., Van Essen, D. C., Schlaggar, B. L., & Petersen, S. E. (2008a). Defining functional areas in individual human brains using resting functional connectivity MRI. Neuroimage, 41(1), 45-57.

Cole, M. W., Bassett, D. S., Power, J. D., Braver, T. S., & Petersen, S. E. (2014). Intrinsic and task-evoked network architectures of the human brain. Neuron, 83(1), 238-251.

Cordes, D., Haughton, V. M., Arfanakis, K., Wendt, G. J., Turski, P. A., Moritz, C. H., Quigley, M. A., & Meyerand, M. E. (2000). Mapping functionally related regions of brain with functional connectivity MR imaging. AJNR Am J Neuroradiol, 21(9), 1636-1644.

Damoiseaux, J. S., Rombouts, S. A., Barkhof, F., Scheltens, P., Stam, C. J., Smith, S. M., & Beckmann, C. F. (2006). Consistent resting-state networks across healthy subjects. Proc Natl Acad Sci U S A, 103(37), 13848-13853.

Devlin, J. T., & Poldrack, R. A. (2007). In praise of tedious anatomy. Neuroimage, 37(4), 1033-1041; discussion 1050-1038.

Dosenbach, N. U., Fair, D. A., Miezin, F. M., Cohen, A. L., Wenger, K. K., Dosenbach, R. A., Fox, M. D., Snyder, A. Z., Vincent, J. L., Raichle, M. E., et al. (2007). Distinct brain networks for adaptive and stable task control in humans. Proc Natl Acad Sci U S A, 104(26), 11073-11078.

Dosenbach, N. U., Nardos, B., Cohen, A. L., Fair, D. A., Power, J. D., Church, J. A., Nelson, S. M., Wig, G. S., Vogel, A. C., Lessov-Schlaggar, C. N., et al. (2010). Prediction of individual brain maturity using fMRI. Science, 329(5997), 1358-1361.

Doucet, G., Naveau, M., Petit, L., Delcroix, N., Zago, L., Crivello, F., Jobard, G., Tzourio-Mazoyer, N., Mazoyer, B., Mellet, E., et al. (2011). Brain activity at rest: a multiscale hierarchical functional organization. J Neurophysiol, 105(6), 2753-2763.

Fair, D. A., Cohen, A. L., Power, J. D., Dosenbach, N. U., Church, J. A., Miezin, F. M., Schlaggar, B. L., & Petersen, S. E. (2009). Functional brain networks develop from a "local to distributed" organization. Plos Computational Biology, 5(5), e1000381.

Felleman, D. J., & Van Essen, D. C. (1991a). Distributed hierarchical processing in the primate cerebral cortex. Cereb Cortex, 1(1), 1-47.

Fox, M. D., & Raichle, M. E. (2007a). Spontaneous fluctuations in brain activity observed with functional magnetic resonance imaging. Nat Rev Neurosci, 8(9), 700-711.

Fransson, P., Aden, U., Blennow, M., & Lagercrantz, H. (2011). The functional architecture of the infant brain as revealed by resting-state fMRI. Cereb Cortex, 21(1), 145-154.

Frost, M. A., & Goebel, R. (2012). Measuring structural-functional correspondence: spatial variability of specialised brain regions after macro-anatomical alignment. Neuroimage, 59(2), 1369-1381.

Greene, D. J., Laumann, T. O., Dubis, J. W., Ihnen, S. K., Neta, M., Power, J. D., Pruett, J. R., Jr., Black, K. J., & Schlaggar, B. L. (2014). Developmental changes in the organization of functional connections between the basal ganglia and cerebral cortex. J Neurosci, 34(17), 5842-5854.

Greicius, M. D., Krasnow, B., Reiss, A. L., & Menon, V. (2003). Functional connectivity in the resting brain: a network analysis of the default mode hypothesis. Proc Natl Acad Sci U S A, 100(1), 253-258.

He, B. J., Zempel, J. M., Snyder, A. Z., & Raichle, M. E. (2010). The temporal structures and functional significance of scale-free brain activity. Neuron, 66(3), 353-369.

Honey, C. J., Sporns, O., Cammoun, L., Gigandet, X., Thiran, J. P., Meuli, R., & Hagmann, P. (2009b). Predicting human resting-state functional connectivity from structural connectivity. Proc Natl Acad Sci U S A, 106(6), 2035-2040.

Honey, C. J., Thivierge, J. P., & Sporns, O. (2010). Can structure predict function in the human brain? Neuroimage, 52(3), 766-776.

Hutchison, R. M., Womelsdorf, T., Allen, E. A., Bandettini, P. A., Calhoun, V. D., Corbetta, M., Della Penna, S., Duyn, J. H., Glover, G. H., Gonzalez-Castillo, J., et al. (2013). Dynamic functional connectivity: promise, issues, and interpretations. Neuroimage, 80, 360-378.

Katz, L. C., & Shatz, C. J. (1996). Synaptic activity and the construction of cortical circuits. Science, 274(5290), 1133-1138.

Kelly, C., & Castellanos, F. X. (2014). Strengthening connections: functional connectivity and brain plasticity. Neuropsychol Rev, 24(1), 63-76.

Kenet, T., Bibitchkov, D., Tsodyks, M., Grinvald, A., & Arieli, A. (2003). Spontaneously emerging cortical representations of visual attributes. Nature, 425(6961), 954-956.

Kopell, N. J., Gritton, H. J., Whittington, M. A., & Kramer, M. A. (2014). Beyond the connectome: the dynome. Neuron, 83(6), 1319-1328.

Krienen, F. M., Yeo, B. T., & Buckner, R. L. (2014). Reconfigurable task-dependent functional coupling modes cluster around a core functional architecture. Philos Trans R Soc Lond B Biol Sci, 369(1653).

Larson-Prior, L. J., Zempel, J. M., Nolan, T. S., Prior, F. W., Snyder, A. Z., & Raichle, M. E. (2009). Cortical network functional connectivity in the descent to sleep. Proc Natl Acad Sci U S A, 106(11), 4489-4494.

Lewis, C. M., Baldassarre, A., Committeri, G., Romani, G. L., & Corbetta, M. (2009). Learning sculpts the spontaneous activity of the resting human brain. Proc Natl Acad Sci U S A, 106(41), 17558-17563.

Lin, W., Zhu, Q., Gao, W., Chen, Y., Toh, C. H., Styner, M., Gerig, G., Smith, J. K., Biswal, B., & Gilmore, J. H. (2008). Functional connectivity MR imaging reveals cortical functional connectivity in the developing brain. AJNR Am J Neuroradiol, 29(10), 1883-1889.

Lowe, M. J., Mock, B. J., & Sorenson, J. A. (1998). Functional connectivity in single and multislice echoplanar imaging using resting-state fluctuations. Neuroimage, 7(2), 119-132.

Mackey, A. P., Miller Singley, A. T., & Bunge, S. A. (2013). Intensive reasoning training alters patterns of brain connectivity at rest. J Neurosci, 33(11), 4796-4803.

Maffei, A., & Fontanini, A. (2009). Network homeostasis: a matter of coordination. Curr Opin Neurobiol, 19(2), 168-173.

McAvoy, M., Larson-Prior, L., Nolan, T. S., Vaishnavi, S. N., Raichle, M. E., & d'Avossa, G. (2008). Resting states affect spontaneous BOLD oscillations in sensory and paralimbic cortex. J Neurophysiol, 100(2), 922-931.

Miall, R. C., & Robertson, E. M. (2006). Functional imaging: is the resting brain resting? Curr Biol, 16(23), R998-1000.

Morcom, A. M., & Fletcher, P. C. (2007). Does the brain have a baseline? Why we should be resisting a rest. Neuroimage, 37(4), 1073-1082.

Mueller, S., Wang, D., Fox, M. D., Yeo, B. T., Sepulcre, J., Sabuncu, M. R., Shafee, R., Lu, J., & Liu, H. (2013). Individual variability in functional connectivity architecture of the human brain. Neuron, 77(3), 586-595.

Nelson, S. M., Cohen, A. L., Power, J. D., Wig, G. S., Miezin, F. M., Wheeler, M. E., Velanova, K., Donaldson, D. I., Phillips, J. S., Schlaggar, B. L., et al. (2010a). A parcellation scheme for human left lateral parietal cortex. Neuron, 67(1), 156-170.

O'Reilly, J. X., Croxson, P. L., Jbabdi, S., Sallet, J., Noonan, M. P., Mars, R. B., Browning, P. G., Wilson, C. R., Mitchell, A. S., Miller, K. L., et al. (2013). Causal effect of disconnection lesions on interhemispheric functional connectivity in rhesus monkeys. Proc Natl Acad Sci U S A, 110(34), 13982-13987.

Palanca, B. J., Mitra, A., Larson-Prior, L., Snyder, A. Z., Avidan, M. S., & Raichle, M. E. (2015). Resting-state Functional Magnetic Resonance Imaging Correlates of Sevoflurane-induced Unconsciousness. Anesthesiology, 123(2), 346-356.

Penn, A. A., & Shatz, C. J. (1999). Brain waves and brain wiring: the role of endogenous and sensory-driven neural activity in development. Pediatr Res, 45(4 Pt 1), 447-458.

Power, J. D., Barnes, K. A., Snyder, A. Z., Schlaggar, B. L., & Petersen, S. E. (2012). Spurious but systematic correlations in functional connectivity MRI networks arise from subject motion. Neuroimage, 59(3), 2142-2154.

Power, J. D., Cohen, A. L., Nelson, S. M., Wig, G. S., Barnes, K. A., Church, J. A., Vogel, A. C., Laumann, T. O., Miezin, F. M., Schlaggar, B. L., et al. (2011). Functional network organization of the human brain. Neuron, 72(4), 665-678.

Power, J. D., Fair, D. A., Schlaggar, B. L., & Petersen, S. E. (2010). The development of human functional brain networks. Neuron, 67(5), 735-748.

Power, J. D., Mitra, A., Laumann, T. O., Snyder, A. Z., Schlaggar, B. L., & Petersen, S. E. (2014). Methods to detect, characterize, and remove motion artifact in resting state fMRI. Neuroimage, 84, 320-341.

Pruett, J. R., Jr., Kandala, S., Hoertel, S., Snyder, A. Z., Elison, J. T., Nishino, T., Feczko, E., Dosenbach, N. U., Nardos, B., Power, J. D., et al. (2015). Accurate age classification of 6 and 12 month-old infants based on resting-state functional connectivity magnetic resonance imaging data. Dev Cogn Neurosci, 12, 123-133.

Redcay, E., Kennedy, D. P., & Courchesne, E. (2007). fMRI during natural sleep as a method to study brain function during early childhood. Neuroimage, 38(4), 696-707.

Satterthwaite, T. D., Wolf, D. H., Loughead, J., Ruparel, K., Elliott, M. A., Hakonarson, H., Gur, R. C., & Gur, R. E. (2012). Impact of in-scanner head motion on multiple measures of functional connectivity: relevance for studies of neurodevelopment in youth. Neuroimage, 60(1), 623-632.

Shannon, B. J., Dosenbach, R. A., Su, Y., Vlassenko, A. G., Larson-Prior, L. J., Nolan, T. S., Snyder, A. Z., & Raichle, M. E. (2013). Morning-evening variation in human brain metabolism and memory circuits. J Neurophysiol, 109(5), 1444-1456.

Shatz, C. J. (1990). Competitive interactions between retinal ganglion cells during prenatal development. J Neurobiol, 21(1), 197-211.

Shehzad, Z., Kelly, A. M., Reiss, P. T., Gee, D. G., Gotimer, K., Uddin, L. Q., Lee, S. H., Margulies, D. S., Roy, A. K., Biswal, B. B., et al. (2009). The resting brain: unconstrained yet reliable. Cereb Cortex, 19(10), 2209-2229.

Smith, S. M., Fox, P. T., Miller, K. L., Glahn, D. C., Fox, P. M., Mackay, C. E., Filippini, N., Watkins, K. E., Toro, R., Laird, A. R., et al. (2009). Correspondence of the brain's functional architecture during activation and rest. Proc Natl Acad Sci U S A, 106(31), 13040-13045.

Smyser, C. D., Inder, T. E., Shimony, J. S., Hill, J. E., Degnan, A. J., Snyder, A. Z., & Neil, J. J. (2010). Longitudinal analysis of neural network development in preterm infants. Cereb Cortex, 20(12), 2852-2862.

Sporns, O., Tononi, G., & Kotter, R. (2005). The human connectome: A structural description of the human brain. Plos Computational Biology, 1(4), 245-251.

Tagliazucchi, E., & Laufs, H. (2014). Decoding wakefulness levels from typical fMRI resting-state data reveals reliable drifts between wakefulness and sleep. Neuron, 82(3), 695-708.

Tagliazucchi, E., von Wegner, F., Morzelewski, A., Brodbeck, V., Borisov, S., Jahnke, K., & Laufs, H. (2013). Large-scale brain functional modularity is reflected in slow electroencephalographic rhythms across the human non-rapid eye movement sleep cycle. Neuroimage, 70, 327-339.

Tambini, A., Ketz, N., & Davachi, L. (2010). Enhanced brain correlations during rest are related to memory for recent experiences. Neuron, 65(2), 280-290.

Van Essen, D. C. (2013). Cartography and connectomes. Neuron, 80(3), 775-790.

Van Essen, D. C., & Dierker, D. (2007). On navigating the human cerebral cortex: response to 'in praise of tedious anatomy'. Neuroimage, 37(4), 1050-1054; discussion 1066-1058.

Vincent, J. L., Kahn, I., Snyder, A. Z., Raichle, M. E., & Buckner, R. L. (2008). Evidence for a frontoparietal control system revealed by intrinsic functional connectivity. J Neurophysiol, 100(6), 3328-3342.

Vincent, J. L., Patel, G. H., Fox, M. D., Snyder, A. Z., Baker, J. T., Van Essen, D. C., Zempel, J. M., Snyder, L. H., Corbetta, M., & Raichle, M. E. (2007a). Intrinsic functional architecture in the anaesthetized monkey brain. Nature, 447(7140), 83-86.

Vogel, A. C., Power, J. D., Petersen, S. E., & Schlaggar, B. L. (2010). Development of the brain's functional network architecture. Neuropsychol Rev, 20(4), 362-375.

Wig, G. S., Laumann, T. O., Cohen, A. L., Power, J. D., Nelson, S. M., Glasser, M. F., Miezin, F. M., Snyder, A. Z., Schlaggar, B. L., & Petersen, S. E. (2014a). Parcellating an individual subject's cortical and subcortical brain structures using snowball sampling of resting-state correlations. Cereb Cortex, 24(8), 2036-2054.

Wig, G. S., Schlaggar, B. L., & Petersen, S. E. (2011b). Concepts and principles in the analysis of brain networks. Ann N Y Acad Sci, 1224, 126-146.

Wilson, M. A., & McNaughton, B. L. (1994). Reactivation of hippocampal ensemble memories during sleep. Science, 265(5172), 676-679.

Wise, R. G., Ide, K., Poulin, M. J., & Tracey, I. (2004). Resting fluctuations in arterial carbon dioxide induce significant low frequency variations in BOLD signal. Neuroimage, 21(4), 1652-1664.

Yeo, B. T., Krienen, F. M., Sepulcre, J., Sabuncu, M. R., Lashkari, D., Hollinshead, M., Roffman, J. L., Smoller, J. W., Zollei, L., Polimeni, J. R., et al. (2011). The

organization of the human cerebral cortex estimated by intrinsic functional connectivity. J Neurophysiol, 106(3), 1125-1165.

Chapter 2: An approach for parcellating human cortical areas using resting-state correlations

This chapter has been published as a journal article. The citation is:

Wig GS*, Laumann TO*, Petersen SE. (2014). An approach for parcellating human cortical areas using resting-state correlations. *Neuroimage*. Jun;93 Pt 2:276-91. doi: 10.1016/j.neuroimage.2013.07.035.

*These authors contributed equally to this work

Steve Petersen, Gagan Wig and I conceived the project and research approach. Gagan Wig and I designed and implemented the methods and performed the data analysis with feedback from Steve Petersen. Gagan Wig and I wrote the paper. Steve Petersen edited the paper.

2.1 Abstract

Resting-state functional correlations (RSFC) reveal properties related to the brains underlying organization and function. Features related to RSFC signals, such as the locations where the patterns of RSFC exhibit abrupt transitions, can be used to identify putative boundaries between cortical areas (RSFC-Boundary Mapping). The locations of RSFC-based area boundaries are consistent across independent groups of subjects. RSFC-based parcellation converges with parcellation information from other modalities in many locations, including task-evoked activity and probabilistic estimates of cellular architecture, providing evidence for the ability of RSFC to parcellate brain structures into functionally meaningful units. We highlight a collection of these observations, but also point out several limitations and observations that mandate careful consideration in using and interpreting RSFC for the purposes of parcellating the brain's cortical and subcortical structures.

2.2 Introduction

The brain is organized at multiple spatial scales ranging from neurons to systems of functionally related areas (Sejnowski et al., 1989). Area1 parcellation has principally relied on discriminating areas based on the convergence of multiple underlying properties including function, architectonics (cyto-, mylo-, and chemo-), connectivity, and in some cases, topographic mapping (e.g., (D.J. Felleman et al., 1991b)). An areal

[1] The term 'area' is conventionally restricted to parcellations of the cerebral cortex and the discussion that follows largely focuses on cortical divisions. It should be noted however, that many of the general ideas regarding parcellation that will be discussed here are applicable to cortical areas as well as subdivisions of subcortical nuclei and the cerebellum.

level of organization as revealed by distinctions in these properties is not limited to primary sensory areas (e.g., (Foerster, 1936; Gennari, 1782; Hubel et al., 1962; Kaas et al., 1979; Marshall et al., 1937)), but rather, is evident across the brain. For example, borders of area MT in the macaque monkey (also known as area V5) can be defined by MT's independent representation of the visual field, the presence of neurons with sensitivity to processing properties of visual motion, distinct patterns of incoming and outgoing connections, and the thick band of myelin that is present in layer IV (e.g., (Van Essen et al., 1981)). Likewise, distinctions in patterns of connectivity and architectonics have been used to parcellate ventral and medial frontal cortex into distinct areas in the macaque monkey (Carmichael et al., 1994, 1996) and human (Ongur et al., 2003). While many of the tools used to identify areal boundaries have typically required invasive measurements or histological analysis of post-mortem brains, recent advances in brain imaging acquisition and analysis have offered an opportunity to parcellate brain areas non-invasively in living subjects (e.g., the present special issue on In Vivo Brodmann Mapping in Neuroimage).

Defining areas using functional distinctions has largely been accomplished by dissociating adjacent locations based on their patterns of task-evoked activity (e.g., (Petersen et al., 1988; Sereno et al., 1995)). More recently, attempts to functionally distinguish brain regions have leveraged the observation that the brain exhibits structured and ordered patterns of low-frequency functional correlations in the absence of overt task demands (Resting State Functional Connectivity (RSFC); (B. Biswal et al., 1995)). The prevalence of organized patterns of RSFC across levels of arousal makes

RSFC well suited to understanding the function and organization of individuals that span ranges of age, mental health, and even species.

The precise significance of RSFC is uncertain; however, accumulating evidence suggests that resting-state correlations identify locations that are functionally similar with one another (for reviews see (B. B. Biswal et al., 2010; M. D. Fox et al., 2007a)). Furthermore, although RSFC relationships are likely mediated by anatomical connectivity, they are not restricted to direct structural connections (e.g., (C J Honey et al., 2009a; Vincent et al., 2007b); for reviews see (Deco et al., 2011; Wig et al., 2011a)). For these reasons, using resting-state correlations as a property by which to understand brain organization is likely drawing on information related to a combination of an area's functional role and its underlying anatomical connectivity.

RSFC has been used to identify putative areal divisions or boundaries by identifying locations where patterns of RSFC exhibit abrupt transitions (RSFC-Boundary Mapping; (Cohen et al., 2008b)). RSFC-based area parcellations using boundary detection have been described for numerous locations including regions of the parietal cortex (Barnes et al., 2011; Nelson et al., 2010b), frontal cortex (Cohen et al., 2008b; Hirose et al., 2012; Nelson et al., 2010c), and across expanses of the whole brain (Wig et al., 2013). Notably, there have been a number of additional applications of RSFC-based analysis with the goal of identifying areas (and also systems) in the brain (e.g., (Deen et al., 2011; Doucet et al., 2011; Goulas et al., 2012; Kahnt et al., 2012; Kelly et al., 2010; D. J. Kim et al., 2012; J. H. Kim et al., 2010; Leech et al., 2012; Margulies et al., 2009; Mars et al., 2012; Mumford et al., 2010; Power et al., 2011; Ryali et al., 2013; Smith et al., 2009; Uddin et al., 2010; Yeo et al., 2011; Zhang et al., 2008)). We return

to the important distinction between boundary detection and alternate RSFC-based methods as means for area parcellation at a later point.

Rather than reviewing the growing body of work that has examined RSFC to identify brain areas and systems, we will utilize this article as a platform to describe some of our recent efforts towards parcellating large expanses of the cerebral cortex using patterns of RSFC. We recognize that the approaches for parcellating brain areas using patterns of RSFC are under continuous revision and refinement, and will continue to improve. Here we will highlight our groups most recent progress in this endeavor and provide descriptions of some important observations, caveats, and places for potential improvement in using RSFC to parcellate brain areas. Our aims are three-fold. First, we aim to demonstrate that the borders revealed by RSFC-Boundary Mapping reflect locations of RSFC pattern transition and are highly similar across independent groups of subjects. Second, we compare the results of RSFC-Boundary Mapping to areal distinctions revealed by other modalities (specifically, task-evoked activity and architectonics) to demonstrate the strong convergence across methods of parcellation in certain locations. Third, we contrast RSFC-Boundary Mapping to other RSFC-based methods that have been used to identify functional area centers or cluster groups of functionally related voxels across large expanses of the brain. Throughout the report, we will also draw attention to a number of observations and limitations for using RSFC to parcellate areas, and discuss their implications towards both the theory and practice of RSFC-based parcellation.

RSFC can be used to identify area borders in groups of individuals

Brain imaging permits areal parcellation in individual subjects and a related article describes our recent efforts towards this endeavor using RSFC (Wig et al., 2013). We draw attention to two observations from that report: (1) RSFC parcellation maps exhibit significantly higher similarity between independent scans of the same individual from different days than between scans from different individuals (see (Wig et al., 2013) Figure 11 and Supplementary Figure 4) . The between subject variability in RSFC parcellation is consistent with reports that have demonstrated subject-wise variability in brain area organization as defined by task-evoked activity (e.g., (Dougherty et al., 2003; Fedorenko et al., 2010; Sabuncu et al., 2010)), architectonics (e.g., (Amunts et al., 2004; Caspers et al., 2006)), anatomical connectivity (e.g., (Johansen-Berg et al., 2005)), and macroscopic anatomy (Van Essen, 2005). (2) Despite the presence of individual differences in area parcellation, numerous features revealed by RSFC parcellation are consistent across individuals (see (Wig et al., 2013) Figure 12). Accordingly, for the present work, rather than focusing on parcellating individual brains that exhibit numerous sources of variation, we adopt a strategy that highlights the commonalities across individuals from a single cohort and report 'group-based' parcellations. While a group-based strategy might obscure important and interesting parcellation variation within a population, it permits identification of the consistent parcellation features across the population.

There are a number of ways to derive a group-based RSFC parcellation. The primary difference across methods relates to the processing stage at which individuals are combined to create group estimates, and each alternative will potentially introduce

the influence of different sources of variation. We refer the interested reader to the appendix of this report for details of the methods we have used here to arrive at group-based RSFC parcellations.

RSFC-Boundary Mapping identifies locations of abrupt transitions in patterns of resting-state correlations

RSFC-Boundary Mapping rests on the assumption that an area's RSFC correlations are relatively uniform within the extent of an area, yet may be distinct from the RSFC of an adjacent area (Cohen et al., 2008b). In this view, locations where the patterns of RSFC exhibit abrupt transitions can be considered putative boundaries between areas across the cortical surface. This concept is illustrated in Figure 1. By computing and comparing the average seed-based RSFC maps from a group of young adults (N=40) for a line of seeds across a portion of the cortical surface, we can see that the RSFC correlation maps do not change smoothly, but rather, exhibit rapid and abrupt changes (Figure 1a). Furthermore, these locations of change are consistent in both directions (i.e., from an inferior location in the posterior extent of the cingulate gyrus to a more superior location in the paracentral lobe, or in reverse), suggesting the presence of a functional boundary between two adjacent areas. This basic approach can be extended across the cortical surface with the aid of image-processing tools to create a vertex-wise estimate of the likelihood with which a location is identified as a RSFC boundary (i.e., a spatial gradient of changes in correlation map similarity, or it's

corresponding edge 2) between two locations in the brain (Figure 1b; See Appendix—Methods for method details)). The RSFC boundary map reveals locations where patterns of RSFC exhibit a transition (hotter colors), and locations where the patterns of RSFC are more locally stable (cooler colors). We hypothesize that the locations of transitions are strong candidates for the locations of boundaries between distinct areas.

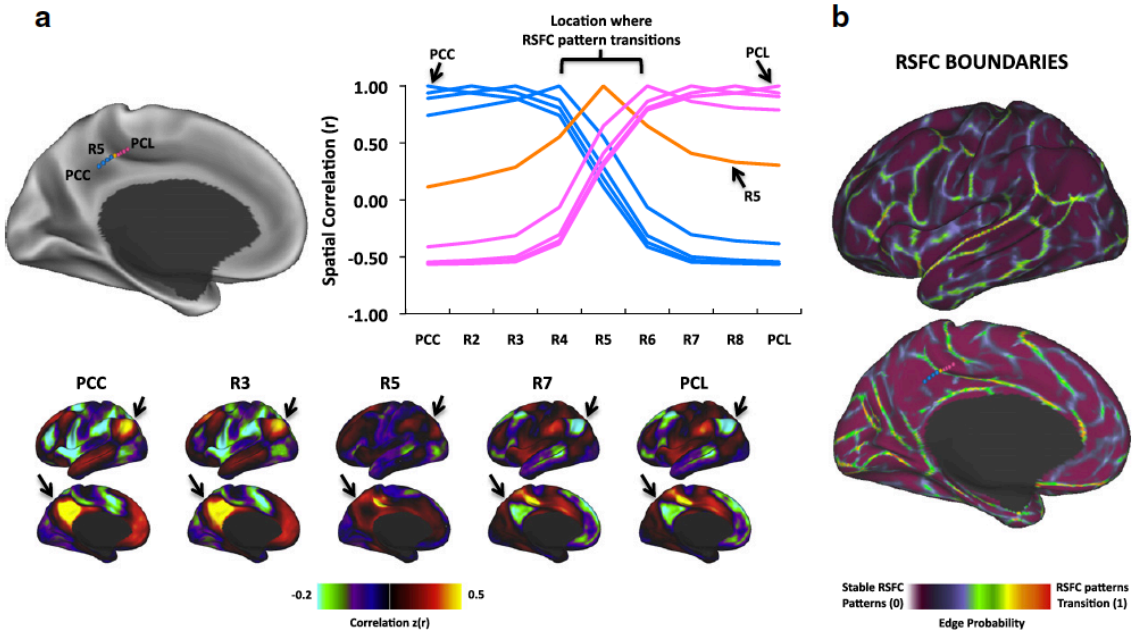

Figure 2-1. Patterns of RSFC exhibit abrupt changes across the cortical surface. (a) RSFC maps were derived for locations (R2-R8) between a region in the posterior extent of the cingulate cortex (PCC) and a region in the paracentral lobe (PCL) in a group of subjects (n=40; defined anatomically; locations are shown as colored balls). The plot to the right depicts the similarity (spatial correlation) of every location's RSFC map with the RSFC map of each of the other locations. RSFC maps are similar from PCC to R4, followed by a location of abrupt change (R5), and then a second set of locations where the maps are highly self-similar.

[2] Spatial gradient maps can exhibit features reflecting a high level of variability in the magnitude of correlation map changes (cf. Figure 9 – step 6, and Wig, et al 2013), suggesting that even adjacent cortical areas identified in this way will not be equally separable from one another in terms of their patterns of RSFC. In the present work, we have applied an edge detection technique that emphasizes the locations where there is a gradient present. The edges are agnostic as to how large the correlation pattern change underlying the transition is. Thus large and small correlation pattern changes can both have high values in the edge probability map as long as the location of transition is consistently identified.

Similarity lines and location balls have been color coded to denote greater RSFC similarity with PCC (blue) or PCL (pink). The location whose RSFC map was not similar to either the PCC or PCL group (R5) is color-coded orange. The RSFC maps of a subset of the regions are depicted on the lower panel, and two locations with prominent differences between maps are highlighted by arrows (the angular gyrus on the lateral views and anterior cingulate gyrus on the medial views). (b) RSFC-Boundary map for a group of subjects (n=40). The coloring highlights where patterns of RSFC exhibit a abrupt transitions (i.e., putative areal borders) and locations where patterns of RSFC are relatively stable. Locations highlighted in panel (a) are displayed on the medial surface –the identified transition point (orange) is at a location of high border likelihood.

RSFC-defined borders are highly similar across independent groups of individuals

We argue that group-based parcellation may deemphasize some of the inherent variability across groups of individuals (both anatomical and otherwise) to reveal the parcellation features (in the current case, areal boundaries3) that are consistent across individuals. If this is the case, then RSFC-Boundary Mapping parcellations from independent groups of individuals sampled from the same cohort should be highly similar. Figure 2a depicts group-based RSFC Boundary Mapping maps from three independent groups of healthy young adults (N = 40 individuals/group). The spatial correlation between the three parcellation maps reveals a high degree of similarity across the groups (average spatial correlation: r = 0.60, range of spatial correlations across three maps: r = 0.60 – 0.61). Visual inspection confirms that the locations of many of the putative boundaries between areas are strikingly similar across the three groups. For example, locations along the middle and inferior frontal gyrus exhibit similar areal boundaries in each of the three groups providing evidence for distinct divisions along the lateral frontal cortex. Likewise, prominent boundaries within medial-superior

[3] Parcellation features may also include an areas interior/extent or an areas geometric center.

frontal cortex, medial parietal cortex (e.g., between posterior cingulate cortex and paracentral lobule), medial occipital cortex, and lateral parietal cortex (e.g., between the angular gyrus and the lateral aspect of the middle occipital gyrus) are evident in all three groups. To demonstrate the overlap in group-based parcellations, each of the group maps was thresholded to reveal the strongest edge probability locations, and a conjunction of these images was created (Figure 2b). Conjunction maps were created over a range of edge probability thresholds (0.10-0.20) to give a more complete picture of the amount of overlap in RSFC-Boundary Mapping features. The putative boundaries highlighted earlier can all be observed in these conjunction images, reinforcing their consistency. In addition, a final group-based parcellation was derived by combining the individuals from the three independent groups into one 120-subject group (Figure 3). Not surprisingly, this last group parcellation map is similar to each of the independent group parcellations. This 120-subject group parcellation map includes the consistent features highlighted in the conjunction maps of figure 2b while also retaining the full range of edge probability values across all cortical vertices; it is used in our subsequent comparisons.

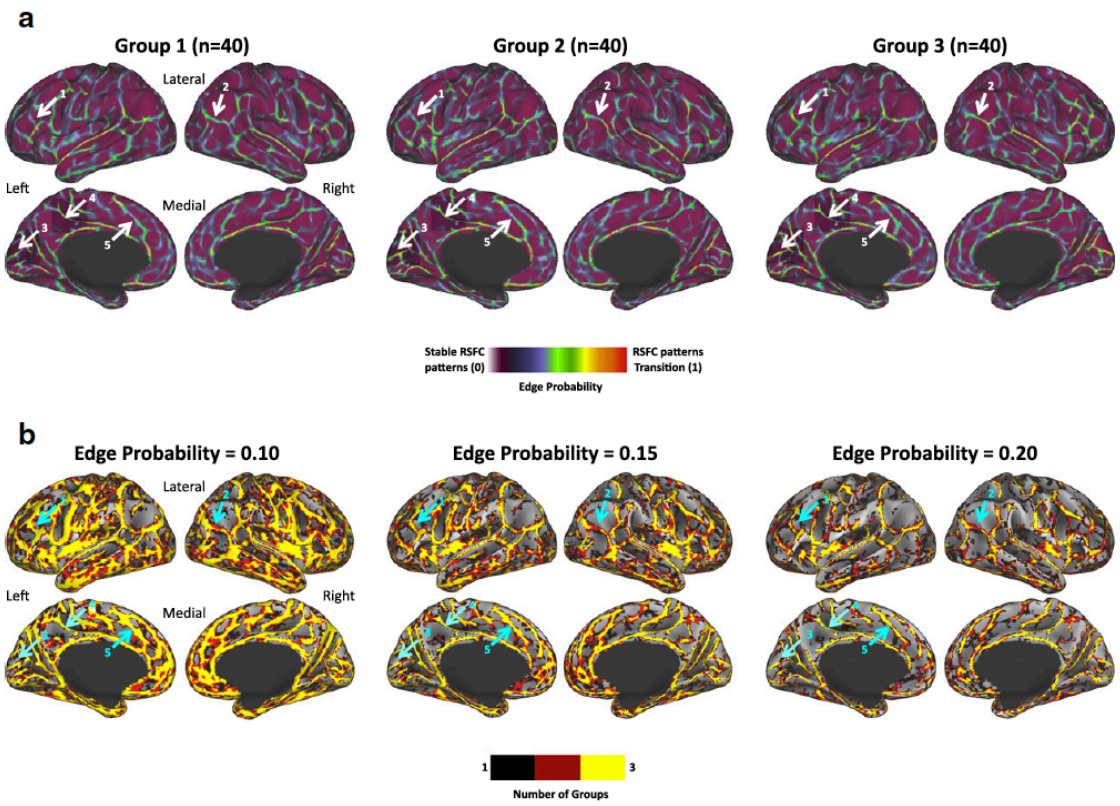

Figure 2-2. RSFC-Boundary Mapping parcellation reliably identifies locations of putative area borders. (a) RSFC-Boundary Mapping parcellations are highly similar across 3 independent groups of healthy young adults. A subset of locations is pointed out with arrows to highlight the high degree of similarity in parcellations. These locations include regions along the inferior and middle frontal gyrus of the left hemisphere (1), a strong border separating angular gyrus from the middle-occipital gyrus in the right hemisphere (2), a strong border parallel to the calcarine sulcus in the medial occiptal lobe (3), a strong border separating posterior extent of the cingulate gyrus from locations in the paracentral lobe (4), and a border which separates locations in the anterior cingulate gyrus from more dorsal regions of the medial frontal cortex (4). (b) The strongest RSFC-Boundary Mapping borders are consistent across groups. Independent conjunction images created by first thresholding each of the three group's RSFC-Boundary Mapping parcellation maps from (a), binarizing the image, and summing the three images to demonstrate the consistency in parcellation features across groups. Three edge probability thresholds are depicted.

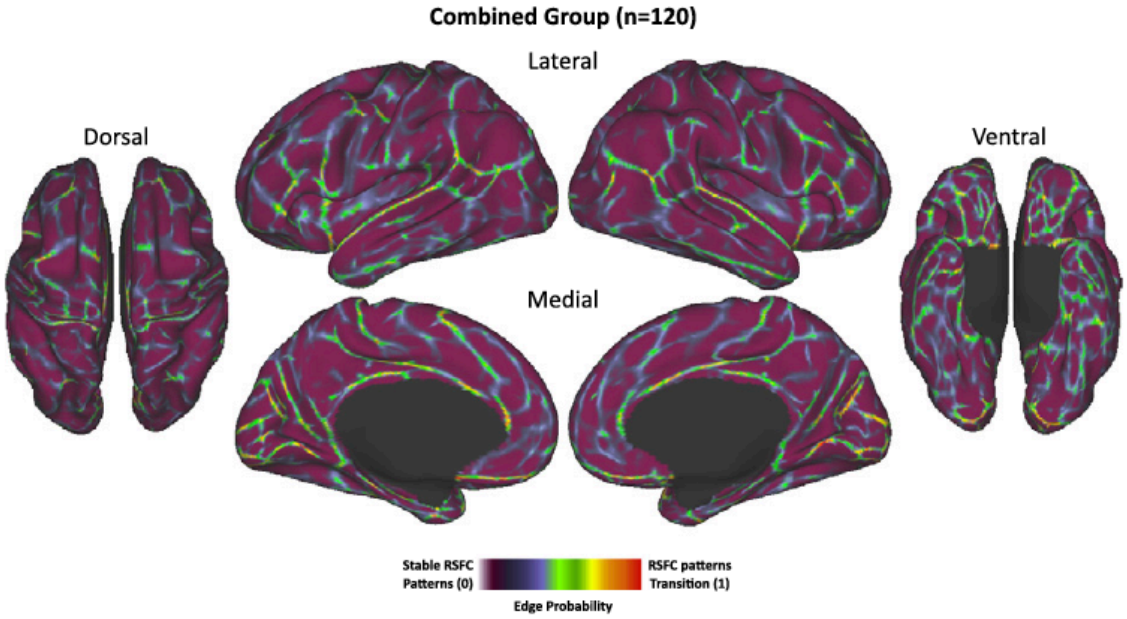

Figure 2-3. RSFC-Boundary Mapping parcellation from combined group (N=120) of healthy young adult subjects. The coloring highlights where patterns of RSFC exhibit abrupt transitions (i.e., putative areal borders) and locations where patterns of RSFC are relatively stable.

RSFC-defined borders exhibit strong correspondence with task-activation maps

To understand the relevance of RSFC-based areal boundaries, it is critical to determine whether parcellations derived from the current approach correspond with parcellations identified by other modalities. Brain areas perform distinct processing operations and a RSFC parcellation map should reveal areal divisions that are functionally plausible based on known processing dissociations. Previous research in both our laboratory and others has taken this approach to begin to inform and validate RSFC parcellations in numerous cortical locations (e.g., (Nelson et al., 2010b; Wig et al., 2013), also see (Smith et al., 2009)). By examining functional activity defined by the meta-analysis of large batteries of task-evoked data, we identified a collection of

independent locations demonstrating unique fingerprints of functional activity that converge with divisions revealed by RSFC borders.

Meta-analysis of task-evoked data reveals locations sensitive to a variety of signal types

Meta-analyses were conducted on a large collection of independent studies in which independent groups of subjects performed different tasks with different stimuli. Each meta-analysis was aimed at identifying brain regions that reliably displayed significant activity when certain tasks were performed (e.g., reading) or certain signal types were expected (e.g., error-related activity). While the analyses were constrained by the available datasets (specifically those collected in our laboratory), we were able to create meta-analytic maps for task-evoked activity focused on error-related processing, task-induced deactivations, task-initiation, memory (episodic retrieval), language (reading), and sensorimotor functions. All study datasets contributing to the meta-analyses were acquired on a single scanner (a Siemens 1.5 Tesla MAGNETOM Vision MRI scanner), which was distinct from the scanner used to acquire the RSFC data (see Appendix –Methods for details). For each dataset, the voxels passing a statistical threshold were identified to create a binary mask, and the resultant maps were summed to create a conjunction image for the corresponding meta-analysis (for subject, dataset and analysis details see (Power et al., 2011)). This conjunction image indicated how often a voxel was identified across all the datasets associated with the given task or signal-type. In this way, each meta-analytic conjunction image represents an estimate of the spatial extent of functional areas defined by task-related activity.

RSFC borders separate clusters of task-evoked data

For comparison to the RSFC-Boundary map, we focus on voxels exhibiting significant activity in at least 60% of the studies contributing to each task-evoked meta-analysis. As the comparison is constrained by available datasets, only a portion of the total cortical surface is available for comparison between modalities. Figure 4 demonstrates that locations demonstrating task-induced activity tend to fall within borders defined by RSFC (for purposes of comparison, the 120-subject RSFC-Boundary map was thresholded at >0.15 edge probability to identify stronger borders). In several locations, RSFC-defined borders tightly surround clusters identified in task-evoked maps. For example, locations demonstrating task-induced deactivations including the medial prefrontal cortex, angular gyrus, and posterior cingulate cortex are surrounded by RSFC borders. In other locations, contiguous voxels of activity which appear to have multiple local maxima and associated sub-clusters are separated by a RSFC border, suggesting the sub-clusters may be parts of different areas (e.g., in the motor-response meta-analytic map a task-related cluster in the anterior portion of the cingulate gyrus is separated by a RSFC-border from a more dorsal cluster in the medial superior frontal cortex likely corresponding to the supplementary motor area, while in the episodic-memory meta-analytic map a task-related cluster in the inferior parietal lobule is separated by a RSFC-border from a cluster in the angular gyrus). As a quantitative confirmation of these qualitative observations, we performed a chi-square test of independence between a composite task-map of all cortical locations exhibiting task-evoked activity in at least one meta-analytic map and the thresholded RSFC-Boundary map. The vertices identified as having a high likelihood of being an RSFC-

defined border and the vertices identified as exhibiting task-evoked data (i.e., putative area interiors) came from non-overlapping populations ($X2$ (1, N = 59412) = 220.9, $p << 0.001$).

It is important to note, however, that the correspondence between task-evoked activity and RSFC-borders is not perfect at all locations (e.g., not all task clusters are perfectly enclosed by RSFC borders). This may be a consequence of the large differences in data acquisition and processing between the two types of data (e.g., different scanners, volume-based analysis for task data vs. surface-based RSFC parcellation). Indeed, a thorough demonstration of the correspondence between RSFC-borders and task activations will require datasets that include both data types in the same subjects. This caveat notwithstanding, there may remain true discrepancies between these modalities that will mandate closer examination of the sources of disparity. Resting state and task-evoked activity may highlight different aspects of the brain's functional organization.

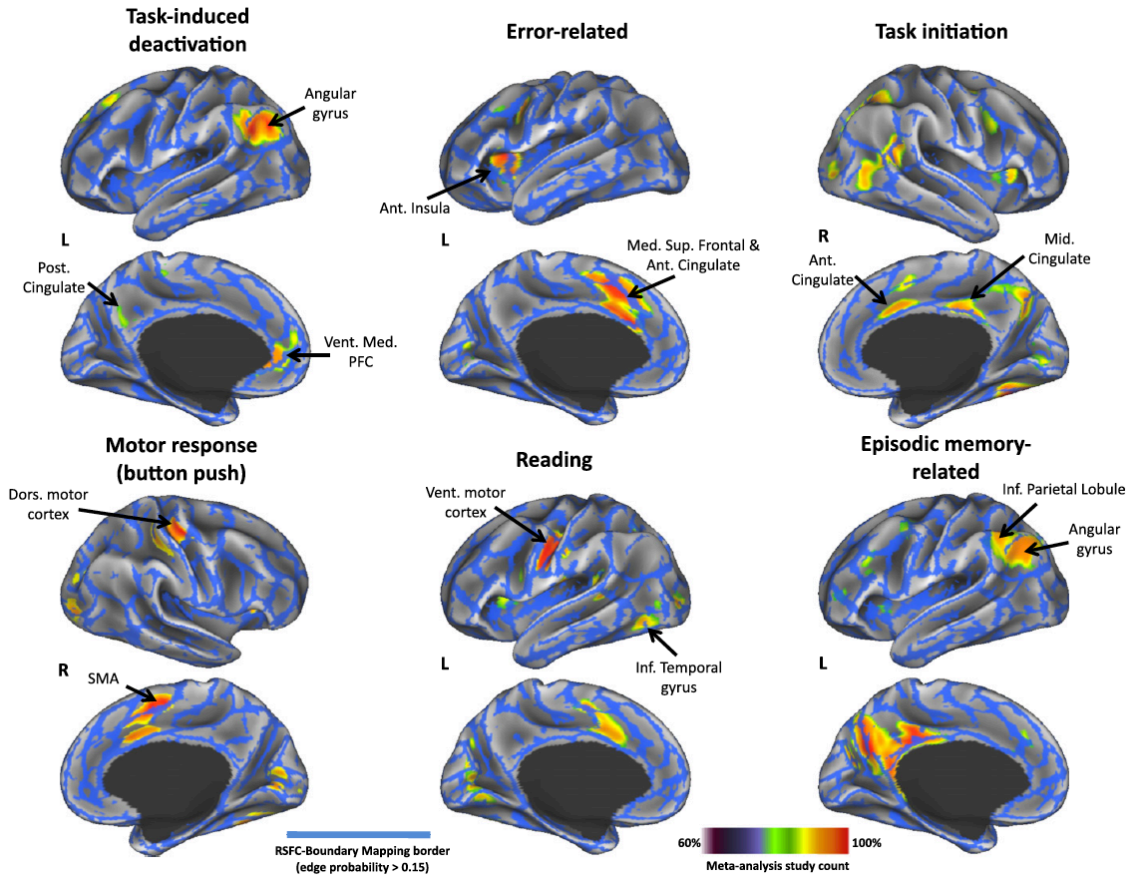

Figure 2-4. RSFC-Boundary Mapping parcellation exhibits a high degree of correspondence with areas defined by task-evoked activity. Task-evoked activity was derived from meta-analyses of multiple studies to highlight locations exhibiting sensitivity to performance of certain tasks (e.g., reading) or certain signal types (e.g., error-related activity). The 120-subject RSFC-Boundary Mapping parcellation was thresholded (edge probability > 0.15) to reveal locations exhibiting a high likelihood of being a border between areas. Many area locations defined by task-evoked activity are surrounded by RSFC-borders (e.g., the cluster of activity in the ventral medial prefrontal cortex in the task-induced deactivation meta-analytic map). In other locations RSFC-borders separate what appears to be distinct clusters of task-evoked activity, suggesting the existence of distinct areas (e.g., a cluster of activity in the inferior parietal lobule is separated from a cluster of activity in the angular gyrus in the episodic memory meta-analysis map). Parcellations are overlaid on inflated cortical surfaces; some surfaces have been tilted to facilitate viewing (i.e., the lateral surface of the right hemisphere in the motor response (button pushing) comparison and the lateral surface of the left hemisphere in the error-related activity comparison).

RSFC-defined borders respect architectonic divisions in some locations

In addition to functional dissociations, identifying the transitions in architectonic features has been a standard approach towards parcellating human cortical areas since

(Brodmann, 1909). More recently, probabilistic maps of a collection of cortical areas have been defined by quantitative procedures that measure changes in the laminar distribution of cell-body density across the cortical surface in a set of post-mortem human brains (Amunts et al., 2000; Schleicher et al., 1990; Schormann et al., 1998). Surface-based representations of these maps, as well as a number of other parcellations, are available in the sumsDB database (http://sumsdb.wustl.edu/) and have been described at greater length elsewhere (Fischl et al., 2008; Van Essen et al., 2011). Direct comparisons between maps derived from post-mortem dissection of human brains and the in-vivo RSFC parcellation described hitherto has clear caveats towards interpretation. Determining the precise convergence between architectonics and RSFC will be best accomplished by incorporating imaging methods that can reveal cellular and sub-cellular features of anatomy, and there are numerous efforts to do so (Dick et al., 2012; Glasser et al., 2011; Toga et al., 2006). Keeping this limitation in mind, we describe preliminary observations that suggest RSFC-based parcellations may converge with features related to underlying cellular anatomy.

RSFC borders exhibit overlap with architectonic divisions defining primary visual cortex

While the precise correspondence between probabilistic maps of cyto-architecture based on post-mortem histology and RSFC-based boundaries may be difficult to ascertain due to the very different methods and underlying properties used to create these parcellations, we highlight here an important instance where they appear to converge. Figure 5a depicts probabilistic estimates of areas 17 and 18 (herein referred to as probabilistic area (PA) 17 and 18). These architectonic areas have been

shown to have reasonable correspondence with retinotopic maps of V1 and V2 (V1 more clearly than V2; (Hinds et al., 2009; Van Essen et al., 2011)). The architectonic boundaries are overlaid on a medial occipital view of the RSFC-Boundary map as black lines. The border between PA 17 and PA 18 overlaps with a prominent border in this map that runs both ventral and dorsal to the calcarine sulcus. These RSFC-based borders were also consistently observed in each of the individual group parcellations (see arrow '3' in Figure 2).

Figure 5b demonstrate how RSFC seed maps differ on either side of the RSFC-Boundary Mapping defined border (calculated across all 120 subjects). When a seed is placed ventral to the calcarine sulcus but dorsal to an RSFC-defined border (grey ball labeled '17' in Figure 5a), resting-state correlations are prominent within PA 17 but bound by the RSFC-defined borders separating PA 17 from PA 18. Conversely, a seed region on the opposing side of the RSFC-defined border (grey ball labeled '18' in Figure 5a) exhibits the strongest resting-state correlations with locations within PA 18, both dorsal and ventral to the calcarine sulcus. The difference between these two seed-based maps is best appreciated in the statistical difference image ($t(119)=3.38$, $p<0.001$); a collection of other more distal locations also exhibit differential connectivity as a function of seed location. Accordingly, the presence of a RSFC-defined border separating PA 17 from PA 18 likely reflects differences in both local and global correlation patterns.

Notably, there are additional borders found by RSFC-Boundary Mapping within PA 17. For example, a border running along the calcarine sulcus (red arrow, labeled '1') approximates the position of the horizontal meridian in retinotopic maps of V1 and may

reflect differences in RSFC between the upper and lower visual fields of V1. Likewise a border running along the dorsal-ventral axis mid-way through PA17 may divide the more central vs. peripheral visual representations of this area. The presence of additional borders within a cortical area characterized by topographic mapping is consistent with the RSFC-based division between mouth and hand regions of primary motor and somatosensory cortex that has been reported by network estimation methods elsewhere (e.g., (Power et al., 2011; Yeo et al., 2011)). This division of motor/somatosensory cortex can also be seen in the parcellation maps presented here (e.g., see borders surrounding the dorsal motor cortex surrounding button-push related task activity and in the ventral motor cortex surrounding reading-related task activity in Figure 5). Importantly, a number of divisions are also apparent along the pre- and post-central gyrus, and exhibit correspondence with other probabilistic area divisions (e.g., PA 1 vs. 2, PA 2 vs. 3b; see post-central gyrus in lateral views in Figure 4). All together, these observations are critical to evaluate: they likely reflect the special nature of the information RSFC brings to bear towards understanding area organization and function, but also stress caution when interpreting the presence of RSFC boundaries in the absence of parcellation information from other modalities.

The RSFC-Boundary Mapping border corresponding to the PA 17/PA 18 border extends somewhat further laterally beyond the occipital pole than the cyto-architectonic boundary (while a lateral view is not presented in Figure 5, a lateral view of the RSFC-Boundary Mapping borders are presented in Figure 3). This discrepancy, along with an aberrant border within PA 17 (Figure 5a: red arrow, labeled ‘2’), may be due to inadequacies in the scan acquisition and processing – in particular, field distortions

and/or signal loss related to vasculature at the occipital pole likely affected the position of borders measured here (see subsequent section 'Additional constraints and considerations' and red arrow labeled '4' in Figure 8a).

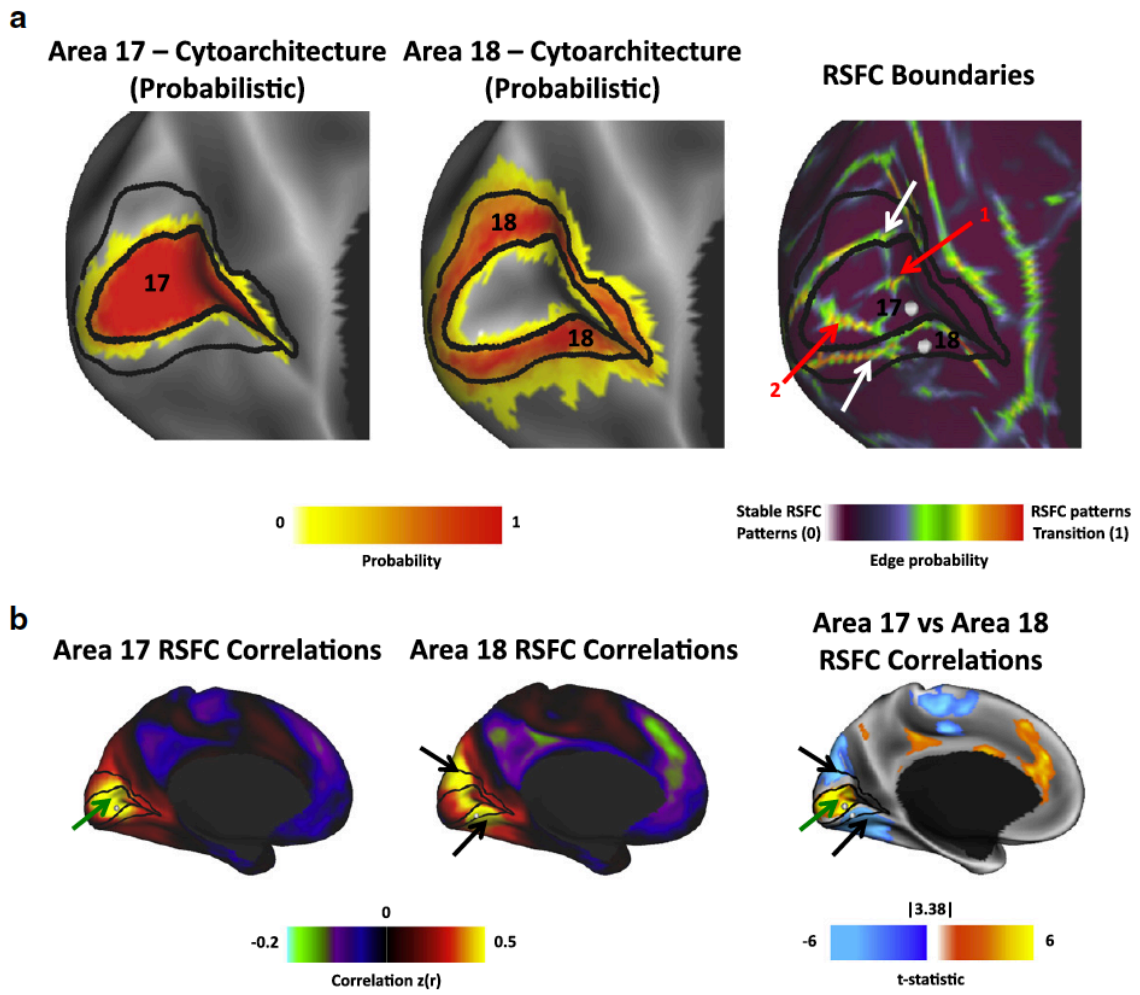

Figure 2-5. RSFC-Boundary Mapping compared to cyto-architectonically-defined probabilistic areas (PA) 17 and 18. (a) Medial occipital view of PA 17 and PA 18 (Fischl, et al 2008) and 120-subject RSFC-Boundary map. Black lines indicate reasonable boundaries between and around areas 17 and 18 as described in Van Essen, et al 2011. The white arrows indicate dorsal and ventral RSFC boundaries that appear to closely correspond to the architectonic boundary. The RSFC-based borders are also apparent in each of the individual groups (see Figure 2). Red arrow 1 indicates a boundary along the calcarine fissure that may correspond to the horizontal meridian of PA 17 (Visual Area 1). Red arrow 2 indicates a boundary that is likely due to susceptibility artifact at the occipital pole (see Figure 8a) (b) Correlation maps generated from ventral PA 17 and PA 18 seeds (white balls) and the differences between them. Green and black arrows highlight the locations of strongest correlations for seeds in PA 17 and PA 18, respectively. The differences between the two seeds can be best appreciated on the statistical

difference map, which is calculated as a surface vertex-wise two-sample t-test between the correlation maps of the two seeds. Note that the contour of the difference image follows the PA 17/18 boundary.

RSFC can be used to identify the location of area centers

RSFC patterns can also be leveraged to reveal alternative features that may relate to area organization. So far, we have described how identifying locations where patterns of RSFC exhibit an abrupt transition can be used for identifying borders between putative areas. An alternative strategy is to focus on identifying the interior (or central) parts of areas rather than the boundaries between them. We use an RSFC approach that aims to directly identify these interior regions and suggests that independent RSFC-based areal center identification may help parcellate areas that are not clearly distinguished by RSFC-Boundary Mapping (Wig et al., 2013). In general, these two approaches to RSFC-based area definition should be highly complimentary to one another.

RSFC-Snowball sampling identifies locations where resting-state correlation peaks aggregate

Our method for identifying candidate locations for the central portions of areas combines seed-based RSFC with principles inspired by social network science and graph theory (Snowball Sampling; (Goodman, 1961; Wasserman et al., 1994)). RSFC-Snowball sampling first identifies the peaks of correlation (i.e., neighbors) from a seed-based RSFC map, and then iteratively tracks the neighbor's of these neighbors through multiple stages. To minimize sampling bias, this basic process is repeated from numerous starting locations across the brain, and the output of each sampling

procedure is aggregated to arrive at a final peak density map. We have previously described the details of using this method for parcellating an individual subject's cortical and subcortical brain structures; RSFC-Snowballing parcellation maps are reliable within an individual scanned over multiple days, and area center locations defined by RSFC-Snowballing correspond with area center locations defined by task-evoked data (Wig et al., 2013). To parallel the present group-based RSFC-Boundary Mapping parcellation observations, a method for extending the RSFC-Snowballing method to the level of groups is presented in the Appendix section.

RSFC-defined centers and borders compliment one-another

An RSFC-Snowballing peak density map was derived for the group of 120 individuals. Rather than being randomly or uniformly distributed, the RSFC-Snowballing map exhibits a structured distribution, with some locations having many peaks, and others having very few. If RSFC-Boundary Mapping identifies the locations of putative boundaries between areas and RSFC-Snowballing identifies the locations of putative centers of areas, peak density values should be less prominent at locations that are transition points (or boundaries) and more prominent within boundary interiors. Simultaneously viewing the strong borders defined by RSFC-Boundary Mapping and the strong centers defined by RSFC-Snowballing suggests this expectation may be true (Figure 6). Importantly, each of the two methods appear to reveal unique parcellation features in some locations (e.g., two area centers identified by RSFC-Snowballing in the posterior-inferior temporal cortex are surrounded by an area border defined by RSFC-Boundary Mapping on the lateral right hemisphere), suggesting the two methods are not

completely redundant with one another and can be used in combination for the purposes of RSFC parcellation (for more detailed examples and discussion see (Wig et al., 2013)). This is consistent with the negative, but non-perfect relationship between the two RSFC-based parcellation maps ($r = -0.14$, $p << 0.001$).

The non-perfect relationship noted above may be surprising, given that both methods of area parcellation focus on patterns of RSFC. This observation may related to a practical as opposed to conceptual difference between the methods — operationally, the thresholds that are most useful for a given method of parcellation may miss distinctions in another method of parcellation and the different processing steps for each method may accentuate and attenuate non-overlapping sources of noise in RSFC. For example, adjacent areas that share very similar patterns of RSFC would have a weak boundary between them, yet the area centers might be highlighted by RSFC-Snowballing. Along these lines, there are trade-offs between methods that focus on borders between areas versus methods that attempt to identify area interiors. Relying on borders may result in parcellations with discontinuous boundaries if there are differences in the strength of RSFC transitions between an area and the various areas that are adjacent to it. Likewise, focusing on area centers may result in a parcellation with a poor representation of area extent. Accordingly, just as it is important to focus on multiple modalities to accurately parcellate areas, it is advantageous to focus on multiple features that may distinguish areas (i.e., boundaries and centers or interiors).

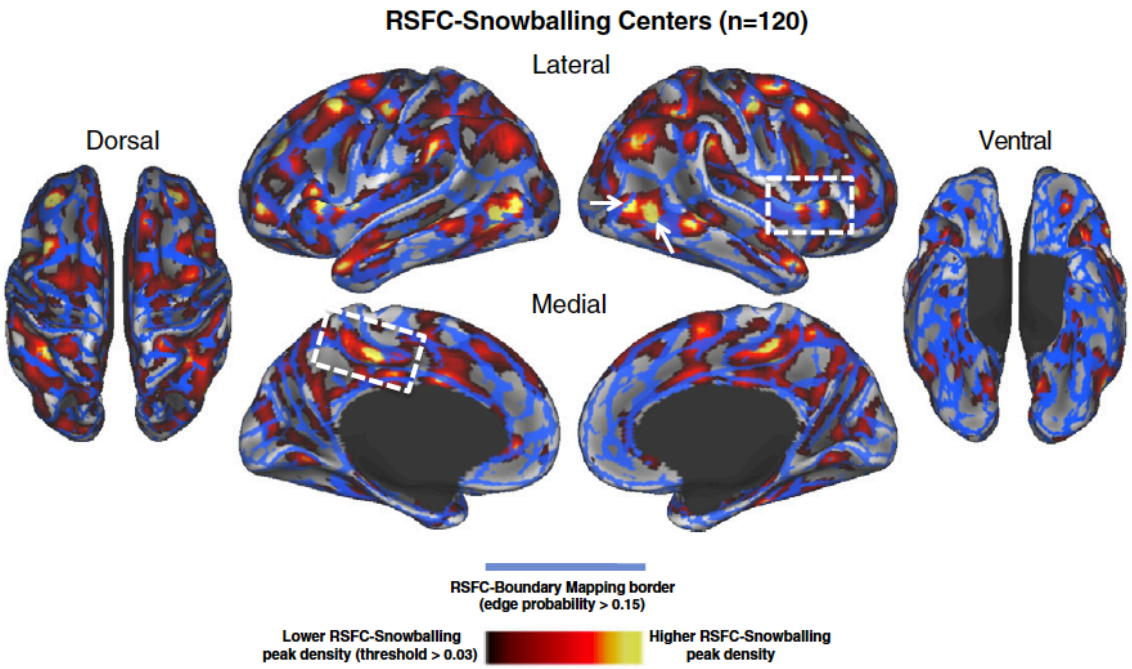

Figure 2-6. Area borders defined by RSFC-Boundary Mapping surround area centers defined by RSFC-Snowballing. RSFC-Snowballing parcellation of 120 subjects reveals the locations of putative area interiors (centers). This RSFC-Snowballing parcellation map was thresholded to highlight vertices with high area center likelihood (peak density > 0.03). The 120-subject RSFC-Boundary Mapping parcellation was thresholded to reveal locations exhibiting a high likelihood (edge probability > 0.15) of being a border between areas. Each parcellation method reveals different area features (i.e., interiors and borders) and many locations exhibit a high degree of correspondence between the methods (e.g., running above the posterior cingulate sulcus in the left medial hemisphere and the right anterior insula in the right lateral hemisphere highlighted by white boxes). In other locations, a given parcellation method may identify features not revealed by the other (e.g., two area centers identified by RSFC-Snowballing [pointed out with white arrows] are surrounded by an area border defined by RSFC-Boundary Mapping on the lateral right hemisphere) encouraging the use of multiple methods for RSFC-based parcellation.

RSFC-defined borders overlap with RSFC-defined system boundaries, but also reveal plausible areal divisions within the identified systems

Voxels can be clustered or grouped based on the similarity of their resting-state time series or their RSFC maps (e.g., using community detection, clustering algorithms,

or independent component analysis (ICA)4; e.g., (Doucet et al., 2011; Mumford et al., 2010; Power et al., 2011; Smith et al., 2009; Yeo et al., 2011)). In some cases, the identified clusters have demonstrated a considerable degree of overlap with functionally defined systems, providing evidence that patterns of RSFC can be used to identify system-level organization (e.g., (Power et al., 2011; Smith et al., 2009)). Although many clustering approaches have been described as methods of parcellation, it is important to recognize that the purpose (and the outcome) of these analyses typically differ from the work presented here. Community detection, clustering, and component separation techniques operate on a data space that is blind to the underlying neuroanatomy. As a consequence, RSFC-based clustering techniques are capable of identifying collections of voxels or locations with similar properties, but these collections are not bound by space and may also group distinct adjacent areas into a single cluster. Accordingly, the majority of clustering analyses have typically identified locations that are functionally similar and may compose a given system (e.g., the visual system or the default system), but do not necessarily parcellate areas themselves (e.g., V1 versus V2 of the visual system, etc.). Direct comparisons of RSFC-defined system divisions and RSFC-based area parcellation provide illustrations of this important distinction

RSFC clusters, communities, and components are not equivalent to areas

Brain systems are defined as groups of functionally related areas (Sejnowski et al., 1989) and RSFC clustering techniques have identified collections of areas (or

[4] While there are important differences across each of these methods, for simplicity we will refer to the collection of methods as 'clustering techniques' and the identified units as 'clusters'.

technically, regions/voxels) that likely represent functional brain systems at the scales that have been prominently explored. It is important to point out that the voxels corresponding to a given cluster are often spatially discontiguous, and can even span the length of the brain (e.g., groupings labeled as the default system typically include voxels in the medial prefrontal cortex and posterior parietal cortex; Figure 7a). It should be clear based on this discontinuity alone that the identification of a cluster may reflect a granularity of organization that should not be confused with the parcellation of an area.

RSFC-defined area borders are consistent with RSFC-defined system boundaries in many locations

If clustering techniques are capable of identifying putative systems, and systems are composed of areas, the locations of system divisions should overlap with the locations of some areal boundaries. Figure 7b depicts the correspondence between system divisions (i.e., transitions between two adjacent clusters) and the 120-subject RSFC-Boundary map. As expected, many locations that are system divisions exhibit high RSFC-Boundary mapping edge probabilities.

A direct comparison of RSFC-defined boundaries and two published systems maps (Power et al., 2011 and Yeo et al., 2011) was conducted. Figure 7c depicts the distribution of edge probability values across all cortical vertices. Two separate distributions are presented in each histogram: the subset of edge probability values located at cortical vertices that were identified as system divisions (colored in yellow (Power et al., 2011) and orange (Yeo et al., 2011)), and the subset of edge probability values located at cortical vertices that were not identified as system divisions (colored in

purple). Locations of system divisions exhibited higher edge probability values than the locations not identified as system divisions[5] (Power et al. (2012) division comparison: Median edge probability at locations that are system divisions: 0.168, median edge probability at locations that are not system divisions: 0.144, W(57034) = 492580832, z = 19.5, p<<0.0001; Yeo et al. (2012) division comparison: Median edge probability at locations that are system divisions: 0.174, median edge probability at locations that are not system divisions: 0.143, W(57034) = 471727456, z = 28.0, p<<0.0001).

RSFC-defined systems contain multiple areal divisions

The locations of putative system divisions revealed by clustering techniques coincide with the locations of several strong putative area boundaries as identified by RSFC-Boundary Mapping. One might try to use clustering techniques for parcellation by segregating a cluster into portions that only contain adjacent voxels and label these sub-clusters as areas. However, there is strong reason to be cautious in this regard. As a prominent example, it should be apparent that this would result in large portions of the visual system highlighted using various methods in Figure 7a (blue community or red cluster) being labeled as a single area. Consistent with this, it is apparent that many locations not identified as system divisions exhibit high edge probability (RSFC boundary) likelihood (see purple bars in histograms depicted in Figure 7c). These

[5] Kolmogorov-Smirnov goodness-of-fit hypothesis tests revealed that the distributions of the RSFC-Boundary Mapping edge probabilities were non-normal and log transformation did not achieve normality. Accordingly, a Wilcoxon rank sum test was used to determine the probability with which the two distributions had equivalent medians.

observations support the notion that system divisions are not a comprehensive representation of area boundaries.

Further comparison of RSFC-derived clusters and communities to RSFC-derived borders confirms that, in some cases, multiple strong boundaries can be found within a single contiguous portion of a cluster or community. We have already pointed out the parcellation of PA17/PA18 using RSFC-Boundary Mapping; here we highlight a portion of the left lateral inferior frontal cortex as an additional example of a location where multiple boundaries are observed within a cluster. Two independent techniques (community detection (yellow in Power et al. (2012)) and clustering (orange in Yeo et al. (2012))) identified similar clusters of continuous voxels spanning the extent of the left inferior/middle frontal gyrus (Figure 7d). However, the RSFC-Boundary Mapping parcellation suggests the presence of 3 strong borders (corresponding to 4 putative areas) within these clusters. While it is possible that the presence of RSFC-Boundary Mapping divisions simply reflect subtle and progressive distinctions within a single area, this would be inconsistent with the architectonic divisions that have been noted along this part of the brain (e.g., Brodmann's areas 44-47 and possibly 10). Furthermore, examination of the seed-based RSFC maps obtained from locations within each of these divisions suggests otherwise (the most posterior location (4) has a RSFC map most similar to the most anterior location (1), which are quite distinct from maps obtained from locations (2) and (3); Figure 7e).

Why do clustering techniques behave differently than the RSFC-Boundary Mapping parcellation method highlighted here? Clustering techniques, for a given a priori or data-determined number of clusters, will identify groups of voxels that minimize

RSFC similarity distance within clusters while simultaneously maximizing RSFC similarity distance between clusters. This focus on maximizing global separation may come at the cost of more local distinctions. In contrast, parcellation methods that rely on local feature changes (such as RSFC-Boundary Mapping) will be more sensitive to transitions in cortical identity (e.g., from V1 to V2 in Figure 6). It may be possible for a clustering technique to identify a collection of voxels that corresponds to a single area if the method is invoked using both an appropriate level of granularity and with spatial constraints. However, complete partitioning at a given spatial scale (e.g., systems or areas) would require a perfectly hierarchical RSFC structure. The appropriate level of the RSFC hierarchy to define a given cortical area may be the same level that defines a system of areas elsewhere. As such, just as is the case with RSFC-Boundary Mapping, appropriate comparisons are necessary to understand the clustering observations further and ensure biological plausibility.

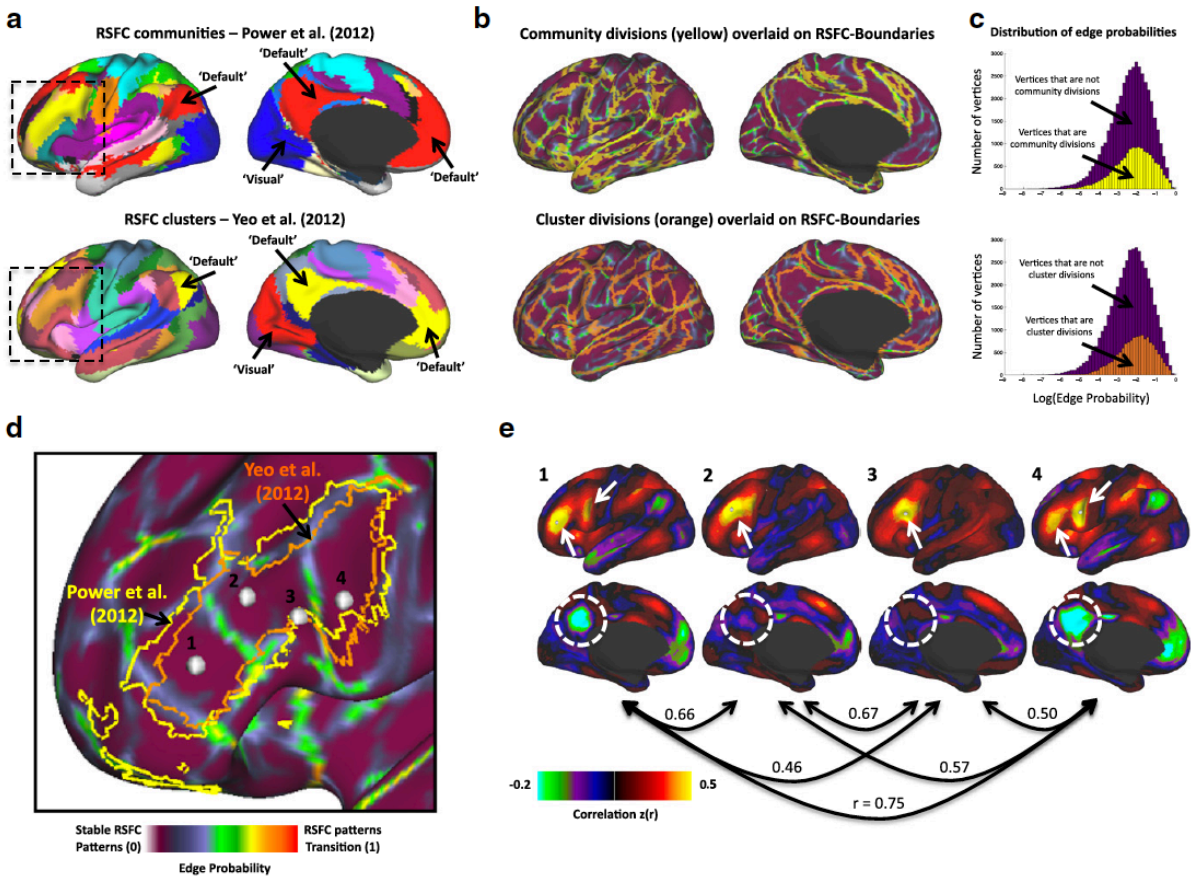

Figure 2-7. RSFC-Boundary Mapping compared to RSFC-defined systems boundaries. (a) Large-scale cortical systems derived from RSFC community detection (Power et al, 2011) and clustering (Yeo et al, 2011). Dotted boxes indicate approximate view in (d). (b) RSFC-based system divisions (community divisions from Power et al., 2011; cluster divisions from Yeo et al., 2011) overlaid on 120-subject RSFC-Boundary map depict the correspondence between the two types of maps. (c) Histograms depicting the distribution of edge probabilities for locations that were identified as system divisions as defined by Power et al. (yellow) and Yeo et al. (orange) and locations that were not identified as system divisions (purple in both). Note that system division edge probabilities are slightly right shifted relative to the edge probabilities of the remaining locations (i.e. tend to have higher edge probabilities), but there remain many locations with high edge probabilities that are not accounted for by system divisions (d) Close-up of lateral frontal cortex showing frontal-parietal system borders overlaid on RSFC-Boundary map. Four white balls indicate local minima in the RSFC-Boundary map. (e) The spatial correlation (Pearson's r) between the four correlation maps generated from the local minima positions indicated in (d). Note that the most anterior (1) and most posterior (4) seeds have very similar correlation maps. The two intermediate seeds (2,3) show similar patterns as seeds 1 and 4, but also differ markedly in certain regions, e.g. along the lateral frontal cortex (arrows) and in posterior cingulate cortex (dotted circle), providing evidence that there are numerous areas within a single system location.

Additional constraints and considerations

While we have attempted to point out potential caveats and sources that require particular further attention, we highlight here additional considerations in the application of RSFC for area parcellation. Specifically, we focus on the relationship between RSFC-defined boundaries and BOLD signal strength and surface geometry, and also make some comments on parcellation of subcortical structures using patterns of RSFC.

Relationship of RSFC-defined borders to BOLD signal strength

It is important to note that observed transitions in the patterns of RSFC may not be neurobiologically relevant. In particular, boundaries that correspond to BOLD signal differences relating to variable BOLD sensitivity across the brain (e.g. due to magnetic field inhomogeneties arising from adjacent structures with different magnetic susceptibilities (Frahm et al., 1988)) are likely of little interest in the context of cortical parcellation. With this in mind, we compared the RSFC-Boundary maps to the BOLD signal strength across the brain. Mean BOLD signal was calculated by averaging the first frame of acquisition (post-steady state magnetization) from all subjects (Ojemann et al., 1997). A small positive correlation (r=0.12) was found between the change in the mean BOLD signal along the cortical surface (measured by the gradient, or spatial derivative, of the mean BOLD signal) and the 120-subject RSFC-Boundary map. BOLD signal strength changes may account for a small amount of variability in the RSFC-Boundary map, but even this may be largely confined to regions known to have significant signal loss. Figure 8a depicts the pattern of BOLD signal dropout in our data. BOLD data was normalized to a mode of 1000 during preprocessing. Accordingly, a

mean BOLD signal of 800 or less (depicted in orange shades) represents a substantial attenuation of signal. Boundaries in the ventral portion of the temporal lobe (red arrow 1) and in orbitofrontal cortex (red arrow 2) are clearly suspect given the large signal loss in these regions. Similarly, the boundaries along the superior temporal gyrus (red arrow 3) and at the occipital pole (red arrow 4) may be explained by the decreased signal in these regions. Leaving out regions with substantial signal loss (i.e. BOLD<800) significantly reduces the correlation between the change in BOLD signal strength and the RSFC-Boundary map (r=0.07). We conclude that for much of the brain changes in BOLD signal strength do not account for the presence of RSFC-defined boundaries. Field map-based distortion correction, which was not carried out here as many subjects in our cohort had not been collected with field maps, may help ameliorate distortion-related effects, but would not be able to repair boundaries related to frank signal loss. Consideration of artifacts such as these are critical to keep in mind when interpreting boundaries and highlight regions of the brain where RSFC-based tools will struggle to generate meaningful parcellation without further processing or acquisition refinements.

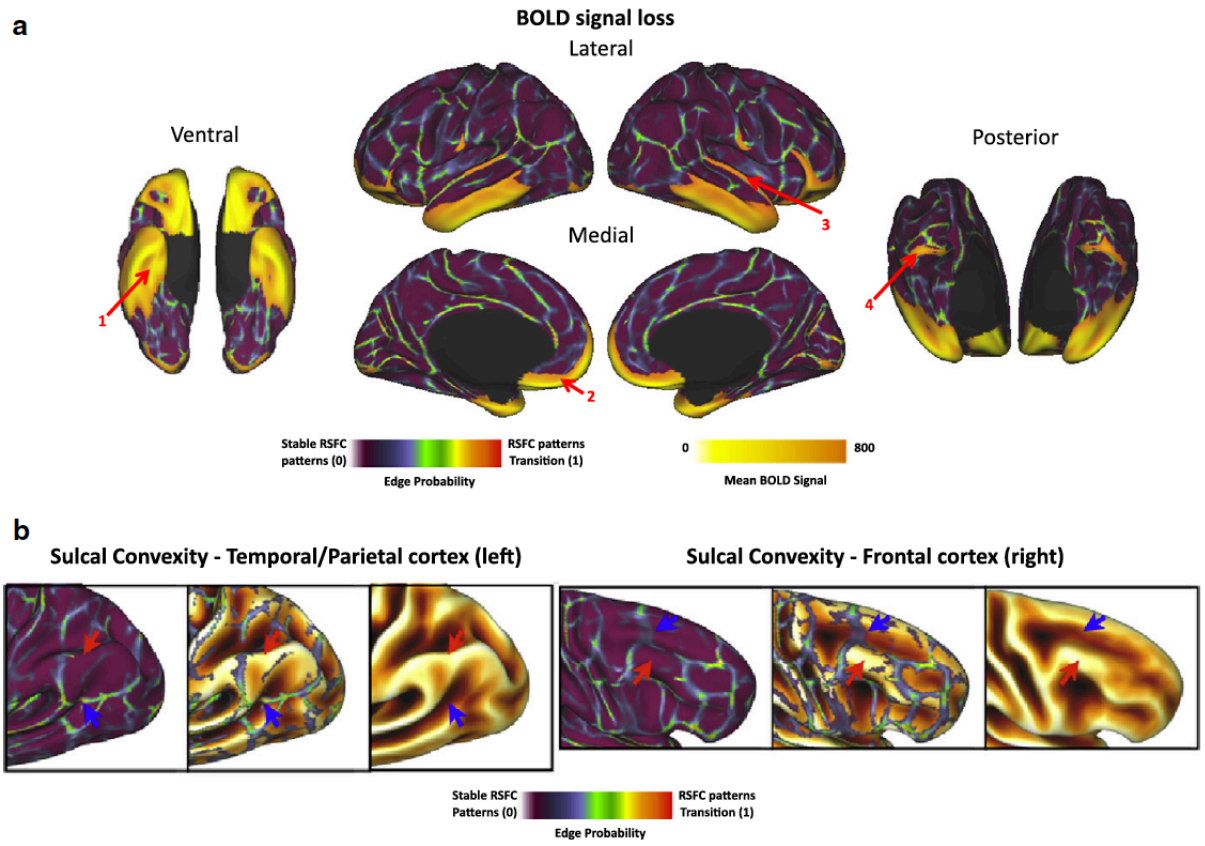

Figure 2-8. RSFC-Boundary Mapping compared to BOLD signal strength and surface geometry. (a) Mean BOLD signal from the first frame of resting state data from 120 subjects overlaid on RSFC-Boundary map. Regions with BOLD signal less than 800 (BOLD signal has been mode 1000 normalized) can be seen in orange-yellow. Signal loss is apparent in ventral temporal (red arrow '1) and orbitofrontal (red arrow '2') regions, superior temporal gyrus (red arrow '3'), and the occipital pole (red arrow '4'). (b) Lateral parietal-occipital (right) and lateral frontal views of RSFC-Boundary map compared to surface geometry. Left panels show full range RSFC-Boundary map, middle panels show RSFC-Boundary map thresholded at 0.15 boundary frequency, and right panels show average surface convexity of Conte-69 atlas (darker and brighter values on this surface represent sulcal and gyral regions respectively). Red arrows indicate gyral crowns where there is an absence of a strong RSFC-defined border and blue arrows indicate regions in which RSFC boundaries cross over sulcal fundi.

Relationship of RSFC-defined borders to surface geometry

Areal borders need not respect morphometric divisions. For example, the primary visual area (V1) spans both sides of the calcarine sulcus, reflecting the upper and lower representations of the visual field in this area (e.g., (Dougherty et al., 2003)). However, a number of strong borders defined by RSFC-Boundary Mapping follow

prominent gyral and sulcal landmarks: strong RSFC borders are present along the central sulcus (from dorsal to ventral) and along the cingulate gyrus (from anterior to posterior). While some of these divisions may be consistent with areal divisions (e.g., the primary motor and somatosensory areas follow the central sulcus along the pre- and post-central gyri, respectively), one concern is that the identification of RSFC-Boundary Mapping borders is biased by surface geometry (for example, as a consequence of the volume-to-surface processing and analysis stream; see methods in Appendix—Methods). Indeed, the RSFC-Boundary map has a small positive correlation with the average convexity of the Conte69 atlas (r=0.11). A number of observations mitigate this concern however. Figure 8b highlights a few examples in the frontal and temporal/parietal cortex where strong RSFC boundaries are not found along gyral crowns (red arrows), as well as examples of regions where strong RSFC boundaries cross over sulcal fundi (blue arrows). While it is conceivable that RSFC borders follow morphometric landmarks in some locations as a consequence of the presence of an areal division, we do not view gyral and sulcal features as the causal source of group-level RSFC borders. We recognize that the previous observations do not completely rule out the possibility that inter-individual variability in surface geometry may be masked when individuals are combined into a group, and that geometric bias may be present when RSFC borders are computed on individual subjects. With respect to the latter point, observations in our laboratory suggests otherwise (e.g., see supplemental figure 3 in (Wig et al., 2013)).

RSFC-based parcellation of subcortical structures

While we have focused our present discussions on parcellation of cortical areas, many of the general points we have made are applicable to subdividing subcortical structures, with some caveats. For example, the gradient-based approach described here is applied primarily for the 2-dimensional parcellation of the cortical sheet; subcortical structures, however, are not arrayed on a sheet, but rather are organized as nuclei having, sometimes complex, 3-dimensional forms. As such, different approaches are necessary for their parcellation. The gradient-based strategy for finding RSFC pattern transitions can naturally be extended into 3-dimensions for this purpose, though we do not present such an approach here. The current form of the RSFC-Snowballing procedure is not limited to the cortical surface and is capable of identifying area centers within subcortical structures, which in fact is highlighted elsewhere (Wig et al., 2013). In addition, clustering approaches have clearly demonstrated the ability to partition subcortical structures according to RSFC correlations (e.g., (Barnes et al., 2010; Zhang et al., 2008)). As with the cortex, much work remains to be done comparing apparent RSFC-based distinctions with other modalities to understand how RSFC information in the subcortical nuclei and the cerebellum converges with and/or diverges from other properties of brain organization and function.

2.3 Concluding comments

Patterns of RSFC exhibit abrupt transitions across the brain and recent advances in BOLD imaging acquisition and analysis have facilitated the development of tools to map the locations of these changes across the cortical surface (RSFC-Boundary Mapping). Throughout this report, we have described some prominent observations where the locations of putative areal divisions as defined by RSFC-Boundary Mapping

converge with features from other parcellation modalities as well as other RSFC analysis methods.

Where possible, we have attempted to highlight observations and issues that necessitate particular attention in order to more fully understand and interpret the parcellation information gleaned from RSFC-based approaches. Of course, as the nature and source of RSFC signals is continually explored, we suspect our understanding of RSFC-based area parcellation will also be modified. For example, deeper understanding of the non-stationary nature of RSFC signals (e.g., (Chang et al., 2010; Smith et al., 2012)) and of the sensitivity of RSFC to various sources of spurious noise (e.g., (Birn et al., 2006; Chang et al., 2009; Power et al., 2012; Satterthwaite et al., 2012; Van Dijk et al., 2012)), as well as improved image acquisition and processing techniques (De Martino et al., 2011; Van Essen et al., 2012b) will likely aid our ability to use RSFC for parcellating cortical and subcortical areas.

The parcellation of brain areas relies on distinctions related to function, architectonics, connectivity and topography. While the earliest parcellation of human cortical areas relied on invasive approaches such as post-mortem dissection (e.g., (Brodmann, 1909; Vogt et al., 1919)) or intra-cranial recording (e.g., (Jasper et al., 1954)), recent advances in brain imaging have enabled continual improvements and refinement in our understanding of the properties and methods for identifying areal divisions ((Toga et al., 2006); the present special issue on In Vivo Brodmann Mapping in Neuroimage). As has been the case with parcellation of non-human cortical areas, it is likely that no single feature will serve to parcellate all cortical and subcortical structures. Accurate and informative parcellation has been accomplished by the careful

consideration of multiple converging features. In additional to distinctions identified by examining patterns of evoked-activity, connectional anatomy, architectonics, and topography, we feel there is sufficient and compelling evidence to suggest that patterns of RSFC provide confirmatory and complementary information for the purposes of parcellating cortical areas and subcortical divisions of the brain. We urge interested readers to explore and utilize our RSFC-based parcellation maps for themselves, we have made these maps available on our laboratory website (http://www.nil.wustl.edu/labs/petersen/Publications.html).

2.4 Appendix – Methods

Subjects

RSFC from a total of 120 healthy young adult subjects was analyzed for parcellation (60 females, mean age = 25 years, age range = 19-32 years). All subjects were native speakers of English and were right-handed. Subjects were recruited from the Washington University community and were screened with a self-report questionnaire to ensure that they had no current or previous history of neurological or psychiatric diagnosis. Informed consent was obtained from all subjects. The study was approved by the Washington University School of Medicine Human Studies Committee and Institutional Review Board

Data acquisition parameters

Structural and RSFC (functional) MRI data were obtained with a Siemens MAGNETOM Trio Tim 3.0T Scanner (Erlangen, Germany) and a Siemens 12 channel Head Matrix Coil. To help stabilize head position, each subject was fitted with a

thermoplastic mask fastened to holders on the headcoil. A T1-weighted sagittal magnetization-prepared rapid acquisition gradient echo (MP-RAGE) structural image was obtained (TE=3.08ms, TR(partition)=2.4s, TI=1000ms, flip angle=8°, 176 slices with 1x1x1mm voxels) (Mugler et al., 1990). An auto align pulse sequence protocol provided in the Siemens software was used to align the acquisition slices of the functional scans parallel to the anterior commissure-posterior commissure (AC-PC) plane and centered on the brain. This plane is parallel to the slices in the Talairach atlas (Talairach et al., 1988).

During RSFC data acquisition, subjects were instructed to relax while fixating on a black crosshair that was presented against a white background. Functional imaging was performed using a blood oxygenation level-dependent (BOLD) contrast sensitive gradient echo echo-planar sequence (TE=27ms, flip angle=90°, in-plane resolution=4x4 mm). Whole brain EPI volumes (MR frames) of 32 contiguous, 4 mm-thick axial slices were obtained every 2.5 seconds. A T2-weighted turbo spin echo structural image (TE=84ms, TR=6.8s, 32 slices with 1x1x4 mm voxels) in the same anatomical planes as the BOLD images was also obtained to improve alignment to an atlas. The number of volumes obtained from subjects ranged from 184 to 729 (mean = 336 frames).

Image preprocessing

Functional images were first processed to reduce artifacts (Miezin et al., 2000). These steps included: (i) correction of odd vs. even slice intensity differences attributable to interleaved acquisition without gaps, (ii) correction for head movement within and across runs and (iii) across-run intensity normalization to a whole brain mode

value of 1000. Atlas transformation of the functional data was computed for each individual using the MP-RAGE scan. Each run was then re-sampled to an isotropic 3-mm atlas space (Talairach et al., 1988), combining movement correction and atlas transformation in a single cubic spline interpolation (Lancaster et al., 1995a; Snyder, 1996). This single interpolation procedure avoids blurring that would be introduced by multiple interpolations. All subsequent operations were performed on the atlas-transformed volumetric time series.

RSFC preprocessing

Several additional preprocessing steps were utilized to reduce spurious variance unlikely to reflect neuronal activity in RSFC data. RSFC preprocessing was performed in two iterations. In the first iteration, RSFC preprocessing included, in the following order: (i) multiple regression of the BOLD data to remove variance related to the whole brain signal (cf. (Scholvinck et al., 2010)), ventricular signal, white matter signal, six detrended head realignment parameters obtained by rigid body head motion correction, and the first-order derivative terms for all aforementioned nuisance variables. (ii) a band-pass filter (0.009 Hz < f < 0.08 Hz), (iii) volumetric spatial smoothing (6 mm full width at half maximum in each direction).[6]

Following the initial RSFC preprocessing iteration, to ameliorate the effect of motion artifact on RSFC correlations, data was processed following the recently described 'scrubbing' procedure (Power et al., 2012). Temporal masks were created to flag motion-contaminated frames so that they could be ignored during subsequent

[6] Volumetric smoothing was only performed as a RSFC preprocessing step for RSFC-Snowballing.

nuisance regression and correlation calculations. Motion contaminated volumes were identified by frame-by-frame displacement (FD, calculated as the sum of absolute values of the differentials of the 3 translational motion parameters and 3 rotational motion parameters) and by frame-by-frame signal change (DVARS). Volumes with FD > 0.3 mm or DVARS > 3% signal change were flagged. In addition, the two frames acquired immediately prior to each of these frames and the two frames acquired immediately after these frames were also flagged to account for temporal spread of artifactual signal resulting from the temporal filtering in the first RSFC preprocessing iteration.

The RSFC preprocessing steps outlined above (steps i – iii; including nuisance regression, temporal filtering, and volumetric smoothing) were applied in the second iteration on RSFC data that excluded volumes flagged during motion scrubbing. The mean percent of frames excluded from the remaining subjects was 26% (range: 1%-26.0%). All subjects had a minimum of 126 frames remaining after RSFC preprocessing (mean = 245 frames).

Surface preprocessing

Following volumetric registration, each subject's MP-RAGE image was processed to generate anatomical surfaces using FreeSurfer's default recon-all processing pipeline (version 5.0). This pipeline included brain extraction, segmentation, generation of white matter and pial surfaces, inflation of the surfaces to a sphere, and surface shape-based spherical registration of the subject's 'native' surface to the fsaverage surface (A. M. Dale et al., 1999; A.M. Dale et al., 1993b; Fischl et al., 1999; F

Ségonne et al., 2004; Florent Ségonne et al., 2005). The fsaverage-registered left and right hemisphere surfaces were brought into register with each other using deformation maps from a landmark-based registration of left and right fsaverage surfaces to a hybrid left-right fsaverage surface ('fs_LR'; (Van Essen et al., 2011)) and resampled to a resolution of 164,000 vertices (164k fs_LR) using Caret tools (Van Essen et al., 2001). Finally, each subject's 164k fs_LR surface was down-sampled to a 32,492 vertex surface (fs_LR 32k), which allowed for analysis in a computationally tractable space while still oversampling the underlying resolution of BOLD data used in subsequent analyses. The various deformations from the 'native' surfaces to the fs_LR 32k surface were composed into a single deformation map allowing for one step resampling. The above procedure results in a surface space that allows for quantitative analysis across subjects as well as between hemispheres. A script for this procedure is available on the Van Essen Lab website (Freesurfer_to_fs_LR Pipeline, http://brainvis.wustl.edu).

RSFC-Boundary Mapping

RSFC-Boundary Mapping identifies transitions in resting state correlations across the cortical surface. Cohen et al.'s (2008) original approach applied 2-D image processing tools to BOLD data sampled from patches on a flattened cortical surface (e.g., (Nelson et al., 2010b)). Flattening the surface induces distortions in the surface representation that could lead to spurious boundary identification. The current implementation of RSFC-Boundary Mapping avoids this issue by performing all computations directly on a closed surface topology. The analysis is now also applied to the entire cortical surface as opposed to small selected patches of cortex. The details of

this procedure have been described for individual subjects elsewhere (Wig et al., 2013). Here we apply the method to groups of individuals.

A flowchart of the RSFC-Boundary Mapping procedure can be seen in Figure 9. The RSFC BOLD time courses7 were first sampled to each subject's individual 'native' midthickness surface (generated as the average of the white and pial surfaces) using the ribbon-constrained sampling procedure available in Connectome Workbench 0.7. This procedure samples data from voxels within the gray matter ribbon (i.e. between the white and pial surfaces) that lay in a cylinder orthogonal to the local midthickness surface weighted by the extent to which the voxel falls within the ribbon—it is designed to minimize partial-volume effects arising from the low sampling resolution of the BOLD data relative to the structural image acquisition (Glasser et al., 2011). Once sampled to the 'native' surface, the time courses were smoothed along the surface using a Gaussian smoothing kernel ($\sigma = 2.55$). The smoothed time courses were deformed and resampled from the individual's 'native' surface to the 32k fs_LR surface in a single step using the deformation map generated as described above.

Each surface vertex's time course was correlated with the time courses from every voxel in a brain mask to generate full volume correlation maps (32492 vertices x 65549 voxels). Each correlation map was transformed using Fisher's r-to-z transformation (Zar, 1996) and averaged across subjects. Full volume correlation maps were used instead of surface correlation maps in order to ensure that sub-cortical correlation relationships contributed to areal parcellation. A RSFC map similarity matrix

[7] No spatial smoothing was performed in the volume during pre-processing for RSFC-Boundary Mapping so as to minimize again partial-volume effects and cross-sulcal data blurring.

was created by calculating the spatial correlation between every vertex's RSFC correlation maps with one another, producing a 32k x 32k matrix. Each row of this matrix corresponds to a map on the cortical surface wherein the values reflect the similarity of a given vertices RSFC map with the RSFC map of every other vertex. To find positions where RSFC similarity exhibited abrupt changes, the similarity maps were first Gaussian smoothed along the surface ($\sigma = 2.55$) and the first spatial derivative was computed using the 'metric-gradient-all' function available in Caret 5.65. This resulted in 32k 'gradient' maps for each hemisphere. These gradient maps represent the essential feature of RSFC transition we aim to identify. As a further refinement relative to whole-brain boundary maps presented in previous work (Wig et al., 2013), in order to sharpen observed borders and facilitate identification of even subtle differences in correlation patterns, we applied a non-maxima suppression procedure to each of the gradient maps, creating 32k 'edge' maps. This technique identifies a vertex as an edge if it is a gradient maxima with respect to at least two pairs of spatially non-adjacent neighboring vertices (each of the 32k vertices has six neighbors, except 12 which have five neighbors). The non-linear nature of this step makes it susceptible to potentially uninteresting noise in the input data; averaging correlation maps from many subjects minimizes this possibility. Finally, the 32k 'edge' maps from each hemisphere were averaged to indicate the frequency with which a given vertex was identified as an edge.

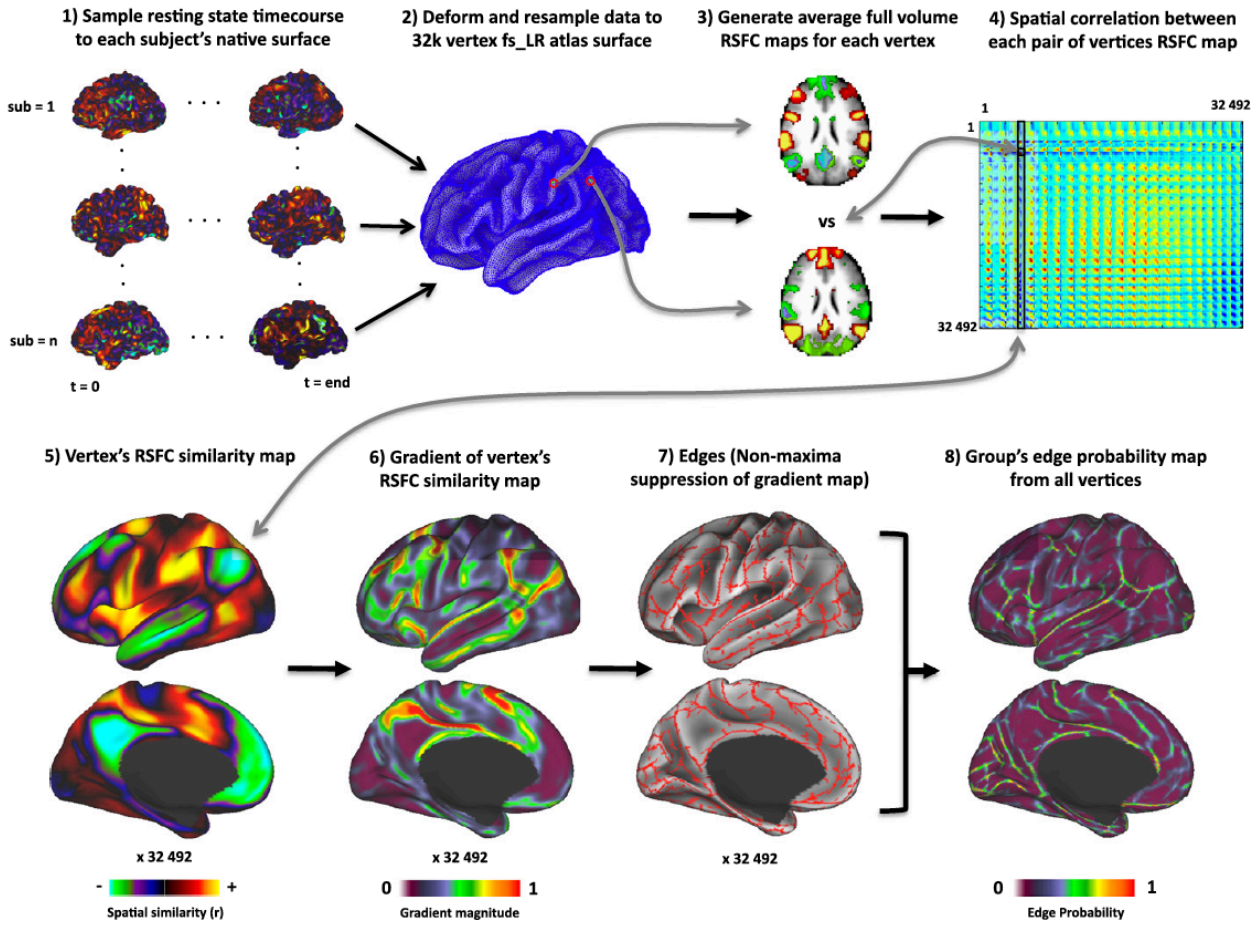

Figure 2-9. RSFC-Boundary Mapping procedure. (1) Resting state time courses are first sampled to each subject's native midthickness surface and smoothed along the surface. (2) The sampled data is then deformed and resampled to the 32k fs_LR surface space (Van Essen, et al 2011). (3) Full volume RSFC maps are calculated for all surface vertices and averaged across all subjects. (4) The spatial correlation between all RSFC maps is calculated generating a 32,492 x 32,492 vertex matrix. (5) Each column of this matrix represents each surface vertex's RSFC similarity map. (6) The spatial gradient of each RSFC similarity map is taken. (7) Edges in the gradient map are then highlighted by non-maxima suppression (where 1 indicates an edge and 0 indicates no edge). (8) Finally, the edge maps from all vertices are averaged together; this generates a final RSFC-Boundary map that indicates how frequently an edge was detected at each vertex (edge probability).

RSFC-Snowball Sampling

RSFC-Snowball sampling (RSFC-Snowballing) identifies locations that exhibit a high density of resting-state correlations to other locations in the brain. Peak density values are lesser at locations that are transition points (or boundaries) between

adjacent areas and greater within an area's interior (or center). Therefore, the voxel-wise distribution of peaks can be used to identify the locations of area centers. A separate report describes RSFC-Snowballing for parcellating cortical and sub-cortical structures in an individual subject (Wig et al., 2013). As with RSFC-Boundary Mapping, we describe here the method for application to groups of individuals.

RSFC-Snowballing is an iterative procedure that uses seed-based RSFC to identify locations correlated with a starting seed location (i.e., the 'neighbors' of the seed, in a graph theoretic sense), and then identifies the neighbors of the neighbors, and so forth over multiple iterations (zones). RSFC-Snowballing is initialized from multiple starting seed locations (i.e., from a pre-defined set of coordinates) creating a peak density map for each starting location. The peak density maps derived from each starting location are combined to arrive at an aggregate peak density map (Figure 10). In the present analysis, the starting location set was defined from a meta-analysis of task-evoked data, which identified 151 task-defined centers across cortical and sub-cortical structures (for details see (Wig et al., 2013)). Aggregating the peak density maps from multiple starting locations minimizes the potential bias of a single starting seed location and provides estimates of area centers across broad expanses of the brain's cortical and subcortical structures.

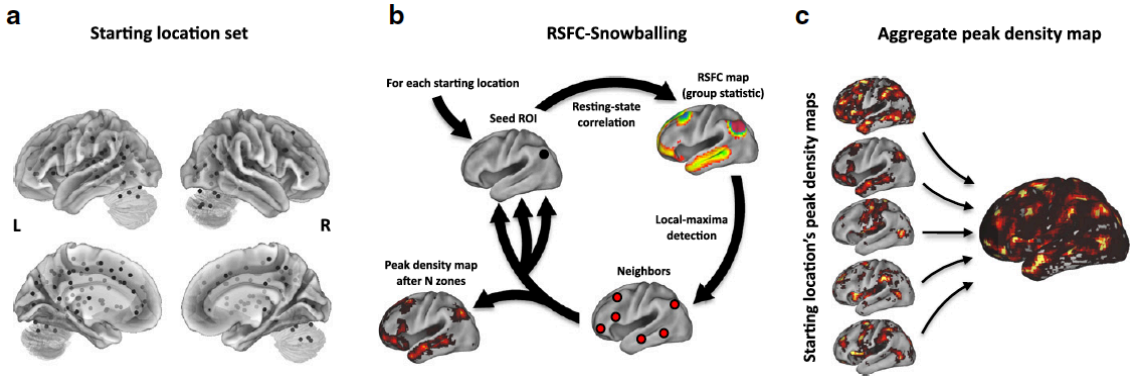

Figure 2-10. Overview of RSFC-Snowballing using multiple starting seed locations. (a) Initialization location set consisting of cortical and sub-cortical seed locations (n=151) defined by meta-analysis of task-evoked data. (b) For each seed location in the initialization location set, RSFC-Snowballing iteratively identifies the neighbors (peaks of RSFC correlation) of seed ROIs over multiple zones and adds these neighbors to a peak density map. (c) The independently derived peak density maps from each of the seed locations of the initialization location set are summed to arrive at an aggregate peak density map presumed to reflect the likelihood with which a given location is an area center.

A neighbor of a given seed need not be physically adjacent to the seed, but rather is defined by the presence of a RSFC relationship above a given correlation threshold. Neighbor identification was conducted by calculating seed-based statistical correlation maps across the group of individuals. For each participant, the average time course was extracted from the seed region of interest (ROI) and Pearson's correlation coefficient was computed between this ROI's time course and the time course for each voxel across the whole brain volume. The resulting correlation map was converted to z values using Fisher's r-to-z transformation (Zar 1996). The individual z(r) images were next submitted to a random-effects analysis, treating participant as the random factor, to create a statistical map using a t-test. To identify the seed ROI's 'neighbors' (i.e. the regions that were correlated with the seed ROI), the statistical t-maps were first smoothed (6 mm FWHM) and the local maxima (peaks) of contiguous clusters of voxels that both surpassed a correlation threshold ($p < 0.001$, uncorrected) and had a minimum distance of 10mm between peaks were identified.

Each starting location was submitted to RSFC-Snowballing over 3 zones. The final aggregate peak density map was spatially smoothed (volumetric smoothing of 6 mm FWHM) and then normalized relative to its maximal value to facilitate viewing.

2.5 Acknowledgements

We thank Alex Cohen, Steven Nelson, Jonathan Power, and Brad Schlaggar for thoughtful discussions and feedback throughout much of this work. We also thank Malcolm Tobias, Avi Snyder, Matt Glasser, and Babatunde Adeyemo for technical support and assistance. This work was supported by a McDonnell Foundation Collaborative Action Award, NIH 32979, NIH 46424, NIH 61144 and the Human Connectome Project (1U54MH091657) from the 16 NIH Institutes and Centers that support the NIH Blueprint for Neuroscience Research.

2.6 References

Amunts, K., Malikovic, A., Mohlberg, H., Schormann, T., & Zilles, K. (2000). Brodmann's areas 17 and 18 brought into stereotaxic space-where and how variable? Neuroimage, 11(1), 66-84.

Amunts, K., Weiss, P. H., Mohlberg, H., Pieperhoff, P., Eickhoff, S., Gurd, J. M., Marshall, J. C., Shah, N. J., Fink, G. R., & Zilles, K. (2004). Analysis of neural mechanisms underlying verbal fluency in cytoarchitectonically defined stereotaxic space--the roles of Brodmann areas 44 and 45. Neuroimage, 22(1), 42-56.

Barnes, K. A., Cohen, A. L., Power, J. D., Nelson, S. M., Dosenbach, Y. B., Miezin, F. M., Petersen, S. E., & Schlaggar, B. L. (2010). Identifying Basal Ganglia divisions in individuals using resting-state functional connectivity MRI. Front Syst Neurosci, 4, 18.

Barnes, K. A., Nelson, S. M., Cohen, A. L., Power, J. D., Coalson, R. S., Miezin, F. M., Vogel, A. C., Dubis, J. W., Church, J. A., Petersen, S. E., et al. (2011). Parcellation in left lateral parietal cortex is similar in adults and children. Cereb Cortex, CerCor-2011-00246.R1.

Birn, R. M., Diamond, J. B., Smith, M. A., & Bandettini, P. A. (2006). Separating respiratory-variation-related fluctuations from neuronal-activity-related fluctuations in fMRI. Neuroimage, 31(4), 1536-1548.

Biswal, B., Yetkin, F. Z., Haughton, V. M., & Hyde, J. S. (1995). Functional connectivity in the motor cortex of resting human brain using echo-planar MRI. Magn Reson Med, 34(4), 537-541.

Biswal, B. B., Mennes, M., Zuo, X. N., Gohel, S., Kelly, C., Smith, S. M., Beckmann, C. F., Adelstein, J. S., Buckner, R. L., Colcombe, S., et al. (2010). Toward discovery science of human brain function. Proc Nat Acad Sci USA, 107(10), 4734-4739.

Brodmann, K. (1909). *Vergleichende lokalisationslehre der grosshirnrinde in ihren prinzipien dargestellt auf grund des zellenbaues*. Leipzig: J. A. Barth.

Carmichael, S. T., & Price, J. L. (1994). Architectonic subdivision of the orbital and medial prefrontal cortex in the macaque monkey. J Comp Neurol, 346(3), 366-402.

Carmichael, S. T., & Price, J. L. (1996). Connectional networks within the orbital and medial prefrontal cortex of macaque monkeys. J Comp Neurol, 371(2), 179-207.

Caspers, S., Geyer, S., Schleicher, A., Mohlberg, H., Amunts, K., & Zilles, K. (2006). The human inferior parietal cortex: cytoarchitectonic parcellation and interindividual variability. Neuroimage, 33(2), 430-448.

Chang, C., Cunningham, J. P., & Glover, G. H. (2009). Influence of heart rate on the BOLD signal: the cardiac response function. Neuroimage, 44(3), 857-869.

Chang, C., & Glover, G. H. (2010). Time-frequency dynamics of resting-state brain connectivity measured with fMRI. Neuroimage, 50(1), 81-98.

Cohen, A. L., Fair, D. A., Dosenbach, N. U., Miezin, F. M., Dierker, D., Van Essen, D. C., Schlaggar, B. L., & Petersen, S. E. (2008b). Defining functional areas in individual human brains using resting functional connectivity MRI. Neuroimage, 41, 45-57.

Dale, A. M., Fischl, B., & Sereno, M. I. (1999). Cortical surface-based analysis. I. Segmentation and surface reconstruction. Neuroimage, 9(2), 179-194.

Dale, A. M., & Sereno, M. I. (1993b). Improved localization of cortical activity by combining EEG and MEG with cortical surface reconstruction: A linear approach. Journal of Cognitive Neuroscience, 5, 162-176.

De Martino, F., Esposito, F., van de Moortele, P. F., Harel, N., Formisano, E., Goebel, R., Ugurbil, K., & Yacoub, E. (2011). Whole brain high-resolution functional imaging at ultra high magnetic fields: an application to the analysis of resting state networks. Neuroimage, 57(3), 1031-1044.

Deco, G., Jirsa, V. K., & McIntosh, A. R. (2011). Emerging concepts for the dynamical organization of resting-state activity in the brain. Nature Reviews. Neuroscience, 12(1), 43-56.

Deen, B., Pitskel, N. B., & Pelphrey, K. A. (2011). Three systems of insular functional connectivity identified with cluster analysis. Cereb Cortex, 21(7), 1498-1506.

Dick, F., Tierney, A. T., Lutti, A., Josephs, O., Sereno, M. I., & Weiskopf, N. (2012). In vivo functional and myeloarchitectonic mapping of human primary auditory areas. J Neurosci, 32(46), 16095-16105.

Doucet, G., Naveau, M., Petit, L., Delcroix, N., Zago, L., Crivello, F., Jobard, G., Tzourio-Mazoyer, N., Mazoyer, B., Mellet, E., et al. (2011). Brain activity at rest: a multiscale hierarchical functional organization. J Neurophysiol, 105(6), 2753-2763.

Dougherty, R. F., Koch, V. M., Brewer, A. A., Fischer, B., Modersitzki, J., & Wandell, B. A. (2003). Visual field representations and locations of visual areas V1/2/3 in human visual cortex. J Vis, 3(10), 586-598.

Fedorenko, E., Hsieh, P. J., Nieto-Castanon, A., Whitfield-Gabrieli, S., & Kanwisher, N. (2010). New method for fMRI investigations of language: defining ROIs functionally in individual subjects. J Neurophysiol, 104(2), 1177-1194.

Felleman, D. J., & Van Essen, D. C. (1991b). Distributed hierarchical processing in the primate cerebral cortex. Cerebral Cortex, 1(1), 1-47.

Fischl, B., Rajendran, N., Busa, E., Augustinack, J., Hinds, O., Yeo, B. T., Mohlberg, H., Amunts, K., & Zilles, K. (2008). Cortical folding patterns and predicting cytoarchitecture. Cereb Cortex, 18(8), 1973-1980.

Fischl, B., Sereno, M. I., & Dale, A. M. (1999). Cortical surface-based analysis. II: Inflation, flattening, and a surface-based coordinate system. Neuroimage, 9(2), 195-207.

Foerster, O. (1936). The motor cortex of man in light of Hughlings Jackson's doctrines. Brain, 58, 135-159.

Fox, M. D., & Raichle, M. E. (2007a). Spontaneous fluctuations in brain activity observed with functional magnetic resonance imaging. Nat Rev Neurosci, 8(9), 700-711.

Frahm, J., Merboldt, K. D., & Hanicke, W. (1988). Direct FLASH MR imaging of magnetic field inhomogeneities by gradient compensation. Magn Reson Med, 6(4), 474-480.

Gennari, F. (1782). Francisci Gennari Parmensis Medicinae Doctoris Collegiati de Peculiari Structura Cerebri Nonnullisque Eius Morbis-Paucae Aliae Anatom. Observat. Accedunt. Parma, Italy: Regio Typographeo.

Glasser, M. F., & Van Essen, D. C. (2011). Mapping human cortical areas in vivo based on myelin content as revealed by T1- and T2-weighted MRI. J Neurosci, 31(32), 11597-11616.

Goodman, L. (1961). Snowball sampling. Annals of Mathematical Statistics, 32(1), 148-170.

Goulas, A., Uylings, H. B., & Stiers, P. (2012). Unravelling the intrinsic functional organization of the human lateral frontal cortex: a parcellation scheme based on resting state fMRI. J Neurosci, 32(30), 10238-10252.

Hinds, O., Polimeni, J. R., Rajendran, N., Balasubramanian, M., Amunts, K., Zilles, K., Schwartz, E. L., Fischl, B., & Triantafyllou, C. (2009). Locating the functional and anatomical boundaries of human primary visual cortex. Neuroimage, 46(4), 915-922.

Hirose, S., Watanabe, T., Jimura, K., Katsura, M., Kunimatsu, A., Abe, O., Ohtomo, K., Miyashita, Y., & Konishi, S. (2012). Local signal time-series during rest used for areal boundary mapping in individual human brains. PLoS ONE, 7(5), e36496.

Honey, C. J., Sporns, O., Cammoun, L., Gigandet, X., Thiran, J. P., Meuli, R., & Hagmann, P. (2009a). Predicting human resting-state functional connectivity from structural connectivity. Proc Natl Acad Sci USA, 106(6), 2035-2040.

Hubel, D. H., & Wiesel, T. N. (1962). Receptive fields, binocular interaction and functional architecture in the cat's visual cortex. J Physiol, 160, 106-154.

Jasper, H., & Penfield, W. (1954). *Epilepsy and the Functional Anatomy of the Human Brain* (2nd ed.).

Johansen-Berg, H., Behrens, T. E., Sillery, E., Ciccarelli, O., Thompson, A. J., Smith, S. M., & Matthews, P. M. (2005). Functional-anatomical validation and individual variation of diffusion tractography-based segmentation of the human thalamus. Cereb Cortex, 15(1), 31-39.

Kaas, J. H., Nelson, R. J., Sur, M., Lin, C. S., & Merzenich, M. M. (1979). Multiple representations of the body within the primary somatosensory cortex of primates. Science, 204(4392), 521-523.

Kahnt, T., Chang, L. J., Park, S. Q., Heinzle, J., & Haynes, J. D. (2012). Connectivity-based parcellation of the human orbitofrontal cortex. J Neurosci, 32(18), 6240-6250.

Kelly, C., Uddin, L. Q., Shehzad, Z., Margulies, D. S., Castellanos, F. X., Milham, M. P., & Petrides, M. (2010). Broca's region: linking human brain functional connectivity data and non-human primate tracing anatomy studies. Eur J Neurosci, 32(3), 383-398.

Kim, D. J., Park, B., & Park, H. J. (2012). Functional connectivity-based identification of subdivisions of the basal ganglia and thalamus using multilevel independent component analysis of resting state fMRI. Hum Brain Mapp.

Kim, J. H., Lee, J. M., Jo, H. J., Kim, S. H., Lee, J. H., Kim, S. T., Seo, S. W., Cox, R. W., Na, D. L., Kim, S. I., et al. (2010). Defining functional SMA and pre-SMA subregions in human MFC using resting state fMRI: functional connectivity-based parcellation method. Neuroimage, 49(3), 2375-2386.

Lancaster, J. L., Glass, T. G., Lankipalli, B. R., Downs, H., Mayberg, H., & Fox, P. T. (1995a). A Modality-Independent Approach to Spatial Normalization of Tomographic Images of the Human Brain. Hum Brain Mapp, 3, 209-223.

Leech, R., Braga, R., & Sharp, D. J. (2012). Echoes of the brain within the posterior cingulate cortex. J Neurosci, 32(1), 215-222.

Margulies, D. S., Vincent, J. L., Kelly, C., Lohmann, G., Uddin, L. Q., Biswal, B. B., Villringer, A., Castellanos, F. X., Milham, M. P., & Petrides, M. (2009). Precuneus shares intrinsic functional architecture in humans and monkeys. Proc Natl Acad Sci U S A, 106(47), 20069-20074.

Mars, R. B., Sallet, J., Schuffelgen, U., Jbabdi, S., Toni, I., & Rushworth, M. F. (2012). Connectivity-based subdivisions of the human right "temporoparietal junction area": evidence for different areas participating in different cortical networks. Cereb Cortex, 22(8), 1894-1903.

Marshall, W. H., Woolsey, C. N., & Bard, P. (1937). Cortical Representation of Tactile Sensibility as Indicated by Cortical Potentials. Science, 85(2207), 388-390.

Miezin, F. M., Maccotta, L., Ollinger, J. M., Petersen, S. E., & Buckner, R. L. (2000). Characterizing the hemodynamic response: Effects of presentation rate, sampling procedure, and the possibility of ordering brain activity based on relative timing. Neuroimage, 11, 735-759.

Mugler, J. P., 3rd, & Brookeman, J. R. (1990). Three-dimensional magnetization-prepared rapid gradient-echo imaging (3D MP RAGE). Magn Reson Med, 15(1), 152-157.

Mumford, J. A., Horvath, S., Oldham, M. C., Langfelder, P., Geschwind, D. H., & Poldrack, R. A. (2010). Detecting network modules in fMRI time series: a weighted network analysis approach. Neuroimage, 52(4), 1465-1476.

Nelson, S. M., Cohen, A. L., Power, J. D., Wig, G. S., Miezin, F. M., Wheeler, M. E., Velanova, K., Donaldson, D. I., Phillips, J. S., Schlaggar, B. L., et al. (2010b). A parcellation scheme for human left lateral parietal cortex. Neuron, 67(1), 156-170.

Nelson, S. M., Dosenbach, N. U., Cohen, A. L., Wheeler, M. E., Schlaggar, B. L., & Petersen, S. E. (2010c). Role of the anterior insula in task-level control and focal attention. Brain Struct Funct, 214(5-6), 669-680.

Ojemann, J. G., Akbudak, E., Snyder, A. Z., McKinstry, R. C., Raichle, M. E., & Conturo, T. E. (1997). Anatomic localization and quantitative analysis of gradient refocused echo-planar fMRI susceptibility artifacts. Neuroimage, 6(3), 156-167.

Ongur, D., Ferry, A. T., & Price, J. L. (2003). Architectonic subdivision of the human orbital and medial prefrontal cortex. J Comp Neurol, 460(3), 425-449.

Petersen, S. E., Fox, P. T., Posner, M. I., Mintun, M., & Raichle, M. E. (1988). Positron emission tomographic studies of the cortical anatomy of single-word processing. Nature, 331(6157), 585-589.

Power, J. D., Barnes, K. A., Snyder, A. Z., Schlaggar, B. L., & Petersen, S. E. (2012). Spurious but systematic correlations in functional connectivity MRI networks arise from subject motion. Neuroimage, 59(3), 2142-2154.

Power, J. D., Cohen, A. L., Nelson, S. M., Wig, G. S., Barnes, K. A., Church, J. A., Vogel, A. C., Laumann, T. O., Miezin, F. M., Schlaggar, B. L., et al. (2011). Functional network organization of the human brain. Neuron, 72(4), 665-678.

Ryali, S., Chen, T., Supekar, K., & Menon, V. (2013). A parcellation scheme based on von Mises-Fisher distributions and Markov random fields for segmenting brain regions using resting-state fMRI. Neuroimage, 65, 83-96.

Sabuncu, M. R., Singer, B. D., Conroy, B., Bryan, R. E., Ramadge, P. J., & Haxby, J. V. (2010). Function-based intersubject alignment of human cortical anatomy. Cereb Cortex, 20(1), 130-140.

Satterthwaite, T. D., Wolf, D. H., Loughead, J., Ruparel, K., Elliott, M. A., Hakonarson, H., Gur, R. C., & Gur, R. E. (2012). Impact of in-scanner head motion on multiple measures of functional connectivity: relevance for studies of neurodevelopment in youth. Neuroimage, 60(1), 623-632.

Schleicher, A., & Zilles, K. (1990). A quantitative approach to cytoarchitectonics: analysis of structural inhomogeneities in nervous tissue using an image analyser. J Microsc, 157(Pt 3), 367-381.

Scholvinck, M. L., Maier, A., Ye, F. Q., Duyn, J. H., & Leopold, D. A. (2010). Neural basis of global resting-state fMRI activity. Proc Natl Acad Sci U S A, 107(22), 10238-10243.

Schormann, T., & Zilles, K. (1998). Three-dimensional linear and nonlinear transformations: an integration of light microscopical and MRI data. Hum Brain Mapp, 6(5-6), 339-347.

Ségonne, F., Dale, A. M., Busa, E., Glessner, M., Salat, D., Hahn, H. K., & Fischl, B. (2004). A hybrid approach to the skull stripping problem in MRI. Neuroimage, 22(3), 1060-1075.

Ségonne, F., Grimson, E., & Fischl, B. (2005). A genetic algorithm for the topology correction of cortical surfaces. Inf Process Med Imaging, 19, 393-405.

Sejnowski, T. J., & Churchland, P. S. (1989). Brain and Cognition. In M. Posner (Ed.), *Foundations of Cognitive Science* (pp. 888). Cambridge: MIT Press.

Sereno, M. I., Dale, A. M., Reppas, J. B., Kwong, K. K., Belliveau, J. W., Brady, T. J., Rosen, B. R., & Tootell, R. B. (1995). Borders of multiple visual areas in humans revealed by functional magnetic resonance imaging. Science, 268(5212), 889-893.

Smith, S. M., Fox, P. T., Miller, K. L., Glahn, D. C., Fox, P. M., Mackay, C. E., Filippini, N., Watkins, K. E., Toro, R., Laird, A. R., et al. (2009). Correspondence of the brain's functional architecture during activation and rest. Proc Natl Acad Sci U S A, 106(31), 13040-13045.

Smith, S. M., Miller, K. L., Moeller, S., Xu, J., Auerbach, E. J., Woolrich, M. W., Beckmann, C. F., Jenkinson, M., Andersson, J., Glasser, M. F., et al. (2012). Temporally-independent functional modes of spontaneous brain activity. Proc Natl Acad Sci U S A, 109(8), 3131-3136.

Snyder, A. Z. (1996). Difference image vs. ratio image error function forms in PET-PET realignment. In R. Myer, V. J. Cunningham, D. L. Bailey, & T. Jones (Eds.), *Quantification of Brain Function Using PET* (pp. 131-137). San Diego, CA: Academic Press.

Talairach, J., & Tournoux, P. (1988). *Co-Planar Stereotaxic Atlas of the Human Brain* (M. Rayport, Trans.). New York: Thieme Medical Publishers, Inc.

Toga, A. W., Thompson, P. M., Mori, S., Amunts, K., & Zilles, K. (2006). Towards multimodal atlases of the human brain. Nat Rev Neurosci, 7(12), 952-966.

Uddin, L. Q., Supekar, K., Amin, H., Rykhlevskaia, E., Nguyen, D. A., Greicius, M. D., & Menon, V. (2010). Dissociable connectivity within human angular gyrus and intraparietal sulcus: evidence from functional and structural connectivity. Cereb Cortex, 20(11), 2636-2646.

Van Dijk, K. R., Sabuncu, M. R., & Buckner, R. L. (2012). The influence of head motion on intrinsic functional connectivity MRI. Neuroimage, 59(1), 431-438.

Van Essen, D. C. (2005). A Population-Average, Landmark- and Surface-based (PALS) atlas of human cerebral cortex. Neuroimage, 28(3), 635-662.

Van Essen, D. C., Drury, H. A., Dickson, J., Harwell, J., Hanlon, D., & Anderson, C. H. (2001). An integrated software suite for surface-based analyses of cerebral cortex. J Am Med Inform Assoc, 8(5), 443-459.

Van Essen, D. C., Glasser, M. F., Dierker, D. L., Harwell, J., & Coalson, T. (2011). Parcellations and Hemispheric Asymmetries of Human Cerebral Cortex Analyzed on Surface-Based Atlases. Cereb Cortex.

Van Essen, D. C., Maunsell, J. H., & Bixby, J. L. (1981). The middle temporal visual area in the macaque: myeloarchitecture, connections, functional properties and topographic organization. J Comp Neurol, 199(3), 293-326.

Van Essen, D. C., Ugurbil, K., Auerbach, E., Barch, D., Behrens, T. E., Bucholz, R., Chang, A., Chen, L., Corbetta, M., Curtiss, S. W., et al. (2012b). The Human Connectome Project: a data acquisition perspective. Neuroimage, 62(4), 2222-2231.

Vincent, J. L., Patel, G. H., Fox, M. D., Snyder, A. Z., Baker, J. T., Van Essen, D. C., Zempel, J. M., Snyder, L. H., Corbetta, M., & Raichle, M. E. (2007b). Intrinsic functional architecture in the anesthetized monkey brain. Nature, 447(7140), 46-47.

Vogt, O., & Vogt, C. (1919). Allgemeine Ergebnisse unserer Hirnforschung. Journal für Psychologie und Neurologie, 25, 273-462.

Wasserman, S., & Faust, K. (1994). *Social network analysis: Methods and applications*. Cambridge: Cambridge University Press.

Wig, G. S., Laumann, T. O., Cohen, A. L., Power, J. D., Nelson, S. M., Glasser, M. F., Miezin, F. M., Snyder, A. Z., Schlaggar, B. L., & Petersen, S. E. (2013). Parcellating an Individual Subject's Cortical and Subcortical Brain Structures Using Snowball Sampling of Resting-State Correlations. Cereb Cortex.

Wig, G. S., Schlaggar, B. L., & Petersen, S. E. (2011a). Concepts and principles in the analysis of brain networks. Annals of the New York Academy of Sciences, 1224(1), 126-146.

Yeo, B. T., Krienen, F. M., Sepulcre, J., Sabuncu, M. R., Lashkari, D., Hollinshead, M., Roffman, J. L., Smoller, J. W., Zollei, L., Polimeni, J. R., et al. (2011). The organization of the human cerebral cortex estimated by intrinsic functional connectivity. J Neurophysiol, 106(3), 1125-1165.

Zar, J. (1996). *Biostatistical Analysis*. Upper Saddle River, NJ: Prentice Hall.

Zhang, D., Snyder, A. Z., Fox, M. D., Sansbury, M. W., Shimony, J. S., & Raichle, M. E. (2008). Intrinsic functional relations between human cerebral cortex and thalamus. J Neurophysiol, 100(4), 1740-1748.

Chapter 3: Generation and evaluation of cortical areal parcellation from resting-state correlations

This chapter has been published as a journal article. The citation is:

Gordon, E.M.*, Laumann, T.O.*, Adeyemo, B., Huckins, J.F., Kelley, W.M., and Petersen, S.E. (2014). Generation and Evaluation of a Cortical Area Parcellation from Resting-State Correlations. *Cereb. Cortex*. Published online October 14, 2014. http://dx.doi.org/10.1093/cercor/bhu239.

*These authors contributed equally to this work

Evan Gordon, Steve Petersen, and I conceived the project and research approach. Evan Gordon and I designed the analyses with feedback from Babatunde Adeyemo and Steve Petersen. Evan Gordon, Babatunde Adeyemo and I processed the data. Jeremy Huckins and William Kelley provided and processed additional datasets. Evan Gordon and I wrote the paper. Babatunde Adeyemo and Steve Petersen edited the paper.

3.1 Abstract

The cortical surface is organized into a large number of cortical areas; however, these areas have not been comprehensively mapped in the human. Abrupt transitions in resting state functional connectivity (RSFC) patterns can noninvasively identify locations of putative borders between cortical areas (RSFC boundary mapping; Cohen et al., 2008). Here we describe a technique for using RSFC boundary maps to define parcels that represent putative cortical areas. These parcels had highly homogenous RSFC patterns, indicating that they contained one unique RSFC signal; further, the parcels were much more homogenous than a null model matched for parcel size when tested in two separate datasets. Several alternative parcellation schemes were tested this way, and no other parcellation was as homogenous or had as large a difference compared to its null model. The boundary map-derived parcellation contained parcels that overlapped with architectonic mapping of areas 17, 2, 3, and 4. These parcels had a network structure similar to the known network structure of the brain, and their connectivity patterns were reliable across individual subjects. These observations suggest that RSFC boundary map-derived parcels provide information about the location and extent of human cortical areas. A parcellation generated using this method is available at

http://www.nil.wustl.edu/labs/petersen/Resources.html

3.2 Introduction

The cortical surface of the brain is organized into a large number of interacting cortical areas (Sejnowski and Churchland 1989). Accurate identification of these cortical

areas is a major goal of modern systems neuroscience, as it would provide substantial benefits to many areas of neuroscientific investigation. For example, identification and functional characterization of visual areas in the macaque has provided a detailed hierarchical wiring diagram of the primate visual system, which has greatly aided our understanding of visual processing (Felleman and Van Essen 1991). Identifying human cortical areas would be a critical first step towards the same sort of comprehensive characterization of information flow within the brain's various processing systems. Second, identification of cortical areas would greatly improve investigations of brain function using graph theory (Bullmore and Sporns 2009), because such areas could serve as rationally defined, neurobiologically-based network "nodes" (Wig et al. 2011; Power et al. 2013). Third, identified areas can serve as a priori regions of interest for analysis of functional neuroimaging data. Averaging data within pre-defined areas would improve signal-to-noise and reduce multiple comparisons problems in statistical testing.

Identification of distinct cortical areas is based on observing dissociations in one or more critical underlying brain properties, including functional responses, topography, architectonics, and connectivity (Felleman and Van Essen 1991; Carmichael and Price 1994, 1996). In the macaque, decades of research using these modalities have provided a reasonable first-order approximation of a complete cortical areal parcellation (Lewis and Van Essen 2000; Paxinos et al. 2000; Saleem et al. 2007; Van Essen et al. 2012; Markov et al. 2014). While a limited number of similar areal dissociations have been identified in humans (e.g., Brodmann 1909; Öngür et al. 2003; Schleicher et al. 2005), the measurement of these brain properties often relies either on invasive neural recordings or on post-mortem examinations of brain tissue, both of which are difficult to

obtain for large expanses of cortex in humans. As such, definitions of cortical areas in humans have lagged behind those in other primates.

Advances in functional neuroimaging techniques offer the potential for noninvasive in-vivo recording of brain activity. In principle, cortical areas may be dissociated by their differential responses to specific task conditions (Petersen et al. 1988). However, application of this approach to the cortex broadly has been challenging, as most tasks recruit large networks of coactivated areas. This lack of specificity makes it difficult to identify fine dissociations between adjacent and functionally related areas using a necessarily limited task set.

Recently, an fMRI technique called resting state functional connectivity (RSFC) has emerged that may provide one modality for noninvasive parcellation of human cortex. RSFC relies on the observation that in the absence of any task, spatially distant regions of cortex exhibit highly correlated patterns of BOLD activity (Biswal et al. 1995) that are both spatially structured (Beckmann et al. 2005; Power et al. 2011; Yeo et al. 2011) and relatively reliable across individuals (Damoiseaux et al. 2006; Shehzad et al. 2009). While the precise significance of RSFC is uncertain, accumulating evidence suggests that regions exhibiting RSFC correlations are also functionally coactive during tasks (Fox and Raichle 2007; Smith et al. 2009; Biswal et al. 2010). In this view, these correlations observed during the resting state at least partly reflect the statistical history of regional coactivation (Dosenbach et al. 2007). RSFC correlations also appear to be at least partly constrained by structural connections, though regions with no direct structural connections can also be functionally connected, likely via indirect pathways (Vincent et al. 2007; Honey et al. 2009). Taken together, this evidence suggests that

RSFC measurements reflect some combination of both a region's function, in a manner not limited to any one task, and its direct and indirect connectivity.

RSFC data may be used to perform areal parcellation via a recently proposed approach known as boundary mapping (Cohen et al. 2008; Wig et al., 2014b). The boundary mapping approach relies on the observation that RSFC patterns can abruptly change from one cortical location to a proximate location, mirroring the abrupt changes in function or connections that form the basis of cortical area discrimination in nonhuman primates (Felleman and Van Essen 1991); these locations of abrupt change may thus represent boundaries between cortical areas. The boundary mapping technique has previously been used to identify transition zones in limited sections of cortex, including left lateral parietal cortex (Nelson, et al. 2010a; Barnes et al. 2012) and parts of frontal cortex (Cohen et al. 2008; Nelson, et al. 2010b; Hirose et al. 2012, 2013), as well as in the whole brain (Wig et al. 2014a, 2014b). Boundaries identified in this way have been shown to: 1) separate regions with functionally discrete task activation timecourses (Nelson, et al. 2010a); 2) match functional activation patterns; 3) correspond well with systems-level divisions, but also further subdivide those systems; and 4) match architectonically-defined areal borders between V1 and V2 (Wig et al., 2014b). In sum, boundaries identified using this technique are reasonable candidates for borders between cortical areas. However, no previous work has either used these boundaries to identify cortical areas, or evaluated the resulting cortical areas. Here we present a method for identifying and evaluating putative cortical areas from group average RSFC boundary maps.

A parcellation that accurately represents cortical areas of the brain should have, among others, several properties. First, each parcel should generally be homogenous, in that it should have a similar functional connectivity pattern at all points within the parcel (Craddock et al. 2012; Shen et al. 2013). Second, a parcellation that accurately represents cortical areas should contain parcels that overlap known human cortical areas that have been well-described with cytoarchitectonics (e.g., Fischl et al. 2008). Third, a parcellation that accurately represents cortical areas should have a large-scale network structure that is consistent with the known network structure of the brain (Wig et al. 2011; Power et al. 2011; Yeo et al. 2011). Finally, parcels that accurately represent cortical areas in group average data should serve as reasonable a priori regions of interest in individual subjects. While the known inter-individual variability in areal extent (e.g., Amunts et al. 2000) means that cortical area locations in individual subjects are unlikely to precisely match parcels identified from group average data, these group average parcels should still represent the central tendency of the group. Thus, for any given parcel, the functional connectivity patterns across subjects should reflect that level of reliability.

We note that some of these criteria—particularly parcel homogeneity and overlap with architectonics—are likely to fail for a minority of cortical areas. For example, some cortical areas are topographically organized (e.g., somatotopy in somatomotor cortex), such that subregions within the area have different functional responses (Rao et al. 1995), including different RSFC responses (Long et al. 2014). These functional dissociations would likely either reduce the observed RSFC homogeneity of a parcel

representing the area, or would result in the delineation of sub-areal parcels within a single cortical area. These are unavoidable limitations of any RSFC-based technique.

In this paper, we constructed a set of parcels derived from a group average RSFC boundary map that represent putative cortical areas. We assessed the homogeneity of these parcels, and we compared those homogeneities against an appropriate null model. We additionally assessed the homogeneity of these boundary map-derived parcels using an independent dataset, collected on a different scanner model at a different institution. Further, we compared the homogeneity of the boundary map-derived parcellation to the homogeneities of several other alternative parcellations (Brodmann, 1909; Tzourio-Mazoyer et al., 2002), including other candidate approaches for performing whole-brain areal partitioning using RSFC data (Power et al., 2011; Yeo et al. 2011; Craddock et al. 2012; Shen et al. 2013). Each of these sets of parcel homogeneities was also compared to a tailored null model, all within the independent dataset. We also identified boundary map-derived parcels that overlapped with several known human architectonic areas. We further identified the network structure of the boundary map-derived parcellation and compared this structure to the network structure identified using all gray matter points in the brain. Finally, we assessed the level of inter-subject reliability of subject-level RSFC patterns from these boundary map-derived parcels.

3.3 Methods

For a graphical summary of the methods, see Figure 1

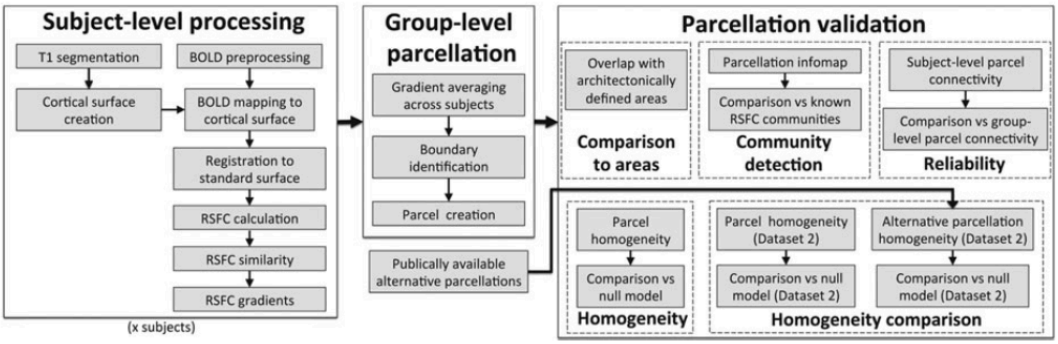

Figure 3-1. Visual outline of analysis methods

We acquired two independent datasets: Dataset 1, which we used to create an RSFC boundary map and generate parcels; and Dataset 2, which we used to compare the boundary map-derived parcellation against other putative areal parcellations.

Dataset 1

Subjects

Data was collected from 120 healthy young adult subjects during relaxed eyes-open fixation (60 females, mean age = 25 years, age range = 19-32 years). All subjects were native speakers of English and right-handed. Subjects were recruited from the Washington University community and were screened with a self-report questionnaire to ensure that they had no current or previous history of neurological or psychiatric diagnosis. Informed consent was obtained from all subjects. The study was approved by the Washington University School of Medicine Human Studies Committee and Institutional Review Board

Data Acquisition

Structural and functional MRI data were obtained with a Siemens MAGNETOM Trio Tim 3.0T Scanner (Erlangen, Germany) and a Siemens 12 channel Head Matrix Coil. A T1-weighted sagittal magnetization-prepared rapid acquisition gradient echo (MP-RAGE) structural image was obtained (TE=3.08ms, TR(partition)=2.4s, TI=1000ms, flip angle=8°, 176 slices with 1x1x1mm voxels) (Mugler and Brookeman 1990). An auto align pulse sequence protocol provided in the Siemens software was used to align the acquisition slices of the functional scans parallel to the anterior commissure-posterior commissure (AC-PC) plane of the MP-RAGE and centered on the brain. This plane is parallel to the slices in the Talairach atlas (Talairach and Tournoux 1988).

During functional MRI data acquisition, subjects were instructed to relax while fixating on a black crosshair that was presented against a white background. Functional imaging was performed using a blood oxygenation level-dependent (BOLD) contrast sensitive gradient echo echo-planar sequence (TE=27ms, flip angle=90°, in-plane resolution=4x4 mm). Whole brain EPI volumes (MR frames) of 32 contiguous, 4 mm-thick axial slices were obtained every 2.5 seconds. A T2-weighted turbo spin echo structural image (TE=84ms, TR=6.8s, 32 slices with 1x1x4 mm voxels) in the same anatomical planes as the BOLD images was also obtained to improve alignment to an atlas. The number of volumes collected from subjects ranged from 184 to 729 (mean = 336 frames, 14.0 mins).

Dataset 2

Subjects

Data was collected from 108 healthy young adult subjects during relaxed eyes-open fixation (69 females, mean age = 21 years, age range = 18-33 years). Subjects were recruited from the Dartmouth College community and were screened with a self-report questionnaire to ensure that they had no neurological problems, were not using psychoactive medications and had normal or corrected to normal vision. Participants were given course credit or monetary compensation in exchange for their participation and were provided informed consent in accordance with the guidelines set by the Committee for the Protection of Human Subjects at Dartmouth College. These subjects were selected as the subjects with minimal in-scan head motion from a larger cohort of 746 subjects.

Data Acquisition

Structural and functional MRI data were obtained with a Philips Achieva 3.0 Tesla scanner and a thirty-two channel phased array coil. A T1-weighted sagittal MP-RAGE structural image was obtained (TE=4.6ms, TR=9.9ms, flip angle=8°, 160 slices with 1x1x1mm voxels.

During functional MRI data acquisition, subjects were instructed to relax while fixating on a white crosshair that was presented against a black background. Functional imaging was performed using a BOLD contrast sensitive gradient echo echo-planar sequence (TE=35ms, flip angle=90°, in-plane resolution=3x3 mm, sense factor = 2). Whole brain EPI volumes (MR frames) of 36 3.5 mm-thick axial slices were obtained

every 2.5 seconds with .5mm skip between slices. Two 5:00 minute runs (240 volumes total) were collected from each subject.

Further analysis of both datasets was identical, except where noted.

Preprocessing

Functional images were first processed to reduce artifacts (Miezin et al. 2000). These steps included: (i) correction of odd vs. even slice intensity differences attributable to interleaved acquisition without gaps, (ii) correction for head movement within and across runs and (iii) across-run intensity normalization to a whole brain mode value of 1000. Atlas transformation of the functional data was computed for each individual using the MP-RAGE scan. Each run was then re-sampled to an isotropic 3-mm atlas space (Talairach and Tournoux 1988), combining movement correction and atlas transformation in a single cubic spline interpolation (Lancaster et al. 1995; Snyder 1996). All subsequent operations were performed on the atlas-transformed volumetric time series.

Functional connectivity processing

Additional preprocessing steps to reduce spurious variance unlikely to reflect neuronal activity were executed as recommended in Power et al. (2014). RSFC preprocessing was performed in two iterations. In the first iteration, the processing steps were: (i) demeaning and detrending, (ii), multiple regression including: whole brain, ventricular and white matter signals, and motion regressors derived by Volterra expansion (Friston et al., 1996), and (iii) a band-pass filter ($0.009\ Hz < f < 0.08\ Hz$).

Following the initial RSFC preprocessing iteration, temporal masks were created to flag motion-contaminated frames. Motion contaminated volumes were identified by frame-by-frame displacement (FD, described in Power et al., 2012). Volumes with FD > 0.2 mm (Dataset 1) / FD > .25mm (Dataset 2; different thresholds were used based on observations of different motion "noise floors" in the two datasets, following Power et al., 2012), as well as uncensored segments of data lasting fewer than 5 contiguous volumes were flagged for removal. In Dataset 1, these masks censored 16% ± 14% (range: 0.7% – 66%) of the data across subjects; on average, subjects retained 279 ± 107 volumes (range: 151 – 719). In Dataset 2, these masks censored 8% ± 2% (range: 4% – 12%) of the data across subjects; on average, subjects retained 221 ± 5 volumes (range: 212 – 230).

The data was then re-processed in a second iteration incorporating the temporal masks described above. This reprocessing was identical to the initial processing stream, but ignored cencored data. Finally, the data was interpolated across censored frames using least squares spectral estimation (Power et al. 2014) of the values at censored frames so that continuous data can be passed through (iv) a band-pass filter (0.009 Hz < f < 0.08 Hz) without contaminating frames near high motion frames (Power et al. 2012; Carp 2013). It should be noted that even following this processing censored frames are still ignored during the final correlation calculations between timecourses.

Surface processing and CIFTI creation

Surface generation and sampling of functional data to anatomical surfaces followed a similar procedure as described in Glasser et al. (2013). First, following

volumetric registration, anatomical surfaces were generated from each subject's MP-RAGE image using FreeSurfer's default recon-all processing pipeline (version 5.0). This pipeline included brain extraction, segmentation, generation of white matter and pial surfaces, inflation of the surfaces to a sphere, and surface shape-based spherical registration of the subject's 'native' surface to the fsaverage surface (Dale and Sereno 1993; Dale et al. 1999; Fischl et al. 1999; Ségonne et al. 2004, 2005). The fsaverage-registered left and right hemisphere surfaces were then brought into register with each other (Van Essen et al., 2012) and resampled to a resolution of 164,000 vertices using Caret tools (Van Essen et al. 2001). Finally, each subject's surface was down-sampled to a 32,492 vertex surface (fs_LR 32k), which allowed for analysis in a computationally tractable space while still oversampling the underlying resolution of BOLD data used in subsequent analyses. The above procedure results in a surface space that allows for quantitative analysis across subjects. A script for this procedure is available on the Van Essen Lab website (Freesurfer_to_fs_LR Pipeline, http://brainvis.wustl.edu/wiki/index.php/Caret:Operations/Freesurfer_to_fs_LR).

Surface processing of the BOLD data proceeded through the following steps. First, the BOLD volumes are sampled to each subject's individual 'native' midthickness surface (generated as the average of the white and pial surfaces) using the ribbon-constrained sampling procedure available in Connectome Workbench 0.84, which samples data from voxels within the gray matter ribbon (i.e. between the white and pial surfaces) (Glasser and Van Essen 2011). Voxels with a timeseries coefficient of variation 0.5 standard deviations higher than the mean coefficient of variation of nearby voxels (within a 5 mm sigma Gaussian neighborhood) are excluded from the volume to

surface sampling, as described in Glasser et al. (2013). Once sampled to the 'native' surface, timecourses were deformed and resampled from the individual's 'native' surface to the 32k fs_LR surface. Finally, the time courses were smoothed along the 32k fs_LR surface using a Gaussian smoothing kernel ($\sigma = 2.55$).

These surfaces are then combined with volumetric subcortical and cerebellar data into the CIFTI format using Connectome Workbench (Glasser et al. 2013), creating full brain timecourses that exclude non-gray matter tissue. Subcortical (including accumbens, amygdala, caudate, hippocampus, pallidum, putamen, and thalamus) and cerebellar voxels were selected based on a mask generated by finding the modal assignment of voxels by Freesurfer segmentation across all subjects. Volumetric data was smoothed within this mask with a Gaussian kernel ($\sigma = 2.55$) before being combined with the surface data.

Boundary map generation

RSFC-Boundary Mapping identifies transitions in resting state correlations across the cortical surface. The original approach described in Cohen et al. (2008) applied 2-D image processing tools to BOLD data sampled from patches on a flattened cortical surface. The current implementation performs all calculations directly on a closed surface topology and applies to the entire cortical surface. The RSFC-Boundary Mapping procedure is implemented using Connectome Workbench and Matlab (Version 7.14, Mathworks, Inc., Sherborn, MA, USA) and follows a similar sequence as described in Wig et al. (2014b) with some notable distinctions that will be highlighted below.

For each subject, the time course of each surface vertex was correlated with the time courses from every other surface vertex and subcortical voxel in CIFTI space. Each correlation map was transformed using Fisher's r-to-z transformation. For each hemisphere, the subject's RSFC map similarity matrix was created by calculating the pairwise spatial correlations between all vertex's RSFC correlation maps, producing a 32k x 32k matrix. To find positions where RSFC similarity exhibited abrupt changes, the first spatial derivative was computed using the 'cifti-gradient' function in Connectome Workbench. This resulted in 32k 'gradient' maps for each hemisphere. These gradient maps were then averaged across subjects. At this point, instead of using non-maxima suppression to identify boundaries in the gradient maps, as in Wig et al. (2014b), we used the "watershed by flooding" algorithm (Beucher & Lantuejoul, 1979), implemented using custom Matlab scripts. This standard image segmentation procedure defines regions in the gradient maps by starting from local minima (vertices with values smaller than of their neighbors that were less than three vertices away) and iteratively growing until reaching locations that could ambiguously be assigned to more than one region. These boundary locations identify putative boundaries in the gradient maps. Finally, the 32k boundary maps from each hemisphere were averaged to indicate the frequency with which a given vertex was identified as a boundary.

Boundary map reliability

To determine the reliability of the boundary maps, we calculated the degree of spatial correlation between the boundary maps from the two datasets as an overall measure of reliability. To further determine whether the strongest boundaries in

particular were highly reliable, we then thresholded the two boundary maps to retain the top quartile of boundary values (i.e., retaining the cortical vertices most likely to be boundaries) and assessed the overlap of the two thresholded boundaries by calculating Dice's coefficient.

Parcel creation

Parcels were created from the Dataset 1 boundary map only using custom Matlab scripts. We identified all local minima on the boundary map image as seeds to be used for parcel creation. Parcels were grown from these seeds using the "watershed by flooding" procedure described above, such that parcels were allowed to expand outward from the seed until they either reached a height threshold on the boundary map or met another parcel. This resulted in a large number of parcels tiling the cortical surface (>1000), with one-vertex wide borders (i.e., the watershed zones) separating them. Pairs of parcels were then merged together based on the values of the boundary map in the border vertices between the parcels, which represent the local change in connectivity patterns, and therefore can be considered a measure of the dissimilarity of the parcels. If the median boundary value between two parcels was below a threshold, then the parcels were considered not sufficiently dissimilar and were merged together. We visually examined multiple border thresholds, and the optimal threshold that captured all major divisions in the boundary map image appeared to be at the 60^{th} percentile of the values in the boundary map (see Supplemental Figure 3 for parcellations resulting from other threshold values). As areas of the cortex with very high boundary map values are likely to be transition zones between parcels rather than

parcels themselves, we then eliminated all parcels and portions of parcels in vertices with high boundary map values (defined as the top quartile of values in the boundary map).

This procedure produced an anatomically plausible number of parcels that visually appeared to well fit the contours of the boundary map. Parcels in low-SNR areas (defined as regions with mean BOLD signal < 750, consisting primarily of orbitofrontal cortex and anterior ventral lateral temporal lobe; see Ojemann et al. 1997; Wig et al. 2014b), which are likely to be noisy and unreliable, were excluded from further analysis. Finally, we eliminated parcels containing fewer than 15 cortical vertices (~30mm^2) because the effective resolution of the BOLD data (originally 4x4x4mm, then upsampled and smoothed on the surface) suggested that accurate identification and evaluation of objects that small might be dubious.

Parcel evaluation

The parcel creation procedure outlined above creates parcels based on strong boundaries, which indicate large differences in connectivity patterns between adjacent cortical regions. However, a parcel that accurately represents a cortical area should not only be distinct from its neighbors but, in most cases (i.e. non-topographic regions), it should also have a single, consistent connectivity pattern across the parcel—in other words, its connectivity pattern should be homogenous within the parcel. Thus, the degree to which the created parcels are homogenous can serve as a quality metric of the parcellation (Craddock et al. 2012; Shen et al. 2013). We assessed the homogeneity of our created parcels using the following technique: for each parcel, we

computed the average whole-brain connectivity pattern of each vertex in the parcel across subjects in Dataset 1. We then entered the connectivity patterns from all vertices in a parcel into a principal components analysis. The homogeneity of the parcel was calculated as the percent of total variance across all vertices' connectivity patterns that can be explained by the first (largest) principal component. A higher homogeneity value indicates that the connectivity patterns of vertices within the parcel can be better described by a single connectivity pattern. We then averaged the homogeneity values across parcels to determine the overall homogeneity of the whole parcellation. Compared to other metrics of parcel homogeneity, this novel metric has the advantage of being highly interpretable: the homogeneity of a parcel represents the percent of variance in the parcel explained by the most common connectivity pattern. Homogeneity analyses conducted with a previously devised homogeneity metric (average z-transformed pairwise correlations between all vertex connectivity patterns within a parcel, from Craddock et al., 2012) yielded very similar results (see Supplemental Figure 11).

However, we note that any metric of parcel homogeneity is likely to be dependent on parcel size, with smaller parcels being intrinsically more homogenous. To illustrate this fact, consider that a large, perfectly homogenous parcel could be divided in half, and both halves would still be perfectly homogenous. Further, a direct comparison of the homogeneities of the large and small parcels would not indicate one scheme as superior to the other, even though the large perfectly homogenous parcel is much more likely to represent a single cortical area. Even in a purely random parcellation scheme, randomly placed small parcels are more likely to contain a single connectivity pattern

than randomly placed large parcels, which will more often span multiple cortical areas. Thus, any homogeneity-based evaluation of a parcellation must be compared to a null model—it should consider not only how homogenous the parcels are, but also whether they are more homogenous than would be expected from randomly placed parcels of the same size and shape. Thus, we assessed the degree to which a parcellation was more homogenous than a null model consisting of many parcellations with randomly placed parcels of the same size, shape, and relative position to each other.

To create such random parcellations, we rotated each hemisphere of the original parcellation a random amount around each of the x, y, and z axes on the spherical expansion of the 32k fs_LR cortical surface. This procedure randomly relocated each parcel while maintaining the relative positions of parcels to each other. Each parcel was then slightly dilated or contracted to adjust for vertices gained or lost due to the nonuniform vertex density across the surface of the sphere, thus maintaining the same number of vertices within the rotated parcel while approximately maintaining the same shape. Random rotation was repeated 1000 times to generate distributions of average homogeneities calculated from randomly placed versions of each tested parcellation. Notably, in any random rotation, some parcels will inevitably be rotated into the medial wall (where no data exists) or into low-SNR regions (where we believe the homogeneity of data to be particularly low). The homogeneity of a parcel rotated into one of these regions was not calculated; instead, we assigned this parcel the average homogeneity of all random versions of the parcel that were rotated into valid (high-SNR) cortical regions.

The average homogeneity of the original parcellation was compared to the homogeneities of the set of rotated parcellations. We assessed 1) the number of rotated parcellations that had worse average homogeneity than the original parcellation, and 2) the difference between the original parcellation homogeneity and the distribution of random homogeneities, calculated as a Z-score ((original homogeneity – mean of random homogeneities) / standard deviation of random homogeneities).

Comparison of parcel homogeneity against alternative parcellations

We compared the homogeneities of boundary-derived parcels against those of several alternative parcellations, created using a variety of methods (and excluding all parcels in low-SNR regions). These alternative parcellations included: “Power ROIs”: a set of functional ROIs derived from a combination of meta-analytic and functional connectivity analyses (Power et al., 2011); “Craddock”: a parcellation created by the NCUT method (Craddock et al., 2012); “Shen”: a parcellation created using a multiclass spectral clustering approach to the NCUT criterion (Shen et al. 2013); “Power communities”: a parcellation created using the Infomap community detection technique (Power et al. 2011); “Yeo”: a parcellation created using a signal clustering technique (Yeo et al., 2011); “Brodmann”: a parcellation created from canonical Brodmann areas (Brodmann 1909); and “AAL”: a parcellation created from the Automated Anatomical Labeling atlas (Tzourio-Mazoyer et al. 2002). Each parcellation was sampled to the cortical surface where necessary, and parcels containing less than 15 cortical vertices outside of low-SNR regions were eliminated from further analysis. For parcellation approaches with multiple solutions (the Craddock and Shen parcellations), we selected

the solution with the number of parcels most similar to the boundary map-derived parcellation. We repeated these analysis for all other available Craddock and Shen parcellations with at least 50 parcels; these produced similar results to the chosen parcellation (see Supplemental Figures 8 and 9). Table 1 provides additional details for each of these parcellations.

Name	Reference	Number of parcels	Notes
Power ROIs	ROI centers from Power et al. (2011), with subcortical ROIs excluded; available from http://www.nil.wustl.edu/labs/petersen/Resources_files/Consensus264.xls	226 (111 L, 115 R)	10 mm radius circles drawn around cortical locations. ROIs based, in part, on the same dataset used to create the boundary map.
Craddock	Craddock et al. (2012); available from http://ccraddock.github.io/cluster_roi/	353 (175 L, 178 R)	Sampled from volume to surface. Used 400-cluster parcellation generated by two-level group clustering using temporal correlation.
Shen	Shen et al. (2013); available from http://www.nitrc.org/frs/?group_id=51	213 (106 L, 107 R)	Sampled from volume to surface. Used 300-cluster parcellation.
Power communities	Power et al. (2011); available from http://sumsdb.wustl.edu:8081/sums/index.jsp	103 (53 L, 50 R)	Sampled from volume to surface. "Consensus" procedure applied to collapse across multiple thresholds. Separate parcel created from each spatially contiguous community cluster.
Yeo	Yeo et al. (2011); available from http://sumsdb.wustl.edu:8081/sums/index.jsp	98 (49 R, 49 L)	Used 17-cluster parcellation. Separate parcel created from each spatially contiguous cluster.
Brodmann	Brodmann (1909); available from http://sumsdb.wustl.edu:8081/sums/index.jsp	77 (39 L, 38 R)	Sampled from volume to surface.
AAL	Tzourio-Mazoyer et al. (2002); available from http://www.gin.cnrs.fr/AAL/aal_for_SPM8.tar.gz	74 (36 L, 38 R)	Sampled from volume to surface.

Table 3-1. Previously published parcellations compared against present boundary map-derived parcellation.

To ensure that the boundary map-derived parcellation created using Dataset 1 was not advantaged by being tested in the same dataset, we tested all parcellations' homogeneity using Dataset 2. For each parcellation scheme, we evaluated homogeneity using Dataset 2, and compared it to the homogeneity of randomly rotated versions of the parcellation.

Comparison of parcels with known cytoarchitectonic areas

If the boundary-derived parcellation created above is an accurate representation of the cortical areas in the brain, then it should contain parcels that are similar to known

human cytoarchitectonic areas. We visually compared the boundary map-derived parcels to the probabilistic borders of areas 17, 1, 2, 3 (combining 3a and 3b), 4 (combining 4a and 4p), and hOc5 that were mapped to the 32k fs_LR by Van Essen et al. (2012) (publically available through the SumsDB database, http://sumsdb.wustl.edu:8081/sums/index.jsp) based on cytoarchtectonic mapping by Fischl et al. (2008).

Identification of parcel network structure

If the boundary-derived parcels created above are accurate representations of the cortical areas in the brain, then the network structure of the temporal correlations between these parcels should be highly similar to previously published descriptions of the network structure of the temporal correlations between all gray matter voxels.

Closely following Power et al. (2011), we assessed the network structure of the parcel-wise graph using the Infomap algorithm (Rosvall and Bergstrom 2008). In each subject we calculated the average timecourse of each parcel from Dataset 1, and cross-correlated these timecourses to form the parcel-wise correlation matrix. These correlation matrices were then Fisher transformed and averaged across subjects. The resulting average correlation matrix was thresholded at a variety of correlation thresholds calculated to create connection matrices with specific degrees of sparseness (ranging from 1% to 3% of all possible connections surviving the threshold, in steps of .1%). Further, connections passing these thresholds were removed if the geodesic distance along the cortex between the centroids of the connected parcels was less than 20mm. The resulting connection matrices at each threshold were then evaluated using

the Infomap algorithm, which assigned parcels to communities at each correlation threshold based on the maximization of within-community random walks in the connection matrix. Communities with five or fewer parcels were eliminated from consideration, and those parcels were considered unassigned.

We then collapsed across Infomap thresholds using a “consensus” procedure, with the goal of incorporating information both from more sparse thresholds, in which smaller networks were likely to emerge, and more dense thresholds, in which more parcels were likely to be successfully assigned. In this procedure, each node was given the community assignment it had at the sparsest possible threshold at which it was successfully assigned. The node assignments were “cleaned up” by removing small communities that were only present at one threshold. This procedure is nearly identical to the method used to collapse previously published voxel-wise community assignments (Power et al. 2011) across thresholds to create a single network map (the “Power communities” map described above). We note that this procedure does not attempt to comprehensively describe all features of the network, and may be especially poor at capturing non-hierarchical network features (which do occur infrequently). Rather, it provides a single, summary view of the brain’s networks.

We assessed the overlap between the consensus parcel-wise network communities and the surface-mapped voxelwise Power consensus communities described above. Overlap was calculated as the number of cortical vertices that had the same community identity in both parcel-wise and voxel-wise Infomap analyses divided by the total number of vertices that were assigned to a community in both analyses.

Use of parcels in individual subjects

Ideally, the boundary-derived parcellation could be used to interrogate individual subject data. However, applying a group-level parcellation to individual subjects should only be performed if there is reasonable confidence that the parcellation truly does reflect the central tendency of the overall group, such that data in a given parcel from an individual will tend to look like the average data in that parcel across individuals. Thus, to determine whether the parcellation derived from the group boundary map could also be used to investigate individual subjects, we examined how reliably individual subjects' parcel connectivity maps looked like the group average parcel connectivity maps.

For each parcel in each Dataset 1 subject, we calculated the whole-brain subject-level connectivity pattern of the parcel by extracting the parcel's mean timecourse in that subject's data and correlating it against the timecourses from every other gray matter point in the brain. We then averaged the Fisher's Z-transformed correlation patterns across subjects. Finally, we calculated the spatial correlation between the group average Fisher-transformed connectivity pattern for that parcel and all of the Fisher-transformed subject-level connectivity patterns for the same parcel. This analysis produced a subject-group similarity (i.e., spatial correlation value) for each parcel in each subject.

We then explored two dimensions of variability in connectivity patterns: at the subject level and at the parcel level. First, we examined whether some subjects tended to be more or less similar to the group average than others, and whether the degree of similarity was related to the quantity of data remaining for each subject after motion correction. This was done by averaging similarity scores across parcels, for each

subject, and then plotting these subject average scores against the number of uncensored timepoints in each subject's resting state scan. Second, we examined whether some parcels' subject-specific connectivity patterns tended to be more or less similar to the group average than others. This was done by averaging similarity scores across subjects, for each parcel. Parcels with low average similarity scores can be considered unreliable for use in cross-subject analysis.

3.4 Results

Boundary map characteristics

Visually, the group boundary map (Figure 2) appears very similar to our previously published boundary map (Wig et al. 2014b), though close examination indicates that the present boundary map appears cleaner, with sharper boundaries and lower minimum boundary values. Comparison of histograms of the values in the current boundary map and the previously published boundary map (Supplemental Figure 1) supports this observation, as the value distribution of the current map is markedly shifted to the left, suggesting a reduction of measurement noise in the map.

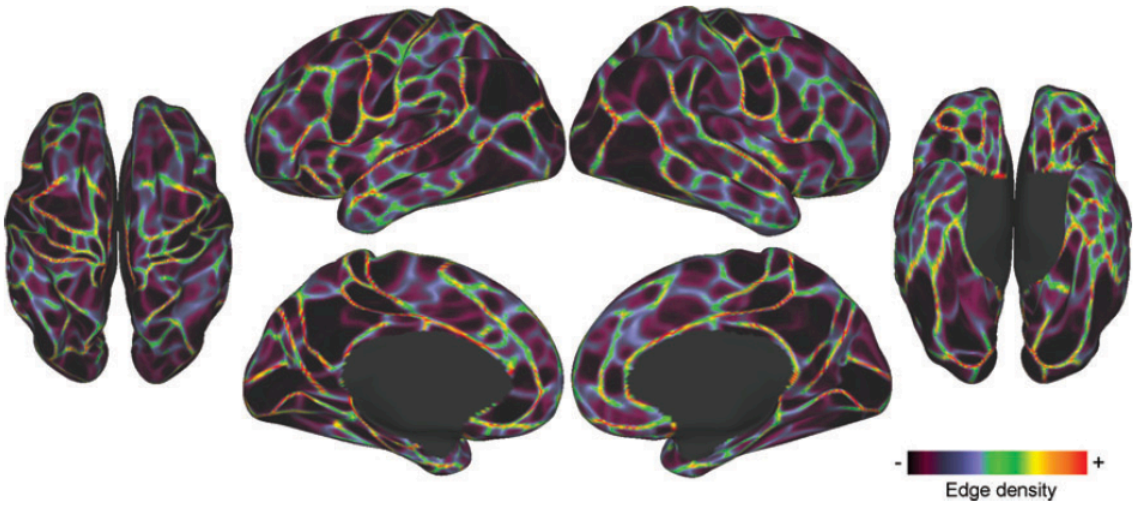

Figure 3-2. RSFC-boundary map from Dataset 1. Bright colors indicate locations where abrupt transitions in RSFC pattersn were reliably found across many cortical vertices, representing putative boundaries between cortical areas. Dim colors represent relatively stable RSFC patterns.

Boundary map reliability

Boundary maps from the two datasets appeared visually very similar. When thresholded at the top quartile of boundary map values, the boundary maps from the two datasets overlapped closely (Supplemental Figure 2), with a Dice's coefficient of .71.

Parcel creation

The parcel creation procedure produced 422 cortical parcels (206 in the left hemisphere, 216 in the right hemisphere; see Figure 3). Of these parcels, 356 (178 in each hemisphere) parcels were at least partly (>= 15 vertices, ~30mm^2) outside low SNR areas (Wig et al., 2014b). The remaining 66 parcels were considered unreliable due to low SNR and were excluded from further analysis.

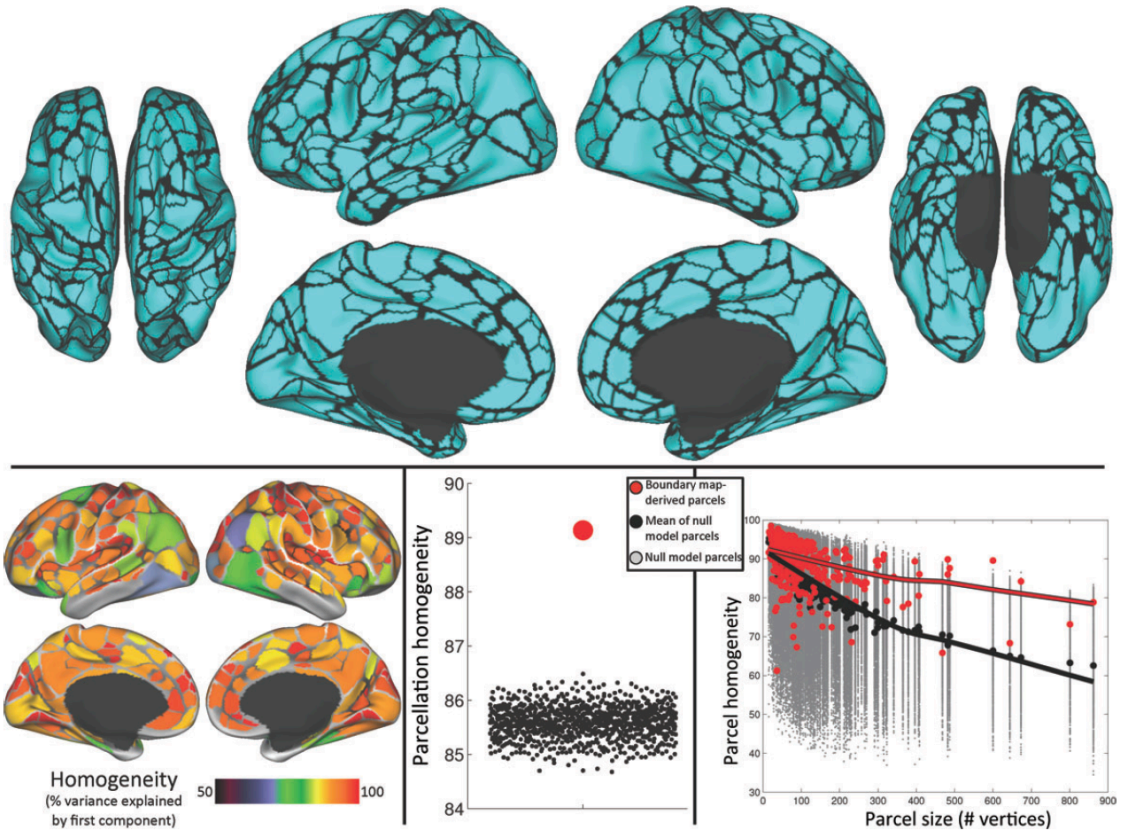

Figure 3-3. Boundary map-derived parcels are both highly homogenous and more homogenous than a null model. Top: 422 cortical parcels were created from the Dataset 1 boundary map. Bottom left: homogeneity of each parcel, calculated as the percent of the variance in RSFC patterns explained by the parcel's first PCA eigenvariate. Green indicates a parcel is >70% homogenous; red indicates >90% homogenous. Bottom middle: average homogeneity across parcels (red dot) was significantly higher than that across parcels of each null model iteration (black dots). Bottom right: homogeneity of individual real parcels (red dots) was higher than that of null model parcels (gray dots) when plotted against parcel size. Black dots indicate the median homogeneity across iterations for each null model parcel. Lowess fit lines in red and black emphasize the homogeneity–size relationship for the real and null model parcels, respectively.

Parcel homogeneity

We calculated the homogeneity of each of these parcels within Dataset 1. Homogeneity represents the degree to which the parcel has a uniform connectivity pattern, and is thus a metric of parcel quality. Parcel homogeneities are mapped onto

the brain in Figure 3. Mean parcel homogeneity across all parcels was 89.1% ± 5.8% (max 98.4%, min 61.2%).

We then compared the mean homogeneity of this parcellation to a null model consisting of mean homogeneities from 1000 matched parcellations randomly rotated on the cortex. We observed that the mean homogeneity of the boundary-derived parcellation was much higher than any of the 1000 randomly rotated null model parcellation homogeneities (Figure 3); the parcellation was thus significantly more homogenous than random at $p<.001$. These null model parcellations had a mean homogeneity of 85.6%, with a standard deviation of .29% across parcellations; the boundary-derived parcellation had a homogeneity Z score of 12.07 (i.e. was 12.07 standard deviations away from the mean of the null model parcellations).

We further examined the relationship between parcel homogeneity and parcel size to determine whether the homogeneity measure was dependent on parcel size. The homogeneities of the real parcels (in red) and null model parcels (in grey, medians in black) are plotted against parcel size in Figure 3. We observed a close relationship between homogeneity and parcel size that can be appreciated with the Lowess fit line plotted on top; this relationship was observed both for the boundary-derived parcels (in red) and for the random matched parcels (in grey; mean homogeneities of random parcels in black).

In sum, parcels derived from boundary maps are highly homogenous. Overall, this parcellation is also much more homogenous than a null model consisting of randomly replaced versions of the parcellation, suggesting that the present parcels are well placed. We further established that the homogeneity measure has a strong

relationship with parcel size, justifying our use of the present null model, which accounts for parcel size and shape.

Comparison of parcel homogeneity against alternative parcellations

To demonstrate external validity of the parcellation, we evaluated the homogeneity of the Dataset 1 boundary map-derived parcels using data from Dataset 2. The mean homogeneity across the boundary map-derived parcels was 87.4% ± 6.4%, which was similar to, but slightly lower than, the homogeneities of the parcels derived from and tested in Dataset 1 (89.1% ± 5.8%, as stated above).

As above, we compared the homogeneities of the boundary map-derived parcels to the null model consisting of randomly rotated versions of the parcellations. Once again, the boundary map-derived parcellation tested in Dataset 2 was more homogenous than any randomly rotated parcellation ($p<.001$); it had a Z score of 10.91 compared to the distribution of random parcellations.

We further evaluated the homogeneity of several alternative parcellations using Dataset 2. Parcel homogeneities from these alternative parcellations can be seen in Figure 4; average homogeneities of each parcellation are listed in Table 2.

We then compared the homogeneities of each alternative parcellation against the homogeneities of a null model consisting of 1000 randomly placed versions of the parcellation. See Table 2 for comparisons to the null model parcellations. The Power ROIs, Yeo parcels, and Brodmann parcels were more homogenous than any of their null model parcellations, while the Shen parcellation and Power communities were significantly better than the set of random parcellations, but not better than all possible

random parcellations. The Craddock and AAL parcellations were not significantly more homogenous than their null models.

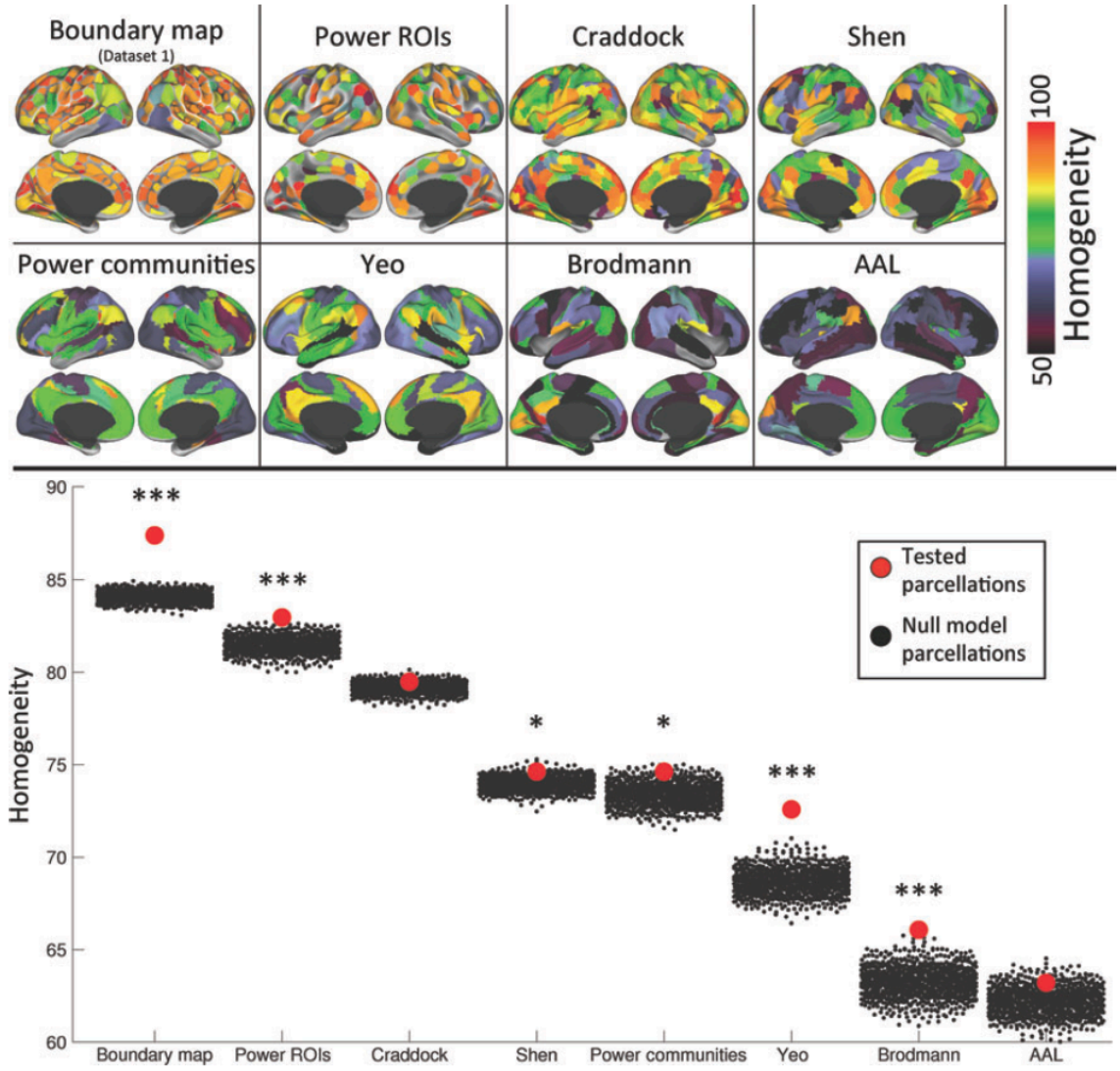

Figure 3-4. When tested in an independent dataset, the boundary map-derived parcellation is more homogenous than any other parcellation, and does better relative to its null model than any other parcellation. Top: parcel homogeneities of each competing parcellation when tested in Dataset 2. Bottom: average homogeneity across parcels of each parcellation (red dots) compared with the average homogeneity across parcels of each of 1000 null model iterations (black dots), which vary in homogeneity because of differing parcel sizes. ***indicates the parcellation was more homogenous than all of its 1000 null model iterations (i.e., $P<0.001$); *indicates the parcellation was more homogenous than at least 950 of its null model iterations ($P<0.05$).

Parcellation	Mean ± SD homogeneity (tested in Dataset 2)	Number of null model iterations with worse homogeneity	*Z*-score relative to null model
Boundary map-derived	87.4 ± 6.4%	1000 ($P < 0.001$)	10.91
Power ROIs	83.0 ± 9.7%	1000 ($P < 0.001$)	3.29
Craddock	79.5 ± 10.4%	871 ($P = 0.129$)	1.12
Shen	74.6 ± 11.6%	960 ($P = 0.040$)	1.71
Power communities	74.6 ± 15.7%	976 ($P = 0.024$)	1.97
Yeo	72.6 ± 14.9%	1000 ($P < 0.001$)	5.70
Brodmann	66.1 ± 14.0%	1000 ($P < 0.001$)	3.51
AAL	63.2 ± 11.7%	920 ($P = 0.080$)	1.38

Table 3-2. Average homogeneity and comparison of homogeneity against a null model for each parcellation

Finally, we examined homogeneity vs parcel size relationships for the boundary map-derived parcellation, as well as for each alternative parcellation (see Supplemental Fig 4). Relationships between homogeneity and size were observed for each parcellation and the null model of each parcellation, though size-homogeneity relationships appeared weaker for parcellations with less variance in parcel size, as would be expected. When the fit lines of all of the parcellations and random parcellations were plotted on the same scale (Supplemental Fig 5), it became evident that while all parcels exhibited homogeneity decreases as size increased, the boundary map-derived parcels had superior homogeneity even when parcel size was taken into account.

Comparison of parcels with known cytoarchitectonic areas

We observed strong visual overlap between the boundary map-derived parcels and several known cytoarchitectonic areas. The left side of Figure 5 illustrates these

overlaps on the left hemisphere (see Supplemental Figure 6 for right hemisphere overlap). The architectonic boundary of area 17 almost perfectly encompassed a single RSFC-defined parcel in both hemispheres. By contrast, area hOc5 also appeared to correspond with a single parcel in the left hemisphere, but that parcel extended significantly beyond the probabilistic border of the area. In the right hemisphere, no parcel corresponded with area hOc5. Area 1 did not correspond with any parcels, falling directly on top of a border between parcels in both hemispheres.

In both hemispheres, cytoarchitectonically defined areas 2, 3, and 4 aligned well with a string of parcels running down the pre- and postcentral gryri. Taken together, these strings of parcels matched areas 3 and 4 almost perfectly, and overlapped most of area 2, failing only to capture a ventral posterior section of the area. Thus, we hypothesized that while the parcels do not conform well to strict anatomical definitions of cortical areas, they may be capturing some unknown functional subdivisions within the areas.

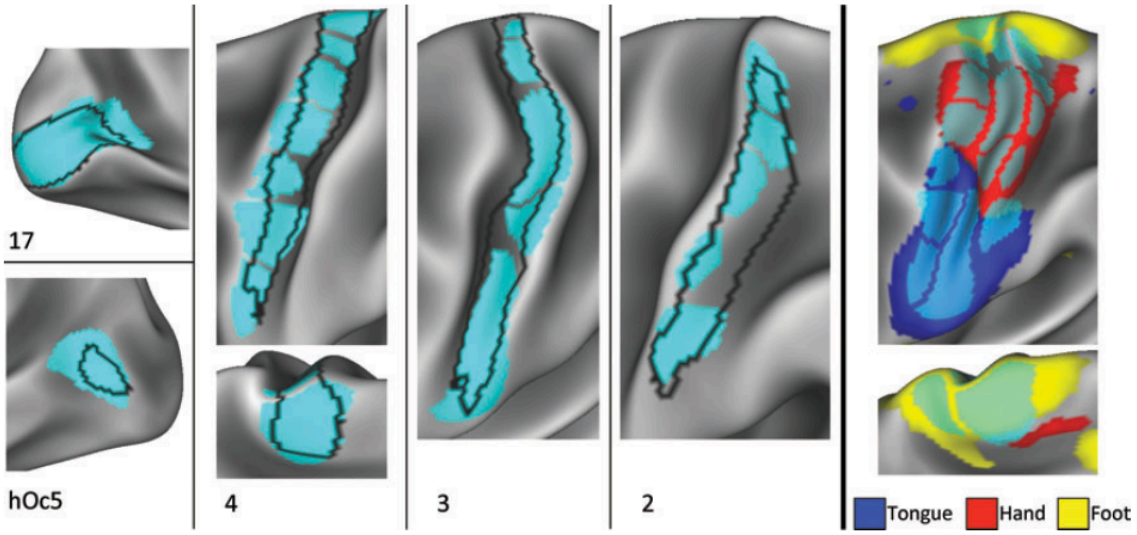

Figure 3-5. Boundary map-derived parcels match known cortical areas and functional activation

patterns. Left and middle: a variety of cytoarchitectonically defined cortical areas (Fischl et al. 2008) were matched by boundary map-derived parcels. Area 17 overlapped very well with one parcel, whereas area hOc5 overlapped moderately well with another parcel. Areas 2, 3, and 4 overlapped with several adjacent parcels. Right: parcel divisions within cytoarchitectonic areas 2, 3, and 4 corresponded with divisions between activation clusters from motor movements of the right foot, right hand, and tongue (Barch et al. 2013).

One possible functional subdivision these parcels could be capturing is the known somatotopic divisions within areas 2-4, in which dorsomedial somatomotor cortex receives sensory input and projects motor output to the feet, dorsolateral somatomotor cortex to the hands, and ventrolateral somatomotor cortex to the mouth and tongue. We conducted a post-hoc investigation of this possibility using results from a motor fMRI task collected as part of the Human Connectome Project. This task involved blocks of cued left or right finger tapping, left or right toe squeezing, and tongue movement (see Barch et al. 2013 for details). Preliminary findings from this task conducted in 20 subjects were presented in Barch et al. (2013); the present investigation used results from 219 subjects, analyzed using the same procedures as in Barch et al. (2013). We thresholded this data at a very high statistical threshold (arbitrarily selected to be $Z > 8.0$, though similar results were observed for any threshold between $Z>5.0$ and $Z>10.0$) and examined the overlap between the task activations and the various parcels in the pre- and postcentral gyri.

We observed that each task activation cluster very well matched multiple parcels in the pre- and postcentral gyri (left hemisphere activations shown in Fig 5, right; see Supplemental Figure 6 for right hemisphere activations). The correspondence was particularly clear for the hand and tongue activation clusters. The left hemisphere (though not right hemisphere) foot cluster extended anterior and posterior to the pre- and postcentral gyri. Importantly, the dorsal/ventral borders of each activation cluster

very well conformed to some of the parcel borders that split the putative cytoarchitectonic areas into multiple parcels. This suggests that these borders represent differences in function within a topographically organized area that are not captured by cytoarchitectonics.

Parcel network structure

We conducted community detection in the parcel-wise graph across many density thresholds (see Supplemental Figure 7 for results from all thresholds), and we collapsed across thresholds using a consensus procedure. There was considerable visual overlap between the cross-threshold consensus parcel-wise communities (Fig 6, top) and the Power communities (Fig 6, middle). Every community found in the Power communities was also observed in the parcel communities except for one in anterior medial temporal lobe. These included all of the classic large scale RSFC networks/systems that have been consistently identified using multiple techniques (community detection, Power et al., 2011; ICA, Beckmann et al. 2005, Smith et al. 2009; signal clustering, Yeo et al. 2011), such as Visual (dark blue in Fig 6), Dorsal somatomotor (light blue), Ventral somatomotor (orange), Auditory (light purple), Default (red), Fronto-parietal (yellow), Dorsal attention (green), Cingulo-opercular (purple), Ventral attention (teal), and Salience (black). They also included a number of less well-known systems that have been identified only in more recent investigations (Power et al., 2011; Yeo et al., 2011), such as: 1) a superior temporal sulcus-centered community (pink in Fig 6); 2) a community in anterior and posterior lateral frontal cortex, ventral inferior parietal lobule, and dorsomedial prefrontal cortex (tan); 3) a community in

retrosplenial and ventral temporal cortex (white); and 4) a community in posterior cingulate and ventral posterior precuneus (medium blue). Meanwhile, only one community emerged in the parcels was not found in the Power communities: a community in the marginal sulcus and frontal eye fields (colored magenta in Fig 6, top).

Overall, the overlap between the two methods was 71.2%. Multiple parcels with 100% overlap were observed in medial prefrontal, parietal, and occipital cortex, anterior and posterior insula, and pre- and postcentral gyrus. By contrast, parcels with poor overlap between the two methods were observed in lateral occipital and retrosplenial cortex, marginal sulcus, and frontal eye fields (Figure 6, bottom).

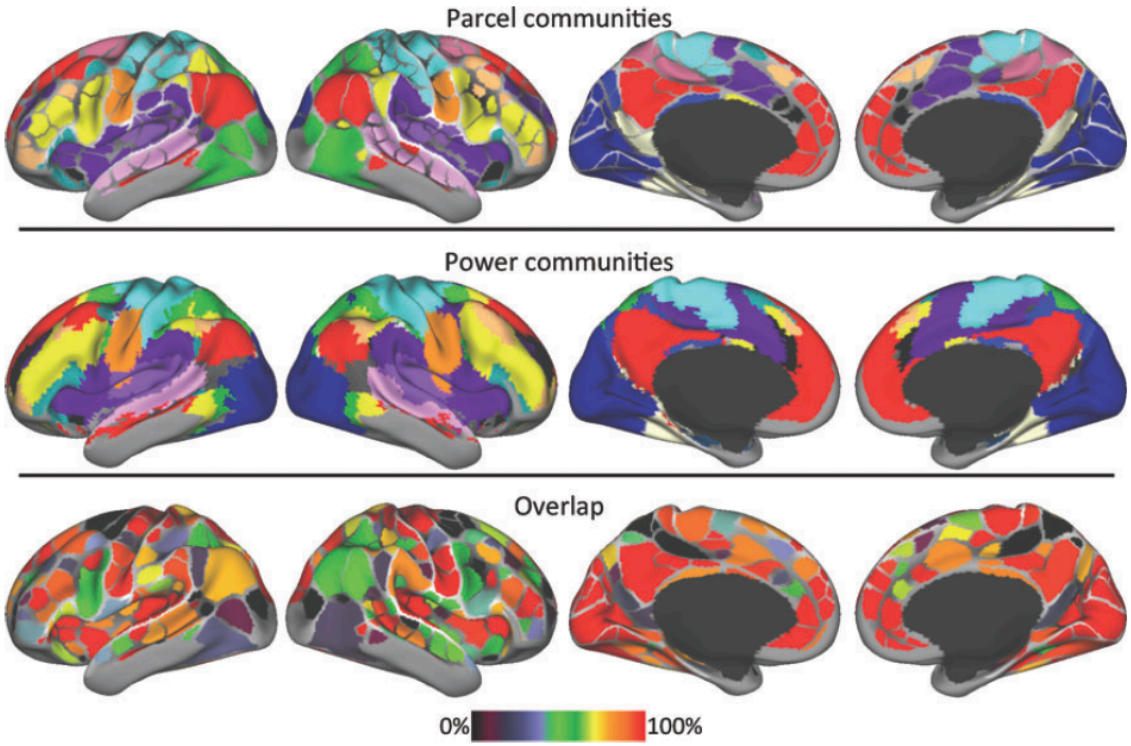

Figure 3-6. The network structure of the boundary map-derived parcellation closely corresponds with the previously described network structure of the brain. Top: communities identified with the Infomap community detection procedure using the boundary map-derived parcels as network nodes. See the text for names of each colored community. Middle: the network structure of the brain calculated using every voxel as a network node (Power et al. 2011). Bottom: spatial overlap of the parcel- and voxel-wise community assignments.

Use of parcels in individual subjects

We examined how similar the group-average parcel connectivity patterns were to the connectivity patterns seeded from the same parcel in each individual. Across all subjects and parcels, the average Fisher transformed spatial correlation (Z(r)) between subject and group connectivity patterns was .57 ± .15. However, we observed that the average Z(r) across parcels was not uniform across subjects, ranging from .34 to .69. We tested whether this variability was related to how much data had been collected on a subject. We observed a nonlinear relationship between the number of timepoints analyzed and the average subject-group Z(r) across parcels (Figure 7, left). The average Z(r) for 84 subjects with less than 300 uncensored timepoints (12.5 min) ranged from .35 to .64, with 48 subjects having a Z(r) less than .55, but the average Z(r) for 36 subjects with more than 300 uncensored timepoints ranged from .56 to .68.

We also observed that subject-group Z(r)s were not uniform across different parcels, ranging from .32 to .73 (Figure 7, top right). Specifically, parcels in medial occipital cortex, lateral and medial parietal cortex, insular cortex, medial prefrontal cortex, and pre/postcentral gyrus tended to have a Z(r) around .6 or above, with parietal Default mode parcels (posterior cingulate/precuneus and angular gyrus) having the highest Z(r), around .7. When analysis was restricted to the 36 subjects with more than 300 timepoints, Z(r) values increased in 355 of 356 parcels; however, the spatial pattern of Z(r) across parcels did not change (Figure 7, bottom right). This suggests that including subjects with insufficient data reduces the reliability of parcel connectivity estimates globally rather than in specific parcels.

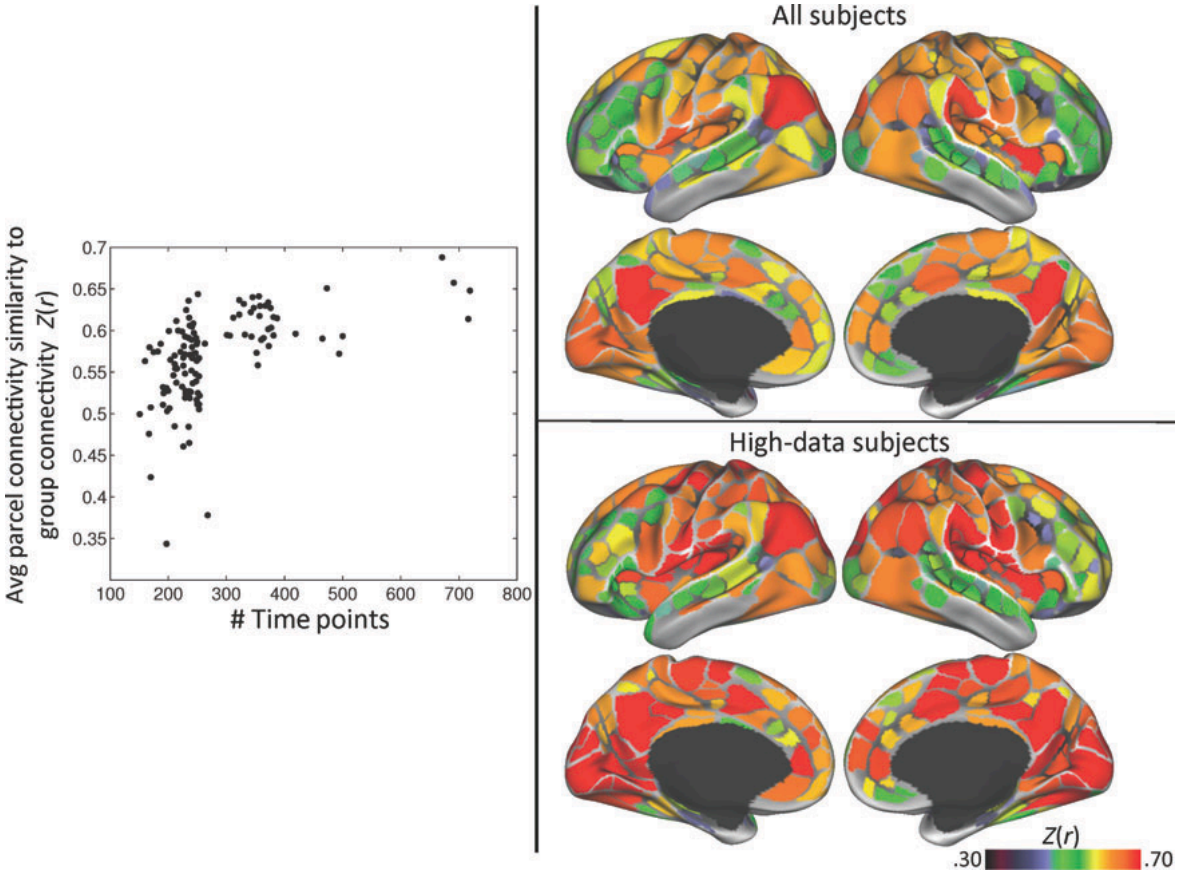

Figure 3-7. Group-average parcel connectivity is similar to subject-level connectivity, but this similarity varies across parcels and subjects. Left: the average Fisher-transformed correlation between group- and subject-level parcel connectivity patterns for each subject, plotted against the number of time points in each subject's resting-state data. Top right: the average group–subject correlation for each parcel, averaged across all subjects. Bottom right: the average group–subject correlation for each parcel, averaged across subjects with >300 time points (12.5 min) of resting-state data.

3.5 **Discussion**

In this study we described a method for building discrete parcels from RSFC boundary maps. We also described a homogeneity-based metric to evaluate the quality of the parcellation, and we demonstrated that the boundary map-derived parcels were highly homogenous. We found that the parcellation was significantly more homogenous than size and shape-matched random parcellations in two independent datasets. We also found that the boundary map-derived parcellation had higher overall homogeneity and performed better relative to random parcellations than a number of alternative parcellations. We additionally observed a high degree of overlap between the boundary map-derived parcels and several known cytoarchitectonic areas, with subdivisions within the cytoarchitectonic areas corresponding to functional differences. We further examined the network structure of the boundary map-derived parcels, and we found that it closely matched the previously described voxelwise structure of the brain. Finally, we observed that boundary-derived parcel connectivity patterns were mostly reliable across individual subjects.

There are good a priori reasons to believe that RSFC boundary maps have real utility for areal parcellation of human cortex. First, RSFC-based techniques are noninvasive and can be applied to any subject population that does not exhibit severe movement during scanning. Second, RSFC is believed to represent some combination of direct and indirect structural connectivity (Honey et al., 2009; Vincent et al., 2007) and a statistical history of functional coactivations (e.g., Dosenbach et al., 2007); as such, it reflects some combination of a region's function and connectivity, which are two of the major measures proposed to dissociate cortical areas (Felleman & Van Essen,

1991). Third, RSFC boundary maps in particular have been shown to not only identify where RSFC patterns change, but also to correspond with task activation patterns and to known areal borders based on architectonic divisions (Wig et al. 2014b). This cross-modality validation indicates that strong RSFC boundaries are very likely to index cortical area divisions in many cases.

Boundary Map-Based Parcellation Generates Parcels that Conform to Cytoarchitectonic Areas

We observed that the boundary map-derived parcellation contained parcels that had very strong overlap with the known extent of area 17, as defined by Fischl et al. (2008) and mapped to the cortical surface by Van Essen et al. (2012). Other known cortical areas, such as somatomotor areas 2, 3, and 4, were overlapped by a combination of several parcels. These observations—that parcel borders conform to cytoarchtectonically-based estimates of human cortical areas—lend substantial face validity to the parcellation.

However, the fact that somatomotor areas were subdivided into multiple parcels suggests that the present parcellation does not faithfully replicate all architectonic areas, but may instead over-parcellate some areas. We predicted that over-parcellation would be most likely to occur in topographically organized architectonic areas, such as somatomotor cortex, that are known to have subregions with dissociable functional responses (Rao et al., 1995), including dissociable RSFC responses (Long et al., 2014). Indeed, over-parcellation based on function is the most likely explanation for the subdivisions within somatomotor areas, as we observed that at least some of those

subdivisions were functionally relevant, conforming to the boundaries between different functional activation patterns resulting from motor movements of different body parts. The present boundary map-derived parcellation should thus be considered a functional parcellation; as such, it provides complementary information about brain organization that cannot be observed via anatomy.

By contrast, area hOc5 (also known as the MT+ complex) was only moderately well-matched by a too-large parcel in the left hemisphere, and did not match any parcel in the right hemisphere. This failure to parcellate the area may be related to the known individual variability in hOc5 (Malikovic et al. 2007), which is greater than that of any other area investigated here (Van Essen et al., 2012). Inconsistent locations of cortical areas across subjects would reduce the likelihood that the boundary mapping procedure can successfully identify the area's border.

In total, the boundary map-derived parcellation consisted of 422 discrete parcels. This number of parcels falls above the range of 150 to 200 human cortical areas per hemisphere estimated by Van Essen et al. (2012). It is possible that, like the somatomotor cortex, various other architectonic cortical areas may be functionally subdivided by the present parcellation, resulting in an inflated number of parcels.

Boundary Map-Based Parcellation Generates Parcels that are Functionally Homogenous

Overall, the boundary-derived parcels had highly homogenous RSFC patterns, with an average parcel homogeneity of almost 90%. This high degree of homogeneity in

RSFC patterns indicates that most parcels represented regions of uniform BOLD signal, which is an expected characteristic of most cortical areas.

Only a few parcels had low homogeneity (see Figure 3). Some of these parcels—e.g., in medial and anterior inferior temporal lobe, and in inferior insula—were near low-SNR areas, and may have had somewhat degraded signal; thus, low homogeneity is not surprising in these parcels. Other parcels—in right angular gyrus, right occipital cortex, bilateral occipitotemporal cortex, and left frontal eye fields—more likely represent local failures of the RSFC boundary mapping procedure, in which a true border between cortical areas was not successfully delineated.

Homogeneity-based Parcellation Evaluation Must Account for Parcel Size and Shape

The boundary map-derived parcels were not only highly homogenous, they were also much more homogenous than a null model consisting of 1000 identical parcellations that were randomly rotated into a new position on the cortical surface. The use of a null model is necessary for true evaluation of a parcellation, as the homogeneity measure of a given parcel is strongly dependent on the parcel's size (see Figure 3 and Supplemental Figures 4 and 5). A similar effect was reported by Craddock et al. (2012), who found that the homogeneity of both clustering-derived and random parcels varied strongly as a function of the number of clusters specified (which will vary inversely with parcel size). By examining homogeneities of individual parcels, we show that this effect is specifically driven by parcel size; this can be appreciated by examination of the parcel size vs homogeneity plots of the randomly rotated parcels

(gray points in Fig 3; black points represent the mean homogeneity across rotations). As discussed in the Methods, this effect likely arises because small randomly placed parcels are more likely to fall within large homogenous regions such as the medial posterior parietal cortex, while large randomly placed parcels are more likely to sprawl across multiple cortical areas. The effect of parcel size is also likely constrained by the smoothness of the data, which is affected by averaging across variable subjects, the application of geodesic Gaussian smoothing during data processing, and the intrinsic spatial autocorrelation of the BOLD signal. If these explanations are correct, then a parcel's homogeneity will depend not only on its size, but also on the regularity of the parcel's shape, as an elongated parcel is more likely to sprawl across multiple cortical areas and extend beyond the intrinsic smoothness of the data than a circular parcel with the same surface area. This means that any appropriate null model of homogeneity must account both for a parcel's size and its shape. Of previously published RSFC-based parcellation approaches, only Craddock et al. (2012) compared their parcellation to a null model; however, that null model was simply the same number of randomly generated parcels. That null model thus maintains the average parcel size, but it does not attempt to match these sizes on a parcel-to-parcel basis or to maintain the shape of parcels, as the present null model does.

Boundary Map-Derived Parcellation Performs Better Than Alternative Parcellations

We tested the homogeneity of the boundary map-derived parcellation using a second dataset, such that the parcel creation procedure was completely independent of

the data in which it was tested. We found that the parcellation was still highly homogenous, and still much more homogenous than its null model, suggesting that these boundary map-derived parcels represent a robust central tendency of the population and can be applied to other datasets, even ones collected with different sequences on different scanners. Further, the boundary map-derived parcellation was both more homogenous and more homogenous compared to its null model than any other putative areal-level parcellation tested, suggesting that it better represents functionally homogenous cortical areas than any of the other parcellations.

Parcellations derived from network detection approaches (the clustering-based approach proposed by Yeo et al. (2011) and the community detection procedure described in Power et al. (2011)) performed reasonably well when compared to their null models (particularly the Yeo parcellation), suggesting that these parcellations contain substantial information about the structure in the data. However, the raw homogeneities of the parcels in this parcellation were only moderate. This likely indicates that these approaches, which are designed to identify large-scale brain systems or networks, do not parcellate the brain finely enough to represent sub-systems-level distinctions between adjacent regions. Such distinctions, as demonstrated by Wig et al. (2014b), likely reflect areal divisions in the brain, as they indicate where multiple regions with similar but discrete connectivity patterns interact within larger systems. The fact that such divisions are not reflected in the Yeo and Power parcellations indicates that those parcellations are closer to systems-level divisions of the brain than true parcellations of cortical areas.

Parcellations based on the NCUT criterion (Craddock et al., 2012, Shen et al., 2013) were moderately homogenous; however, the Shen parcellation was only marginally more homogenous than its null model, while the Craddock parcellation was not more homogenous than its null model. This poor performance on a homogeneity-based measure is surprising, given that clustering techniques such as these are designed to group similar signals together, which in theory should produce homogenous parcels. Blumensath et al. (2013) recently argued that parcels produced using the NCUT criterion described in Craddock et al. (2012) are dependent primarily on the specified cluster number rather than on the underlying data, as highly reproducible NCUT parcels could be produced using random data. The present results are a further demonstration that NCUT-derived parcels do not represent the underlying data structure well.

The Brodmann parcellation (Brodmann, 1909) had low homogeneity, but was more homogenous than any of its null model parcellations. This suggests that, like the Yeo and Power parcellations, this parcellation does successfully represent structure in the data, but is too under-parcellated to represent true cortical areas. This perspective agrees with modern attempts to anatomically parcellate human cortex, which frequently observe more fine-grained architectonic divisions than those reported by Brodmann (e.g., Morris et al. 2000, retrosplenial cortex; Öngür et al. 2003, orbitofrontal cortex; Morosan et al. 2005, superior temporal gyrus; Caspers et al. 2006, inferior parietal cortex; Scheperjans et al. 2008, superior parietal cortex; Kujovic et al. 2013, extrastriate visual cortex).

The AAL parcellation (Tzourio-Mazoyer et al. 2002) had the lowest homogeneity of all parcellations and was not better than its null model. Indeed, there was no expectation that the AAL parcellation would represent the structure of RSFC data, as previous work has indicated that AAL regions are worse than RSFC-based parcellation schemes at representing cortical areas (Craddock et al. 2012; Blumensath et al. 2013; Shen et al. 2013).

The Power ROIs (from Power et al., 2011) had both high homogeneity and were significantly better than all null model parcellations. These ROIs, which were derived partly from an earlier, less precise version of the present boundary mapping procedures, have been used in the field for a variety of purposes, including investigation of motion-related artifacts (Power et al. 2012), functional connectivity dynamics (Glerean et al. 2012), task control processes (Cole et al. 2013), and deficits related to neuropsychological disorders such as Autism (Rudie et al. 2013), attention deficit hyperactivity disorder (Eloyan et al. 2012), and schizophrenia and bipolar disorders (Argyelan et al. 2014). The present results suggest that these ROIs are reasonable estimates of cortical area centers, though not of full cortical areas, as they do not attempt to define the boundaries of areas.

One other RSFC-based whole-brain areal parcellation scheme has recently been proposed (Blumensath et al. 2013), but we were not able to compare this scheme against the present boundary map-derived parcellation, as it was never applied to group average data. Blumensath et al. reported that subject-level parcels could be created using a region growing approach constrained by hierarchical clustering. Further, they reported that, compared to parcels derived using the NCUT technique (Craddock et al.

2012), these parcels were more reliable, better represented RSFC pattern transitions, and better aligned with task activation patterns. However, it is unclear if this method could produce reasonable group average parcels.

Parcel-based Network Structure Corresponds With Voxelwise Network Structure

We used a community detection procedure (Infomap; Rosvall and Bergstrom et al., 2008) to identify the network structure of boundary map-derived parcels, and we compared it to the previously described network structure of the brain defined using every voxel in the brain as a node (the “Power communities” described above; Power et al., 2011). Every community found in the Power communities was also observed in the parcel communities except for one in anterior medial temporal lobe. These included a number of large, highly replicated communities such as the Default, Fronto-parietal, and Cingulo-Opercular communities. They also included smaller communities, such as a retrosplenial/temporal community, a cingulate-precuneus community, and a superior temporal lobe community, which have been identified only recently using advanced network analysis techniques (Power et al., 2011; Yeo et al., 2011). The observation that parcel-based communities replicate both large, easily detected RSFC systems and small, subtle RSFC systems indicates that the present parcellation captures the overall network structure of the brain in considerable detail. The fact that this detailed structure is represented without the need for voxel level granularity suggests that the present parcellation is appropriate for use in certain network analyses, such as graph theory

analysis, which benefit from a limited number of rational, neurobiologically-based nodes in order to be interpretable (Power et al., 2013; Wig et al., 2011).

One additional community was observed in the parcel-wise analysis that has not been observed in previous work: a community in the marginal sulcus and frontal eye fields (magenta in Figure 6). These areas were incorporated into the Cingulo-opercular and Dorsal attention systems, respectively, in the Power communities. We are not aware of any work demonstrating that these regions operate as a coherent unit; by contrast, it is well established that the frontal eye fields are a central node of the Dorsal attention system (Corbetta and Shulman 2002). Further, we observed that this community only emerged at relatively sparse thresholds; at more dense thresholds, it was split and incorporated into Cingulo-opercular and Dorsal attention communities, as in the Power voxelwise communities (see Supplemental Figure 7). We thus speculate that this newly observed community may represent an over-separation of existing communities rather than a real brain system.

Most Group-Defined Parcels Reliably Represent Individual Subject Connectivity, Especially for High-Data Subjects

An important goal of this work is to create parcels representing cortical areas that can be interrogated in individual subject data. Conducting fMRI analysis in a parcel-wise fashion is an ideal form of data reduction (Wig et al. 2011), as it involves analyzing several hundred relatively independent, homogenous parcel-averaged signals rather than 65,000+ noisy, non-independent voxel signals. In principle, applying these parcels to subject-level task analysis would thus not only decrease the need for multiple

comparisons correction, but would greatly increase the power of the analysis, as averaging a homogenous signal across a parcel would reduce noise levels. We examined whether the boundary map-derived parcels could be used for individual subject analysis. We found that on average, subject connectivity maps had high spatial correlations to group level maps, suggesting that in general, extracting and averaging subject-level data from a group-average parcel is a valid approach.

However, we also observed that this degree of similarity was not uniform across subjects and parcels. For a given subject, connectivity similarity with the group was observed to be strongly and nonlinearly related to the amount of data the subject retained after motion censoring: subjects with greater than 12.5 minutes of data had high average similarity to the group, while subjects with less than 12.5 minutes of data were variable in how similar they were to the group. This finding emphasizes the need to acquire large amounts of data for reliable RSFC estimates, which has been well characterized by Anderson et al. (2011), who similarly demonstrated nonlinear effects of scanning time on RSFC reliability. Specifically, they found that reliability increased as 1/sqrt(scanning time). A similar relationship may be present in the current data, though we found that fitting this curve to the scanning time/group similarity relationship explained only about 33% of the variance in group similarity, so we hesitate to draw any strong conclusions about the nature of this effect.

A number of parcels were observed to have high homogeneity, indicating that the parcel was well-formed in the group, but nevertheless had relatively low subject-group similarity. The most likely explanation for this phenomenon is inter-individual variability in functional connectivity. Indeed, the locations of the most variable parcels—in lateral

prefrontal cortex and lateral temporal-occipital cortex (green and purple in Figure 3)—correspond to regions previously reported to have particularly high inter-subject variability in RSFC patterns (Mueller et al. 2013). While most boundary map-derived parcels are appropriate for subject-level data analysis, these few parcels may be too variable for such a purpose. Ideally, issues of inter-subject variability could be avoided by creating single-subject parcels from subject-level boundary mapping. In theory, such subject-level parcels could then be matched to each other for averaging or comparison across subjects; this procedure would constitute an areal-level registration. Blumensath et al. (2013) previously demonstrated that whole brain parcellations can be created at the individual subject level, though in that work no attempt was made to match parcels to each other across subjects, which would be needed for true parcel-level cross-subject analysis. Future work may explore the feasibility and utility of subject-level parcel matching.

Limitations

While this parcellation scheme is homogenous, replicates the network structure of the brain well, and has similar connectivity patterns across individuals, it may not yet constitute a truly reliable whole-brain parcellation. Most parcels are highly homogenous, but some (e.g. in lateral occipital cortex) appear to be inaccurate and/or under-parcellated. Other regions may be somewhat over-parcellated. For example, while the parcellation describes some subdivisions in somatomotor cortex that correspond with functional activation patterns, other subdivisions have no known functional relevance, and they divide the motor and somatosensory strips into an arguably implausible

number of parcels. It is likely that more accurate parcellations addressing these issues may be generated in the future as higher resolution datasets with more per-subject timepoints become available.

It should also be noted that the present approach results in a purely functional parcellation that, while containing substantial information about the location and extent of anatomical cortical areas, nevertheless does not perfectly converge with a true anatomical areal parcellation. Indeed, the topological functional organization of some cortical areas makes it unlikely that specific anatomical area boundaries could ever be derived from purely functional measures like RSFC. In their classic parcellation of macaque visual cortex, Felleman and Van Essen (1991) remark that ideally, each cortical area should be uniquely identifiable using any of several modalities (connectivity, architectonics, topographic organization, functional responses, or behavioral consequences of lesions). In practice, they found that not every area could be identified using every method; often only one or two of these methods dissociated a specific area. This suggests that comprehensive categorization of all cortical areas in the human cortex will require further data from additional modalities.

Conclusions

Here we demonstrate that parcels created from RSFC boundary maps overlap with known architectonic areas and have highly homogenous connectivity patterns. We also demonstrate that these parcels are far more homogenous than a null model in two independent datasets, indicating that the parcellation not only captures the structure of the data, but that it generalizes across different subject pools, scanners, and scanning

sequences. Further, no other parcellation tested was as homogenous or had as large a homogeneity difference compared to its null model. The proposed parcellation scheme thus appears to better represent functional divisions within the human brain than any other RSFC-based parcellation scheme yet published. A modified version of this parcellation created by combining both datasets (Supplemental Figure 10) is publically available at http://www.nil.wustl.edu/labs/petersen/Resources.html.

3.6 Acknowledgements

This work was supported by the National Institutes of Health (grant numbers NS061144 to S.E.P.; DA022582, MH059282, HL114092, and AA021347 to W.M.K.; MH100872 to T.O.L; and MH091657 to David Van Essen); the McDonnell Foundation (Collaborative Action Award to S.E.P.); and the Simons Foundation (Award 95177 to S.E.P.).

3.7 Supplementary Figures

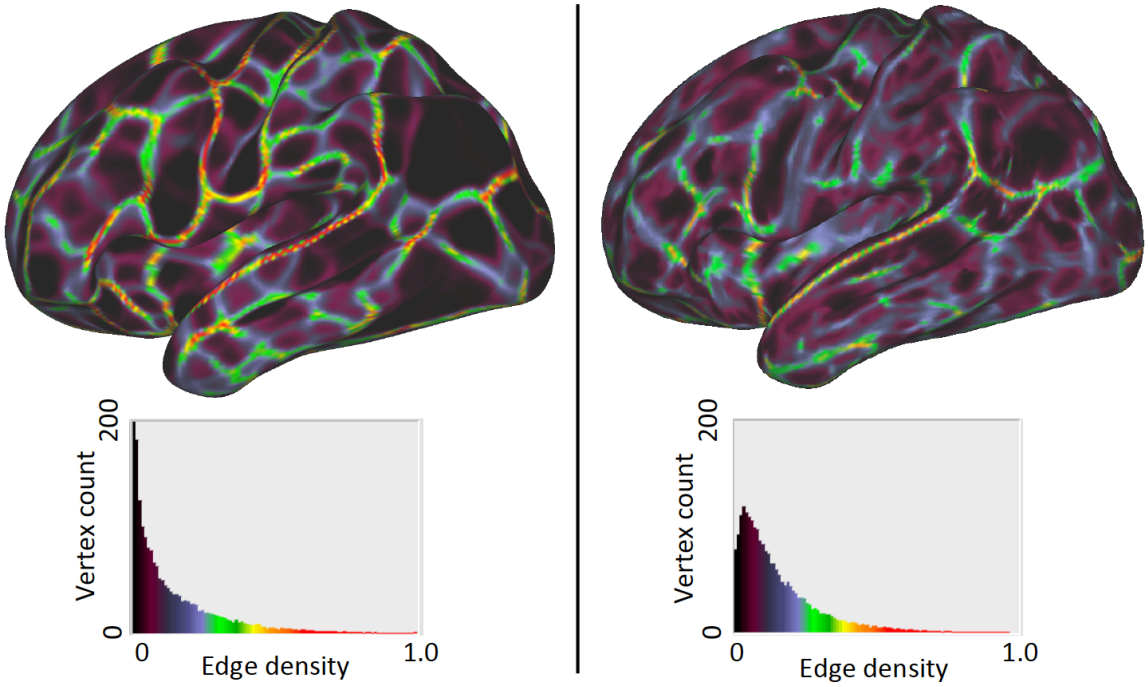

Supplementary Figure 3-1. Improved RSFC boundary mapping procedures reduce noise in boundary maps, resulting in stronger edges and "deeper" non-edge areas. Left: boundary map (top) and histogram of boundary map values (bottom) created using procedures described in the main text. Right: boundary map (top) and histogram of boundary map values (bottom) created using procedures from Wig et al. (2013).

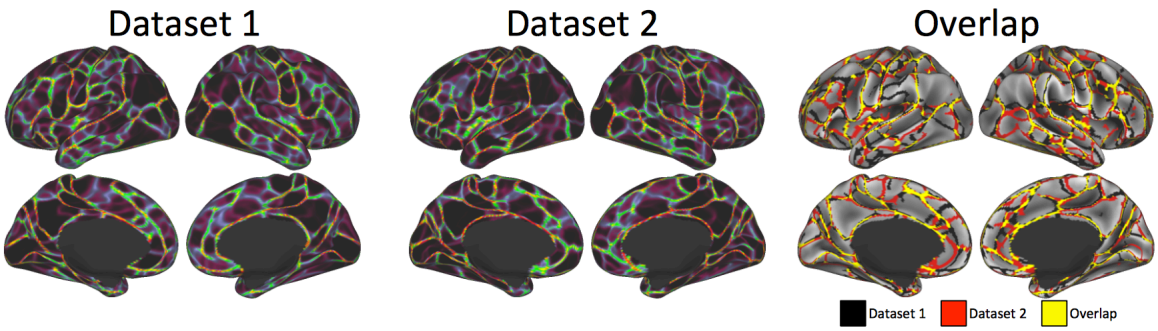

Supplementary Figure 3-2. Boundary maps from Dataset 1 (left) and Dataset 2 (middle) are highly similar. Right: overlap between boundary maps from Datasets 1 and 2 after thresholding both at the 75th percentile of boundary map values. Black: Dataset 1 boundaries; red: Dataset 2 boundaries; yellow: boundaries overlapping between datasets.

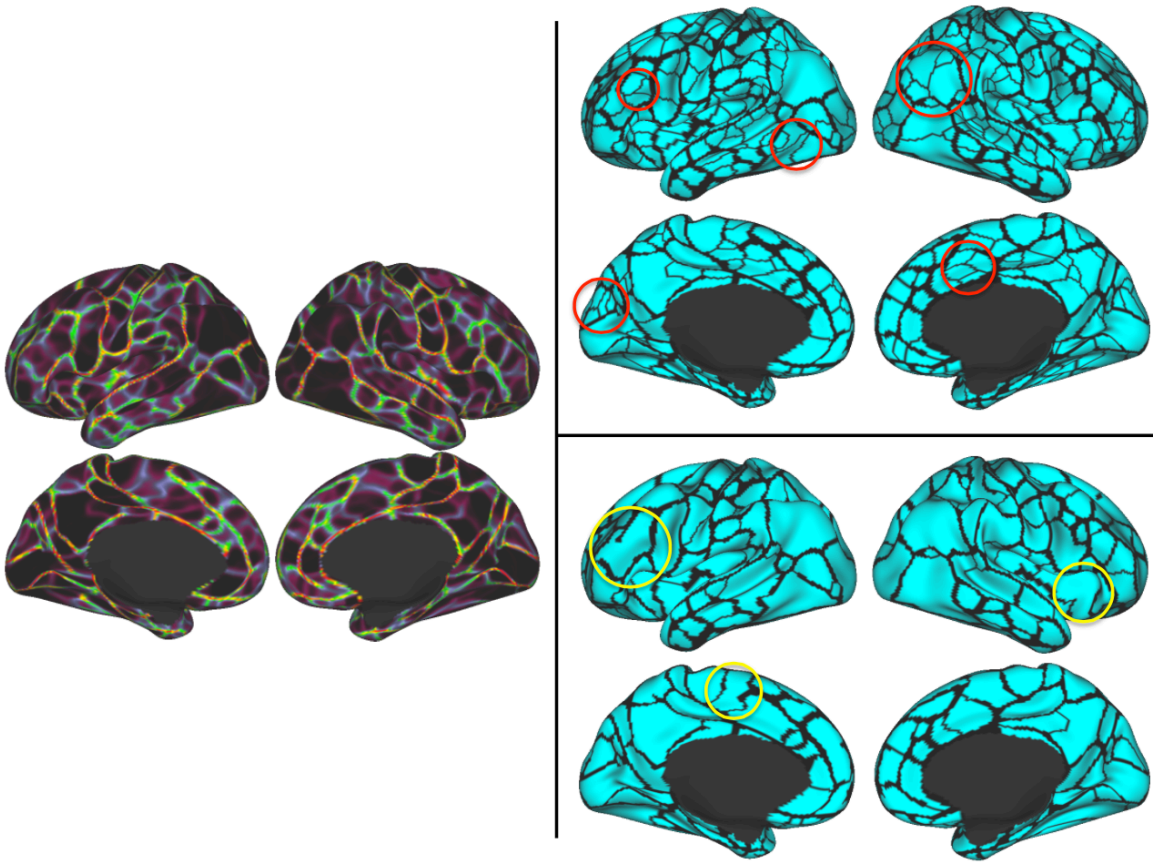

Supplementary Figure 3-3. Parcels created using other thresholds for parcel merging do not well-fit the features of the boundary map. Left: boundary map. Top right: parcels created using the 20th percentile of boundary map values as a merge threshold. Many regions appear over-parcellated (red circles). Bottom right: parcels created using the 70th percentile as a merge threshold. Many regions appear under-parcellated (green circles).

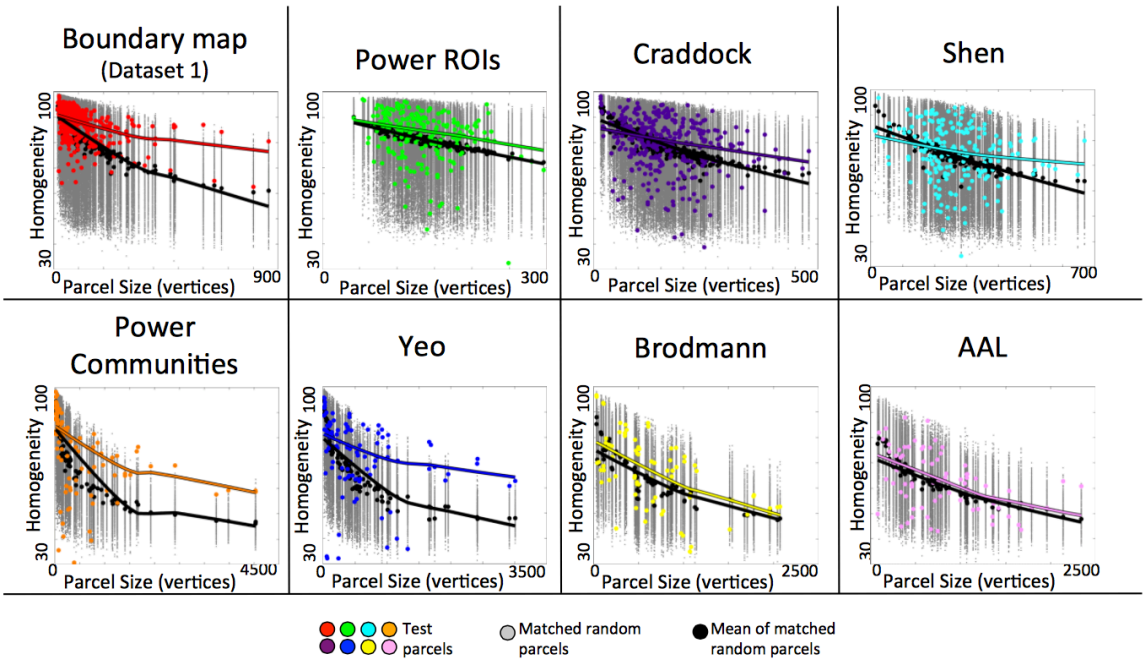

Supplementary Figure 3-4. Parcel homogeneity is dependent on parcel size across all parcellation schemes tested. Colored dots in each plot indicate the homogeneities of the tested parcels. Gray dots indicate the homogeneities of null model versions of each parcel (rotated to a different cortical location), while black dots indicate the means of the null model parcel homogeneities. Colored and black lines represent lowess fit curves of the real parcel homogeneities and null model parcel homogeneities, respectively.

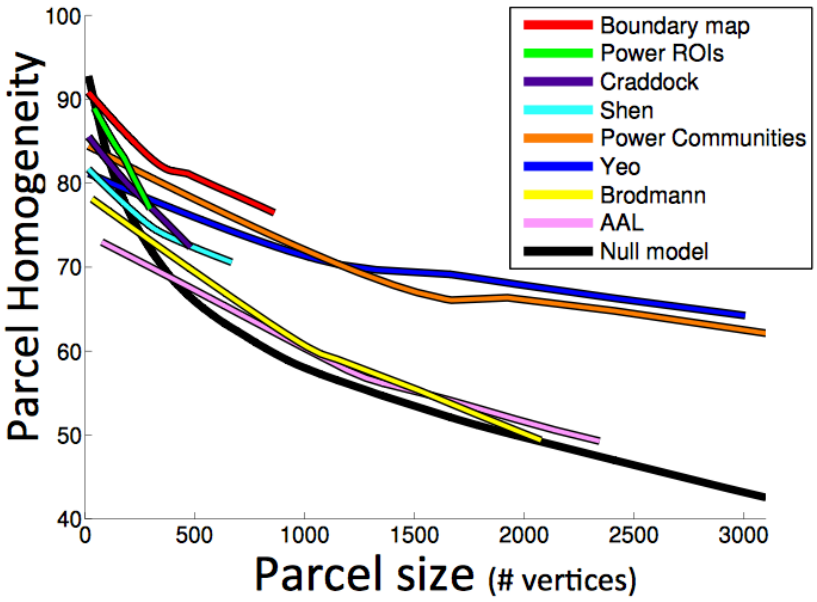

Supplementary Figure 3-5. Boundary map-derived parcels are the most homogenous even when parcel size is taken into account. Colored lines indicate lowess fit curves of parcel homogeneities against parcel size (as in Supplementary Figure XX); black line indicates fit curve of null model parcels from all parellations. The boundary map-derived parcel

homogeneities depend on parcel size, but the fit curve is elevated above the curve of every other alternative parcellation scheme.

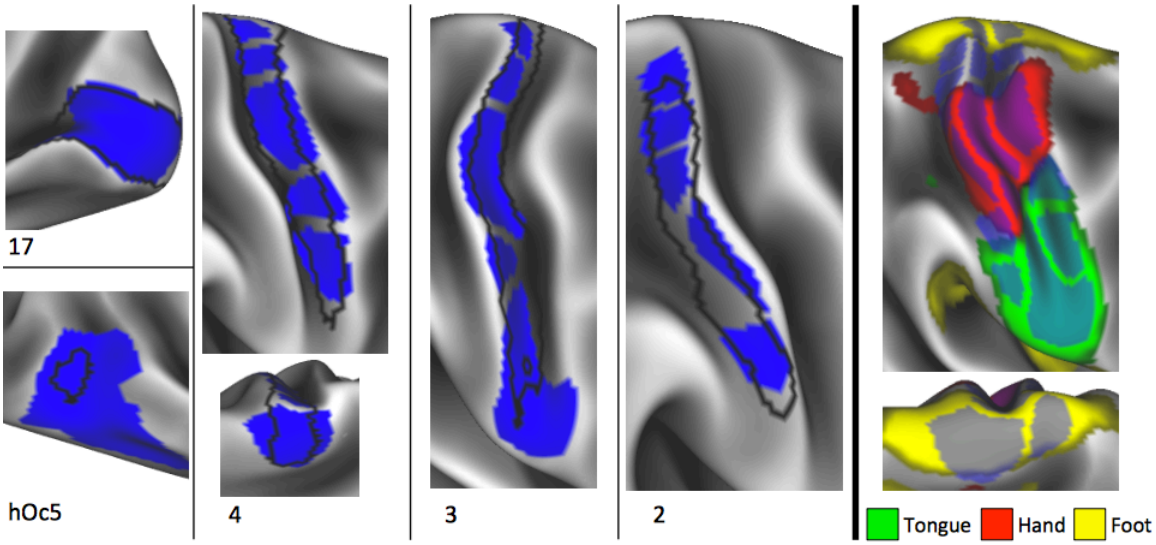

Supplementary Figure 3-6. Boundary map-derived parcels match known cortical areas and functional activation patterns in the right hemisphere. Left and middle: a variety of cytoarchitectonically-defined cortical areas (Fischl et al., 2008) were matched by boundary map-derived parcels. Area 17 overlapped very well with one parcel, but area hOc5 did not overlap well with any parcel. Area 2, 3, and 4 overlapped with several adjacent parcels. Right: parcel divisions within cytoarchitectonic areas 2, 3, and 4 corresponded with divisions between activation clusters from motor movements of the left foot, left hand, and tongue (Barch et al., 2013).

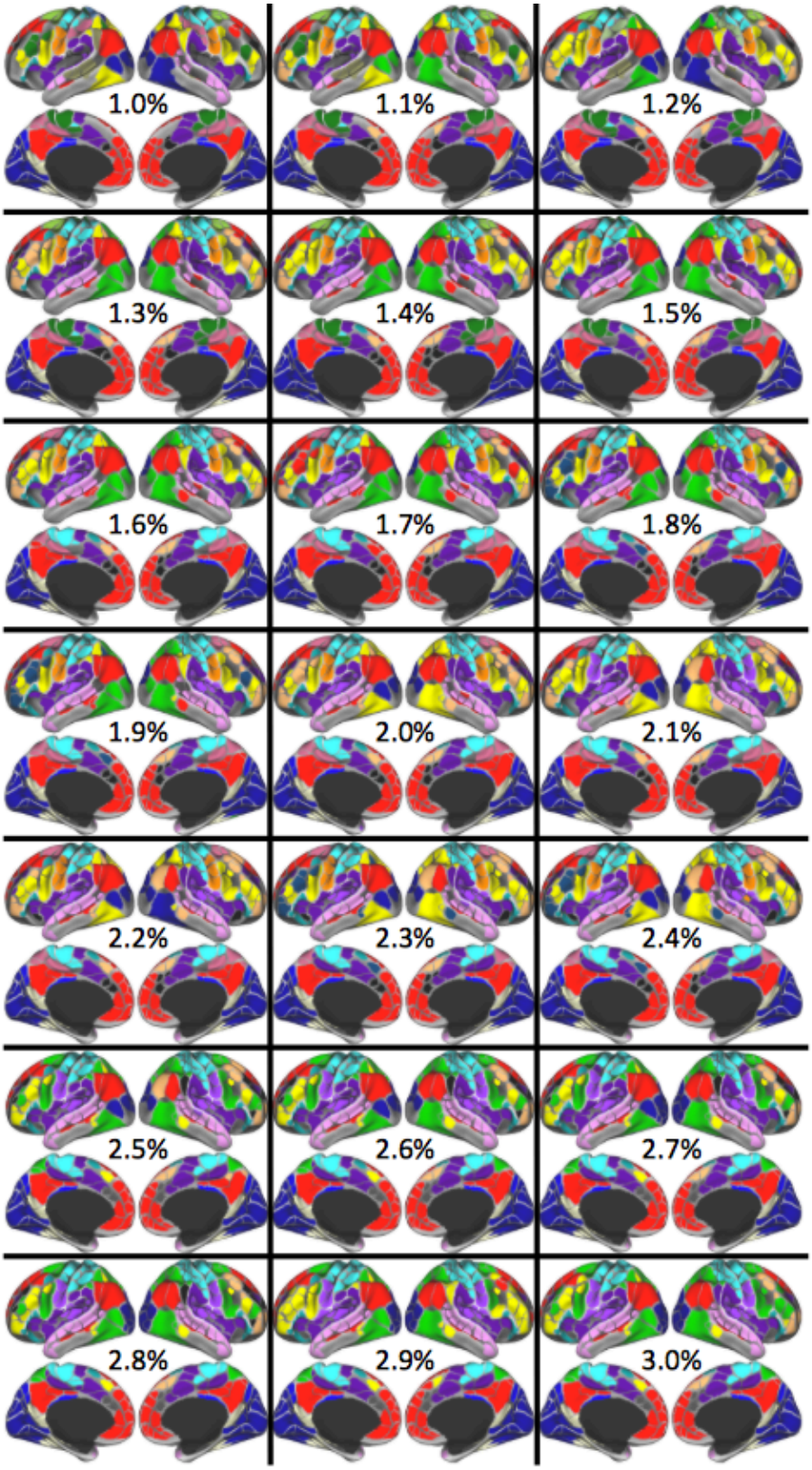

Supplementary Figure 3-7. Infomap community assignments at every network density threshold tested, from 1.0% to 3.0%.

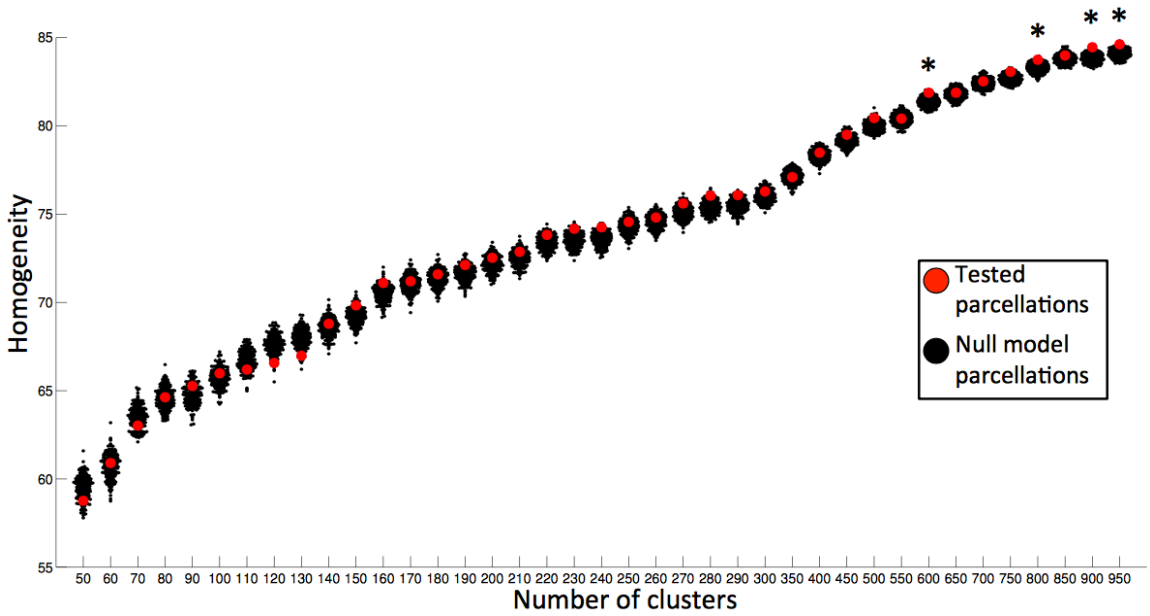

Supplementary Figure 3-8. Most parcellations created by Craddock et al. (2012) are not significantly homogenous compared to 200 iterations of a tailored null model, across different numbers of clusters. Red dots indicate mean parcel homogeneity for a given parcellation with cluster number indicated by the x-axis; black dots indicate mean homogeneity of each null model iteration. * indicates p<.05 (i.e., mean parcel homogeneity was better than homogeneities from at least 190 null model iterations). No tested parcellations were more homogenous than all null model iterations.

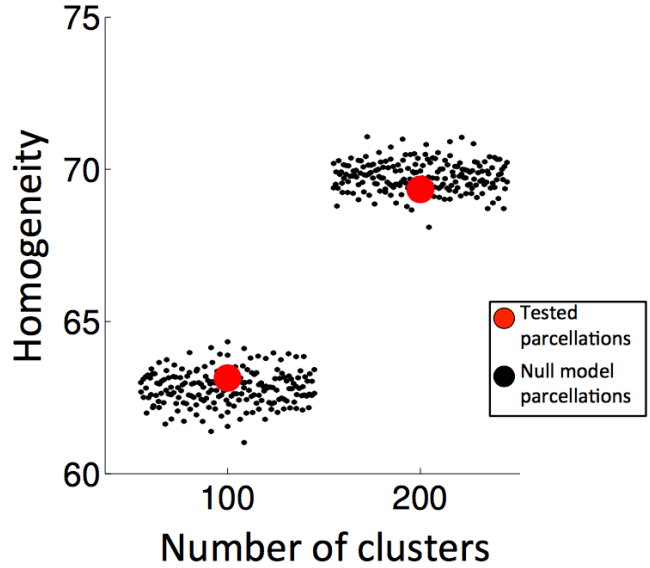

Supplementary Figure 3-9. Parcellations created by Shen et al. (2013) with cluster numbers 100 and 200 are not significantly homogenous compared to 200 iterations of a tailored null model. Red dots indicate mean parcel homogeneity for a given parcellation with cluster number indicated by the x-axis; black dots indicate mean homogeneity of each null model iteration. Neither tested parcellation reached significance (i.e. was more homogenous than at least 190 null model iterations).

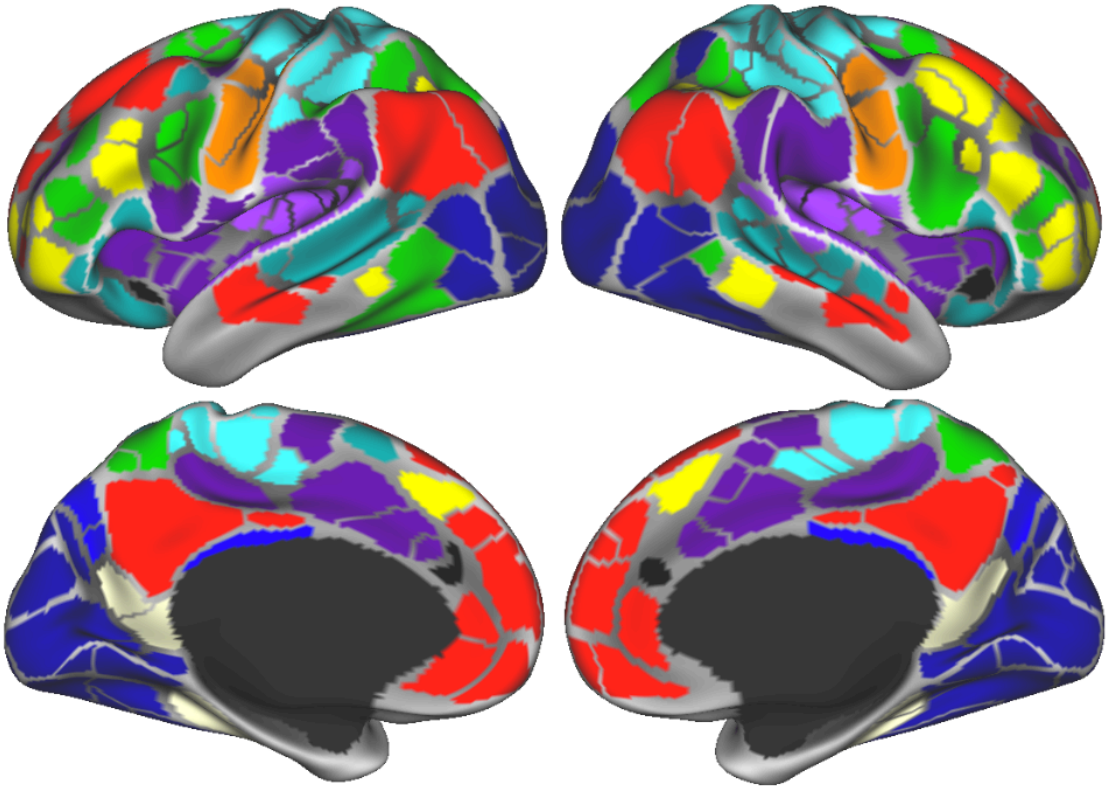

Supplementary Figure 3-10. Parcellation derived by combining Datasets 1 and 2 and applying the boundary mapping procedure to the combined dataset. Colors represent the community structure of the parcellation calculated using the infomap procedure, with the same color mapping described in the main text. This parcellation is publically available at http://www.nil.wustl.edu/labs/petersen/Resources.html.

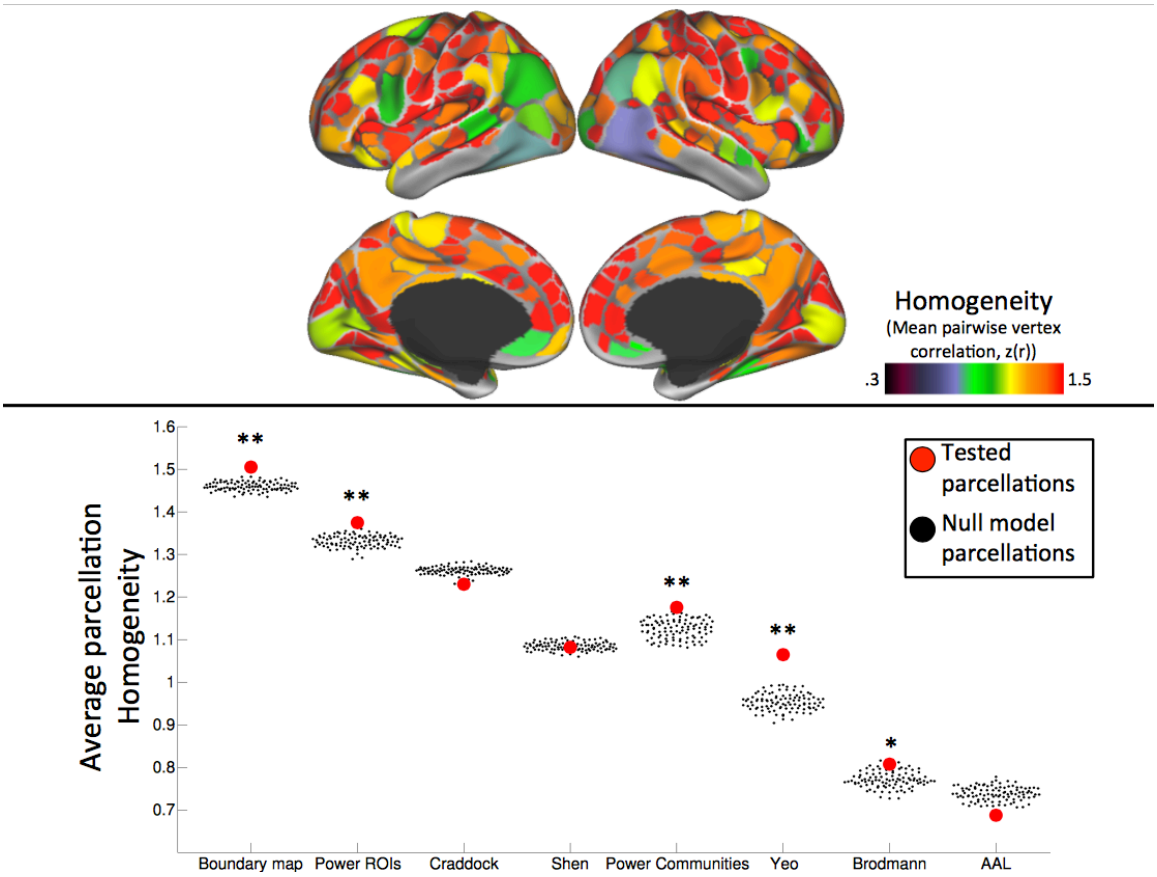

Supplementary Figure 3-11. When tested in Dataset 2 using a previously devised homogeneity metric (from Craddock et al., 2012), results are very similar to results obtained using the PCA-based homogeneity metric. Top: the spatial distribution of boundary map-derived parcel homogeneities is very similar to those obtained from the PCA-based homogeneity metric (top left of Figure 4, main text). Bottom: the average homogeneity across parcels of each parcellation (red dots) compared to the average homogeneity across parcels of each of 100 null model iterations (black dots) demonstrated a pattern very similar to that obtained from the PCA-based homogeneity metric (bottom of Figure 4, main text). ** indicates the parcellation was more homogenous than all of its 100 null model iterations (i.e., $p<.01$); * indicates the parcellation was more homogenous than at least 95 of its null model iterations ($p<.05$).

3.8 References

Amunts K, Malikovic A, Mohlberg H, Schormann T, Zilles K. 2000. Brodmann's areas 17 and 18 brought into stereotaxic space—where and how variable? Neuroimage. 11:66–84.

Anderson JS, Ferguson MA, Lopez-Larson M, Yurgelun-Todd D. 2011. Reproducibility of single-subject functional connectivity measurements. AJNR Am J Neuroradiol. 32:548–555.

Argyelan M, Ikuta T, DeRosse P, Braga RJ, Burdick KE, John M, Kingsley PB, Malhotra AK, Szeszko PR. 2014. Resting-State fMRI Connectivity Impairment in Schizophrenia and Bipolar Disorder. Schizophr Bull. 40:100–110.

Barch DM, Burgess GC, Harms MP, Petersen SE, Schlaggar BL, Corbetta M, Glasser MF, Curtiss S, Dixit S, Feldt C, Nolan D, Bryant E, Hartley T, Footer O, Bjork JM, Poldrack R, Smith S, Johansen-Berg H, Snyder AZ, Van Essen DC. 2013. Function in the human connectome: Task-fMRI and individual differences in behavior. NeuroImage, Mapping the Connectome. 80:169–189.

Barnes KA, Nelson SM, Cohen AL, Power JD, Coalson RS, Miezin FM, Vogel AC, Dubis JW, Church JA, Petersen SE, Schlaggar BL. 2012. Parcellation in Left Lateral Parietal Cortex Is Similar in Adults and Children. Cereb Cortex. 22:1148–1158.

Beckmann CF, DeLuca M, Devlin JT, Smith SM. 2005. Investigations into resting-state connectivity using independent component analysis. Philos Trans R Soc Lond B Biol Sci. 360:1001–1013.

Beucher S, Lantuejoul C. 1979. Use of watersheds in contour detection.

Biswal BB, Mennes M, Zuo X-N, Gohel S, Kelly C, Smith SM, Beckmann CF, Adelstein JS, Buckner RL, Colcombe S, Dogonowski A-M, Ernst M, Fair D, Hampson M, Hoptman MJ, Hyde JS, Kiviniemi VJ, Kötter R, Li S-J, Lin C-P, Lowe MJ, Mackay C, Madden DJ, Madsen KH, Margulies DS, Mayberg HS, McMahon K, Monk CS, Mostofsky SH, Nagel BJ, Pekar JJ, Peltier SJ, Petersen SE, Riedl V, Rombouts SARB, Rypma B, Schlaggar BL, Schmidt S, Seidler RD, Siegle GJ, Sorg C, Teng G-J, Veijola J, Villringer A, Walter M, Wang L, Weng X-C, Whitfield-Gabrieli S, Williamson P, Windischberger C, Zang Y-F, Zhang H-Y, Castellanos FX, Milham MP. 2010. Toward discovery science of human brain function. Proceedings of the National Academy of Sciences. 107:4734 –4739.

Biswal BB, Yetkin FZ, Haughton VM, Hyde JS. 1995. Functional connectivity in the motor cortex of resting human brain using echo-planar MRI. Magn Reson Med. 34:537–541.

Blumensath T, Jbabdi S, Glasser MF, Van Essen DC, Ugurbil K, Behrens TEJ, Smith SM. 2013. Spatially constrained hierarchical parcellation of the brain with resting-state fMRI. NeuroImage. 76:313–324.

Brodmann K. 1909. Vergleichende Lokalisationslehre der Grosshirnrinde in ihren Prinzipien dargestellt auf Grund des Zellenbaues. Leipzig: Barth.

Bullmore E, Sporns O. 2009. Complex brain networks: graph theoretical analysis of structural and functional systems. Nature Reviews Neuroscience. 10:186–198.

Carmichael S t., Price J l. 1996. Connectional networks within the orbital and medial prefrontal cortex of macaque monkeys. J Comp Neurol. 371:179–207.

Carmichael ST, Price JL. 1994. Architectonic subdivision of the orbital and medial prefrontal cortex in the macaque monkey. J Comp Neurol. 346:366–402.

Carp J. 2013. Optimizing the order of operations for movement scrubbing: Comment on Power et al. NeuroImage. 76:436–438.

Caspers S, Geyer S, Schleicher A, Mohlberg H, Amunts K, Zilles K. 2006. The human inferior parietal cortex: cytoarchitectonic parcellation and interindividual variability. Neuroimage. 33:430–448.

Cohen AL, Fair DA, Dosenbach NUF, Miezin FM, Dierker D, Van Essen DC, Schlaggar BL, Petersen SE. 2008. Defining functional areas in individual human brains using resting functional connectivity MRI. Neuroimage. 41:45–57.

Cole MW, Reynolds JR, Power JD, Repovs G, Anticevic A, Braver TS. 2013. Multi-task connectivity reveals flexible hubs for adaptive task control. Nat Neurosci. 16:1348–1355.

Corbetta M, Shulman GL. 2002. Control of goal-directed and stimulus-driven attention in the brain. Nat Rev Neurosci. 3:201–215.

Craddock RC, James GA, Holtzheimer PE, Hu XP, Mayberg HS. 2012. A whole brain fMRI atlas generated via spatially constrained spectral clustering. Human Brain Mapping. 33:1914–1928.

Dale AM, Fischl B, Sereno MI. 1999. Cortical Surface-Based Analysis: I. Segmentation and Surface Reconstruction. NeuroImage. 9:179–194.

Dale AM, Sereno MI. 1993. Improved Localizadon of Cortical Activity by Combining EEG and MEG with MRI Cortical Surface Reconstruction: A Linear Approach. Journal of Cognitive Neuroscience. 5:162–176.

Damoiseaux JS, Rombouts SA, Barkhof F, Scheltens P, Stam CJ, Smith SM, Beckmann CF. 2006. Consistent resting-state networks across healthy subjects. Proc Natl Acad Sci U S A. 103:13848–13853.

Dosenbach NUF, Fair DA, Miezin FM, Cohen AL, Wenger KK, Dosenbach RAT, Fox MD, Snyder AZ, Vincent JL, Raichle ME, Schlaggar BL, Petersen SE. 2007. Distinct brain networks for adaptive and stable task control in humans. Proceedings of the National Academy of Sciences. 104:11073–11078.

Eloyan A, Muschelli J, Nebel MB, Liu H, Han F, Zhao T, Barber AD, Joel S, Pekar JJ, Mostofsky SH, Caffo B. 2012. Automated diagnoses of attention deficit hyperactive disorder using magnetic resonance imaging. Front Syst Neurosci. 6:61.

Felleman DJ, Van Essen DC. 1991. Distributed Hierarchical Processing in the Primate. Cereb Cortex. 1:1–47.

Fischl B, Rajendran N, Busa E, Augustinack J, Hinds O, Yeo BTT, Mohlberg H, Amunts K, Zilles K. 2008. Cortical Folding Patterns and Predicting Cytoarchitecture. Cereb Cortex. 18:1973–1980.

Fischl B, Sereno MI, Dale AM. 1999. Cortical Surface-Based Analysis: II: Inflation, Flattening, and a Surface-Based Coordinate System. NeuroImage. 9:195–207.

Fox MD, Raichle ME. 2007. Spontaneous fluctuations in brain activity observed with functional magnetic resonance imaging. Nat Rev Neurosci. 8:700–711.

Friston KJ, Williams S, Howard R, Frackowiak RSJ, Turner R. 1996. Movement-Related effects in fMRI time-series. Magn Reson Med. 35:346–355.

Glasser MF, Sotiropoulos SN, Wilson JA, Coalson TS, Fischl B, Andersson JL, Xu J, Jbabdi S, Webster M, Polimeni JR, Van Essen DC, Jenkinson M, WU-Minn HCP Consortium. 2013. The minimal preprocessing pipelines for the Human Connectome Project. Neuroimage. 80:105–124.

Glasser MF, Van Essen DC. 2011. Mapping human cortical areas in vivo based on myelin content as revealed by T1- and T2-weighted MRI. J Neurosci. 31:11597–11616.

Glerean E, Salmi J, Lahnakoski JM, Jääskeläinen IP, Sams M. 2012. Functional Magnetic Resonance Imaging Phase Synchronization as a Measure of Dynamic Functional Connectivity. Brain Connectivity. 2:91–101.

Hirose S, Watanabe T, Jimura K, Katsura M, Kunimatsu A, Abe O, Ohtomo K, Miyashita Y, Konishi S. 2012. Local Signal Time-Series during Rest Used for Areal Boundary Mapping in Individual Human Brains. PLoS ONE. 7:e36496.

Hirose S, Watanabe T, Wada H, Imai Y, Machida T, Shirouzu I, Miyashita Y, Konishi S. 2013. Functional relevance of micromodules in the human association cortex delineated with high-resolution FMRI. Cereb Cortex. 23:2863–2871.

Honey CJ, Sporns O, Cammoun L, Gigandet X, Thiran JP, Meuli R, Hagmann P. 2009. Predicting human resting-state functional connectivity from structural connectivity. Proceedings of the National Academy of Sciences. 106:2035 –2040.

Kujovic M, Zilles K, Malikovic A, Schleicher A, Mohlberg H, Rottschy C, Eickhoff SB, Amunts K. 2013. Cytoarchitectonic mapping of the human dorsal extrastriate cortex. Brain Struct Funct. 218:157–172.

Lancaster JL, Glass TG, Lankipalli BR, Downs H, Mayberg H, Fox PT. 1995. A modality-independent approach to spatial normalization of tomographic images of the human brain. Hum Brain Mapp. 3:209–223.

Lewis JW, Van Essen DC. 2000. Mapping of architectonic subdivisions in the macaque monkey, with emphasis on parieto-occipital cortex. J Comp Neurol. 428:79–111.

Long X, Goltz D, Margulies DS, Nierhaus T, Villringer A. 2014. Functional connectivity-based parcellation of the human sensorimotor cortex. Eur J Neurosci. 39:1332–1342.

Malikovic A, Amunts K, Schleicher A, Mohlberg H, Eickhoff SB, Wilms M, Palomero-Gallagher N, Armstrong E, Zilles K. 2007. Cytoarchitectonic Analysis of the Human Extrastriate Cortex in the Region of V5/MT+: A Probabilistic, Stereotaxic Map of Area hOc5. Cereb Cortex. 17:562–574.

Markov NT, Ercsey-Ravasz MM, Gomes ARR, Lamy C, Magrou L, Vezoli J, Misery P, Falchier A, Quilodran R, Gariel MA, Sallet J, Gamanut R, Huissoud C, Clavagnier S, Giroud P, Sappey-Marinier D, Barone P, Dehay C, Toroczkai Z, Knoblauch K, Essen DCV, Kennedy H. 2014. A Weighted and Directed Interareal Connectivity Matrix for Macaque. Cereb Cortex. 24:17–36.

Miezin FM, Maccotta L, Ollinger JM, Petersen SE, Buckner RL. 2000. Characterizing the Hemodynamic Response: Effects of Presentation Rate, Sampling Procedure, and the Possibility of Ordering Brain Activity Based on Relative Timing. NeuroImage. 11:735–759.

Morosan P, Schleicher A, Amunts K, Zilles K. 2005. Multimodal architectonic mapping of human superior temporal gyrus. Anat Embryol. 210:401–406.

Morris R, Paxinos G, Petrides M. 2000. Architectonic analysis of the human retrosplenial cortex. J Comp Neurol. 421:14–28.

Mueller S, Wang D, Fox MD, Yeo BTT, Sepulcre J, Sabuncu MR, Shafee R, Lu J, Liu H. 2013. Individual Variability in Functional Connectivity Architecture of the Human Brain. Neuron. 77:586–595.

Mugler JP 3rd, Brookeman JR. 1990. Three-dimensional magnetization-prepared rapid gradient-echo imaging (3D MP RAGE). Magn Reson Med. 15:152–157.

Nelson SM, Cohen AL, Power JD, Wig GS, Miezin FM, Wheeler ME, Velanova K, Donaldson DI, Phillips JS, Schlaggar BL, Petersen SE. 2010a. A parcellation scheme for human left lateral parietal cortex. Neuron. 67:156–170.

Nelson SM, Dosenbach NUF, Cohen AL, Wheeler ME, Schlaggar BL, Petersen SE. 2010b. Role of the anterior insula in task-level control and focal attention. Brain Struct Funct. 214:669–680.

Ojemann JG, Akbudak E, Snyder AZ, McKinstry RC, Raichle ME, Conturo TE. 1997. Anatomic localization and quantitative analysis of gradient refocused echo-planar fMRI susceptibility artifacts. Neuroimage. 6:156–167.

Öngür D, Ferry AT, Price JL. 2003. Architectonic subdivision of the human orbital and medial prefrontal cortex. J Comp Neurol. 460:425–449.

Paxinos G, Huang X-F, Toga AW. 2000. The rhesus monkey brain in stereotaxic coordinates. San Diego, CA: Academic Press.

Petersen SE, Fox PT, Posner MI, Mintun M, Raichle ME. 1988. Positron emission tomographic studies of the cortical anatomy of single-word processing. Nature. 331:585–589.

Power JD, Barnes KA, Snyder AZ, Schlaggar BL, Petersen SE. 2012. Spurious but systematic correlations in functional connectivity MRI networks arise from subject motion. NeuroImage. 59:2142–2154.

Power JD, Cohen AL, Nelson SM, Wig GS, Barnes KA, Church JA, Vogel AC, Laumann TO, Miezin FM, Schlaggar BL, Petersen SE. 2011. Functional Network Organization of the Human Brain. Neuron. 72:665–678.

Power JD, Mitra A, Laumann TO, Snyder AZ, Schlaggar BL, Petersen SE. 2014. Methods to detect, characterize, and remove motion artifact in resting state fMRI. NeuroImage. 84:320–341.

Power JD, Schlaggar BL, Lessov-Schlaggar CN, Petersen SE. 2013. Evidence for Hubs in Human Functional Brain Networks. Neuron. 79:798–813.

Rao SM, Binder JR, Hammeke TA, Bandettini PA, Bobholz JA, Frost JA, Myklebust BM, Jacobson RD, Hyde JS. 1995. Somatotopic mapping of the human primary motor cortex with functional magnetic resonance imaging. Neurology. 45:919–924.

Rosvall M, Bergstrom CT. 2008. Maps of random walks on complex networks reveal community structure. PNAS. 105:1118–1123.

Rudie JD, Brown JA, Beck-Pancer D, Hernandez LM, Dennis EL, Thompson PM, Bookheimer SY, Dapretto M. 2013. Altered functional and structural brain network organization in autism. NeuroImage: Clinical. 2:79–94.

Saleem KS, Price JL, Hashikawa T. 2007. Cytoarchitectonic and chemoarchitectonic subdivisions of the perirhinal and parahippocampal cortices in macaque monkeys. J Comp Neurol. 500:973–1006.

Scheperjans F, Eickhoff SB, Hömke L, Mohlberg H, Hermann K, Amunts K, Zilles K. 2008. Probabilistic maps, morphometry, and variability of cytoarchitectonic areas in the human superior parietal cortex. Cereb Cortex. 18:2141–2157.

Schleicher A, Palomero-Gallagher N, Morosan P, Eickhoff SB, Kowalski T, de Vos K, Amunts K, Zilles K. 2005. Quantitative architectural analysis: a new approach to cortical mapping. Anat Embryol. 210:373–386.

Ségonne F, Dale AM, Busa E, Glessner M, Salat D, Hahn HK, Fischl B. 2004. A hybrid approach to the skull stripping problem in MRI. NeuroImage. 22:1060–1075.

Ségonne F, Grimson E, Fischl B. 2005. A Genetic Algorithm for the Topology Correction of Cortical Surfaces. In: Information Processing in Medical Imaging. Springer. p. 393.

Sejnowski TJ, Churchland PS. 1989. Brain and cognition. In: Posner MI, editor. Foundations of cognitive science. MIT Press, Cambridge, MA. p. 888.

Shehzad Z, Kelly AMC, Reiss PT, Gee DG, Gotimer K, Uddin LQ, Lee SH, Margulies DS, Roy AK, Biswal BB, Petkova E, Castellanos FX, Milham MP. 2009. The Resting Brain: Unconstrained yet Reliable. Cereb Cortex. 19:2209–2229.

Shen X, Tokoglu F, Papademetris X, Constable RT. 2013. Groupwise whole-brain parcellation from resting-state fMRI data for network node identification. NeuroImage. 82:403–415.

Smith SM, Fox PT, Miller KL, Glahn DC, Fox PM, Mackay CE, Filippini N, Watkins KE, Toro R, Laird AR, Beckmann CF. 2009. Correspondence of the brain's functional architecture during activation and rest. Proceedings of the National Academy of Sciences. 106:13040–13045.

Snyder AZ. 1996. Difference image versus ratio image error function forms in PET-PET realignment. In: Myer R, Cunningham VJ, Bailey DL, Jones T, editors. Quantification of brain function using PET. San Diego, CA: Academic Press. p. 131–137.

Talairach J, Tournoux P. 1988. Co-planar stereotaxic atlas of the human brain. New York: Thieme Medical Publishers, Inc.

Tzourio-Mazoyer N, Landeau B, Papathanassiou D, Crivello F, Etard O, Delcroix N, Mazoyer B, Joliot M. 2002. Automated Anatomical Labeling of Activations in SPM Using a Macroscopic Anatomical Parcellation of the MNI MRI Single-Subject Brain. NeuroImage. 15:273–289.

Van Essen DC, Drury HA, Dickson J, Harwell J, Hanlon D, Anderson CH. 2001. An Integrated Software Suite for Surface-based Analyses of Cerebral Cortex. J Am Med Inform Assoc. 8:443–459.

Van Essen DC, Glasser MF, Dierker DL, Harwell J, Coalson T. 2012. Parcellations and Hemispheric Asymmetries of Human Cerebral Cortex Analyzed on Surface-Based Atlases. Cereb Cortex. 22:2241–2262.

Vincent JL, Patel GH, Fox MD, Snyder AZ, Baker JT, Van Essen DC, Zempel JM, Snyder LH, Corbetta M, Raichle ME. 2007. Intrinsic functional architecture in the anaesthetized monkey brain. Nature. 447:83–86.

Wig GS, Laumann TO, Cohen AL, Power JD, Nelson SM, Glasser MF, Miezin FM, Snyder AZ, Schlaggar BL, Petersen SE. 2014a. Parcellating an Individual Subject's Cortical and Subcortical Brain Structures Using Snowball Sampling of Resting-State Correlations. Cereb Cortex. 24:2036–2054.

Wig GS, Laumann TO, Petersen SE. 2014b. An approach for parcellating human cortical areas using resting-state correlations. Neuroimage. 93:276–291.

Wig GS, Schlaggar BL, Petersen SE. 2011. Concepts and principles in the analysis of brain networks. Ann N Y Acad Sci. 1224:126–146.

Yeo BTT, Krienen FM, Sepulcre J, Sabuncu MR, Lashkari D, Hollinshead M, Roffman JL, Smoller JW, Zöllei L, Polimeni JR, Fischl B, Liu H, Buckner RL. 2011. The organization of the human cerebral cortex estimated by intrinsic functional connectivity. J Neurophysiol. 106:1125–1165.

Chapter 4: Functional system and areal organization of a highly sampled individual human brain

This chapter has been published as a journal article. The citation is:

Laumann TO, Gordon EM, Adeyemo B, Snyder AZ, Joo SJ, Chen MY, Gilmore AW, McDermott KB, Nelson SM, Dosenbach NU, Schlaggar BL, Mumford JA, Poldrack RA, Petersen SE. *Neuron*. 2015 Aug 5;87(3):657-70. doi: 10.1016/j.neuron.2015.06.037. Epub 2015 Jul 23.

Video abstract available at: https://www.youtube.com/watch?v=-mkeCvtjrtc

Steve Petersen, Russ Poldrack, and I conceived the project and research approach. Evan Gordon and I designed the analyses with feedback from Babatunde Adeyemo and Steve Petersen. Avi Snyder and I developed the correlation reproducibility model. Jeannette Mumford helped conceive the design and statistical approach for data collection. Mei-Yen Chen helped with data collection. Sung Jun Joo helped analyze the retinotopic data. Adrian Gilmore, Kathleen McDermott, Steve Nelson, Nico Dosenbach, and Bradley Schlaggar provided additional datasets. I implemented the analyses and wrote the paper. Evan Gordon, Avi Snyder, Babatunde Adeyemo and Steve Petersen edited the paper.

4.1 Abstract

Resting state functional magnetic resonance imaging (fMRI) has enabled description of group-level functional brain organization at multiple spatial scales. However, cross-subject averaging may obscure patterns of brain organization specific to each individual. Here, we characterized the brain organization of a single individual repeatedly measured over more than a year. We report a reproducible and internally valid subject-specific areal-level parcellation that corresponds with subject-specific task activations. Highly convergent correlation network estimates can be derived from this parcellation if sufficient data are collected – considerably more than typically acquired. Notably, within-subject correlation variability across sessions exhibited a heterogeneous distribution across the cortex concentrated in visual and somato-motor regions, distinct from the pattern of inter-subject variability. Further, although the individual's systems-level organization is broadly similar to the group, it demonstrates distinct topological features. These results provide a foundation for studies of individual differences in cortical organization and function, especially for special or rare individuals.

4.2 Introduction

The human brain exhibits a substantial degree of anatomic and functional variability across individuals. This fundamental observation has both frustrated and intrigued investigators who have sought to relate individual differences in brain organization to normal variability in behavior and cognition, as well as to the pathophysiology of disease (Devlin et al., 2007; Van Essen et al., 2007). Sophisticated strategies for transforming inter-subject anatomical variability into standard volumetric

and, more recently, surface-based common spaces allow meaningful comparisons across individuals (Fischl et al., 1999; P. T. Fox et al., 1985). However, such transformations necessarily obscure individual variability in functional organization. Just as no single brain is representative of a population, no group-averaged brain represents a given individual. Furthermore, an observed pattern of functional brain organization in an individual may reflect persistent traits shaped by development and genetics, but may also relate to current state or environmental effects. Ultimately, accurate identification of brain-behavior relationships will require precise characterization of brain organization in individuals that takes into account both measurement error and intra-individual sources of variability.

Great advances recently have been made in describing group-average functional brain organization using resting state functional connectivity (RSFC). RSFC is based on the observation that the blood oxygen level dependent (BOLD) fMRI signal is correlated between spatially separated but functionally related regions of the brain (Biswal et al. 1995). Using this non-invasive technique, functional organization has been identified at the systems and areal level – two discrete scales of brain organization (Churchland et al., 1988). At the systems level, many investigators have used a variety of methods to produce increasingly comprehensive RSFC-based descriptions of distributed cortical and subcortical systems (Choi et al., 2012; Dosenbach et al., 2007; Doucet et al., 2011; Power et al., 2011; Yeo et al., 2011) that appear to correspond with functional systems co-activated by tasks (Power et al., 2011; Smith et al., 2009). At the areal level, (Cohen et al., 2008a) have shown that RSFC exhibits abrupt transitions between cortical areas, i.e. regions of cortex that classically can be discriminated by multiple convergent

properties including function, architectonics, connectivity, and topographic organization (D. J. Felleman et al., 1991a). Based on this observation, the whole cortex has been divided into discrete functional parcels, some of which correspond to task activations and cytoarchitectonically-defined areas (Gordon et al., 2014b; Wig et al., 2014b; Yeo et al., 2014). Indeed, definition of cortical regions that segregate functional areas of this type should be an important first step in pursuing network-level analyses that reflect relevant neurobiological principles (Power et al., 2011; Smith et al., 2011; Wig et al., 2011b). Thus, RSFC has enabled clear progress in the understanding of brain function and organization at multiple scales in groups of subjects, providing a powerful context for understanding brain function. However, these group-level analyses, which necessarily describe group-average data, provide only an approximate view of any individual's brain organization, potentially obscuring meaningful individual differences in cortical organization.

Here, we develop a detailed description of individual functional areal and systems brain organization, including how such organization differs from group-level estimates of organization. Importantly, precise estimates of individual functional brain organization can only be obtained by acquiring sufficient data to overcome sampling error and other sources of variability. RSFC studies commonly acquire only 5-10 minutes of scan time on each participant, based on recommendations given in past reports (Damoiseaux et al., 2006; Shehzad et al., 2009; Van Dijk et al., 2010). This quantity of individual data may be adequate for characterizing group-level patterns of functional brain organization and group-level differences. However, more recent reports have suggested that reliability is substantially improved with more than 10 minutes of

data (Anderson et al., 2011; Birn et al., 2013; Hacker et al., 2013). Most dramatically, Anderson and colleagues (2011) have reported that at least 25 minutes of scan time and, in some cases, as much as 4 hours is needed to distinguish an individual from the group on the basis of RSFC. The total quantity of data required to accurately estimate whole-brain descriptions of functional organization in an individual remains an open question.

To address these considerations, we repeatedly studied one individual over more than a year, accumulating 14 hours of resting state fMRI, as part of an extensive phenotypic assessment of a single human. Using these data, we define a subject-specific areal parcellation and compare it against task activations acquired in the same subject. We then demonstrate the reliability and inter-session variability of correlation networks derived from this parcellation. Finally, we report the commonalities and idiosyncrasies of system topology, i.e. the specific spatial adjacencies of functional systems with respect to each other as identified by RSFC, in the individual as compared to a group of normal control subjects (and we further validated these observations in a second highly-sampled subject). This approach highlights the challenges that inter- and intra-subject variability bring to understanding functional brain organization. It also sets the stage, in this dataset, for relating longitudinal dynamics of brain function to behavioral and metabolic variability (detailed in Poldrack et al. (in revision)), and, more broadly, provides a model for the detailed characterization of functional brain organization in special or rare individuals using RSFC.

4.3 **Results**

Subject-specific areal parcellation

Evaluation of subject-specific RSFC-based parcellation

An individual subject parcellation was generated using data from 84 resting state sessions following the RSFC-gradient based procedure described in detail in (Gordon et al., 2014b) and (Wig et al., 2014b). In brief, this method uses spatial gradients in the similarity of neighboring RSFC maps to identify transitions in RSFC across the cortical surface. Consistent edges identified in these gradient maps can be used to generate discrete parcels using the watershed transform (see Supplemental Materials). The parcellation defined by this method demonstrated high reproducibility, such that parcellations derived from two distinct subsets of 42 sessions exhibited considerable overlap (yellow vertices in Figure 1A). The Dice coefficient between these parcellations was 0.87. We further evaluated the internal validity of the parcels generated from the entire dataset using a homogeneity measure defined as the percent of variance explained by the first principal component of the RSFC patterns from all the vertices in each parcel (Gordon et al., 2014b). Mean homogeneity across all parcels was 86.5% ± 7.3% (Figure 1B). This mean homogeneity was significantly greater than that obtained in any of 1000 null model parcellations generated by randomly rotating the original parcellation around the cortical surface (Z-score = 23.1, $p<0.001$; Figure 1C on the left). Notably, homogeneity of the RSFC-derived parcels did not strongly vary by parcel size (red line in Figure 1C), unlike the

parcels generated by the null model, which decreased in homogeneity with increasing size (black line), suggesting that the parcellation method can accurately define putative functional areas of variable size. Further, the subject-specific parcellation performed better than our previously-defined group parcellation (Gordon et al., 2014b) evaluated in the same way in the subject data (Z-score = 2.1, p=.015) and much better than the AAL atlas (Z-score = -1.3, p=.907).

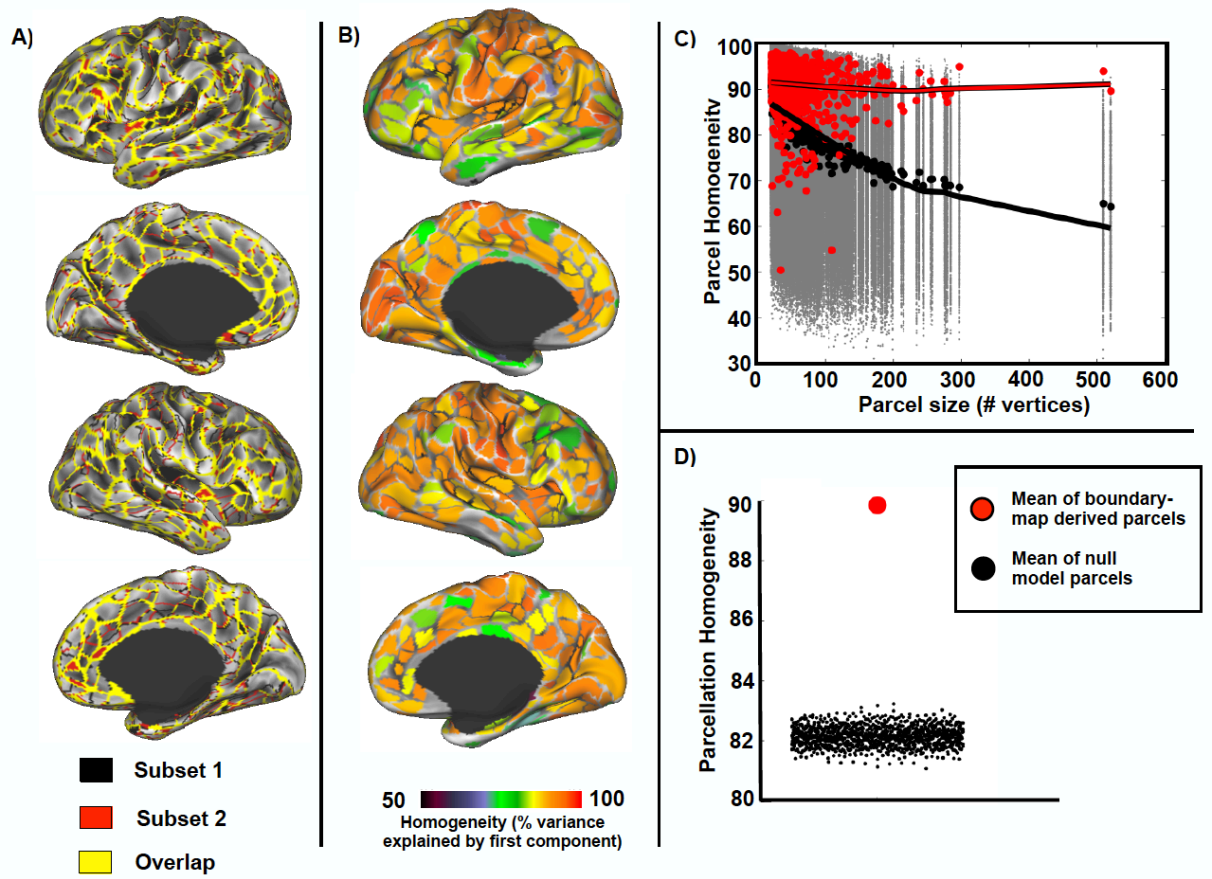

Figure 4-1. Subject-specific parcellation is reproducible and internally valid. A) RSFC-based parcellation produces highly overlapping (yellow) parcel boundaries in two independent subsets of sessions (n = 42 per subset). B) Homogeneity of each parcel calculated as the percent of variance explained by the first eigenvector computed from PCA of the RSFC patterns from vertices in the parcel. C) Homogeneity of real parcels (red dots) by parcel size compared to homogeneity of null model parcels (gray dots). Black dots indicate median homogeneity across iterations for each null model parcel. Lowess fit lines highlight the effect of parcel size on

homogeneity for the individual subject parcels (red line) and the null model parcels (black line). D) Mean homogeneity across parcels in the real parcellation (red dot) is significantly higher (Z-score = 23.1) than the mean homogeneity from null model parcellations (black dots).

Comparison of subject-specific RSFC-based parcels with task fMRI responses

If parcels defined by RSFC plausibly reflect cortical functional areas, they should correspond to areas defined by other measures of brain functional organization. In the past, we have reported alignment of group-average RSFC-boundaries with both probabilistic cytoarchitectonic maps and group-level task activation maps (Gordon et al., 2014b; Wig et al., 2014b). Although we (necessarily) have no histological measurements in this individual, fMRI responses to a large set of tasks were collected, allowing for both qualitative and quantitative assessments of within-subject correspondence between task and rest.

Correspondence with retinotopy

Putative boundaries between early cortical visual areas V1, V2, and V3 were identified by demarcating reversals in the polar angle map responses to a rotating flickering checkerboard stimulus. Both dorsal and ventral borders of the functionally-defined V1 corresponded well to RSFC-defined parcel edges in both hemispheres (Figure 2; magenta arrows). The boundary between dorsal V2 and dorsal V3 also corresponded to parcel edges in both hemispheres. However, there was no apparent parcel edge corresponding to the boundary between

ventral V2 and V3 in either hemisphere. Notably, the RSFC parcellation identified additional boundaries that do not correspond to early visual area boundaries. Some of these boundaries, particularly near the occipital pole, may relate to local changes in signal quality due to magnetization susceptibility inhomogeneity. Further, more boundaries within the left V1 region were observed than in right V1. This hemispheric asymmetry may reflect weak correlation gradients in the right hemisphere below the edge detection threshold. Of particular interest, however, are the boundaries observed both dorsally and ventrally perpendicular to the long axis of areas V2 and V3. These boundaries reflect relatively large correlation gradients that may relate to distinctions between foveal and peripheral representations of the visual field (cyan arrows) as has been observed in group-averaged data (Buckner et al., 2014; Yeo et al., 2011).

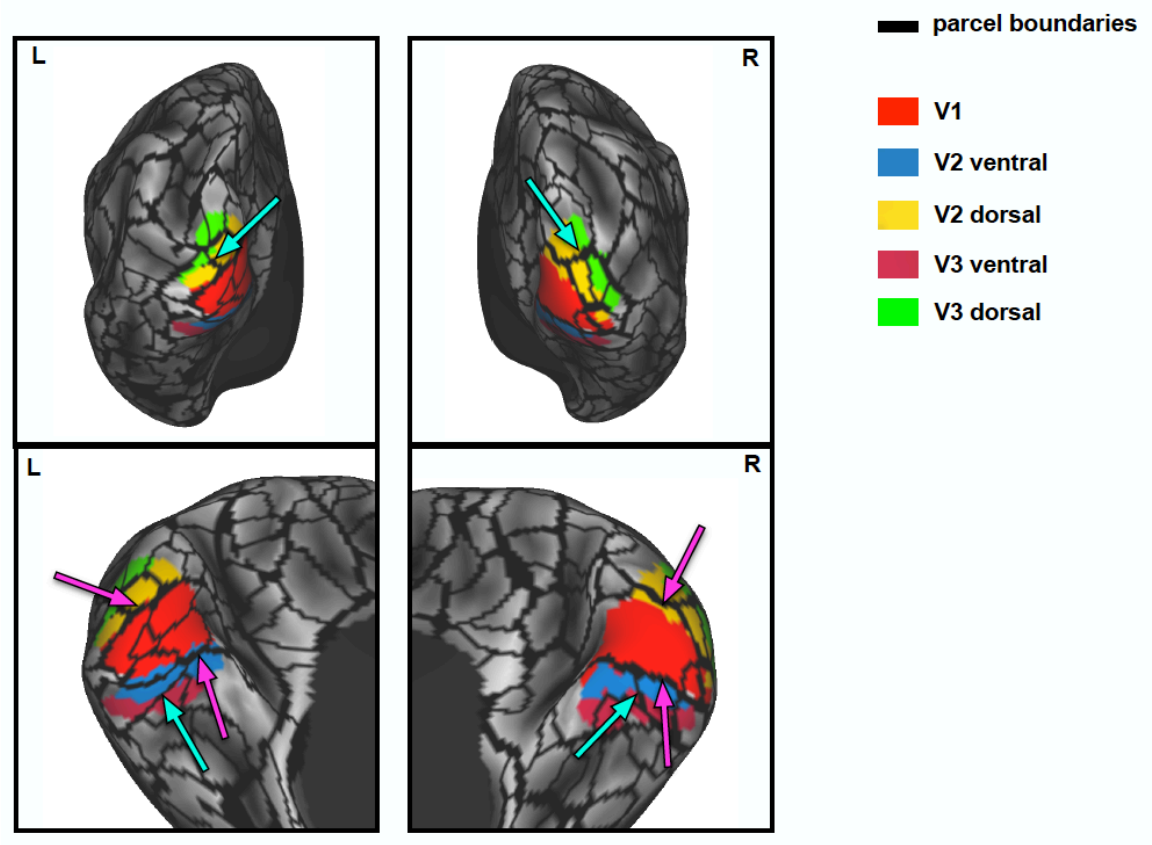

Figure 4-2. Parcel boundaries defined in individual correspond with boundaries between retinotopically defined visual regions derived from the same subject. Magenta arrows indicate correspondence between the RSFC-based parcel boundaries and the boundary between V1 and V2 areas. Cyan arrows indicate RSFC-based parcel boundaries that may represent distinctions between foveal and peripheral representations in the visual field.

Correspondence with evoked responses to a set of tasks

If RSFC-defined parcels correspond to discrete functional areas, then focal responses to tasks should fall within parcel boundaries. To test this correspondence, we evaluated responses to all contrasts in all tasks and computed the fraction of thresholded responses contained within RSFC-defined parcels (fractional overlap). Raising the statistical threshold (reducing the area of "activation") is expected to systematically increase the fractional overlap (Figure

3B). We found that, averaged across all the task contrasts, this fraction was greater than chance at all t-statistic thresholds (Figure 3B). Further, at an arbitrary task map threshold of t=2.3 (two-tailed ~$p<0.1$), 22 of the 27 task contrasts showed significantly higher overlap with the true parcels than the null model ($p<0.05$; Figure 3C). Activation maps from contrasts in the motion discrimination (3 of 5 contrasts with $p<0.01$), object localizer (10 of 10 contrasts with $p<0.01$), and verbal working memory tasks (1of 3 contrasts with $p<0.01$) corresponded particularly well to RSFC parcels, while responses to the N-back (1 of 6 contrasts with $p<0.01$) and spatial working memory (0 of 3 contrasts with $p<0.01$) tasks corresponded somewhat less well.

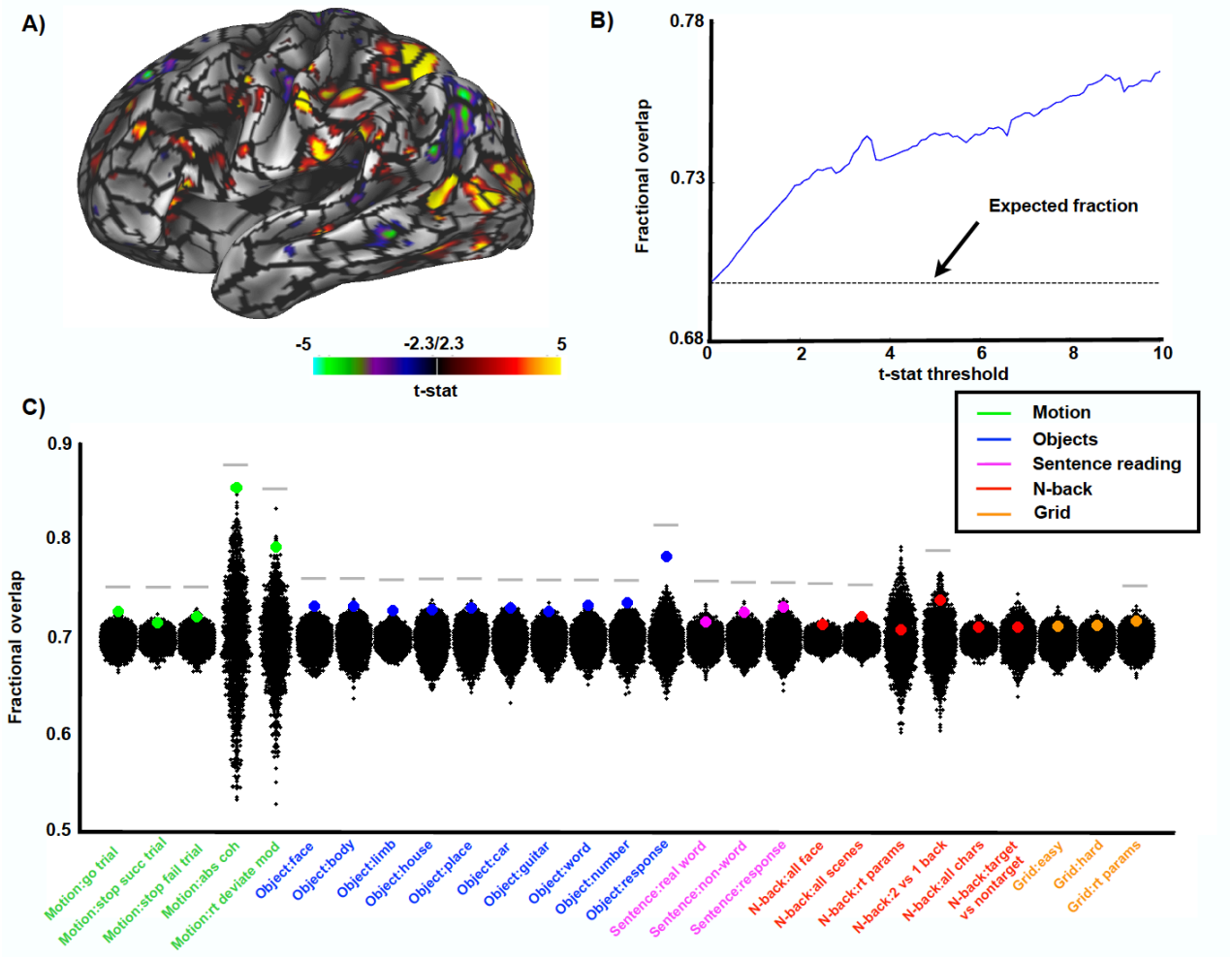

Figure 4-3. RSFC-based parcellation corresponds with task activations. A) Parcellation boundaries overlaid on an example task contrast from the motion discrimination task. B) The average fraction of task-activated vertices that fall within parcels across all 27 task contrasts by t-stat threshold. Expected fraction by chance of task-activated vertices falling within parcel boundaries is 0.696 (dotted line). C) Each colored dot represents the fraction of task-activated vertices that fall within parcel boundaries for each task at a single t-statistic threshold (t=2.3) compared to a null model. The null distribution reflects task/parcel area overlap from rotated real parcel boundaries (black dots). Gray bar indicates real parcellation showed significantly more overlap with task-activated vertices than null parcellations ($p<0.05$).

Areal network reliability and variability

Evaluation of how much data are needed for brain network estimation

Using the parcel-wise correlation matrix as a practical proxy for overall brain organization, we investigated how much resting state fMRI time is needed

to obtain convergent estimates. The results are based on 1000 random samplings of the data acquired over 84 sessions split into two halves. To ensure direct node-to-node comparability, we used the parcels derived from all 84 sessions to define parcel-wise timecourses for both halves of the data (see Figure S1 for system assignment). We observed very high measured correlation (r_M) between the two halves of the data comprising 42 sessions each (r_M=0.99±0.002; Figure 4A). This result defined the upper-limit of correlation network reproducibility to which smaller quantities of data were compared. The average correlation of only one session (9 min) from one half of the data with the full set of sessions from the other half of the data was r_M = .82 ± .04. A steep increase in average similarity (r_M=.92±.01) was observed with three sessions (27 min). Additional improvements were observed up to approximately 10 sessions (90 min; r_M=.97±.005), after which the similarity more slowly approached the asymptotic value of r_M=0.99 (Figure 4B). The graph shown in Figure 4B theoretically is a sigmoid of functional form, $r_M = 1/\sqrt{1+\xi^2}$, where ξ^2 is dominated by a term that is inversely proportional to the quantity of available data (see Figure S2 and the Appendix in Supplemental Materials for an algebraic derivation of the sigmoidal functional form and relevant formulae). This functional form yields a very good fit to the empirical data and can be used to compute a given similarity to the "true" value. The relevant quantities to compute this model are the measurement error of the correlation between a given parcel pair and the

range of correlation values in the set of parcel pairs. Although it is impractical to derive a theoretical reproducibility curve for more complex measurements, e.g., parcellation, limited testing demonstrated that these measurements have lower reproducibility than the correlation matrices with similar quantities of data. For example, the Dice coefficient between a parcellation generated from one session (9 minutes) vs. 42 sessions is ~0.27.

Additionally, we found that the correlation matrices calculated from one half of the data converged just as quickly, or even slightly faster, with the other half of the data when sampling shorter epochs over more sessions (e.g., 4.5 minutes from two sessions compared to 9 minutes from one session; Figure 4C, red line). This rapid convergence was also seen even with contiguous segments as short as 1.125 minutes of data sampled from more sessions (i.e. 1.125 minutes from 8 sessions compared to 9 minutes from one session; Figure 4C, blue line).

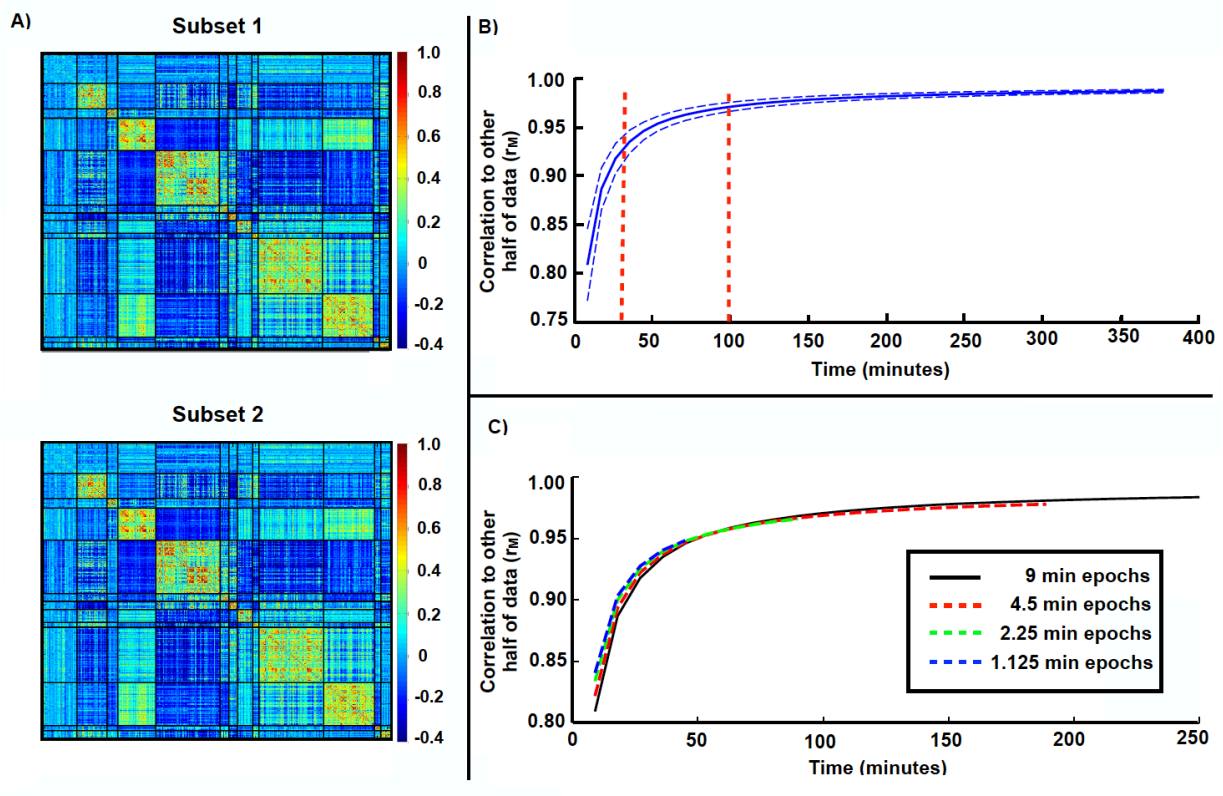

Figure 4-4. Convergence of resting state correlation estimates requires significant amounts of data. A) Example parcel correlation matrices computed from each half of the data. The parcels are sorted by system with black lines indicating system boundaries (see Figure S1 for system assignments). B) Pearson correlation (r_M) of parcel-based correlation matrix from one half of the data with the correlation matrix generated from increasing amounts of data drawn from the other half. Represented are the mean (solid line) and standard deviation (dotted lines) of this correlation from 1000 random samplings of 84 sessions. C) Correlation when the same amount of time is drawn from a larger number of sessions, e.g. 18 minutes drawn from 4.5 minutes of 4 sessions (point on red line) is compared to 18 minutes drawn from 9 minutes of 2 sessions (point on black line).

Comparison of within-subject variability and between-subject variability

Within-subject variability was computed as the standard deviation of the correlation estimated between each parcel-pair across all 84 sessions (using individual system assignment, see Figure S1). Within-subject variability was non-uniformly distributed across systems, with higher variability observed in correlations within and between somato-motor and visual regions (Figure 5A, left).

Relatively less variability was observed between fronto-parietal, default mode, ventral attention, and medial parietal regions. The average variability across all correlations for each parcel confirmed the pattern of relatively larger variability in visual, somato-motor, and dorsal attention regions compared to the rest of the brain (Figure 5A, bottom). This pattern is distinct from the pattern of between-subject variability computed over group-defined parcels observed in our 120-subject dataset (Figure 5B; group system assignment defined in (Gordon et al., 2014b)). Between-subject variability was relatively higher in fronto-parietal, cingulo-opercular, attentional, and default mode regions than in visual, auditory and somato-motor regions, as previously reported (Mueller et al., 2013). It should be noted that correlation variability generally was much higher across individuals than across sessions within the individual, particularly in the fronto-parietal, cingulo-opercular, attentional and default regions.

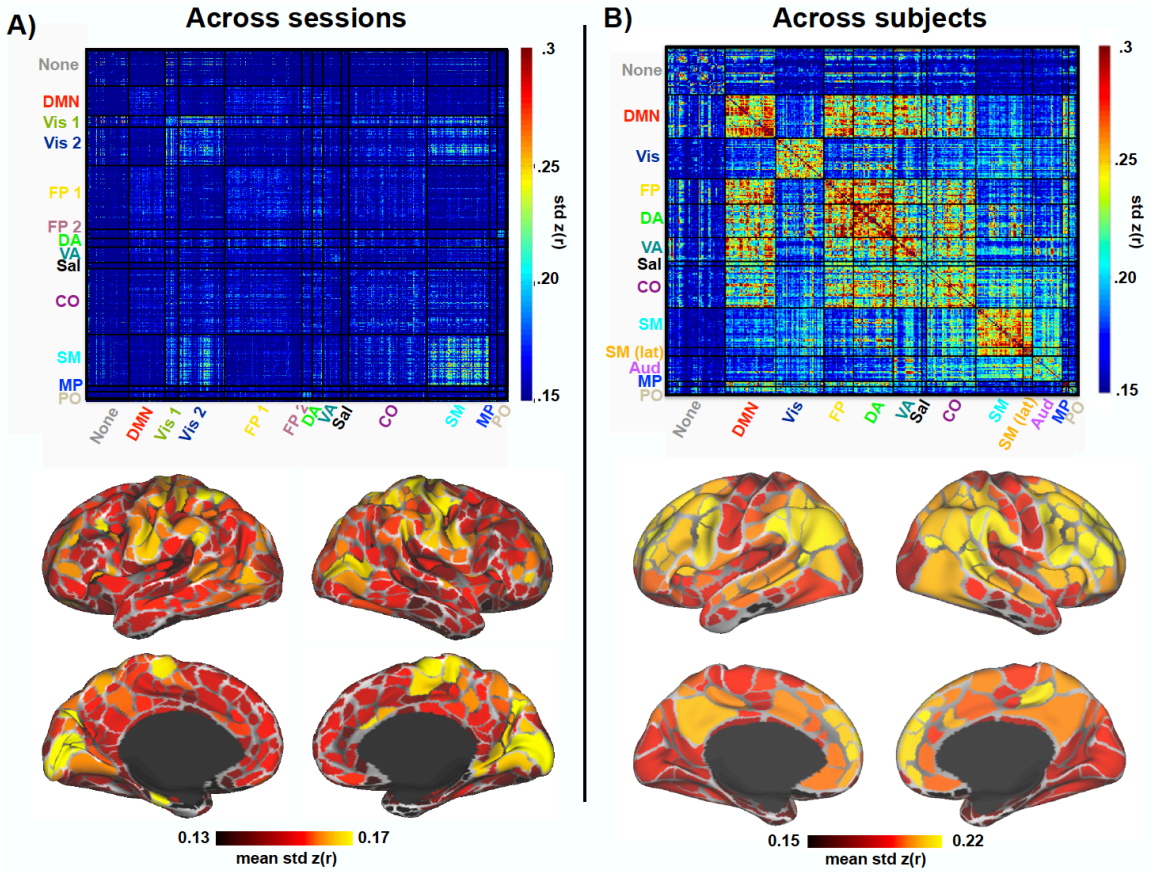

Figure 4-5. Across-session compared to across-subject variability in resting state correlations. A) Above, parcel-to-parcel correlation standard deviation across sessions based on the individual subject parcellation and system assignment (see Figure S1). Below, the average correlation standard deviation for each parcel across all of its connections. B) Above, parcel-to-parcel correlation standard deviation across subjects using the group parcellation and system assignment reported in (Gordon et al., 2014b). Below, the average correlation standard deviation for each parcel across all of its connections.

A potential source of inter-session variability in the individual is that on Tuesdays (n = 40 sessions) the subject fasted and abstained from caffeine to prepare for a blood draw, while on Thursdays (n = 32 sessions) the subject was fed and caffeinated. We observed differences in correlation strengths between Tuesday and Thursday, with increased correlations within and between somato-motor and extrastriate visual regions (Vis 2) on Thursdays relative to Tuesdays (see Figure S3A; further detailed in Poldrack et al (in revision)). Although these

effects of day likely account for some of the observed variability reported above, correlation variability was still relatively higher in visual and somato-motor regions in Tuesday or Thursday acquisitions considered separately (Figure S3B).

Vertex-wise system estimation

Comparison of individual system definition to group system definition

Systems were defined using Infomap-based community detection in the individual and compared to similar results obtained in the group (Figure 6). The systems have been color-coded using the same scheme where possible. Most systems were grossly topologically similar in the individual and the group including: default mode, visual, dorsal attention, ventral attention, fronto-parietal, cingulo-opercular, salience, auditory, somato-motor, medial parietal, and parieto-occipital systems. Furthermore, this commonality extended to detailed features of systems. For example, smaller regions of the fronto-parietal system in the anterior insula and in dorsal medial prefrontal cortex appear in both the individual and the group (magenta circles). The overall Dice coefficient between the individual and group consensus maps is 0.52.

By contrast, some features of the system maps were markedly different between the individual and the group. The Infomap algorithm did not define lateral somato-motor (orange arrows) or medial temporal systems in the individual, as were found in the group. On the other hand, the individual had a clearly defined primary visual system that was not seen in the group (olive

arrows). Prior reports (McAvoy et al., 2008; Xu et al., 2014) suggest that the presence of a primary visual system and the lack of the ventral somato-motor system might relate to a difference in eye state between the individual (eyes closed) and group (eyes open) data. Indeed, an additional 100 minutes of eyes open data collected in the individual as part of a validation dataset confirmed that the effect of eye state is localized primarily to occipital cortex and regions adjacent to the pre- and post-central gyri, identified as visual, somato-motor and dorsal attention regions in this individual (see Figure S4).

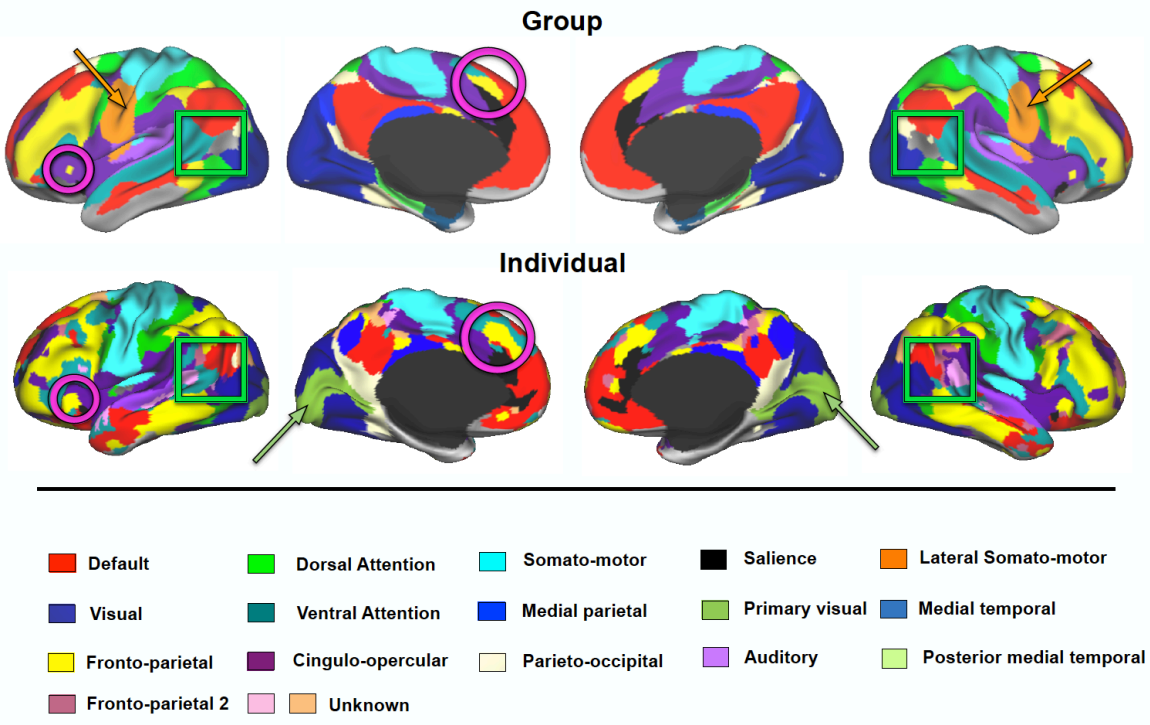

Figure 4-6. Primary subject Infomap-based community detection produces resting state community topology similar to a 120-subject group average dataset. The maps depicted here represent a single view of community identity collapsed across multiple edge density thresholds (additional edge densities are found in Figure S5). Magenta circles highlight similarities between the individual and the group in the fronto-parietal system. Orange arrows point to the lateral somato-motor system present in the group but not the individual, while olive arrows point to the primary visual system present in the individual but not the group.

Several additional systems were also observed in the primary subject that were not present in the group consensus map. Unlike the primary visual system, which was seen at every tested edge density, these unknown systems were only observed at lower edge densities (see Figure S5), indicating that they were less readily separable from other systems and therefore may be of dubious status. One further observation worth noting is that the group consensus map includes a region in the lateral occipital-temporal cortex (between the default mode and visual systems) without system assignment; in the individual, this same region showed unambiguous system affiliation (Figure 6, green squares).

Fine-grained features in the individual's system map were present across many edge densities. Although we cannot specifically address all of these features, we highlight the pattern of correlation in two adjacent regions of the lateral frontal cortex in the individual relative to the group (Figure 7). In the individual, these two adjacent regions showed starkly divergent patterns of functional connectivity: the Infomap algorithm identified the more anterior region as part of the cingulo-opercular system and the more posterior region as part of the fronto-parietal system. In contrast, the same two adjacent regions in the group showed only local differences in functional connectivity and essentially no long-range differences. Furthermore, a direct comparison of RSFC maps, vertex by vertex, between the individual and the group confirmed a group-individual discrepancy in the example lateral frontal region of Figure 7, as well as many other focal regions with distinct patterns of RSFC (Figure S6A, top row). To

ensure that the observed differences between the primary subject and the group were not related to differences between scanners and fMRI sequence parameters, an additional validation dataset (100 minutes eyes-closed rest) was collected on the primary subject at the Washington University site with the same fMRI sequence as the group data. The focal individual vs. group differences were replicated in the validation dataset (Figure S6A, second row).

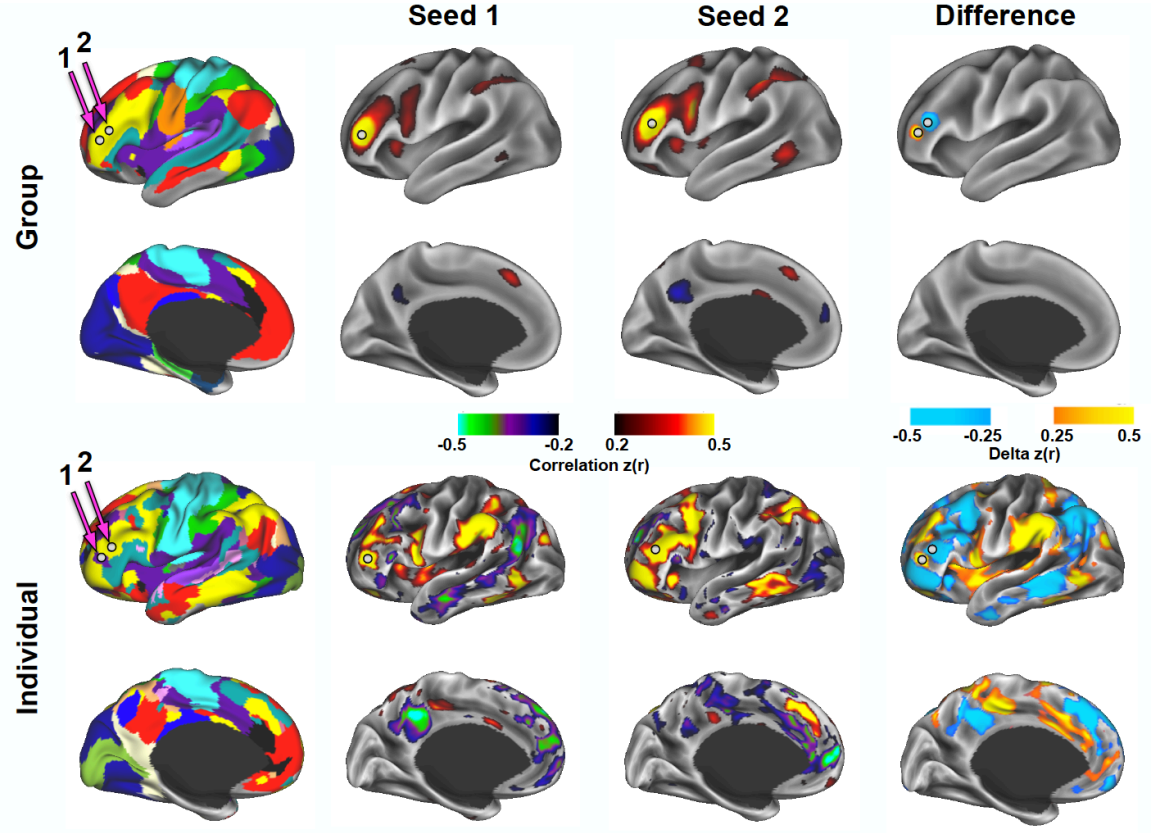

Figure 4-7. Example of idiosyncratic patterns of functional connectivity in an individual. Two nearby regions of interest (white spheres) in the lateral frontal cortex have the same system identity in the group (fronto-parietal) but different system identities in the individual (cingulo-opercular and fronto-parietal). Above, correlation maps from these two regions have very similar patterns in the group, with the largest differences occurring locally. Below, The same two regions demonstrate starkly different correlation patterns in the individual, with large regions of cortex showing large differences in correlation.

To evaluate whether such focal differences are unique to this particular highly-sampled individual or a more general feature of individual brain organization, we collected an extensive dataset (10 runs of 30-minutes) on an additional subject ('secondary subject'). The Infomap-based community detection result at several edge densities are reported for this individual and compared to the group system map in Figure S7. This second individual also exhibited many of the same systems as the group data. As this individual's data were collected with eyes open, it should be noted that, unlike the primary subject, this individual did not have a separate primary visual system but did have a separate ventral somatomotor system (Figure S7, middle rows). Further, focal differences between this second individual and the group were observed primarily in frontal and parietal regions (Figure S7, bottom row), as in the primary subject, although the exact locations were different. Together, these observations illustrate the existence of idiosyncratic topological features in functional brain organization specific to each individual.

4.4 Discussion

We present a description of the functional organization of a single human brain, based on functional MRI measurements repeatedly sampled over more than a year. Resting-state correlation-based functional organization was highly reproducible in this individual. The areal parcellation derived from resting state data corresponded with aspects of retinotopically defined visual areas and fMRI responses to task paradigms in

the same individual. Across-session variability in RSFC was greater in visual, somato-motor, and dorsal attention regions relative to other regions, though considerably less overall than between-subject variability. Finally, we found that functional systems are largely similar in the individual and in the group, but that some features in the individual were topologically distinct.

Subject-specific RSFC-based parcels are reproducible and show internal validity

RSFC-based subject-specific parcellation was reproducible across subsets of data and internally valid according to the criteria defined in (Gordon et al., 2014b). In particular, the subject-specific parcellation exhibited high parcel-wise homogeneity, and the whole parcellation was significantly more homogenous than a null model. This result suggests that, as a whole, the parcellation effectively delineates functionally homogenous cortical areas in this individual, and therefore is likely to represent a neurobiologically meaningful basis for brain network analyses (Power et al., 2011; Smith et al., 2011; Wig et al., 2011b).

The final parcellation included 616 parcels across both cortical hemispheres. This figure is somewhat greater than the 150-200 human cortical areas per hemisphere estimated by (Van Essen et al., 2012a), and also greater than the 333 parcels previously identified in group-average data (Gordon et al., 2014b). RSFC-based parcellation is capable of finding functional subdivisions within traditionally defined cortical areas, e.g., putative distinctions between tongue, hand, and foot representations within Brodmann areas 3 and 4 (Gordon et al., 2014b). Here, even finer delineation of specific functional subdivisions was possible, most likely because imperfect registration

of functional systems across individuals was avoided. Our experience indicates that the precise number of parcels and exact position of the parcel boundaries may vary with processing choices (e.g., smoothing, edge retention threshold), but the general shape and position of parcels does not significantly change. Thus, the current parcel set should be viewed as a current best estimate for this subject.

Subject-specific RSFC-based parcels correspond to task-evoked responses

Correspondence between group-level resting state correlation organization and task co-activation patterns has been amply documented (Cordes et al., 2000; Power et al., 2011; Smith et al., 2009; Wig et al., 2014a). However, subject-specific task-rest correspondence has been more difficult to demonstrate. (Blumensath et al., 2013) have reported that RSFC measurements track task responses in individuals. Here, with the advantage of a much larger dataset, we observed a significant correspondence between subject-specific RSFC-defined parcels and task evoked responses. The V1/V2 boundary defined by retinotopic mapping clearly corresponded to RSFC-based parcel edges. This result replicates, in an individual, our previous observations at the group-level of a correspondence between RSFC-derived parcels and cytoarchitectonic boundaries between probabilistic areas 17 and 18 (Gordon et al., 2014b; Wig et al., 2014b). Areas V2 and V3 also showed correspondence with RSFC-defined parcel edges, albeit less consistently and only dorsally. As noted above, RSFC-defined parcels need not correspond exactly with classically defined cortical areas. Indeed, we observed RSFC-defined parcel edges in this individual that may correspond to foveal vs. peripheral representations of the visual field (Buckner et al., 2014).

Similarly, some task responses corresponded better to the RSFC-based parcellation than others. In particular, the object localizer, verbal working memory, and motion discrimination tasks produced activation patterns that better aligned with parcels than the N-back and spatial working memory tasks. Although the reasons for this observation are uncertain, one possibility is that some task contrasts may be less process-specific than others, leading to a loss of specificity of evoked responses across neighboring functional areas. Reduced specificity may reflect multiple distinct processes invoked in a given task condition or alternate cognitive strategies used in different task sessions. Of course, the set of tasks used for this study does not represent the universe of tasks needed to delineate the full complement of cortical functional areas. However, the presently demonstrated task-rest correspondence so far observed in this dataset validates the principle that subject-specific parcellations can inform future network analyses.

Measures of individual functional brain organization converge with sufficient data

We found that 9 minutes of data generated respectable reproducibility of correlation network estimates with respect to the "true" correlation matrix (average $r_M = 0.82$). However, systematically varying the quantity of data revealed greatly improved precision of correlation matrix estimates as the quantity of data increased from 9 minutes to 27 minutes, and beyond, in accordance with theory taking into account measurement error and the range of values in the correlation matrix (see Supplemental Materials). This result is consistent with recent reports (Anderson et al., 2011; Birn et al., 2013; Hacker et al., 2013). Thus, 5-10 minutes of data, as commonly

collected in many resting-state studies, may not capture a precise representation of stationary functional connectivity features of individual subjects. Further, it should be noted that the presented reproducibility values correspond to the relatively robust measure of correlation estimates from mean parcel timecourses. Achieving similar levels of reproducibility for more fine-grained measures of brain organization (e.g., parcellation) may be expected to require extended per-subject datasets, as collected here.

It is possible to effectively measure individual brain organization with multiple scans of shorter length (e.g., 5 minutes), provided that a sufficient number of scans are acquired. This observation may have implications for study designs in populations in which longer scans may be difficult to obtain (e.g., children). Functional connectivity estimates in the primary subject converged at approximately 100 minutes of total scanning time. Although acquiring this much data in individuals is not feasible in many contexts, 100 minutes could be seen as aspirational for those interested in comprehensively characterizing single-subject features of RSFC, which may be desirable when investigating the network organization of special or rare individuals.

Sources of within-subject variability in functional connectivity are different than sources of between-subject variability

Within-subject variability in RSFC was not uniformly distributed across the cortex. In particular, visual, somato-motor and some dorsal attention regions were more variable than other regions of the brain. In stark contrast, between-subject variability was relatively lower in somato-motor and visual regions than in default mode, attentional, and control network regions. This result expands on previous findings

reported by Mueller et al (2013) and suggests that sources of within-subject variability vs. between-subject variability are distinct. Specifically, the large between-subject variability of correlation estimates in frontal and parietal regions may reflect inter-individual variability in cortical folding patterns (Hill et al., 2010), variable localization of functional areas with respect to sulcal anatomy (Frost et al., 2012), and/or variable system topologies (as discussed below). These factors could lead to misalignment of cortical regions thereby increasing apparent correlation variability as assessed by the group-averaged parcellation used here. However, anatomical variability cannot explain the presently observed pattern of within-subject correlation variability. Other than measurement error (the dominant source of variance according to the model defined in the Appendix), there are several known biological sources of within-subject variability. In particular, slow biological processes such as diurnal rhythms have been shown to significantly modify spontaneous BOLD activity (Hodkinson et al., 2014; Shannon et al., 2013). In the present case, however, the vast majority of scans were collected at the same time of day (7:30 AM). More generally, any intra-day BOLD fluctuations longer than ten minutes are unobservable with this data. Alternatively, numerous studies have demonstrated specific effects of different cognitive and behavioral contexts on resting-state activity (e.g., (Gordon et al., 2014a; Lewis et al., 2009; Tambini et al., 2010). Such cognitive/behavioral contexts could not be entirely controlled from session to session and therefore may have contributed to cross-session variability. A third possible source of variability is metabolic state (i.e. fed or fasted, caffeinated or uncaffeinated) – addressed in more detail below. Other unidentified sources of RSFC variability are likely to exist (e.g., fluctuating hormones, mood, gene expression, longitudinal seasonal or

aging-related changes, etc.), the discovery of which is one of the explicit objectives of acquiring this dataset (described in Poldrack et al (in revision)), but discussion of which is out of scope in the present report. Although sampling error is the primary source of variability in functional connectivity estimates, those additional sources of variability contribute to the necessity of acquiring large quantities of data to obtain stable measurements of brain organization.

Systematic effects attributable to fasted/uncaffeinated (Tuesdays) vs. fed/caffeinated (Thursdays) states were observed in extrastriate visual regions and somato-motor regions. This result is consistent with the previous finding that caffeine reduces measured RSFC in motor cortex (Rack-Gomer et al., 2009). Although fasting/caffeination accounts for some of the increased within-subject variability described above, within-subject variability was still relatively higher in somato-motor and particularly visual regions in Tuesday and Thursday acquisitions considered separately. This residual variability most likely reflects variable arousal across sessions, as (Tagliazucchi et al., 2014) have recently reported increased BOLD variance in somato-motor and visual regions during light sleep relative to waking. Unfortunately, we did not acquire simultaneous EEG-fMRI to confirm this possibility. However, Poldrack et al (in revision) found that the effect of Tuesday vs. Thursday differences on connectivity within these networks was partially attributable to fatigue measured immediately after the scan. In any case, multiple sources of variability potentially affect day-to-day correlation estimates in an individual. Hence, a comprehensive picture of functional organization may not be achievable in a single session. On the other hand, inter-

session variability is dwarfed by between-subject variability. Hence, inter-individual variability is the dominant confound in studies of group-level differences.

Individual functional brain organization shows similar system definition as group but also exhibits distinct functional topology

Almost all of the RSFC systems and their topological relations identified in the individual were also found in the group. Several spatial motifs in the adjacencies of group-average systems observed in prior work (Power et al., 2011) are also present in the individual, including the default/salience/cingulo-opercular and the somato-motor/dorsal-attention/fronto-parietal interfaces. The presence of these topological motifs (salience and dorsal-attention) in both individuals provides further evidence that they are not the result of intermixed signals generated by averaging, a concern posed in the previous work. On the other hand, the frontal-parietal-temporal subgraph found in that work, interposed between default and fronto-parietal systems (light blue in Power 2011), does not have an analogous system in these individuals. Additional highly-sampled subjects will be needed to confirm whether this is a general observation of individual functional brain organization. The two most notable differences between the individual and the group Infomap results are the absence in the individual of the lateral somato-motor system and the presence of an additional system in primary visual cortex. These differences are consistent with previously described effects of eyes closed (individual) vs. eyes open (group) resting state data. The eyes closed state has been shown to increase spontaneous BOLD fluctuations in visual and somato-motor regions (McAvoy et al., 2008), and enhance visual:somato-motor correlations (Xu et al., 2014). Direct comparison of eyes closed and eyes open data collected in our validation dataset

confirm that eye state has localized effects in visual, somato-motor, and adjacent regions (see Figure S4). These differences in RSFC between eye states likely account for several of the system-level differences between the individual and the group. However, eye state does not explain the more focal differences discussed below.

Figure 7 highlights a detailed topological feature that is notably different in the primary subject as compared to the group. This and other topological differences between the primary subject and the group apparent in Figure 6 (e.g., fronto-parietal system patches in the right medial prefrontal and posterior cingulate cortex; ventral attention and default mode patches in left middle frontal gyrus) and between the second subject and the group (see arrows in Figure S7) indicate clear individual differences in RSFC (see Figure S6A and S7 bottom row). The group data were geodesically registered on the surface based on macro-anatomic sulcal and gyral features; this registration represents the current state of the art, but it does not achieve a true area-to-area registration (Frost et al., 2012). Thus, group-level averaging of RSFC patterns necessarily blurs over functionally variable regions, creating the appearance of reduced topological complexity. Such blurring may explain the inability to assign a system identity to the blank region in lateral occipital-temporal cortex in the group result, where there are clear system identities in each individual (Figure 6).

The observation of distinct topological features in individuals raises an interesting possibility concerning brain organization. If we assume that brain systems are composed of functionally related cortical areas, and that cortical areas are unlikely to be translated over large distances across the cortical surface, then the present evidence suggests that some cortical areas are connected to different systems in different

individuals. In other words, some cortical areas may be functionally variable across individuals in their general relationships with other brain areas. Verification of this possibility will require collecting similarly massive data sets on more than just two individuals.

Further, from a methodological standpoint, this observation may have important implications for techniques that attempt to incorporate functional responses into a registration algorithm. Registration strategies have been proposed to improve alignment between subjects taking into account functional variability (Robinson et al., 2014; Sabuncu et al., 2010). However, these schemes rely on having sufficient data in each individual to accurately estimate individual functional topography. Further, such registrations can only align topologically consistent features. If, however, individuals exhibit true topological differences in functional organization, e.g., different numbers of disjoint regions within a given system or different systems attributed to a given cortical area, then complete subject-to-subject alignment in brain space may be not be achievable. Again, confirmation of this possibility will require reliable characterization of the functional brain organization of multiple highly sampled individuals.

Conclusion

This dataset was originally collected in order to comprehensively and longitudinally phenotype a single human with the objective of relating dynamics in brain function to other biological and environmental variables. Successful attribution of such relationships requires accurate description of the individual's functional brain organization. We have used this rich dataset to characterize the functional brain

organization of the individual at multiple scales and to determine how it varies over repeated sessions. We observed broad similarity as well as intriguing specific differences with group data. Any study reporting observations in one or two subjects has necessarily limited generality. Specific features described in these individuals could be explained as idiosyncratic (perhaps reflecting willingness to undergo such extensive self-experimentation). Therefore, we do not assign specific meaning to the detailed features observed here. However, we believe that the reliable presence of these detailed features in each individual must motivate further studies of this type. These studies may inform the understanding of individual differences in brain function and, potentially, cognition. In particular, we believe that the subject-specific approach outlined here may be essential for understanding the functional brain organization of unique or rare subjects (e.g., cognitive savants, rare disease populations, or brain-injured subjects like H.M.). Indeed, the present results provide a foundation for analyses of brain-behavior relationships that respect the specific anatomic and functional contours of a particular individual's brain.

4.5 Experimental Procedures

Ethical review

The University of Texas Office of Research Support reviewed the procedure for collecting the primary subject data and determined that it did not meet the requirements for human subjects research as defined by the Common Rule (45 CFR 46) or FDA Regulations (21 CFR 50 & 56), and thus institutional review board (IRB) approval was not necessary. Transfer of this data to

Washington University for analysis and all datasets collected at Washington University were performed with the approval of the Washington University IRB.

Highly Sampled Subject Characteristics

The primary subject (author RP) is a right-handed Caucasian male, aged 45 years-old at the onset of the study. RP is generally healthy apart from mild plaque psoriasis. Prior to initiation of the pilot period, RP had a physical examination with full blood workup revealing no significant findings. RP has a history of anxiety disorder, but no other neuropsychiatric disorders. An additional extensive dataset was acquired in a right-handed, 34-year-old Caucasian male (author ND). ND was scanned at Washington University.

Primary Subject Data Acquisition

The primary data in the primary subject were collected over the course of 532 days. Scans were performed at fixed times of day: Mondays at 5 pm, and Tuesdays and Thursdays at 7:30 am. Imaging was performed with a Siemens Skyra 3T MRI scanner using a 32-channel coil and a multi-band EPI (MBEPI) sequence [TR = 1.16 seconds; 2.4 mm isotropic voxels] (Moeller et al., 2010). Resting-state fMRI was acquired in the eyes-closed condition. 84 sessions were used in the present analyses. The first minute of each resting state scan was discarded to exclude transient fMRI responses evoked by the scan start and noise-cancelling headphones. A series of tasks also were collected at various

times during the scanning period (n=51 task fMRI sessions) including N-back, motion discrimination, object presentation, verbal working memory, spatial working memory and retinotopy. See Supplemental Materials for acquisition and task fMRI details.

To control for site/scanner differences in comparisons of the primary subject vs. the group, a validation dataset was collected at Washington University using the same fMRI sequence as in the 120-subject group. This dataset comprised ten 10-minute runs of eyes closed resting state data and ten 10-minute runs of eyes open (and fixated) resting state data. All data for this subject are available at the OpenfMRI repository (http://openfmri.org/dataset/ds000031). See Table S1 for comparison of acquisition parameters for all collected datasets.

Secondary Subject Data Acquisition

Subject ND was scanned at Washington University using a 3T TIM TRIO scanner equipped with 12-channel coil and a single-band EPI sequence [TR = 2.2seconds; 4-mm isotropic voxels]. Ten 30-minute eyes open resting-state runs with passive fixation (total 300 minutes) were acquired over 10 days. Subjects ND and RP were analyzed using the same procedures.

Group Data Acquisition and Processing

Group comparisons were based on an extant dataset of 120 subjects studied at Washington University. These subjects have been characterized in great detail elsewhere (Gordon et al., 2014b; Power et al., 2014; Wig et al., 2014b). All subjects were healthy young adults (60 females, mean age = 25 years, age range = 19-32 years), native speakers of English and right-handed. Subjects were screened to exclude a history of neurological or psychiatric diagnoses. Informed consent was obtained in all subjects. Resting state fMRI with eyes open and fixated on a crosshair was acquired using a 3T TIM TRIO system equipped with a 12-channel coil and a single-band EPI sequence [TR = 2.5 seconds; 4 mm isotropic voxels]. The group data were processed as described in (Gordon et al., 2014b). Processing of the group data did not include field distortion correction, as field maps were not acquired in all subjects.

fMRI Preprocessing

Functional data were preprocessed to reduce artifact and to maximize cross-session registration. Data were resampled to 3-mm isotropic atlas space including mean field distortion correction and motion correction in a single interpolation step. Additional RSFC preprocessing followed the procedures described in (Power et al., 2014), including motion scrubbing; white matter, ventricle, and global signal regression; and temporal filtering. See Supplemental

Materials for details of distortion correction, fMRI preprocessing, and RSFC preprocessing.

Surface processing and CIFTI generation

Surface extraction and sampling of functional data to the brain surface followed procedures similar to those previously described in (Glasser et al., 2013). Processed RSFC data were sampled to subject-specific FreeSurfer generated surfaces and registered to a common fs-LR space (Van Essen et al., 2012a). The surface data were combined with volumetric subcortical data into CIFTI format using Connectome Workbench. See Supplemental Materials for more details.

Parcellation Validation

The single-subject parcellation was generated following the procedures described in detail in (Gordon et al., 2014b) and (Wig et al., 2014b); details in supplementary methods). Parcel homogeneity was evaluated as the percent of variance explained by the first eigenvector computed from a principal component analysis (PCA) of the RSFC patterns from all vertices in the parcel (Gordon et al., 2014b). The overall homogeneity of the parcellation was compared to a null model consisting of the homogeneity computed from 1000 random rotations of the parcellation on the surface. The validated parcellation forms the basis for many of the analyses reported here.

Task vs. Rest comparison

Under the assumption that task activations should correspond to RSFC-defined parcels rather than parcel boundaries, we measured the fraction of task-activated vertices that fell within the RSFC-defined parcels. A measured fraction greater than the expected fraction from random placement of non-edge parcel vertices (~70% of the cortical surface) would indicate correspondence between the parcellation and the task activations. However, to account for the known spatial autocorrelation of BOLD fMRI data and the topological dependencies of the parcel detection procedure, i.e. the fact that boundary vertices will by definition neighbor other boundary vertices, we developed a further null model to test for correspondence between task and rest. As in the parcellation homogeneity validation (Gordon et al., 2014b), we randomly rotated the true parcellation along the cortical surface 1000 times. We then computed the fraction of task-activated regions that fell within the randomly rotated parcels. Regions with particularly low SNR as measured by mean BOLD fMRI across all sessions (mode 1000-normalized voxel value < 800) were ignored. From this null distribution, we derived a non-parametric statistic of significance indicating how well each task activation corresponded to the true parcellation.

Evaluating parcel-wise correlation estimate convergence

We used the parcels derived from all 84 sessions to extract parcel-wise resting state timecourses from each session. Cross-correlation of these

timecourses was computed to define parcel-by-parcel correlation matrices representing the areal-level brain network. A split-half procedure was used to evaluate how much data were needed to obtain convergent estimates of this parcel correlation matrix. The 84 sessions were repeatedly split into two randomly selected subsets of sessions. A correlation matrix was computed using concatenated timecourses from all the sessions of one subset (n = 42; 380 minutes of data). The similarity between this 'true' correlation matrix and the correlation matrix derived from varying amounts of the remaining subset of sessions was computed using Pearson's correlation (r_M, measured correlation matrix similarity). To evaluate the effect of session variability over and above pure scan time we also computed the correlation matrix similarity to matrices generated by contiguous sampling of the same number of frames but from a larger number of sessions (e.g., 9 minutes from 1 session compared to 9 minutes from 4.5 minutes of 2 sessions).

System Assignment

The system organization of the vertex/voxel-wise and parcel-wise graphs were computed using the Infomap algorithm (Rosvall et al., 2008), following (Power et al., 2011), where graph nodes represent either cortical surface vertices and sub-cortical/cerebellar voxels, or parcel-based regions of interest. A cross-correlation matrix of the concatenated time courses from all sessions defined the edges between nodes. For parcels, these time courses were computed by

averaging timecourses across all vertices within the parcel. Vertex connections within 10 mm of each other (or 30 mm between parcel centers) were removed from consideration to avoid correlations attributable to spatial smoothing. Geodesic distance was used for surface connections and Euclidean distance for sub-cortical and interhemispheric connections. System assignments were computed at a range of edge densities (0.05% to 5%). Systems with 400 or fewer vertices or voxels (or 8 or fewer parcels) were considered unassigned and removed from further consideration.

The Infomap procedure was also applied to the group dataset. The systems generated in this way followed very closely the results reported in (Power et al., 2011), with the refinement of improved cross-subject alignment attributable to surface registration. A 'consensus' assignment was derived by collapsing across thresholds as described in (Gordon et al., 2014b), giving each node the assignment it has at the sparsest possible threshold at which it was successfully assigned. The subject's Infomap-derived systems were matched to the group consensus systems by computing the average geodesic distance between the vertices of each system in the individual system map and the closest vertex of each system in the group system map, and vice versa. System-to-system assignment was determined by minimizing this distance metric across all systems using the Hungarian algorithm (Bourgeois, 1971). The edge density with the least overall cost to match with the group consensus map formed the basis for the individual consensus map. The present network assignment

procedure is not meant to provide an exhaustive description of network organization and may not capture non-hierarchical network features. We also do not report subcortical or cerebellar Infomap results as network assignment for these regions typically requires specialized analysis procedures (see e.g. (Buckner et al., 2011; Greene et al., 2014; Zhang et al., 2008).

4.6 Acknowledgements

This work was supported by MH100872 (TOL), NS61144 (SEP), NS46424 (SEP), P30NS048056 (AZS), a McDonnell Foundation Collaborative Activity award (SEP), Hope Center for Neurological Disorders Pilot Award (BLS), Intellectual and Developmental Disabilities Research Center at Washington University (NIH/NICHDP30 HD062171), Mallinckrodt Institute of Radiology Pilot Grant (NUFD), Child Neurology Foundation Scientific Research Award (NUFD), WU Child Health Research Center K12-HD076224 (Alan Schwartz), McDonnell Center for Systems Neuroscience New Resource Proposal (NUFD), NS088590 (NUFD), Dart NeuroScience LLC (KBM), MH091657 (Van Essen), and the Texas Emerging Technology Fund (D. Johnston, PI). We thank Alex Huk for facilitating data collection and Jonathan Power for helpful comments on the manuscript. The authors report no conflicts of interest.

4.7 References

Anderson, J. S., Ferguson, M. A., Lopez-Larson, M., & Yurgelun-Todd, D. (2011). Reproducibility of single-subject functional connectivity measurements. AJNR Am J Neuroradiol, 32(3), 548-555.

Birn, R. M., Molloy, E. K., Patriat, R., Parker, T., Meier, T. B., Kirk, G. R., Nair, V. A., Meyerand, M. E., & Prabhakaran, V. (2013). The effect of scan length on the reliability of resting-state fMRI connectivity estimates. Neuroimage, 83, 550-558.

Blumensath, T., Jbabdi, S., Glasser, M. F., Van Essen, D. C., Ugurbil, K., Behrens, T. E., & Smith, S. M. (2013). Spatially constrained hierarchical parcellation of the brain with resting-state fMRI. Neuroimage, 76, 313-324.

Bourgeois, F. L., JC. (1971). An extension of the Munkres algorithm for the assignment problem to rectangular matrices. Communications of the Association for Computing Machinery, 14(12), 802-804.

Buckner, R. L., Krienen, F. M., Castellanos, A., Diaz, J. C., & Yeo, B. T. (2011). The organization of the human cerebellum estimated by intrinsic functional connectivity. J Neurophysiol, 106(5), 2322-2345.

Buckner, R. L., & Yeo, B. T. (2014). Borders, map clusters, and supra-areal organization in visual cortex. Neuroimage, 93 Pt 2, 292-297.

Choi, E. Y., Yeo, B. T., & Buckner, R. L. (2012). The organization of the human striatum estimated by intrinsic functional connectivity. J Neurophysiol, 108(8), 2242-2263.

Churchland, P. S., & Sejnowski, T. J. (1988). Perspectives on cognitive neuroscience. Science, 242(4879), 741-745.

Cohen, A. L., Fair, D. A., Dosenbach, N. U., Miezin, F. M., Dierker, D., Van Essen, D. C., Schlaggar, B. L., & Petersen, S. E. (2008a). Defining functional areas in individual human brains using resting functional connectivity MRI. Neuroimage, 41(1), 45-57.

Cordes, D., Haughton, V. M., Arfanakis, K., Wendt, G. J., Turski, P. A., Moritz, C. H., Quigley, M. A., & Meyerand, M. E. (2000). Mapping functionally related regions of brain with functional connectivity MR imaging. AJNR Am J Neuroradiol, 21(9), 1636-1644.

Damoiseaux, J. S., Rombouts, S. A., Barkhof, F., Scheltens, P., Stam, C. J., Smith, S. M., & Beckmann, C. F. (2006). Consistent resting-state networks across healthy subjects. Proc Natl Acad Sci U S A, 103(37), 13848-13853.

Devlin, J. T., & Poldrack, R. A. (2007). In praise of tedious anatomy. Neuroimage, 37(4), 1033-1041; discussion 1050-1038.

Dosenbach, N. U., Fair, D. A., Miezin, F. M., Cohen, A. L., Wenger, K. K., Dosenbach, R. A., Fox, M. D., Snyder, A. Z., Vincent, J. L., Raichle, M. E., et al. (2007). Distinct brain networks for adaptive and stable task control in humans. Proc Natl Acad Sci U S A, 104(26), 11073-11078.

Doucet, G., Naveau, M., Petit, L., Delcroix, N., Zago, L., Crivello, F., Jobard, G., Tzourio-Mazoyer, N., Mazoyer, B., Mellet, E., et al. (2011). Brain activity at rest: a multiscale hierarchical functional organization. J Neurophysiol, 105(6), 2753-2763.

Felleman, D. J., & Van Essen, D. C. (1991a). Distributed hierarchical processing in the primate cerebral cortex. Cereb Cortex, 1(1), 1-47.

Fischl, B., Sereno, M. I., & Dale, A. M. (1999). Cortical surface-based analysis. II: Inflation, flattening, and a surface-based coordinate system. Neuroimage, 9(2), 195-207.

Fox, P. T., Perlmutter, J. S., & Raichle, M. E. (1985). A stereotactic method of anatomical localization for positron emission tomography. J Comput Assist Tomogr, 9(1), 141-153.

Frost, M. A., & Goebel, R. (2012). Measuring structural-functional correspondence: spatial variability of specialised brain regions after macro-anatomical alignment. Neuroimage, 59(2), 1369-1381.

Glasser, M. F., Sotiropoulos, S. N., Wilson, J. A., Coalson, T. S., Fischl, B., Andersson, J. L., Xu, J., Jbabdi, S., Webster, M., Polimeni, J. R., et al. (2013). The minimal preprocessing pipelines for the Human Connectome Project. Neuroimage, 80, 105-124.

Gordon, E. M., Breeden, A. L., Bean, S. E., & Vaidya, C. J. (2014a). Working memory-related changes in functional connectivity persist beyond task disengagement. Hum Brain Mapp, 35(3), 1004-1017.

Gordon, E. M., Laumann, T. O., Adeyemo, B., Huckins, J. F., Kelley, W. M., & Petersen, S. E. (2014b). Generation and Evaluation of a Cortical Area Parcellation from Resting-State Correlations. Cereb Cortex.

Greene, D. J., Laumann, T. O., Dubis, J. W., Ihnen, S. K., Neta, M., Power, J. D., Pruett, J. R., Jr., Black, K. J., & Schlaggar, B. L. (2014). Developmental changes in the organization of functional connections between the basal ganglia and cerebral cortex. J Neurosci, 34(17), 5842-5854.

Hacker, C. D., Laumann, T. O., Szrama, N. P., Baldassarre, A., Snyder, A. Z., Leuthardt, E. C., & Corbetta, M. (2013). Resting state network estimation in individual subjects. Neuroimage, 82, 616-633.

Hill, J., Dierker, D., Neil, J., Inder, T., Knutsen, A., Harwell, J., Coalson, T., & Van Essen, D. (2010). A surface-based analysis of hemispheric asymmetries and folding of cerebral cortex in term-born human infants. J Neurosci, 30(6), 2268-2276.

Hodkinson, D. J., O'Daly, O., Zunszain, P. A., Pariante, C. M., Lazurenko, V., Zelaya, F. O., Howard, M. A., & Williams, S. C. (2014). Circadian and homeostatic modulation of functional connectivity and regional cerebral blood flow in humans under normal entrained conditions. J Cereb Blood Flow Metab, 34(9), 1493-1499.

Lewis, C. M., Baldassarre, A., Committeri, G., Romani, G. L., & Corbetta, M. (2009). Learning sculpts the spontaneous activity of the resting human brain. Proc Natl Acad Sci U S A, 106(41), 17558-17563.

McAvoy, M., Larson-Prior, L., Nolan, T. S., Vaishnavi, S. N., Raichle, M. E., & d'Avossa, G. (2008). Resting states affect spontaneous BOLD oscillations in sensory and paralimbic cortex. J Neurophysiol, 100(2), 922-931.

Moeller, S., Yacoub, E., Olman, C. A., Auerbach, E., Strupp, J., Harel, N., & Ugurbil, K. (2010). Multiband multislice GE-EPI at 7 tesla, with 16-fold acceleration using partial parallel imaging with application to high spatial and temporal whole-brain fMRI. Magn Reson Med, 63(5), 1144-1153.

Mueller, S., Wang, D., Fox, M. D., Yeo, B. T., Sepulcre, J., Sabuncu, M. R., Shafee, R., Lu, J., & Liu, H. (2013). Individual variability in functional connectivity architecture of the human brain. Neuron, 77(3), 586-595.

Power, J. D., Cohen, A. L., Nelson, S. M., Wig, G. S., Barnes, K. A., Church, J. A., Vogel, A. C., Laumann, T. O., Miezin, F. M., Schlaggar, B. L., et al. (2011). Functional network organization of the human brain. Neuron, 72(4), 665-678.

Power, J. D., Mitra, A., Laumann, T. O., Snyder, A. Z., Schlaggar, B. L., & Petersen, S. E. (2014). Methods to detect, characterize, and remove motion artifact in resting state fMRI. Neuroimage, 84, 320-341.

Rack-Gomer, A. L., Liau, J., & Liu, T. T. (2009). Caffeine reduces resting-state BOLD functional connectivity in the motor cortex. Neuroimage, 46(1), 56-63.

Robinson, E. C., Jbabdi, S., Glasser, M. F., Andersson, J., Burgess, G. C., Harms, M. P., Smith, S. M., Van Essen, D. C., & Jenkinson, M. (2014). MSM: a new flexible framework for Multimodal Surface Matching. Neuroimage, 100, 414-426.

Rosvall, M., & Bergstrom, C. T. (2008). Maps of random walks on complex networks reveal community structure. Proc Natl Acad Sci U S A, 105(4), 1118-1123.

Sabuncu, M. R., Singer, B. D., Conroy, B., Bryan, R. E., Ramadge, P. J., & Haxby, J. V. (2010). Function-based intersubject alignment of human cortical anatomy. Cereb Cortex, 20(1), 130-140.

Shannon, B. J., Dosenbach, R. A., Su, Y., Vlassenko, A. G., Larson-Prior, L. J., Nolan, T. S., Snyder, A. Z., & Raichle, M. E. (2013). Morning-evening variation in human brain metabolism and memory circuits. J Neurophysiol, 109(5), 1444-1456.

Shehzad, Z., Kelly, A. M., Reiss, P. T., Gee, D. G., Gotimer, K., Uddin, L. Q., Lee, S. H., Margulies, D. S., Roy, A. K., Biswal, B. B., et al. (2009). The resting brain: unconstrained yet reliable. Cereb Cortex, 19(10), 2209-2229.

Smith, S. M., Fox, P. T., Miller, K. L., Glahn, D. C., Fox, P. M., Mackay, C. E., Filippini, N., Watkins, K. E., Toro, R., Laird, A. R., et al. (2009). Correspondence of the brain's functional architecture during activation and rest. Proc Natl Acad Sci U S A, 106(31), 13040-13045.

Smith, S. M., Miller, K. L., Salimi-Khorshidi, G., Webster, M., Beckmann, C. F., Nichols, T. E., Ramsey, J. D., & Woolrich, M. W. (2011). Network modelling methods for FMRI. Neuroimage, 54(2), 875-891.

Tagliazucchi, E., & Laufs, H. (2014). Decoding wakefulness levels from typical fMRI resting-state data reveals reliable drifts between wakefulness and sleep. Neuron, 82(3), 695-708.

Tambini, A., Ketz, N., & Davachi, L. (2010). Enhanced brain correlations during rest are related to memory for recent experiences. Neuron, 65(2), 280-290.

Van Dijk, K. R., Hedden, T., Venkataraman, A., Evans, K. C., Lazar, S. W., & Buckner, R. L. (2010). Intrinsic functional connectivity as a tool for human connectomics: theory, properties, and optimization. J Neurophysiol, 103(1), 297-321.

Van Essen, D. C., & Dierker, D. (2007). On navigating the human cerebral cortex: response to 'in praise of tedious anatomy'. Neuroimage, 37(4), 1050-1054; discussion 1066-1058.

Van Essen, D. C., Glasser, M. F., Dierker, D. L., Harwell, J., & Coalson, T. (2012a). Parcellations and hemispheric asymmetries of human cerebral cortex analyzed on surface-based atlases. Cereb Cortex, 22(10), 2241-2262.

Wig, G. S., Laumann, T. O., Cohen, A. L., Power, J. D., Nelson, S. M., Glasser, M. F., Miezin, F. M., Snyder, A. Z., Schlaggar, B. L., & Petersen, S. E. (2014a).

Parcellating an individual subject's cortical and subcortical brain structures using snowball sampling of resting-state correlations. Cereb Cortex, 24(8), 2036-2054.

Wig, G. S., Laumann, T. O., & Petersen, S. E. (2014b). An approach for parcellating human cortical areas using resting-state correlations. Neuroimage, 93 Pt 2, 276-291.

Wig, G. S., Schlaggar, B. L., & Petersen, S. E. (2011b). Concepts and principles in the analysis of brain networks. Ann N Y Acad Sci, 1224, 126-146.

Xu, P., Huang, R., Wang, J., Van Dam, N. T., Xie, T., Dong, Z., Chen, C., Gu, R., Zang, Y. F., He, Y., et al. (2014). Different topological organization of human brain functional networks with eyes open versus eyes closed. Neuroimage, 90, 246-255.

Yeo, B. T., Krienen, F. M., Eickhoff, S. B., Yaakub, S. N., Fox, P. T., Buckner, R. L., Asplund, C. L., & Chee, M. W. (2014). Functional Specialization and Flexibility in Human Association Cortex. Cereb Cortex.

Yeo, B. T., Krienen, F. M., Sepulcre, J., Sabuncu, M. R., Lashkari, D., Hollinshead, M., Roffman, J. L., Smoller, J. W., Zollei, L., Polimeni, J. R., et al. (2011). The organization of the human cerebral cortex estimated by intrinsic functional connectivity. J Neurophysiol, 106(3), 1125-1165.

Zhang, D., Snyder, A. Z., Fox, M. D., Sansbury, M. W., Shimony, J. S., & Raichle, M. E. (2008). Intrinsic functional relations between human cerebral cortex and thalamus. J Neurophysiol, 100(4), 1740-1748.

4.8 Supplemental Materials

Supplemental Figures

	Subject(s)	Site	Sessions	Eye State	Scanner	TR	Voxelsize	Fieldmap
Primary Datasets	Primary subject	University of Texas	84, 10-minute runs	closed	Skyra 3T	1.16 sec	2.4 x 2.4 x 2.4 mm	Yes
	120-subject group	Washington University	Single sessions (average 14 minutes)	open	TRIO 3T	2.5 sec	4 x 4 x 4 mm	No
Validation Datasets	Primary Subject	Washington University	20, 10-minute runs	10 runs closed, 10 runs open	TRIO 3T	2.5 sec	4 x 4 x 4 mm	Yes
	Secondary subject	Washington University	10, 30-minute runs	open	TRIO 3T	2.2 sec	4 x 4 x 4 mm	Yes

Supplementary Table 4-1. Data acquisition parameters for single subject and group datasets.

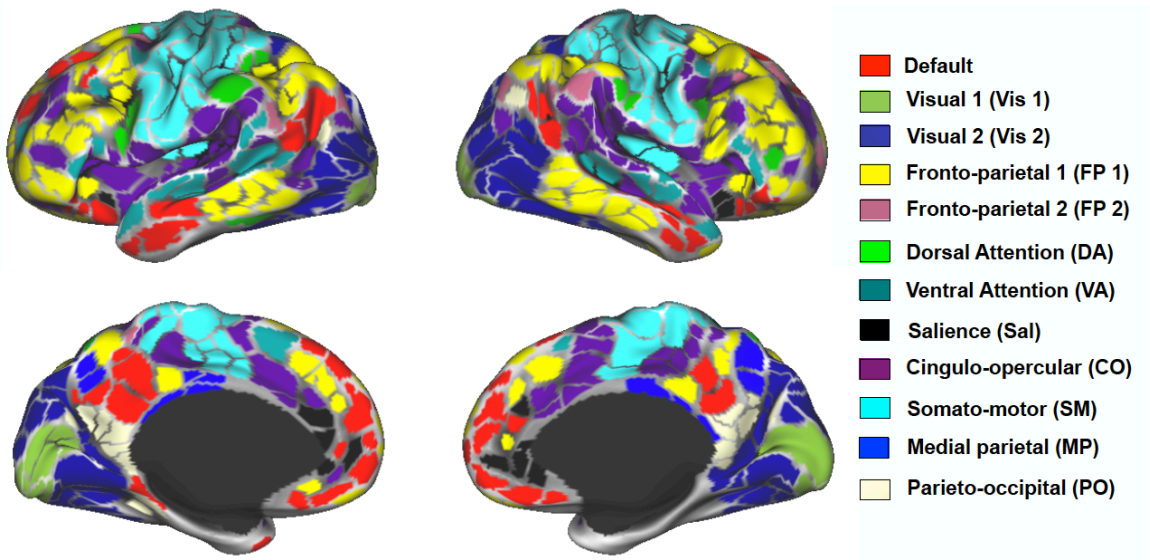

Supplementary Figure 4-1. Consensus system assignments of RSFC-defined parcels derived by the Infomap algorithm. Naming conventions follow, where possible, prior literature defining these systems, in particular: default (Raichle et al., 2001), fronto-parietal, cingulo-opercular (Dosenbach et al., 2008; Dosenbach et al., 2006), dorsal attention (Corbetta et al., 2002), ventral attention (Corbetta et al., 2008), and salience (Seeley et al., 2007).

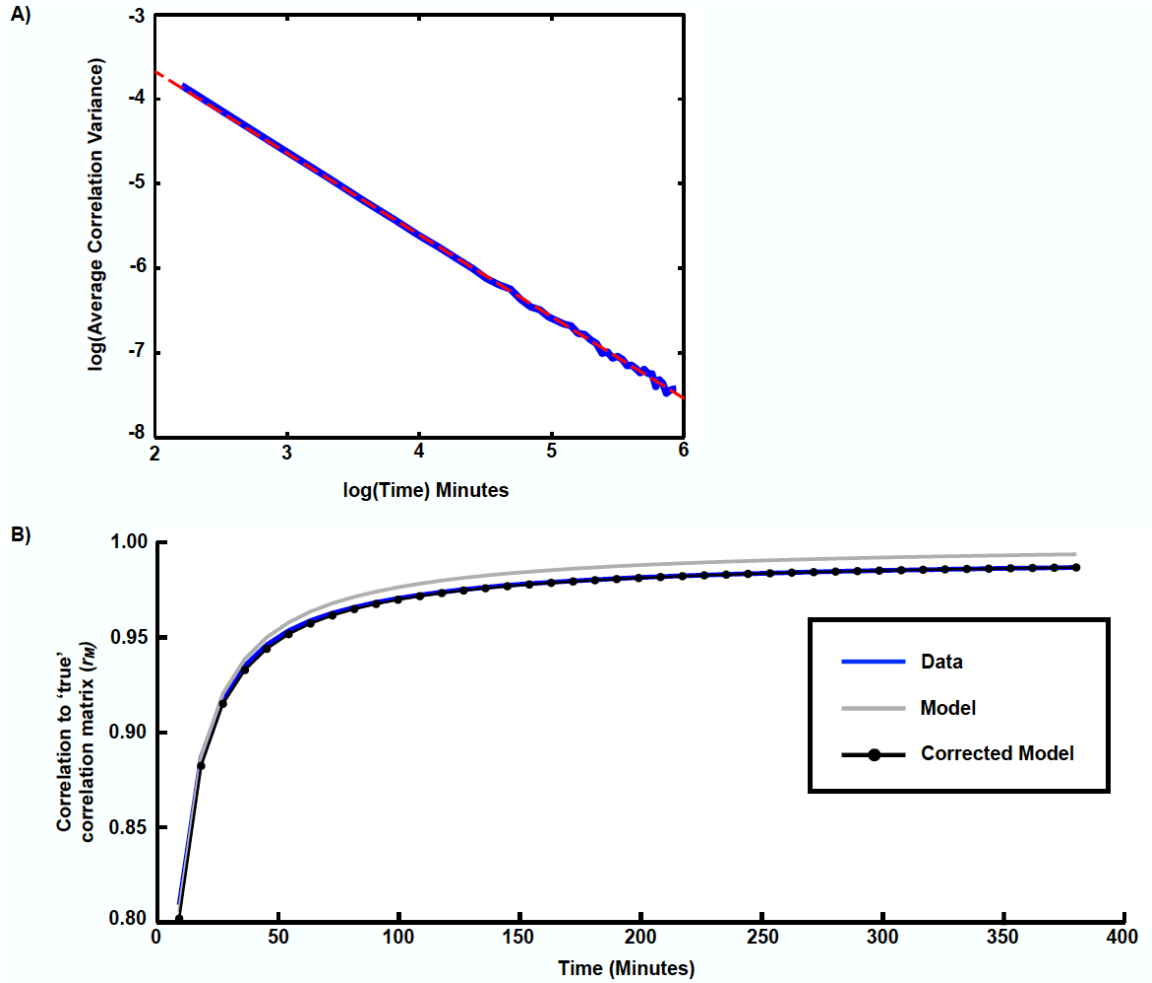

Supplementary Figure 4-2. A) Mean squared error (over parcel pairs) vs. measurement time plotted on logarithmic coordinates. See Appendix for complete theory. Attributing measurement error entirely to the quantity of available fMRI data leads to $\boldsymbol{\sigma_\delta^2 = \epsilon^2/T}$, where $\boldsymbol{T}$ is in units of minutes. Equivalently, $\boldsymbol{ln\sigma_\delta^2 = ln\epsilon^2 - lnT}$. The unconstrained linear fit equation is $\boldsymbol{ln\sigma_\delta^2 = -1.7 - 0.96lnT}$. However, if the slope is assumed to be exactly -1 (i.e, not -0.96), the fit equation is $\boldsymbol{ln\sigma_\delta^2 = -1.49 - lnT}$. Thus, $\boldsymbol{\epsilon^2 = e^{-1.49} = 0.225}$. B) Model-based correlation similarity curve compared to empirical correlation similarity curve (same as in Figure 4B). The uncorrected model omits variance not attributable to sampling error. The corrected model is $\boldsymbol{r_M = 1/\sqrt{1 + (1/\sigma_{z(r)}^2)[\epsilon^2/T + \sigma_n^2]}}$, where $\boldsymbol{\sigma_{z(r)}^2}$= 0.0461 and $\boldsymbol{\sigma_n^2}$ = 0.00065.

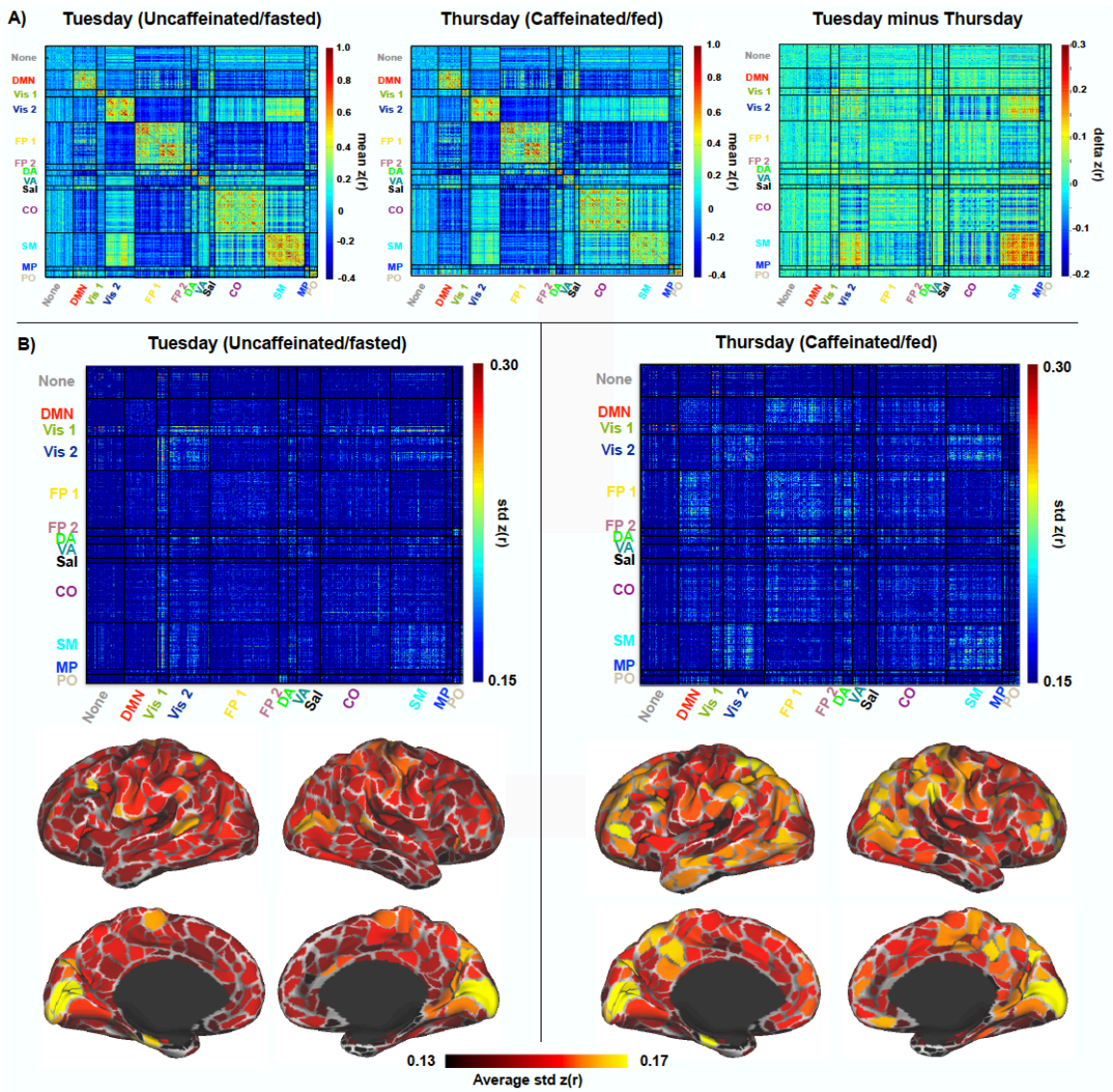

Supplementary Figure 4-3. A) Differences in correlation matrices derived from Tuesday and Thursday sessions. Mean parcel-correlation matrix on Tuesdays (Uncaffeinated/fasted) and Thursdays (Caffeinated/fed). Far right, the difference in correlation between Tuesdays and Thursdays. The module assignments follow the key in Figure S1. B) Intra-subject correlation variability computed separately for Tuesday (Uncaffeinated/fasted) and Thursday (Caffeinated/fed) sessions. Above: Across-session standard deviation of parcel-to-parcel correlations. Below: For each parcel, the average standard deviation of correlation between that parcel and every other parcel.

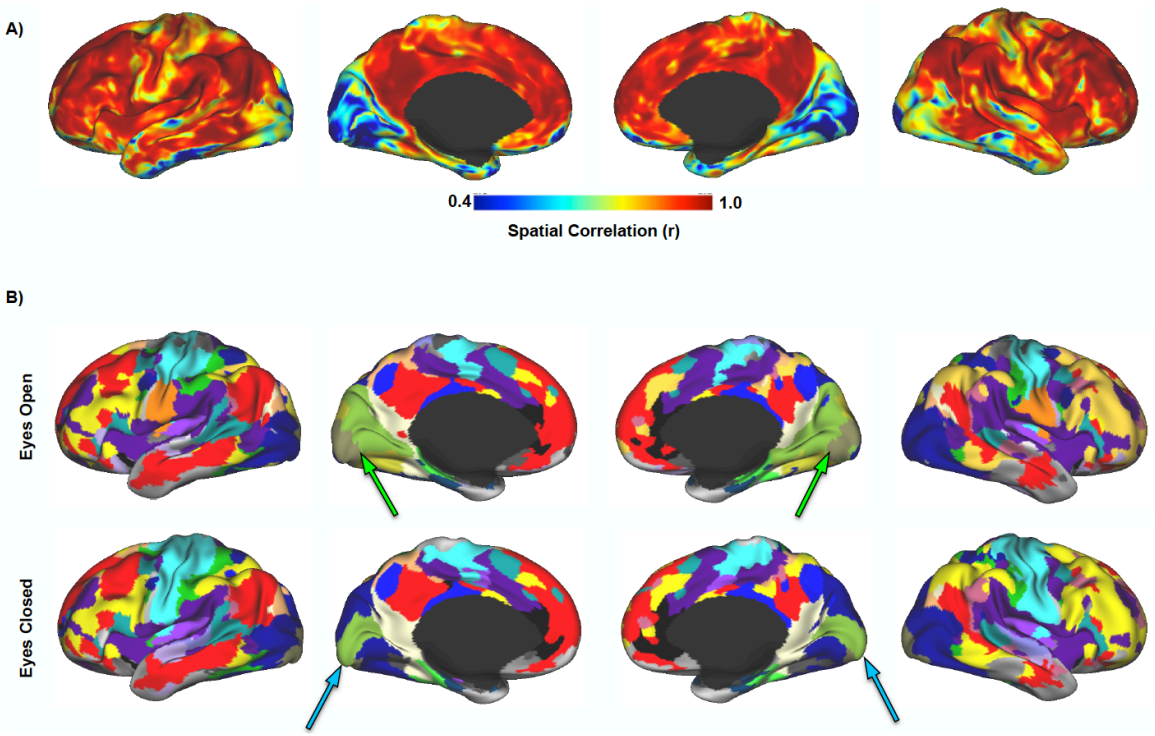

Supplementary Figure 4-4. Comparison of eyes open to eyes closed data collected at Washington University. A) Spatial correlation at each vertex between correlation maps from eyes closed and eyes open data. The least similarity can be observed in visual cortex. There is also relatively less similarity in regions along the pre- and post-central gyri, identified as parts of the somatomotor and dorsal attention systems in this individual. B) Infomap-based community detection from eyes open and eyes closed data. Results represent a single view of community organization at 1.4% edge density in each condition. The system affiliation is largely similar between the two conditions. Notable differences are present in medial visual cortex, in which the eyes closed condition exhibits a primary visual/extriatriate cortex division (blue arrows) that is not present in the eyes open condition, while the eyes open condition exhibits a potential foveal/peripheral division (green arrows) that is not present in the eyes closed condition. Additional differences are in the central sulcus, in which the eyes open condition has a ventral somatomotor system (orange) not present in the eyes closed condition. Finally, at this edge density, the eyes open condition exhibits a separation between left and right fronto-parietal systems (yellow and orange-yellow, respectively) not apparent in the eyes closed condition.

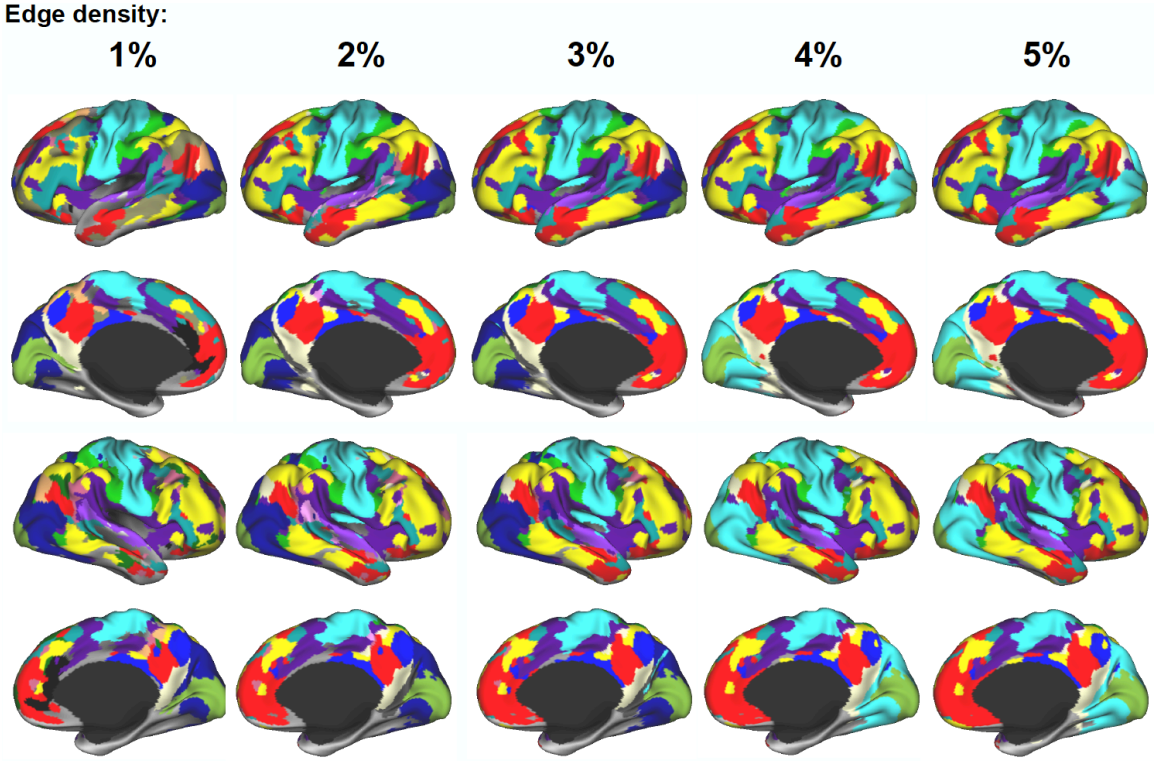

Supplementary Figure 4-5. Individual subject system assignments derived by Infomap from multiple edge density thresholds. Note that the unknown systems are only observed at lower edge densities. Also, the somato-motor and visual systems join together at higher edge densities, while most other large distributed systems remain relatively unchanged.

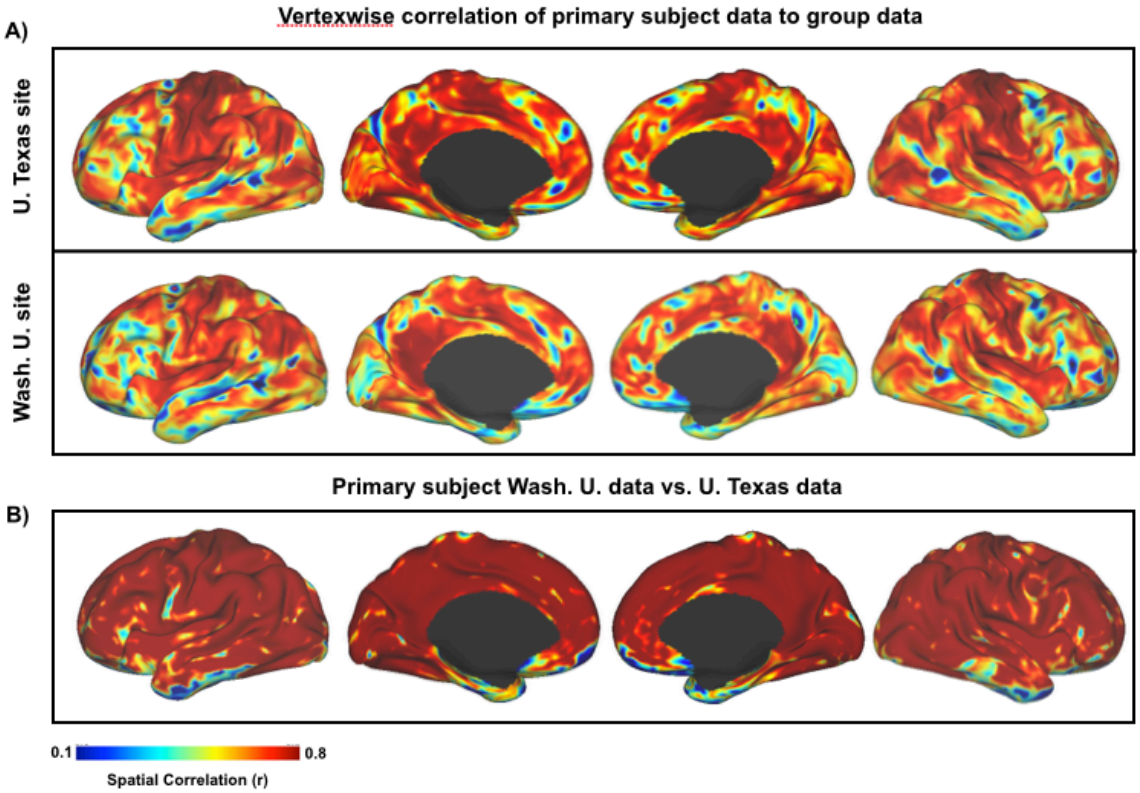

Supplementary Figure 4-6. Cortical regions that are similar between the individual and group in RSFC. At each vertex, the RSFC maps were computed for both the individual and the group-averaged data and then compared to each other by spatial correlation (r). Blue regions indicate generally focal regions with starkly different patterns of RSFC between the individual and the group.

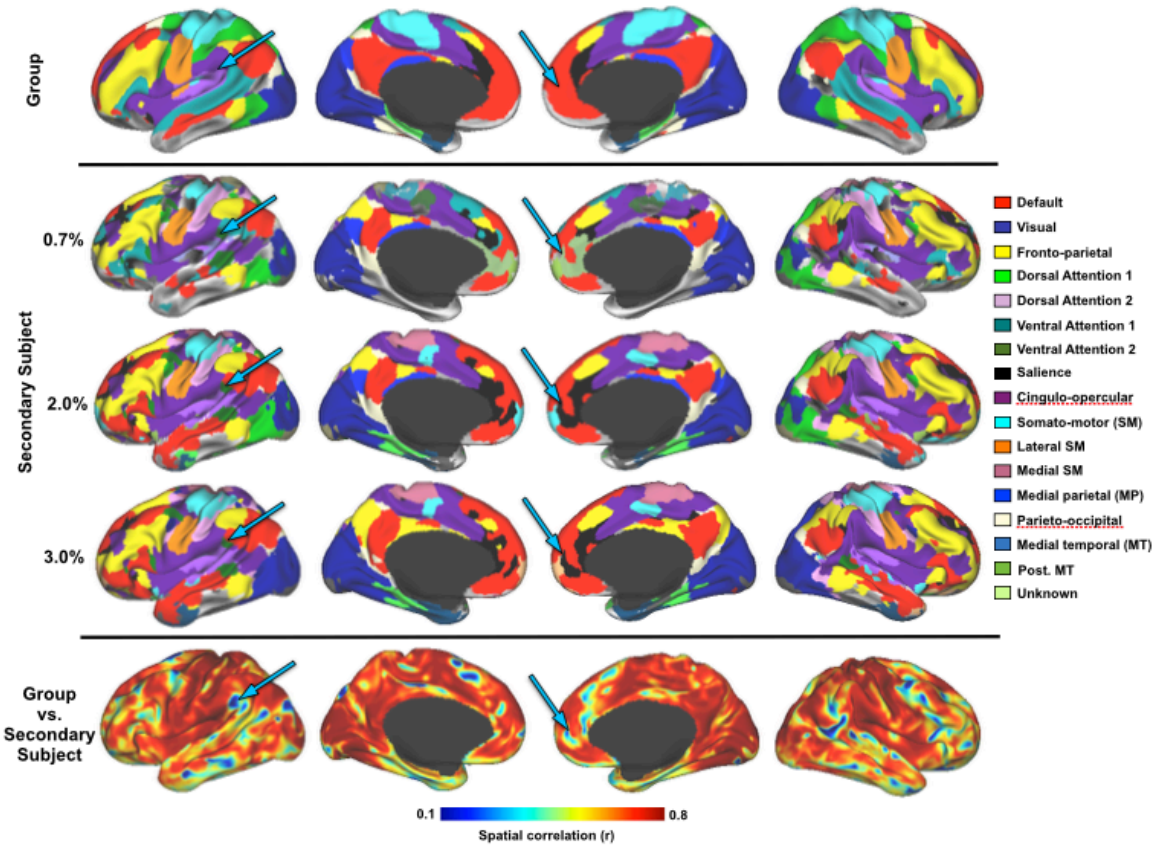

Supplementary Figure 4-7. Secondary subject functional brain organization compared to group organization. (Top row) Infomap-based systems in group average data (same image as in Figure 6). (Middle rows) Infomap-based community detection at multiple edge densities (0.7%, 2%, 3%) from 300 minutes of eyes open resting-state data in secondary subject. (Bottom row) Spatial correlation at each vertex between correlation maps from secondary subject and group average data. Blue arrows highlight regions that show focal discrepancies in RSFC between the secondary subject and the group data that correspond with distinct system topology.

Supplemental Experimental Procedures

Primary Subject Data Acquisition

The primary dataset on the individual was performed on a Siemens Skyra 3T MRI scanner with a 32-channel head coil at the University of Texas at Austin. Additional data on this individual was collected at the Washington University site using the exact same BOLD sequence as the group data (described below under 'Group Data Acquisition').

Anatomical MRI

T1- and T2-weighted anatomical images were acquired using a protocol patterned after the Human Connectome Project (Van Essen et al., 2012b). These data were collected for 14 Monday afternoon sessions through 4/30/2013, with a one-year follow-up collected on 11/4/2013. T1-weighted data were collected using an MP-RAGE sequence (sagittal, 256 slices, 0.7 mm isotropic resolution, TE=2.14 ms, TR=2400 ms, TI=1000 ms, flip angle = 8 degrees, PAT=2, 7:40 scan time). T2-weighted data were collected using a T2-SPACE sequence (sagittal, 256 slices, 0.7 mm isotropic resolution, TE=565 ms, TR=3200 ms, PAT=2, 8:24 scan time).

Field maps

A gradient echo field map sequence was acquired with the same prescription as the functional images. In addition, spin echo field maps were collected with A-P and P-A phase encoding. Collection of field maps was discontinued as of 4/30/2013, after acquisition of 38 datasets.

Resting state fMRI

Eyes-closed resting-state fMRI (RS-fMRI) was performed in each of the 104 regular scan sessions throughout the data collection period, using a multi-band echo-planar imaging (MBEPI) sequence (Moeller et al., 2010) (TR=1.16 seconds, TE = 30 ms, flip angle = 63 degrees, voxel size = 2.4 mm X 2.4 mm X 2 mm, distance factor=20%, 68 slices, oriented 30 degrees back from AC/PC, 96x96 matrix, 230 mm FOV, MB factor=4, 10:00 minute scan length). Starting with session 27 (12/3/2012), the number of slices was changed to 64 because of an update to the multiband sequence that increased the minimum TR beyond 1.16 for 68 slices. Acoustic noise cancellation for the resting-state scan was attempted in each session using the Optoacoustics active noise cancellation system, but the system occasionally failed to cancel the noise.

Task fMRI

Task fMRI was acquired with the same scanner sequence as the resting state data.

N-Back: An n-back task was performed using a blocked design, with a factorial combination of memory load (1 vs. 2 back) and stimulus type (faces, houses, and Chinese characters) across blocks. 20% of items were targets, and 20% were non-target foils (acquisition time = 8:00 minutes). This task was performed 15 times across different sessions.

Motion/stop signal: A motion discrimination task with an embedded stop signal task was performed 8 times across different sessions. On each trial, a moving dot stimulus (Britten et al., 1992) was presented, with coherence of either upward or downward motion varying across trials (levels: 0%, 10%, 30%, and 70% coherence). On 25% of

trials, a visual stop signal (change of the fixation cross from white to red) was presented, at a delay controlled by a 1 up/1down staircase in order to ensure 50% stopping accuracy (Logan, 1994). The subject's task was to perform the motion discrimination as quickly as possible, but withhold responses when the stop signal occurred (acquisition time = 7:11).

Object localizer: A multiple-object localizer (including both cropped and naturalistic faces, human bodies, human limbs, houses, places, cars, guitars, words, and numbers) was performed 8 times (twice each across four sessions; (Troiani et al., 2014)). Each stimulus class was presented in 4-second mini-blocks with items presented at 2 Hz (8 items per mini-block). In each run, 12 mini-blocks of each class were presented along 12 interspersed 4-second fixation blocks (acquisition time: 5:13). Half of the blocks included a single phase-scrambled image; the subject's task was to press a button whenever a phase-scrambled item appeared.

Verbal working memory localizer: A verbal working memory localizer (Fedorenko et al., 2010) was performed 5 times across separate sessions. In each trial, a string of 12 words (400 ms per word) - either a sentence or a string of non words - was presented sequentially, followed by a 1 second probe item; the subject's task was to decide whether the probe item matched any of the words in the preceding string.

Spatial working memory localizer: A spatial working memory localizer (Fedorenko et al., 2013) was performed four times across separate sessions. On each trial, a 4 X 2 spatial grid was presented, and locations in that grid were presented sequentially (1000 ms per location), followed by a forced-choice probe between two grids, one of which

contained all of the locations presented in the preceding series. In the easy condition, one location was presented on each presentation, whereas in the hard condition two locations were presented. Twelve 32-second experimental blocks were interspersed with 4 16-second fixation blocks (acquisition time = 7:28).

Retinotopic mapping: Polar angle (with reference to the vertical meridian, with the center of fovea as the origin) was mapped using a flickering checkerboard wedge (45 deg) rotating periodically in a counterclockwise direction through the visual field with a cycle duration of 20 seconds. This stimulus creates a wave of activation throughout retinotopically organized visual areas, successively and systematically stimulating portions of each map. In this way, the entire visual field is represented by a time-dependent pattern of activity across space. In each of four fMRI runs, the wedge completed 12 cycles of rotation (acquisition time = 4:00 per run).

Secondary Subject Data Acquisition

One additional highly sampled subject was acquired at the Washington University site on a Siemens TRIO 3T MRI scanner with a 12-channel head coil.

Anatomical MRI

Four T1-weighted images were obtained for this subject using an MP-RAGE sequence (sagittal, 224 slices, 0.8 mm isotropic resolution, TE=3.74 ms, TR=2400 ms, TI=1000 ms, flip angle = 8 degrees). Four high-resolution T2-weighted images were also collected (sagittal, 224 slices, 0.8 mm isotropic resolution, TE=479 ms, TR=3200 ms).

Resting state fMRI

Ten 30-minute runs of resting state fMRI were collected over the course of two weeks on this subject. The subject was instructed to relax while fixating on a black crosshair that was presented against a white background. Functional imaging was performed using a gradient-echo EPI sequence (TR = 2.2 s, TE = 27 ms, flip angle = 90°, voxel size = 4 mm x 4 mm × 4 mm, 36 slices). In each session, a gradient echo field map sequence was acquired with the same prescription as the functional images.

Group Data Acquisition

All imaging data for the group dataset was obtained on a Siemens TRIO 3T MRI scanner with a 12-channel head coil at Washington University in St. Louis.

Anatomical MRI

A single T1-weighted image was obtained for each subject using an MP-RAGE sequence (sagittal, 176 slices, 1 mm isotropic resolution, TE=3.08 ms, TR=2400 ms, TI=1000 ms, flip angle = 8 degrees. To facilitate registration, a T2-weighted turbo spin-echo structural image (TE = 84 ms, TR = 6.8 s, 32 slices with 1 × 1 × 4 mm voxels) in the same anatomical planes as the BOLD images was also obtained.

Resting state fMRI

During functional MRI data acquisition, subjects were instructed to relax while fixating on a white crosshair that was presented against a black background. Functional imaging was performed using a gradient-echo EPI sequence (TR = 2.5 s, TE = 27 ms,

flip angle = 90°, voxel size = 4 mm x 4 mm × 4 mm, 32 slices). The number of volumes collected from subjects ranged from 184 to 729 (mean = 336 frames, 14 min).

Data Processing

Distortion correction

Mean field map creation: As field maps were not available for all sessions, a mean field map was generated based on the available data. This mean field map was then applied to all sessions for distortion correction. To generate the mean field map the following procedure was used: (1) Poor quality field maps (4 out of 38) were excluded based on visual inspection. (2) Field map magnitude images from selected sessions were mutually co-registered. (3) Transforms between all sessions were resolved. Transform resolution reconstructs the n-1 transforms between all images using the n*(n-1)/2 computed transform pairs. (4) The resolved transforms were applied to generate a mean magnitude image. (5) The mean magnitude image was registered to an atlas representative template. (6) Individual session magnitude image to atlas space transforms were computed by composing the session-to-mean and mean-to-atlas transforms. (7) Phase images were then transformed to atlas space using the composed transforms, and a mean phase image in atlas space was computed.

Application of mean field map to individual sessions: (1) For each session, field map uncorrected data was registered to atlas space. (2) The generated transformation matrix was then inverted and applied to the mean field map to bring the mean field map into the session space. (3) The mean field map was used to correct distortion in the session

space. (4) The undistorted data was then re-registered to atlas space. (5) This new transformation matrix and the mean field map then were applied together to resample the session data to undistorted atlas space in a single step.

fMRI Preprocessing

Functional data was preprocessed to reduce artifact and to maximize cross-session registration. All sessions underwent intensity normalization to a whole brain mode value of 1000 and within run correction for head movement. Atlas transformation was computed by registering the mean intensity image from a single BOLD session to atlas space via the average (primary subject n = 9; second subject n = 4) high-resolution T2-weighted image and average (primary subject n = 10; second subject n = 4) high-resolution T1-weighted image. All subsequent BOLD sessions were linearly registered to this first session (including additional data from the Washington University site). Atlas transformation, distortion correction, and resampling to 3-mm isotropic atlas space were combined into a single interpolation using FSL's applywarp tool (Smith et al 2004). All subsequent operations were performed on the atlas-transformed volumetric time series.

FMRI processing for each of the subjects in the group data was the same as for the individual, except atlas registration was performed via a single low-resolution (4 mm) T2-weighted image and a single high-resolution (1 mm) T1-weighted image, and no distortion correction was performed.

RSFC preprocessing

Artifacts were reduced using frame censoring, nuisance regression (excluding censored frames), and spectral filtering following (Power et al., 2014). Several sessions were discarded based on poor quality on visual inspection, leaving 84 sessions for subsequent RSFC processing. Frames with framewise displacement (FD) > 0.25 mm were censored, as well as uncensored segments of data lasting fewer than 5 contiguous volumes (mean frames kept across sessions: 97.1% ± 3.7%). Data from the primary subject collected at the Washington University site was censored at FD> 0.5 mm, as well as uncensored segments of data lasting fewer than 5 contiguous frames (frames kept: 93% ± 9%). For group data and the second highly sampled participant, frames with FD > 0.2 mm were censored, as well as uncensored segments of data lasting fewer than 5 contiguous frames (frames kept across subjects: 84% ± 16%; frames kept in second highly sampled subject: 89% ± 14%). Nuisance regressors included whole brain, white matter, and ventricular signals and their derivatives, in addition to 24 movement regressors derived by expansion (Friston et al., 1996). Interpolation over censored frames was computed by least squares spectral estimation to prepare continuous data for subsequent bandpass filtering ($0.009 < f < 0.08$ Hz; (Power et al., 2014)). Censored frames were ignored during the final correlation calculations between timecourses.

Surface processing and CIFTI generation

Surface generation and sampling of functional data to anatomical surfaces for both the individual and the group followed a procedure similar to that previously

described in (Glasser et al., 2013). First, following volumetric registration, anatomical surfaces were generated from the subject's MP-RAGE image using FreeSurfer's default recon-all processing pipeline (version 5.0). This pipeline included brain extraction, segmentation, generation of white matter and pial surfaces, inflation of the surfaces to a sphere, and surface shape-based spherical registration of the subject's 'native' surface to the fsaverage surface (A. M. Dale et al., 1999; A. M. Dale et al., 1993a; Fischl et al., 1999; Segonne et al., 2005). The fsaverage-registered left and right hemisphere surfaces were brought into register with each other using deformation maps from a landmark-based registration of left and right fsaverage surfaces to a hybrid left-right fsaverage surface ('fs_LR'; (Van Essen et al., 2012a) and resampled to a resolution of 164,000 vertices (164k fs_LR) using Caret tools (Van Essen et al., 2001). Finally, each subject's 164k fs_LR surface was down-sampled to a 32,492 vertex surface (fs_LR 32k). The various deformations from the 'native' surfaces to the fs_LR 32k surface were composed into a single deformation map allowing for one step resampling. A script for this procedure is available on the Van Essen Lab website (Freesurfer_to_fs_LR Pipeline, http://brainvis.wustl.edu).

Surface processing of the BOLD data proceeded through the following steps. First, the BOLD fMRI volumes are sampled to the subject's individual 'native' midthickness surface (generated as the average of the white and pial surfaces) using the ribbon-constrained sampling procedure available in Connectome Workbench 0.84. This procedure samples data from voxels within the gray matter ribbon (i.e. between the white and pial surfaces) that lie in a cylinder orthogonal to the local midthickness surface weighted by the extent to which the voxel falls within the ribbon (Glasser et al.,

2011). Voxels with a timeseries coefficient of variation 0.5 standard deviations higher than the mean coefficient of variation of nearby voxels (within a 5 mm sigma Gaussian neighborhood) were excluded from the volume to surface sampling, as described in (Glasser et al., 2013). Once sampled to the 'native' surface, timecourses were deformed and resampled from the individual's 'native' surface to the 32k fs_LR surface in a single step using the deformation map generated as described above. This resampling allows point-to-point comparison between the individual and any other data registered to this surface space. Finally, the time courses were geodesically smoothed along the 32k fs_LR surface using a Gaussian smoothing kernel ($\sigma = 2.55$).

These surfaces were then combined with volumetric subcortical and cerebellar data into the CIFTI format using Connectome Workbench (Glasser et al., 2013), creating full brain timecourses excluding non-gray matter tissue. Subcortical (including accumbens, amygdala, caudate, hippocampus, pallidum, putamen, and thalamus) and cerebellar voxels were selected based on the FreeSurfer segmentation of the individual subject. Volumetric data were smoothed within this mask with a 3D Gaussian kernel ($\sigma = 2.55$) before being combined with the surface data.

Parcellation and Validation

An individual subject parcellation was generated following the procedures described in detail in (Gordon et al., 2014b) and (Wig et al., 2014b), with minor modifications related to processing single subject as opposed to group average data. For each hemisphere, whole-brain CIFTI-space correlation maps were computed at every surface vertex from the BOLD time courses concatenated across all sessions. For

each vertex, spatial gradients of the similarity of resting state correlation maps were computed along the cortical surface. Edges in the spatial gradients were identified by the watershed transform (Beucher et al., 1979) and averaged across all vertices to generate an 'RSFC-boundary map' indicating the frequency with which a given vertex was identified as an edge. To produce discrete parcels, the watershed transform was applied again starting from all local minima. Parcels were merged together if they were considered insufficiently dissimilar based on the edge frequency value (below the 55^{th} percentile) in the RSFC-boundary map. We then eliminated all parcels and portions of parcels in vertices with high boundary map values (top quartile of values in the boundary map), and parcels containing fewer than 20 cortical vertices (~40mm^2).

The internal validity of the parcellation was evaluated following (Gordon et al., 2014b). First, consistency was assessed by evaluating the overlap of parcellations obtained in two independent groups of 42 concatenated sessions. Second, the homogeneity of each parcel was calculated as the percent of variance explained by the first eigenvector computed from a PCA of the RSFC patterns from vertices in the parcel. The homogeneity indicates the extent to which a given parcel has a uniform functional connectivity pattern, and thus represents a measure of parcel quality. Finally, the overall homogeneity of the parcellation was compared to a null model consisting of the homogeneity computed from 1000 random rotations of the parcellation on the surface. The validated parcellation forms the basis for many of the subsequent analyses reported here.

Appendix

As in Figure 4, we evaluate the similarity of a measured vs. "true" functional connectivity matrix as the Pearson correlation,

$$r_M = \frac{\langle \hat{z}(r)_{ij} - \langle \hat{z}(r) \rangle | z(r)_{ij} - \langle z(r) \rangle \rangle}{\left[\sigma_{\hat{z}(r)} \cdot \sigma_{z(r)}\right]}, \quad \text{[S1]}$$

where $\hat{z}(r)_{ij}$ is the measured Fisher z-transformed correlation between parcels i and j, and $z(r)_{ij}$ is the corresponding "true" value. The bra-ket notation denotes the expectation value over all unique ($i \neq j$) parcel pairs. Thus, $\sqrt{\langle [X_{ij} - \langle X \rangle]^2 \rangle} = \sigma_X$ is the standard deviation (over parcel pairs) of quantity X. Let δ_{ij} denote the measurement error associated with a particular parcel pair. Then, $\hat{z}(r)_{ij} = z(r)_{ij} + \delta_{ij}$, and

$$r_M = \frac{\left[\sigma^2_{z(r)} + \langle z(r)|\delta \rangle\right]}{\left[\sigma^2_{z(r)} + 2\langle z(r)|\delta \rangle + \sigma^2_{\delta}\right]^{1/2} \sigma_{z(r)}}, \quad \text{[S2]}$$

in which explicit notation of parcel pair subscripts has been omitted. Since the sampling distribution of a Fisher z-transformed Pearson correlation is very nearly normal, it is reasonable to assume that the measurement error is zero mean and independent of the "true" correlation, i.e., $\langle \delta \rangle = 0$ and $\langle z(r)|\delta \rangle = 0$. It may be noted that variance differs over parcel pairs (see Figure 5). However, this does not matter because the relevant relationship is the dependence of $\langle \delta^2 \rangle$, i.e., the squared error averaged over parcel pairs, on the quantity of available data (N.B.: $\sigma^2_{\delta} = \langle \delta^2 \rangle$). Proceeding on this basis, we obtain

$$r_M = \frac{\sigma^2_{z(r)}}{\left[\sigma^2_{z(r)} + \sigma^2_{\delta}\right]^{1/2} \sigma_{z(r)}} = \frac{1}{\sqrt{1 + \sigma^2_{\delta}/\sigma^2_{z(r)}}} = \frac{1}{\sqrt{1 + \xi^2}}, \quad \text{[S3]}$$

where $\xi^2 = \sigma^2_{\delta}/\sigma^2_{z(r)}$.

If σ^2_{δ} is entirely attributable to sampling error, then $\sigma^2_{\delta} = \epsilon^2/T$, where ϵ^2 is an empirical constant. The value of ϵ^2 then may be obtained by assuming that σ^2_{δ} is exactly

inversely proportional to T (see Figure S2A). The obtained value is $\epsilon^2 = 0.225$ for T (observation time) in units of minutes. The model also requires evaluating the variance of $z(r)$ over parcel pairs. In the present data, $\sigma^2_{z(r)}$= 0.0461.

This is a satisfactory approximation in the regime of small T, as demonstrated in Figure S2B. However, the model in which σ^2_δ is entirely attributed to sampling error modestly deviates from measured values at large T. Thus, the measured value of r_M at $T = 380$ minutes is 0.987, whereas the model obtained so far yields 0.994. This discrepancy implies that variance not attributable to sampling error, e.g., inconsistent arousal over sessions, also is present. This source of variance is accommodated by adding a term to the expression for ξ^2. Thus, $\xi^2 = \left(1/\sigma^2_{z(r)}\right)[\epsilon^2/T + \sigma^2_n]$, where σ^2_n is the component of variance not attributable to sampling error. At low T, ϵ^2/T dominates ξ^2. However, as $T \to \infty$, only $\sigma^2_n/\sigma^2_{z(r)}$ remains. Therefore, the value of σ^2_n can be determined by comparing the data vs. the model at the maximum available value of T. This evaluation leads to σ^2_n = 0.00065. Thus, in the present results, σ^2_n constitutes at most a minor source of variance, numerically equal to 1.4% of $\sigma^2_{z(r)}$.

Supplemental References

Beucher, S., & Lantuejoul, C. (1979). *Use of watersheds in contour detection.* Paper presented at the Proceedings, International Workshop on Image Processing, CCETT/IRISA, Rennes, France.

Britten, K. H., Shadlen, M. N., Newsome, W. T., & Movshon, J. A. (1992). The analysis of visual motion: a comparison of neuronal and psychophysical performance. J Neurosci*,* 12(12), 4745-4765.

Corbetta, M., Patel, G., & Shulman, G. L. (2008). The reorienting system of the human brain: from environment to theory of mind. Neuron*,* 58(3), 306-324.

Corbetta, M., & Shulman, G. L. (2002). Control of goal-directed and stimulus-driven attention in the brain. Nat Rev Neurosci*,* 3(3), 201-215.

Dale, A. M., Fischl, B., & Sereno, M. I. (1999). Cortical surface-based analysis. I. Segmentation and surface reconstruction. Neuroimage*,* 9(2), 179-194.

Dale, A. M., & Sereno, M. I. (1993a). Improved Localizadon of Cortical Activity by Combining EEG and MEG with MRI Cortical Surface Reconstruction: A Linear Approach. J Cogn Neurosci*,* 5(2), 162-176.

Dosenbach, N. U., Fair, D. A., Cohen, A. L., Schlaggar, B. L., & Petersen, S. E. (2008). A dual-networks architecture of top-down control. Trends Cogn Sci*,* 12(3), 99-105.

Dosenbach, N. U., Visscher, K. M., Palmer, E. D., Miezin, F. M., Wenger, K. K., Kang, H. C., Burgund, E. D., Grimes, A. L., Schlaggar, B. L., & Petersen, S. E. (2006). A core system for the implementation of task sets. Neuron*,* 50(5), 799-812.

Fedorenko, E., Duncan, J., & Kanwisher, N. (2013). Broad domain generality in focal regions of frontal and parietal cortex. Proc Natl Acad Sci U S A, 110(41), 16616-16621.

Fedorenko, E., Hsieh, P. J., Nieto-Castanon, A., Whitfield-Gabrieli, S., & Kanwisher, N. (2010). New method for fMRI investigations of language: defining ROIs functionally in individual subjects. J Neurophysiol, 104(2), 1177-1194.

Fischl, B., Sereno, M. I., & Dale, A. M. (1999). Cortical surface-based analysis. II: Inflation, flattening, and a surface-based coordinate system. Neuroimage, 9(2), 195-207.

Friston, K. J., Williams, S., Howard, R., Frackowiak, R. S., & Turner, R. (1996). Movement-related effects in fMRI time-series. Magn Reson Med, 35(3), 346-355.

Glasser, M. F., Sotiropoulos, S. N., Wilson, J. A., Coalson, T. S., Fischl, B., Andersson, J. L., Xu, J., Jbabdi, S., Webster, M., Polimeni, J. R., et al. (2013). The minimal preprocessing pipelines for the Human Connectome Project. Neuroimage, 80, 105-124.

Glasser, M. F., & Van Essen, D. C. (2011). Mapping human cortical areas in vivo based on myelin content as revealed by T1- and T2-weighted MRI. J Neurosci, 31(32), 11597-11616.

Gordon, E. M., Laumann, T. O., Adeyemo, B., Huckins, J. F., Kelley, W. M., & Petersen, S. E. (2014b). Generation and Evaluation of a Cortical Area Parcellation from Resting-State Correlations. Cereb Cortex.

Logan, G. D., Dagenbach, D., Carr, T. (1994). On the ability to inhibit though and action: a users' guide to the stop signal paradigm. In D. C. Dagenbach, T.H (Ed.),

Inhibitory processes in attention, memory, and language (pp. 189-240): Academic Press.

Moeller, S., Yacoub, E., Olman, C. A., Auerbach, E., Strupp, J., Harel, N., & Ugurbil, K. (2010). Multiband multislice GE-EPI at 7 tesla, with 16-fold acceleration using partial parallel imaging with application to high spatial and temporal whole-brain fMRI. Magn Reson Med*,* 63(5), 1144-1153.

Power, J. D., Mitra, A., Laumann, T. O., Snyder, A. Z., Schlaggar, B. L., & Petersen, S. E. (2014). Methods to detect, characterize, and remove motion artifact in resting state fMRI. Neuroimage*,* 84, 320-341.

Raichle, M. E., MacLeod, A. M., Snyder, A. Z., Powers, W. J., Gusnard, D. A., & Shulman, G. L. (2001). A default mode of brain function. Proc Natl Acad Sci U S A*,* 98(2), 676-682.

Seeley, W. W., Menon, V., Schatzberg, A. F., Keller, J., Glover, G. H., Kenna, H., Reiss, A. L., & Greicius, M. D. (2007). Dissociable intrinsic connectivity networks for salience processing and executive control. J Neurosci*,* 27(9), 2349-2356.

Segonne, F., Grimson, E., & Fischl, B. (2005). A genetic algorithm for the topology correction of cortical surfaces. Inf Process Med Imaging*,* 19, 393-405.

Troiani, V., Stigliani, A., Smith, M. E., & Epstein, R. A. (2014). Multiple object properties drive scene-selective regions. Cereb Cortex*,* 24(4), 883-897.

Van Essen, D. C., Drury, H. A., Dickson, J., Harwell, J., Hanlon, D., & Anderson, C. H. (2001). An integrated software suite for surface-based analyses of cerebral cortex. J Am Med Inform Assoc*,* 8(5), 443-459.

Van Essen, D. C., Glasser, M. F., Dierker, D. L., Harwell, J., & Coalson, T. (2012a). Parcellations and hemispheric asymmetries of human cerebral cortex analyzed on surface-based atlases. Cereb Cortex, 22(10), 2241-2262.

Van Essen, D. C., Ugurbil, K., Auerbach, E., Barch, D., Behrens, T. E., Bucholz, R., Chang, A., Chen, L., Corbetta, M., Curtiss, S. W., et al. (2012b). The Human Connectome Project: a data acquisition perspective. Neuroimage, 62(4), 2222-2231.

Wig, G. S., Laumann, T. O., & Petersen, S. E. (2014b). An approach for parcellating human cortical areas using resting-state correlations. Neuroimage, 93 Pt 2, 276-291.

Chapter 5: Resting state BOLD fluctuations are fundamentally stationary

5.1 Abstract

The human brain must be flexible, dynamic and adaptive, yet, at the same time, capable of maintaining long-term stability of functional relationships over decades of life. Spontaneous BOLD activity measured during the resting-state has proven to be a powerful tool for understanding the large-scale functional organization of the brain within which these essential activities are embedded. Recently, ongoing changes in cognition and behavior have been claimed as evident in reports of dynamic, 'non-stationary', behavior in spontaneous BOLD activity. Here, we evaluate the claim that resting-state BOLD activity is non-stationary. First, we find that observations of dynamics in resting-state BOLD activity are largely explained by sampling variability. Second, we find that the largest part of bona fide non-stationarity is accounted for by head motion. Additional non-stationarity may be accounted for by fluctuating wakefulness. Our results suggest that, aside from these factors, resting-state BOLD activity is essentially stationary. We conclude that spontaneous BOLD activity primarily reflects processes that contribute to the long-term stability of functional brain organization.

5.2 Introduction

Spontaneous neural activity plays a major role in learning and memory (Wilson et al., 1994) as well as synaptic homeostasis (Katz et al., 1996; Penn et al., 1999). In humans, study of spontaneous neural activity has greatly accelerated over the last two decades following the advent of 'resting-state' fMRI, wherein ongoing blood oxygen level dependent (BOLD) signal is measured while subjects 'rest' in a scanner. This

approach has demonstrated significant potential for understanding the brain's functional architecture, as it has been observed that fluctuations in the BOLD signal during rest exhibit distributed patterns of correlation that correspond to known functional systems (B. Biswal et al., 1995; Power et al., 2011; Smith et al., 2009; Yeo et al., 2011). Although the physiological basis of resting state functional connectivity (RSFC) is incompletely understood, it is believed to be constrained by axonal connectivity (C. J. Honey et al., 2009b), with the caveat that at least some RSFC relationships must reflect multi-synaptic pathways (Vincent et al., 2007a). Under this view, RSFC has been understood to reflect stable features of brain organization on a timescale of minutes, hours, or even days, which accounts for the relative reliability of RSFC estimates (Laumann et al., 2015; Shehzad et al., 2009). More recently, however, observations of 'dynamics' in RSFC, i.e. correlations appearing to fluctuate dramatically over shorter segments of time (e.g. 1-2 minutes), have been reported (Chang et al., 2010; Hutchison et al., 2012) and a large literature has developed trying to characterize these 'dynamics' and explain their sources (Calhoun et al., 2014; Hutchison et al., 2013; Kopell et al., 2014).

A variety of techniques that highlight different aspects of the BOLD signal have been used to measure dynamics in RSFC. The most commonly used approach is the sliding window technique (Allen et al., 2012; Chang et al., 2010; Hutchison et al., 2012; Zalesky et al., 2014) in which an estimate of functional correlation is computed within a fixed window around each timepoint in a BOLD dataset. Dynamic behavior has also been reported based on transient patterns of co-activation at single or just a few timepoints (Karahanoglu et al., 2015; Liu et al., 2013; Tagliazucchi et al., 2012).

Frequently, patterns of co-activation or correlation documented with these techniques are then clustered into groups representing a set of ‘dynamically’ recurring patterns.

Observations of ‘dynamic’ RSFC patterns with these methods have been interpreted as evidence of ‘non-stationary’ phenomena in the resting state BOLD signal and presumed to reflect relevant changes in brain state on a short time-scale. Since the content of consciousness varies over time, especially in the absence of imposed tasks, it is natural to suppose that RSFC should vary accordingly. Moreover, it is generally believed that BOLD fMRI signals indirectly reflect neural activity. Brain activity is expected to be dynamic, adaptive, and state-dependent. Indeed, brain recordings in other modalities (electrophysiology, EEG, MEG) unambiguously show non-stationary behavior related to changes in arousal or task state (Betti et al., 2013; de Pasquale et al., 2012). Thus, it follows that resting state BOLD data should be similarly non-stationary.

In the present context, it is essential to define what is meant by ‘stationary’. Stationarity is a statistical descriptor that applies to the temporal characteristics of a process. Specifically, a process is stationary if its moments (mean, variance, kurtosis, etc.) are constant over time. Stationarity does not imply that a process is still. For example, a frictionless pendulum will remain indefinitely in oscillatory motion, but if the amplitude and frequency of the motion are constant then the pendulum is stationary. The pendulum in this example does not have constant velocity, but its second-order statistics are stationary. The pendulum differs from BOLD timeseries in that it is periodic, while BOLD is aperiodic and 1/f-like (He et al., 2010). Nevertheless, the pendulum example suffices to illustrate what is meant by stationarity. It is this property that is

implicitly evaluated in studies that aim to report the 'dynamic' activity of BOLD correlations.

However, there remain significant challenges to interpreting observed dynamics in resting state BOLD as representative of non-stationary brain phenomena in the sense defined above. First, as a number of authors have begun to point out, current analytic techniques are susceptible to spurious 'non-stationary' observations if not properly employed (Leonardi et al., 2015; Lindquist et al., 2014; Zalesky et al., 2014). In concurrence, we believe that much of the literature on this topic has not adequately appreciated the nature of sampling variability in second-order statistics (e.g. correlation) when measured on limited quantities of data. This failure is illustrated here by applying dynamic analyses to simulated stationary BOLD data.

Second, and perhaps more importantly, there are potential sources of artifactual and bona fide non-stationary processes that complicate interpretation of dynamic behavior in resting state BOLD. In particular, just as it has clouded interpretation of standard RSFC analyses (Power et al., 2012), head motion is not well-accounted for in most analyses of RSFC dynamics. In addition, as Tagliazucchi et al have reported, most resting state datasets are contaminated by true 'state' changes, namely the passage from wake to sleep, and intermediate stages of drowsiness (Tagliazucchi et al., 2014). To evaluate the role of these processes on resting state 'dynamics', we propose a simple statistic to measure the multivariate kurtosis of resting state BOLD data (Mardia, 1970). Deviations from normality in this statistic should provide evidence for changes in the covariance structure of a multivariate process (Martins, 2007). Using this statistic, we find that resting state BOLD timecourses behave much like stationary,

normal simulations and observed deviations from normality can be explained by movement and/or sleep state. Thus, we show that spontaneous neural activity is essentially stationary, or at least, much more stationary than has been recently claimed.

5.3 Results

Simulation maintains covariance and spectral content of real data

The sampling variability of correlation poses a serious, and increasingly recognized (Lindquist), challenge to identifying true fluctuations in resting state functional connectivity. Signals with the frequency spectrum of typical BOLD data will exhibit large apparent fluctuations in correlation over the time scales often assessed in analyses of RSFC 'dynamics'. Thus, to disambiguate real non-stationarity from sampling variability, it is necessary to develop an adequate null model of expected fluctuations in the context of stationary correlation. To do this, we generated a simulation of BOLD activity that retains both the stationary covariance and spectral structure of real BOLD data. The procedure to generate timeseries with these properties is outlined in Figure 1. First, we sample a timeseries of random normal deviates of the same dimensionality as a real dataset (step 1). These timeseries are then projected onto the eigenvectors derived from the stationary covariance structure of a session of real data (step 2). Finally, these timeseries are then multiplied in the spectral domain by the power spectrum derived from a full-length real dataset (step 3). This procedure produces random stationary timeseries with the covariance and spectral structure of real data (compare last two rows of Figure 1). These simulated timeseries can then act as a null against which to evaluate non-stationary features of real data.

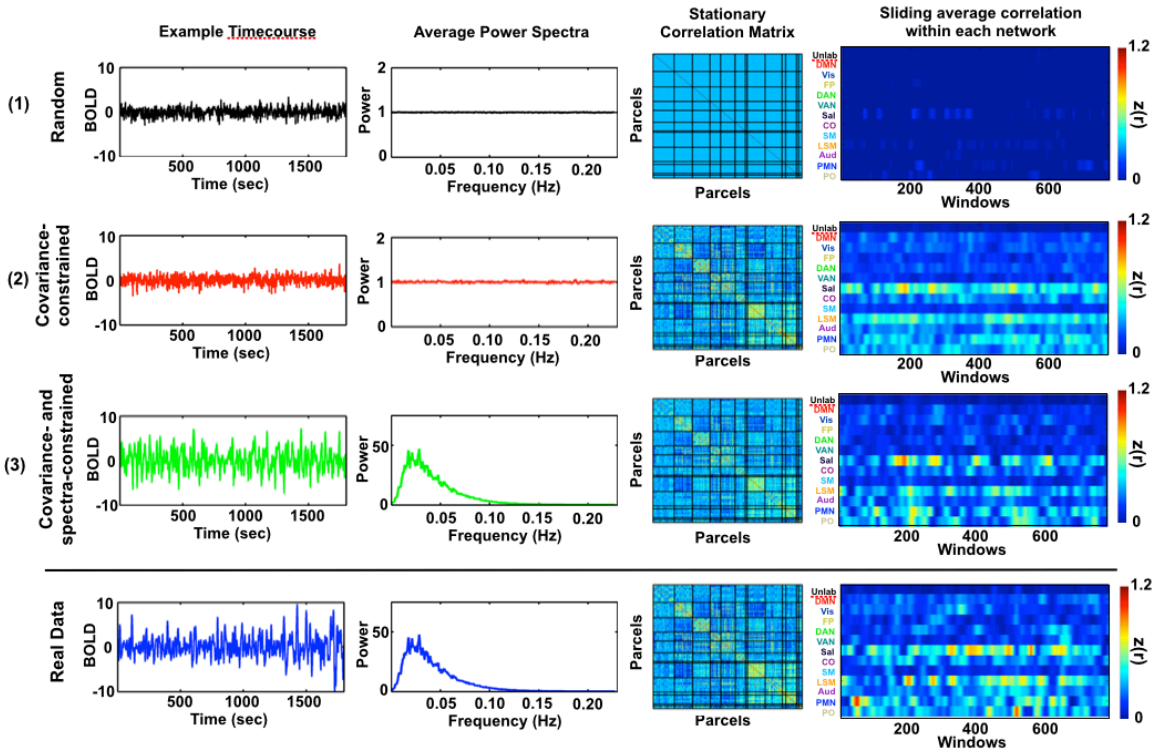

Figure 5-1. Steps of stationary BOLD simulation. (1) BOLD timeseries are simulated by first sampling random normal deviates. (2) These timeseries are projected onto the eigenvectors computed from the average covariance matrix of ten 30-minute sessions of real data from each subject. (3) The projected timeseries are then matched to the average parcel-wise power spectrum of the real data by multiplication in the spectral domain. The final simulated data share the stationary covariance and spectral features of real data (compare to bottom row).

Simulated data produce apparently 'dynamic' patterns

Simulated datasets generated using the stationary model exhibit remarkably similar patterns of fluctuation as real data. The rightmost panel of Figure 1 shows the sliding correlation computed on the average sliding within-network correlation over time (100-second windows) for each stage of the simulation and for real data. The covariance- and spectrally-constrained stationary simulation for a given subject exhibits fluctuations in within-network correlation that have similar magnitude as real data.

Further, these stationary simulations can also produce transient full matrix patterns of correlation that resemble ‘states’, as have been described in several recent publications (Allen et al., 2012; Hutchison et al., 2015). In Figure 2, we have performed a k-means clustering analysis of the sliding correlation matrices computed from both real and simulated data. Real sessions with fewer than 50% frames kept after frame censoring (FD < 0.2) were ignored in this analysis (see below for more on frame censoring). Ten sessions of simulated data based on each subject were used for the simulation dataset. As can be seen in Figure 2A, the clustering extracts matrices that have distinctive patterns of correlation. However, the clustered ‘states’ from both real and simulated data are nearly identical (k = 7). Further, figure 2B depicts the set of sliding correlation matrices (and their ‘state’ assignment) projected onto 2 dimensions, illustrating that apparent states in real data are not discernably different from those found in stationary simulation. The cluster validity index also indicates that there is no distinction in the rank of the divisibility of real and simulated data. Taken together the results suggest that there are not observable ‘states’ in real data that are readily distinguishable from ‘states’ arising from sampling variability measured in stationary simulated data.

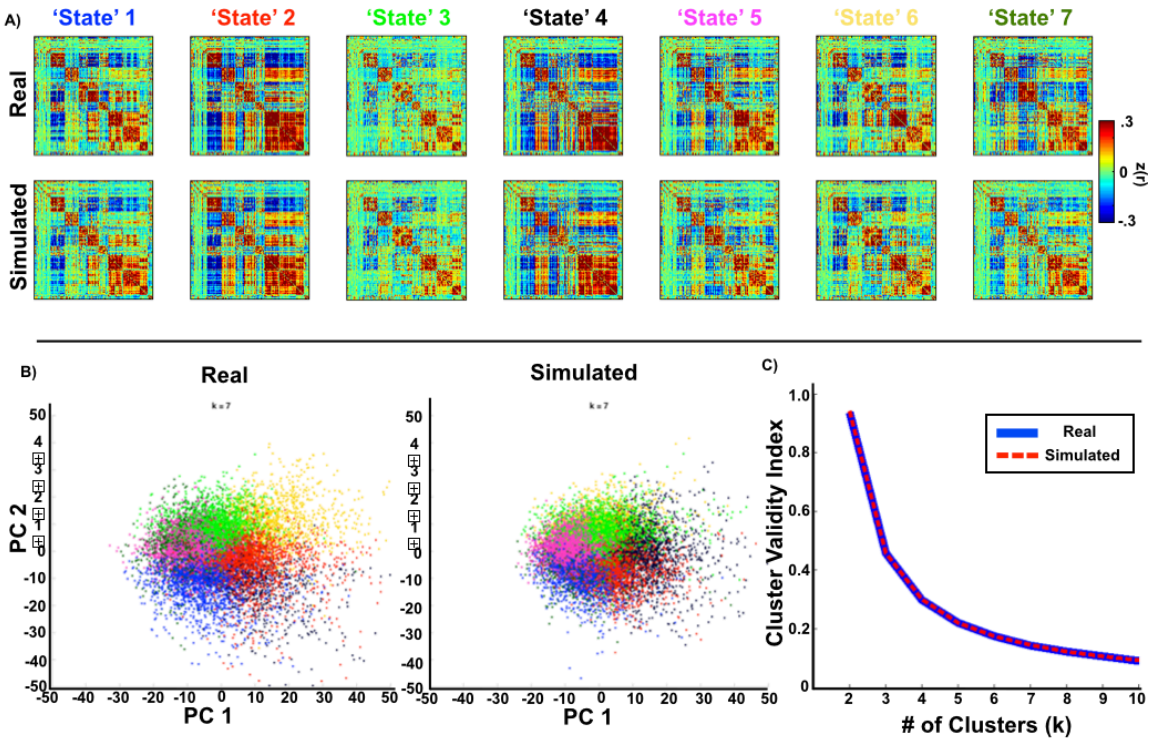

Figure 5-2. Real and simulated data have the same 'states'. A) Average correlation matrix from each cluster in clustering analysis (k = 7) of sliding correlation. Real and simulated data produce very similar 'state' patterns. B) Trajectories of sliding correlation matrices from all subjects and sessions (except sessions with mean FD>.2) have no obvious state organization when projected onto the first principal components. Colors correspond to 'state' identity in A). C) Cluster validity index by number of clusters is nearly identical between real and simulated data.

Multivariate kurtosis can be used to detect presence of non-stationary behavior in multivariate timeseries

The presence of non-stationarity in a timeseries of the form under consideration here, namely a change in second-order statistics, should be reflected in the kurtosis of the timeseries' distribution (e.g., (Martins, 2007)). Therefore, to detect the presence of non-stationarity in a set of BOLD timeseries extracted from cortical parcels of interest, we adopt a straightforward measure of multivariate kurtosis introduced by Mardia (Henze, 2002; Mardia, 1970). This statistic can be used as a test of multivariate

normality and is consequently sensitive to changes in the covariance structure of a multivariate process. To illustrate this sensitivity to changes in covariance, we have generated two simulations of 333-parcel multivariate processes based on the differing covariance of real data in eyes open and eyes closed conditions collected as part of the MyConnectome Project (Figure 3A; Laumann et al., 2015; Poldrack et al., 2015). In one simulation, a single 'eyes-open' stationary covariance structure was assumed for the entire epoch. In the second simulation, the covariance structure changed from 'eyes-open' to 'eyes-closed' halfway through the epoch. While a seemingly large change in external stimulation, this represents a well-documented (Laumann et al., 2015; McAvoy et al., 2008) but relatively minor change to the overall covariance structure (difficult to detect by the naked eye without computing the difference matrix). Prior to kurtosis calculation, the process was dimensionality reduced via principal components analysis to 30 timeseries. In the limit, the expected kurtosis of a normal stationary multivariate process of dimensionality d is d*(d+2). In this work, the multivariate kurtosis of real data will always be contextualized with respect to the multivariate kurtosis derived from simulated data of the same length but defined to have stationary covariance and spectral content. The multivariate kurtosis measure detected increased kurtosis in the two-state simulation relative to the one-state simulation (Figure 3B, right). This observation suggests that multivariate kurtosis is sensitive to non-stationary features of simulated BOLD timeseries.

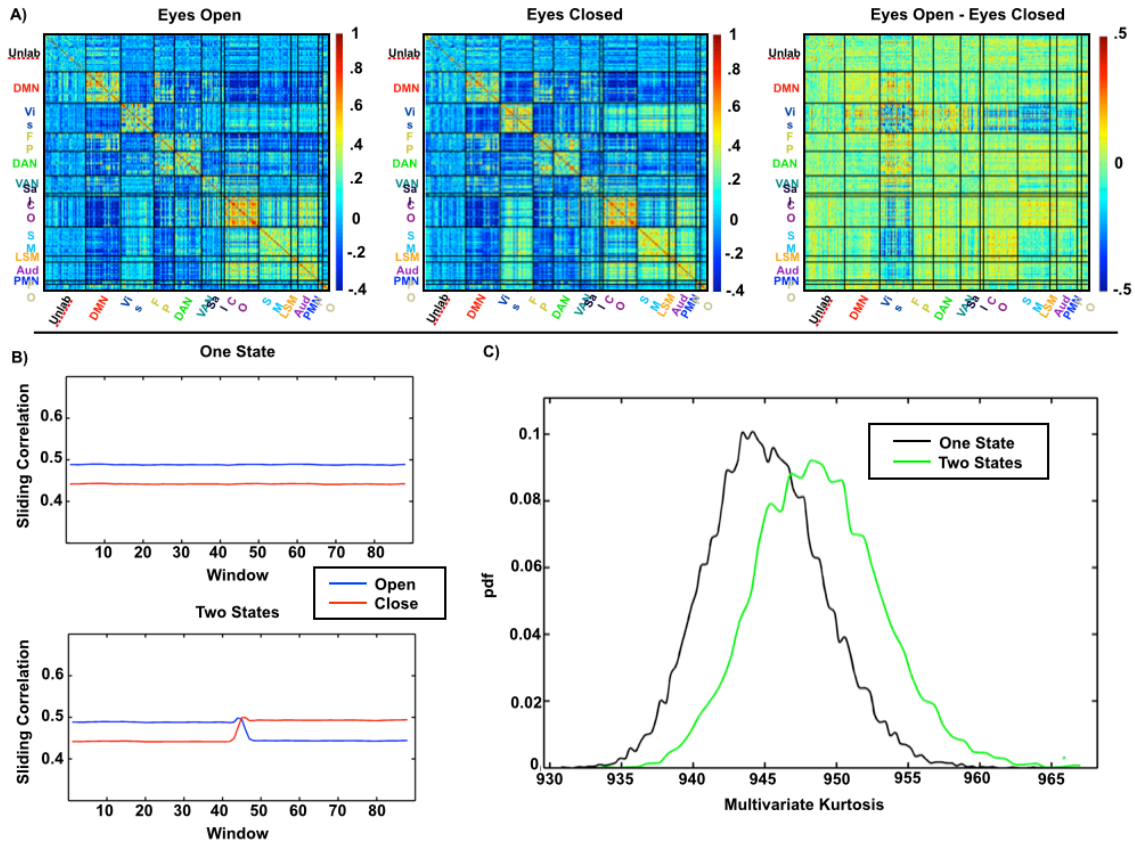

Figure 5-3. Multivariate kurtosis is sensitive to state changes in simulated multivariate data. Simulated data with eyes open vs. eyes closed state changes was used to demonstrate that multivariate kurtosis is sensitive to bona fide state changes. A) Average correlation matrices from real data acquired in eyes open (ten 10-minute sessions) and eyes closed (ten 10-minute session) conditions. The primary differences are in visual and somatomotor cortex. B) Average sliding correlation of windowed correlation matrix to eyes open and eyes closed correlation matrix for two simulations (n = 10000). One simulation is eyes open throughout and the other simulation switches to eyes closed halfway through the session. C) Distribution of computed multivariate kurtosis values for 10000 iterations of each simulation. Multivariate kurtosis is greater for the two-state simulation relative to the one-state simulation.

Timeseries approach normality if high motion frames are removed

Using the multivariate kurtosis measure, we now consider possible contributing sources to apparent non-stationarity in real data. The first, and most obvious, source of non-stationarity is head motion. Head motion is known to cause transient whole-brain changes in BOLD signal that substantially change measured RSFC (Power et al., 2012;

Van Dijk et al., 2012). It is therefore likely to be a source of non-stationarity in the BOLD signal.

As expected, the mean framewise displacement (FD) of each session significantly correlates with multivariate kurtosis (Figure 4A). Without FD-based censoring or temporal interpolation mean FD correlates with kurtosis at $r = 0.50$. If we apply modern procedures for reducing the impact of head motion by removing and interpolating over frames with FD > 0.2 (Power et al., 2014), the correlation decreases to $r = -0.47$. This negative correlation is likely related to several outlier sessions that have particularly high head motion and thus few frames remaining after FD censoring. If we discard all sessions with fewer than 50% of frames remaining, the correlation is $r = -0.08$ ($n=81$; Figure 4A, bottom). Thus, these head motion correction procedures substantially reduce the kurtosis of the timeseries. It is worth noting that there are several sessions among the subjects that exhibit multivariate kurtosis values that are very close to the kurtosis exhibited by stationary simulated data (blue dots that lie near the red lines in Figure 4A). Therefore, by this measure, there are at least some 30-minute long sessions that exhibited practically no detectable non-stationary phenomena, especially after head motion correction.

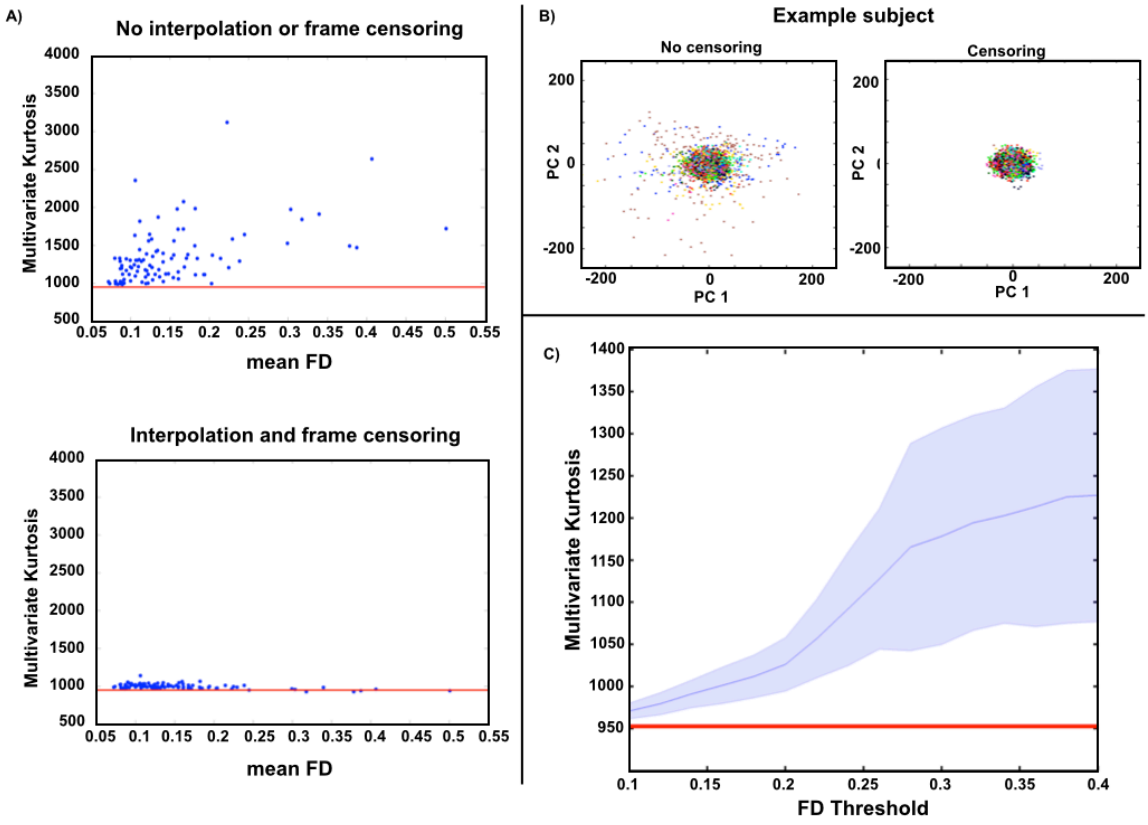

Figure 5-4. Multivariate kurtosis is related to motion. A) Multivariate kurtosis correlations with mean framewise displacement (FD) using all 10 sessions from each of 10 subjects. Kurtosis is computed on the first 30 principal components derived from each session. The average kurtosis of simulated stationary data is indicated by the red line (~950). Correlation with motion is substantially reduced after interpolation and masking of censored frames (bottom). B) Timepoints from all 10 sessions from one example subject projected on first two principal components. Dot color indicates the different sessions. If all timepoints are included there are many timepoints with large deviations from the rest of the data. These will contribute to measures of excess kurtosis. If timepoints with high FD are censored (here, FD>0.2; the censoring procedure also removes stretches of time with less than 5 contiguous frames.), almost all of the deviant timepoints are removed and the projection becomes nearly Gaussian. B) Multivariate kurtosis as a function of frame censoring FD threshold across all sessions and subjects. The shaded error indicates the standard deviation. The red line indicates the average multivariate kurtosis from simulated datasets.

To further illustrate the incremental effect of head motion on kurtosis, we present timepoints from ten sessions of data (818 frames per session) from a single subject after dimensionality reduction (Figure 4B). If all timepoints were included, there were a number of timepoints with significant deviations from the rest of the data. These deviant

timepoints contributed to excess kurtosis in the data. However, for this subject, many of the very deviant timepoints were eliminated if we censored frames with high motion (FD > 0.2). In general, across all subjects and sessions, excess multivariate kurtosis increases as a function of FD (Figure 4C). Put another way, as more and more high motion frames were removed from consideration by applying more stringent FD thresholds, the multivariate kurtosis approaches normality (dotted line; Figure 4C). Unfortunately, for many sessions, all of the data would be eliminated before we reach this point.

Session by session multivariate kurtosis is correlated with sleep index

Motion is an obvious source of spurious non-stationarity, but there is another known potential source of non-stationarity that we may crudely be able to identify in our data. In an essential study, Tagliazucchi and colleagues (Tagliazucchi et al., 2014) demonstrated that many datasets that were collected with the intention of acquiring awake resting state data are contaminated by sleep. Further, sleep has been documented to produce changes in the underlying correlation structure, representing a separate state. Thus, unstable wakefulness would be a likely source of bona fide non-stationarity in resting-state timeseries.

Following their work, we have developed a simple procedure to assess how sleep-like are each of the sessions in our dataset and thus evaluate how much shifting between wake and sleep may exist. This mixture of states should be related to measures of kurtosis. In particular, we have used the Tagliazucchi dataset, in which sleep stage is known, to define a set of voxels by which it is possible to discriminate

different stages of sleep. The best regions of the brain to do this are in visual and somatomotor cortex, and the thalamus. We ignore the visual regions because our data was collected with eyes open (as opposed to the Tagliazucchi data which was collected with eyes closed), which may confound the measure. Thus, a covariance matrix of somatomotor and thalamic voxels can be computed for stage 0 (awake) and state 1 and stage 2 (light) sleep. We then compared covariance of these same voxels from the 30-minute resting sessions in our dataset to these stage 0 and stage 1/2 exemplars. The difference in similarity to stage 1/2 vs. stage 0 sleep is defined as the sleep index, i.e. the higher the value of the sleep index the more 'sleep'-like the session was, suggesting unstable wakefulness. Figure S2 illustrates that the sleep index tends to increase over the course of scanning session across subjects, as might be expected, providing circumstantial evidence that the index may be a useful measure of sleepiness. When we compare the sleep index to the multivariate kurtosis of interpolated, frame-censored data (excluding sessions with <50% frames, and one session with multivariate kurtosis 4.7 std greater than the mean), we find a significant correlation between the two measures ($r = 0.31$, $p=0.0044$; Figure 5). This result provides evidence that, in addition to motion, observed non-stationarity may also be related to changing levels of sleep over the course of a resting state session.

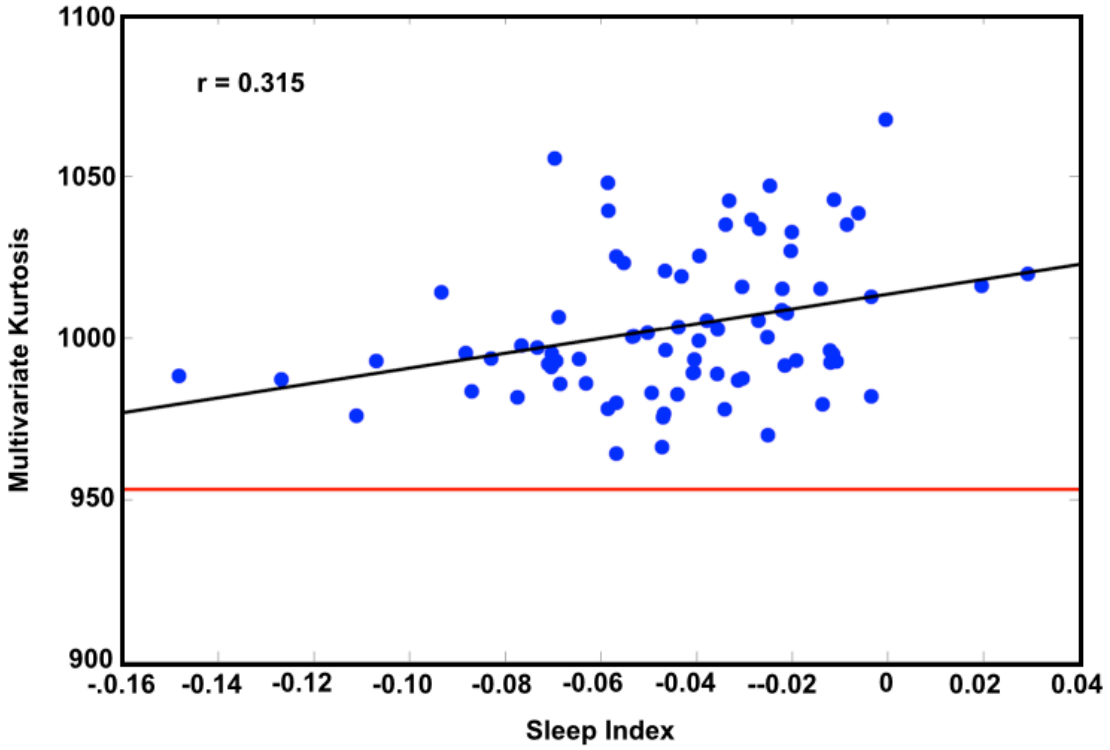

Figure 5-5. Multivariate kurtosis correlates with sleep index. Kurtosis is computed on the first 30 principal components derived from each session. Sessions have been interpolated and frame censored. Any session with mean FD > 0.2 has been removed. One session with a kurtosis measure 4.7 standard deviations from the mean was excluded. The average kurtosis of simulated stationary data is indicated by the red line (~950).

5.4 Discussion

Using a multivariate kurtosis statistic and comparing against a stationary simulation, we evaluated the presence of 'non-stationary' phenomena in resting-state BOLD data. We found that resting-state BOLD data appears to be essentially stationary to second order. Observed fluctuations in second-order statistics can, to a large extent, be attributed to three major factors: 1. sampling variability intrinsic to small quantities of data; 2. artifactual signal changes related to head motion; and 3. bona-fide signal

changes related to sleep state. These sources of real and apparent non-stationarity, as well as the implications of stationary resting-state BOLD, are discussed below.

Much of observed 'dynamics' is sampling variability of second-order statistics

The literature has begun to recognize the fundamental importance of adopting appropriate techniques and statistical models to assess non-stationarity in resting-state BOLD timeseries (Leonardi et al., 2015; Lindquist et al., 2014; Zalesky et al., 2015). Standard techniques, especially the sliding window technique, can generate apparent fluctuations in correlation. The essential problem is that the sampling error of second-order statistics is inversely proportional to the period of observation (Laumann et al., 2015).

Our observations confirm and expand on these warnings. By using an appropriate stationary simulation of BOLD data that incorporates the spectral content and system-specific patterns of covariance of real BOLD data, we demonstrate how sampling variability can masquerade as 'dynamics'. Specifically, the observed variability of windowed correlations in simulated stationary timeseries is similar in magnitude to fluctuations observed in real data (see Figure 1). Moreover, if subjected to a clustering analysis, simulated stationary timeseries produce clustered correlation matrices ('states') very similar to those obtained in real data. Therefore, the appearance of discrete 'states' in resting-state BOLD timeseries appears to be illusory.

Head motion is a large source of artifactual non-stationarity

Head motion has been clearly demonstrated to bias estimates of correlation in standard RSFC analyses (Power et al., 2012; Satterthwaite et al., 2012; Van Dijk et al., 2012), but the problem it poses for dynamic RSFC analyses is perhaps even more obvious (Hutchison et al., 2013). While sampling variability can give the appearance of 'dynamics' in resting-state BOLD timeseries, head motion will introduce 'true' non-stationarity into BOLD data, though of no biological interest. Indeed, even small movements of the head may be expected to corrupt measures specifically designed to detect transient changes in the BOLD signal. As such, we found that measured kurtosis is correlated with the level of head motion in a scanning session. Importantly, if we adopted modern head motion censoring procedures, including interpolation of high motion frames (FD > 0.2) and removal of these frames from analysis (Power et al., 2014), we substantially reduced the observed multivariate kurtosis. In some cases, this maneuver reduced the multivariate kurtosis to be nearly indistinguishable from simulated stationary timeseries. Figure 4C suggests that if even more strict movement criteria are used more sessions may reach this baseline. These results imply that a substantial portion of non-stationarity observed in resting-state BOLD timeseries may be related to head motion and urge maximal caution when interpreting measurements of dynamic RSFC. Indeed, subject by subject and day by day differences in motion may significantly contribute to the variability in dynamic RSFC measures, as others have observed (Lindquist et al., 2014), making reliable associations with behavioral measures a serious challenge.

Unstable wakefulness may introduce bona fide non-stationarity into the resting state

While head motion can introduce true, but artifactual, non-stationarity into resting-state BOLD timeseries, real changes in physiological state over the course of a scanning session may introduce bona fide non-stationarity. In particular, sleep is associated with significant changes in neural activity with specific EEG signatures (Dement et al., 1957). Tagliazucchi and colleagues have demonstrated that sleep is a real contaminant of many resting state datasets that warrants serious consideration when interpreting standard RSFC analyses (Tagliazucchi et al., 2014). Following this observation, we hypothesized that fluctuating sleep state may contribute to measured non-stationarity in our data, even though subjects were asked to stay awake and keep their eyes open for the duration of the scan. This request is a legitimate challenge for 30-minute scan sessions, as collected here, especially as all sessions were collected in the middle of the night (approx. 12 midnight – 2 PM). Consistent with this expectation, we found that, after aggressive motion correction, a sleep index based on the Tagliazucchi dataset correlated with the remaining measured multivariate kurtosis. Thus, at least some observed non-stationarity is likely related to unstable wakefulness over the course of the scan.

Our sleep analysis here has several important caveats. The sleep index is, at best, an indirect measure of the presence of sleep stages. We do not have combined EEG or other independent measures to verify the characteristic patterns of descent into sleep. We also did not use visual cortex in defining the sleep index, even though visual cortex can be used to distinguish different stages of sleep in subjects with their eyes

closed, as our subject had their eyes open. Finally, accurate measurement of resting-state functional connectivity in an individual who is struggling to stay awake is very challenging as this behavior is frequently associated with increased head motion. Thus, periods of unstable wakefulness may have been largely discarded through the motion censoring procedure, reducing our sensitivity to the presence of alternate sleep states over the course of the scan.

Resting-state BOLD may be essentially stationary to second order over short time-scales

Our results suggest that resting-state BOLD timeseries are essentially stationary, or, at least, observable non-stationarity is largely attributable to identified explanatory variables (head motion and sleep state). If resting-state BOLD timeseries are indeed stationary, what are the neurobiological implications?

Resting state BOLD fluctuations do not primarily reflect online cognitive processes

The property of stationarity may provide further support for the notion that resting-state BOLD fluctuations do not primarily reflect online cognitive processes. This perspective has been argued previously based on several forms of evidence (Raichle et al., 2007): 1. The topography of correlated BOLD activity within functional systems, while modified sufficiently to be distinguishable (Tagliazucchi et al., 2014), remains largely intact in slow-wave sleep (Samann et al., 2011) and under anesthesia (Palanca et al., 2015). Under these conditions, online cognitive activity is presumed to be

essentially absent; 2. BOLD responses elicited by a task (i.e. online activity) do not perturb ongoing resting-state activity very much, necessitating substantial trial repetition to observe task-related effects (Raichle et al., 2006); and we may further add, 3. Correlation patterns of resting-state BOLD activity are fairly consistent across subjects (Damoiseaux et al., 2006) and within subjects across sessions (Laumann et al., 2015). Unconstrained online cognition, on the other hand, might be expected to vary considerably from subject to subject or from scan to scan. The observation of stationarity on shorter time scales adds further evidence to this argument. Unconstrained cognitive processes may be expected to vary considerably over the course of a scan, and, at some level, must be reflected in non-stationary neural activity. Resting-state BOLD, however, does not appear to reflect this property, suggesting that it may not substantially relate to such online neural activity. Rather, resting-state BOLD activity may primarily reflect spontaneous offline processes unrelated to immediate cognitive experience.

In particular, stationary spontaneous activity may relate to a necessary feature of effective brain function. While the brain must allow for processing of new experiences and adaptive plasticity, it must also store information and maintain its functional architecture over substantial periods of time, as much as decades. Evidence for stability of brain structure has been well established at small spatial scales (Marder et al., 2006), and spontaneous activity has been implicated in this process. Indeed, spontaneous activity has been shown to play a key role in maintaining functionally appropriate patterns of connectivity during development and has been postulated to serve a similar role throughout life (Katz et al., 1996; Penn et al., 1999). Thus, patterns of spontaneous

activity may both reflect preferred synaptic relationships as well as serve to maintain them. In this view, at the larger spatial scale studied here, spontaneous activity may be expected to significantly change over long time-scales following persistent changes in functional co-activation, as has been demonstrated (Lewis et al., 2009), but, in fact, may generally serve to restore synaptic balance in the wake of experience-dependent perturbations of synaptic weights (Davis, 2006). Stationarity in resting-state BOLD signals over short time-scales may thus reflect the essential long-term stability of systems-level neuronal relationships.

Stationarity is consistent with known 'dynamic' features of resting-state BOLD

It is important to note that stationarity of second-order statistics in resting-state BOLD is compatible with a large repertoire of dynamic behavior and functional associations. For example, stationarity does not imply that resting-state BOLD fluctuations have no relation to behavior. Several studies have reported effects of fluctuations in resting-state activity on cognition (M. D. Fox et al., 2007b; Hesselmann et al., 2008; Sadaghiani et al., 2010), and they are in no way gainsaid by the observations here. A stationary process can have different properties depending on when it is observed. For example, a frictionless pendulum could complete a circuit to turn on a light only at one end of its swing. Further, stationarity is consistent with the presence of specific spatiotemporal propagating processes as have been reported in resting-state data (Majeed et al., 2009; Mitra et al., 2015a). A wave machine operating with fixed frequency and intensity on a pool of water will generate a stationary wave that

translates through space. Similarly, stationary offline processes may manifest as structured spatiotemporal features in BOLD activity.

Conclusion

This set of analyses does not definitively prove that resting-state-BOLD is devoid of non-stationary features. However, we believe that any evaluation of RSFC dynamics needs to carefully account for sampling variability and known sources of non-stationarity (like head motion and sleep state) to appropriately interpret observations of dynamics. Taking these considerations into account, on the other hand, exposes the intriguing possibility that resting-state BOLD activity may be essentially stationary, pointing to a specific role for this activity distinct from online cognitive processing.

5.5 Methods

Subjects

Data were collected on ten healthy, right-handed, young adult subjects (5 females; age: 24-34). Two of the subjects are authors (ND and SN), and the remaining subjects were recruited from the Washington University community. Informed consent was obtained from all participants. Imaging was performed over 12 days on a Siemens TRIO 3T MRI scanner.

Structural data

Four T1-weighted images (sagittal, 224 slices, 0.8 mm isotropic resolution, TE=3.74 ms, TR=2400 ms, TI=1000 ms, flip angle = 8 degrees) and four high-resolution

T2-weighted images (sagittal, 224 slices, 0.8 mm isotropic resolution, TE=479 ms, TR=3200 ms) were obtained for each subject.

Surface processing and CIFTI generation

Surface generation and sampling of functional data to anatomical surfaces followed a procedure similar to that previously described in (Glasser et al., 2013). First, following volumetric registration, anatomical surfaces were generated from the subject's MP-RAGE image using FreeSurfer's default recon-all processing pipeline (version 5.0). This pipeline included brain extraction, segmentation, generation of white matter and pial surfaces, inflation of the surfaces to a sphere, and surface shape-based spherical registration of the subject's 'native' surface to the fsaverage surface (A. M. Dale et al., 1999; A. M. Dale et al., 1993a; Fischl et al., 1999; Segonne et al., 2004). The fsaverage-registered left and right hemisphere surfaces were brought into register with each other using deformation maps from a landmark-based registration of left and right fsaverage surfaces to a hybrid left-right fsaverage surface ('fs_LR'; (Van Essen et al., 2012a)) and resampled to a resolution of 164,000 vertices (164k fs_LR) using Caret tools (Van Essen et al., 2001). Finally, each subject's 164k fs_LR surface was down-sampled to a 32,492 vertex surface (fs_LR 32k). The various deformations from the 'native' surfaces to the fs_LR 32k surface were composed into a single deformation map allowing for one step resampling. A script for this procedure is available on the Van Essen Lab website (Freesurfer_to_fs_LR Pipeline, http://brainvis.wustl.edu).

Surface processing of the BOLD data proceeded through the following steps. First, the BOLD fMRI volumes are sampled to each subject's individual 'native'

midthickness surface (generated as the average of the white and pial surfaces) using the ribbon- constrained sampling procedure available in Connectome Workbench 0.84. This procedure samples data from voxels within the gray matter ribbon (i.e. between the white and pial surfaces) that lie in a cylinder orthogonal to the local midthickness surface weighted by the extent to which the voxel falls within the ribbon (Glasser et al., 2011). Voxels with a timeseries coefficient of variation 0.5 standard deviations higher than the mean coefficient of variation of nearby voxels (within a 5 mm sigma Gaussian neighborhood) were excluded from the volume to surface sampling, as described in (Glasser et al., 2013). Once sampled to the 'native' surface, timecourses were deformed and resampled from the individual's 'native' surface to the 32k fs_LR surface in a single step using the deformation map generated as described above. This resampling allows point-to-point comparison between each individual registered to this surface space. Finally, the time courses were geodesically smoothed along the 32k fs_LR surface using a Gaussian smoothing kernel ($\sigma = 2.55$).

These surfaces were then combined with volumetric subcortical and cerebellar data into the CIFTI format using Connectome Workbench (Glasser et al., 2013), creating full brain timecourses excluding non-gray matter tissue. Subcortical (including accumbens, amygdala, caudate, hippocampus, pallidum, putamen, and thalamus) and cerebellar voxels were selected based on the FreeSurfer segmentation of the individual subject. Volumetric data were smoothed within this mask with a 3D Gaussian kernel ($\sigma = 2.55$) before being combined with the surface data.

Functional data

For each subject, thirty contiguous minutes of resting state data were collected on ten separate days (total time = 300 minutes per subject). Subjects were passively fixated on a white crosshair that was presented against a black background. Functional imaging was performed using a gradient-echo EPI sequence (TR = 2.2 s, TE = 27 ms, flip angle = 90°, voxel size = 4 mm x 4 mm × 4 mm, 36 slices). In each session, a gradient echo field map sequence was acquired with the same prescription as the functional images.

Distortion correction

Mean field map creation: A mean field map was generated based the field maps collected in each subject (Laumann et al., 2015). This mean field map was then applied to all sessions for distortion correction. To generate the mean field map the following procedure was used: (1) Field map magnitude images were mutually co-registered. (2) Transforms between all sessions were resolved. Transform resolution reconstructs the n-1 transforms between all images using the n*(n-1)/2 computed transform pairs. (3) The resolved transforms were applied to generate a mean magnitude image. (4) The mean magnitude image was registered to an atlas representative template. (5) Individual session magnitude image to atlas space transforms were computed by composing the session-to-mean and mean-to-atlas transforms. (6) Phase images were then transformed to atlas space using the composed transforms, and a mean phase image in atlas space was computed.

Application of mean field map to individual sessions: (1) For each session, field map uncorrected data was registered to atlas space. (2) The generated transformation matrix was then inverted and applied to the mean field map to bring the mean field map into the session space. (3) The mean field map was used to correct distortion in the session space. (4) The undistorted data was then re-registered to atlas space. (5) This new transformation matrix and the mean field map then were applied together to resample the session data to undistorted atlas space in a single step.

fMRI Preprocessing

Functional data was preprocessed to reduce artifact and to maximize cross-session registration. All sessions underwent intensity normalization to a whole brain mode value of 1000 and within run correction for head movement. Atlas transformation was computed by registering the mean intensity image from a single BOLD session to atlas space via the average high-resolution T2- weighted image (n = 4) and average high- resolution T1-weighted image (n = 4). All subsequent BOLD sessions were linearly registered to this first session. Atlas transformation, distortion correction, and resampling to 3-mm isotropic atlas space were combined into a single interpolation using FSL's applywarp tool (Smith et al., 2004). All subsequent operations were performed on the atlas-transformed volumetric time series.

RSFC preprocessing

Artifacts were reduced using frame censoring, nuisance regression (excluding censored frames), interpolation and spectral filtering following (Power et al., 2014).

Nuisance regressors included whole brain, white matter, and ventricular signals and their derivatives, in addition to 24 movement regressors derived by expansion (Friston et al., 1996). To assess the impact of motion on measures of non-stationarity, results are presented both with and without the frame censoring and interpolation steps. Frames with framewise displacement (FD) > 0.2 mm were censored, as well as uncensored segments of data lasting fewer than 5 contiguous volumes (mean frames kept across sessions: 72.5% ± 25%). Interpolation over censored frames was computed by least squares spectral estimation to prepare continuous data for subsequent bandpass filtering (Power et al., 2014).

Region of interest (ROI) definition

All analyses presented here are based on timeseries extracted using a group-level cortical parcellation described in (Gordon et al., 2014b). This 333-area parcellation covers most of the cortical surface, and has been divided into 12 networks based on the Infomap community detection technique (Power et al., 2011; Rosvall et al., 2008). The parcels and their network assignments can be seen in Figure S1.

BOLD simulation

To simulate a stationary surrogate with both the covariance and spectral properties of real BOLD we performed the following procedure, outlined in Figure 1. First, we sample a timeseries of random normal deviates of the same dimensionality as a real dataset (step 1). These timeseries are then projected onto the eigenvectors derived from the stationary covariance structure of real data (step 2). Finally, these

timeseries are multiplied in the spectral domain by the power spectrum derived from a full-length real dataset (step 3). This procedure produces random surrogate timeseries with the covariance and spectral structure of real data (compare last two rows of Figure 1) that is stationary by construction. These simulated timeseries can then act as a null against which to evaluate non-stationary features of real data.

Sliding Window Analysis

To estimate fluctuating connectivity over time, we adopt the sliding window strategy commonly used in the literature (Hutchison et al., 2012; Zalesky et al., 2014). Specifically, we extract timeseries from the cortical surface using the 333-area parcellation described in (Gordon et al., 2014b). Correlations are then computed at each timepoint between windowed samples of the timeseries tapered by a Gaussian function to center-weight the contribution of proximal timepoints. Window size is adjustable by changing the number of frames specified as the full width at half maximum. The timeseries are highpass filtered at the frequency of the lowest frequency allowing a full cycle given the window length. Here, we use 100s windows, so the timeseries are high-pass filtered at 0.01 Hz (Leonardi et al., 2015; Zalesky et al., 2015). To illustrate sliding window fluctuations at the network level, we averaged all correlations between regions within each network at each window. Real and simulated timecourses of within-network connectivity can be seen in Figure 1 in the far right column.

State analysis

To group the correlation patterns generated by the sliding window procedure we adopted the k-means clustering algorithm commonly used in the literature (Allen et al., 2012; Hutchison et al., 2015). The correlation patterns were dimensionality reduced from 55278 (333 parcels x 333 parcels) to 30 dimensions by principal component analysis (PCA) prior to clustering to reduce computational demand. The Mahalanobis (L1) distance function was used to compute the separation between each window's correlation pattern and the k-means algorithm was iterated 100 times with random centroid positions to avoid local minima. Windows from all sessions and all subjects were used in the clustering, excluding 19 sessions (8 from one subject) that had more than half of their frames discarded because of excessive head motion. The window length for this analysis was 100 seconds and the windows were overlapping with a separation of 11 seconds between window centers, generating 155 windows per session. The windowed correlation patterns were mean-centered by run to eliminate run-level or subject-level features from contributing to the clustering result. K-means clustering was applied in the same manner to 100 sessions of simulated data, where each subject's BOLD power spectrum and covariance was used to generate 10 sessions. The cluster validity index was used to evaluate the quality of clustering for a range of cluster numbers (k=2-10). The cluster validity index was computed as the ratio of within-cluster distance to between-cluster distance.

Kurtosis of Mardia

In the general case, tests of second-order multivariate stationarity are evaluated in terms of spectral measures (Jentsch et al., 2015). This approach frequently is used in the context of electrophysiology e.g., (Halliday et al., 2009; Wong et al., 2006). Here, we take a different approach based on demonstrating that BOLD fMRI timeseries are consistent with a multivariate normal process.

In greater detail, we evaluate the multivariate fourth moment (kurtosis) of BOLD fMRI data. To obtain a heuristic understanding of the relevance of kurtosis to evaluating the stationarity of a second order statistic, recall that statistical theory shows that the variance of the mth moment is given by the moment of order $2m$ (Weatherburn, 1961). Thus, the variance of the mean (m = 1) is given by the variance (m = 2). Correspondingly, the variance of a second order statistic, i.e., the covariance (m = 2) of a multivariate process, is related to the multivariate kurtosis (m = 4). Hence, evidence of second order stationarity, e.g., lack of significant changes in the covariance structure of a multivariate process, is obtained if the multivariate fourth moment (kurtosis) of BOLD fMRI data equals that of a perfectly normal and stationary synthetic surrogate.

Here, we adopt a straightforward measure of multivariate kurtosis introduced by Mardia (Henze, 2002; Mardia, 1970). Following the formalism of Henze, let $X_1,\ldots,X_n$ denote a random sample of size n of a d-dimensional vector, X. The sample covariance matrix is defined as:

$$S_n = \frac{1}{n}\sum_{j=1}^{n}(X_j - \overline{X_n})(X_j - \overline{X_n})', \quad (1)$$

where $\overline{X_n}$ is the mean over n samples. Given S_n, we can compute the squared Mahalonobis distance, which reflects the dissimilarity between any particular sample and the sample mean:

$$D_{n,jk} = (X_j - \overline{X_n})' S_n^{-1} (X_k - \overline{X_n}). \quad (2)$$

Multivariate kurtosis in the sense of Mardia, $b_{n,d}$, is simply the trace of the square of the squared Mahalanobis distance. Thus,

$$b_{n,d} = \frac{1}{n} \sum_{j=1}^{n} D_{n,jj}^2. \quad (3)$$

In the analyses presented here, multi-dimensional timeseries (both simulated and real) were extracted from 333 cortical areas. This number of regions exceeds the dimensionality of BOLD fMRI (Cordes & Nandy, NI 2006). Thus, the 333 × 333 covariance matrix of the data would be rank deficient, and the inversion required by Eq. (2) would be unstable. Accordingly, the dimensionality of the "raw" data was reduced via principal components analysis from 333 to 30, thereby stabilizing the kurtosis calculation while still retaining a reasonable number of independent signals. In the limit of an infinite sample size ($n \to \infty$), the expected multivariate kurtosis of a normal stationary multivariate process of dimensionality d is d·(d+2). In practice, the obtained value depends on the sample size. Therefore, in this work, the surrogate data were always matched in size to the real data in comparisons of multivariate kurtosis.

Sleep Index

To assess the level of wakefulness in each session we developed a sleep index (SI). This sleep index was based on a separate high quality resting state fMRI dataset acquired on subjects in known states of wake and sleep as determined by EEG (Tagliazucchi et al., 2014). Using these data, we computed the difference between the sleep (averaged over N1 and N2 sleep) and wake covariance matrices (wake minus sleep), and applied spatial principal components analysis (PCA) to the difference matrix. The weights in the first PC highlight those voxels whose covariance structure is maximally altered in wake vs. sleep (Mitra et al., 2015b). To select voxels exhibiting maximal change, we applied a Fischer-Z transform to the weights in the first PC, and selected only voxels whose weights were in the 95th percentile. Voxels in the occipital cortex were manually excluded, to avoid confounds arising from the fact that the data in the main analysis were acquired in the eyes-open state, whereas the sleep data were acquired in the eyes-closed state (during both wake and sleep). Covariance matrices from these voxels were computed for each session of each subject in the main dataset. These covariance matrices were then compared by Pearson correlation to the covariance matrices from the sleep and wake states of the sleep dataset. The sleep index was computed as the similarity to the sleep state minus the similarity to the wake state. A higher value of the sleep index means the session had covariance relatively more similar to sleep than wake.

5.6 Supplemental Figures

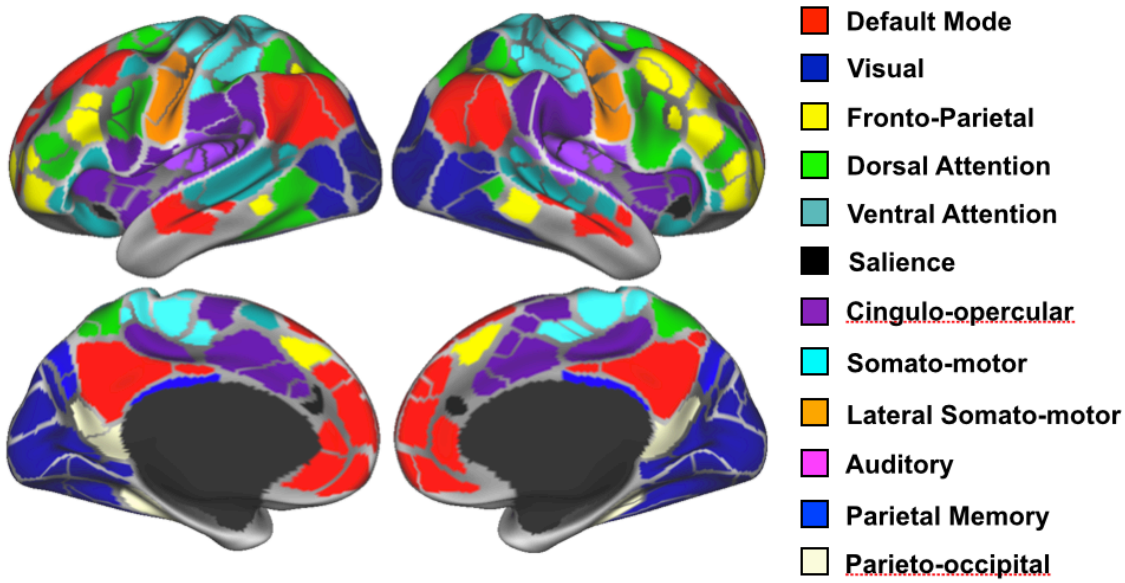

Supplementary Figure 5-1. Cortical parcels and their network assignments.

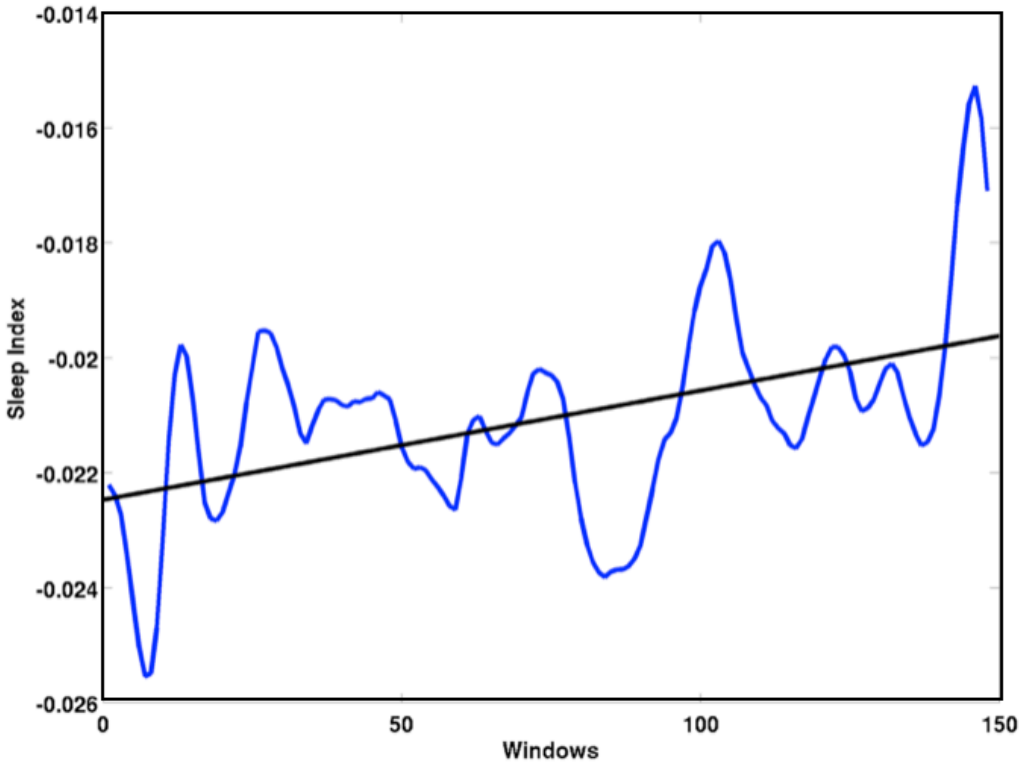

Supplementary Figure 5-2. Sleep index increases with time in scanner. The blue trace is the average value of the sleep index by time in scanner across all sessions and subjects.

5.7 References

Allen, E. A., Damaraju, E., Plis, S. M., Erhardt, E. B., Eichele, T., & Calhoun, V. D. (2012). Tracking Whole-Brain Connectivity Dynamics in the Resting State. Cereb Cortex.

Betti, V., Della Penna, S., de Pasquale, F., Mantini, D., Marzetti, L., Romani, G. L., & Corbetta, M. (2013). Natural scenes viewing alters the dynamics of functional connectivity in the human brain. Neuron, 79(4), 782-797.

Biswal, B., Yetkin, F. Z., Haughton, V. M., & Hyde, J. S. (1995). Functional connectivity in the motor cortex of resting human brain using echo-planar MRI. Magn Reson Med, 34(4), 537-541.

Calhoun, V. D., Miller, R., Pearlson, G., & Adali, T. (2014). The chronnectome: time-varying connectivity networks as the next frontier in fMRI data discovery. Neuron, 84(2), 262-274.

Chang, C., & Glover, G. H. (2010). Time-frequency dynamics of resting-state brain connectivity measured with fMRI. Neuroimage, 50(1), 81-98.

Dale, A. M., Fischl, B., & Sereno, M. I. (1999). Cortical surface-based analysis. I. Segmentation and surface reconstruction. Neuroimage, 9(2), 179-194.

Dale, A. M., & Sereno, M. I. (1993a). Improved Localizadon of Cortical Activity by Combining EEG and MEG with MRI Cortical Surface Reconstruction: A Linear Approach. J Cogn Neurosci, 5(2), 162-176.

Damoiseaux, J. S., Rombouts, S. A., Barkhof, F., Scheltens, P., Stam, C. J., Smith, S. M., & Beckmann, C. F. (2006). Consistent resting-state networks across healthy subjects. Proc Natl Acad Sci U S A, 103(37), 13848-13853.

Davis, G. W. (2006). Homeostatic control of neural activity: from phenomenology to molecular design. Annu Rev Neurosci, 29, 307-323.

de Pasquale, F., Della Penna, S., Snyder, A. Z., Marzetti, L., Pizzella, V., Romani, G. L., & Corbetta, M. (2012). A cortical core for dynamic integration of functional networks in the resting human brain. Neuron, 74(4), 753-764.

Dement, W., & Kleitman, N. (1957). The relation of eye movements during sleep to dream activity: an objective method for the study of dreaming. J Exp Psychol, 53(5), 339-346.

Fischl, B., Sereno, M. I., & Dale, A. M. (1999). Cortical surface-based analysis. II: Inflation, flattening, and a surface-based coordinate system. Neuroimage, 9(2), 195-207.

Fox, M. D., Snyder, A. Z., Vincent, J. L., & Raichle, M. E. (2007b). Intrinsic fluctuations within cortical systems account for intertrial variability in human behavior. Neuron, 56(1), 171-184.

Friston, K. J., Williams, S., Howard, R., Frackowiak, R. S., & Turner, R. (1996). Movement-related effects in fMRI time-series. Magn Reson Med, 35(3), 346-355.

Glasser, M. F., Sotiropoulos, S. N., Wilson, J. A., Coalson, T. S., Fischl, B., Andersson, J. L., Xu, J., Jbabdi, S., Webster, M., Polimeni, J. R., et al. (2013). The minimal preprocessing pipelines for the Human Connectome Project. Neuroimage, 80, 105-124.

Glasser, M. F., & Van Essen, D. C. (2011). Mapping human cortical areas in vivo based on myelin content as revealed by T1- and T2-weighted MRI. J Neurosci, 31(32), 11597-11616.

Gordon, E. M., Laumann, T. O., Adeyemo, B., Huckins, J. F., Kelley, W. M., & Petersen, S. E. (2014b). Generation and Evaluation of a Cortical Area Parcellation from Resting-State Correlations. Cereb Cortex.

Halliday, D. M., Rosenberg, J. R., Rigas, A., & Conway, B. A. (2009). A periodogram-based test for weak stationarity and consistency between sections in time series. Journal of neuroscience methods, 180(1), 138-146.

He, B. J., Zempel, J. M., Snyder, A. Z., & Raichle, M. E. (2010). The temporal structures and functional significance of scale-free brain activity. Neuron, 66(3), 353-369.

Henze, N. (2002). Invariant test for multivariate normality: a critical review. Statistical Papers, 43, 467-506.

Hesselmann, G., Kell, C. A., & Kleinschmidt, A. (2008). Ongoing activity fluctuations in hMT+ bias the perception of coherent visual motion. J Neurosci, 28(53), 14481-14485.

Honey, C. J., Sporns, O., Cammoun, L., Gigandet, X., Thiran, J. P., Meuli, R., & Hagmann, P. (2009b). Predicting human resting-state functional connectivity from structural connectivity. Proc Natl Acad Sci U S A, 106(6), 2035-2040.

Hutchison, R. M., & Morton, J. B. (2015). Tracking the Brain's Functional Coupling Dynamics over Development. J Neurosci, 35(17), 6849-6859.

Hutchison, R. M., Womelsdorf, T., Allen, E. A., Bandettini, P. A., Calhoun, V. D., Corbetta, M., Della Penna, S., Duyn, J. H., Glover, G. H., Gonzalez-Castillo, J., et al. (2013). Dynamic functional connectivity: promise, issues, and interpretations. Neuroimage, 80, 360-378.

Hutchison, R. M., Womelsdorf, T., Gati, J. S., Everling, S., & Menon, R. S. (2012). Resting-state networks show dynamic functional connectivity in awake humans and anesthetized macaques. Hum Brain Mapp.

Jentsch, C., & Subba Rao, S. (2015). A test for second order stationarity of a multivariate time series. Journal of Econometrics, 185 124–161.

Karahanoglu, F. I., & Van De Ville, D. (2015). Transient brain activity disentangles fMRI resting-state dynamics in terms of spatially and temporally overlapping networks. Nat Commun, 6, 7751.

Katz, L. C., & Shatz, C. J. (1996). Synaptic activity and the construction of cortical circuits. Science, 274(5290), 1133-1138.

Kopell, N. J., Gritton, H. J., Whittington, M. A., & Kramer, M. A. (2014). Beyond the connectome: the dynome. Neuron, 83(6), 1319-1328.

Laumann, T. O., Gordon, E. M., Adeyemo, B., Snyder, A. Z., Joo, S. J., Chen, M. Y., Gilmore, A. W., McDermott, K. B., Nelson, S. M., Dosenbach, N. U., et al. (2015). Functional System and Areal Organization of a Highly Sampled Individual Human Brain. Neuron, 87(3), 657-670.

Leonardi, N., & Van De Ville, D. (2015). On spurious and real fluctuations of dynamic functional connectivity during rest. Neuroimage, 104, 430-436.

Lewis, C. M., Baldassarre, A., Committeri, G., Romani, G. L., & Corbetta, M. (2009). Learning sculpts the spontaneous activity of the resting human brain. Proc Natl Acad Sci U S A, 106(41), 17558-17563.

Lindquist, M. A., Xu, Y., Nebel, M. B., & Caffo, B. S. (2014). Evaluating dynamic bivariate correlations in resting-state fMRI: a comparison study and a new approach. Neuroimage, 101, 531-546.

Liu, X., & Duyn, J. H. (2013). Time-varying functional network information extracted from brief instances of spontaneous brain activity. Proc Natl Acad Sci U S A, 110(11), 4392-4397.

Majeed, W., Magnuson, M., & Keilholz, S. D. (2009). Spatiotemporal dynamics of low frequency fluctuations in BOLD fMRI of the rat. J Magn Reson Imaging, 30(2), 384-393.

Marder, E., & Goaillard, J. M. (2006). Variability, compensation and homeostasis in neuron and network function. Nat Rev Neurosci, 7(7), 563-574.

Mardia, K. V. (1970). Measures of multivariate skewness and kurtosis with applications. Biometrika, 57(3), 519-530.

Martins, A. C. R. (2007). Non-stationary correlation matrices and noise. Physica A, 379, 552-558.

McAvoy, M., Larson-Prior, L., Nolan, T. S., Vaishnavi, S. N., Raichle, M. E., & d'Avossa, G. (2008). Resting states affect spontaneous BOLD oscillations in sensory and paralimbic cortex. J Neurophysiol, 100(2), 922-931.

Mitra, A., Snyder, A. Z., Blazey, T., & Raichle, M. E. (2015a). Lag threads organize the brain's intrinsic activity. Proc Natl Acad Sci U S A, 112(17), E2235-2244.

Mitra, A., Snyder, A. Z., Tagliazucchi, E., Laufs, H., & Raichle, M. E. (2015b). Propagated infra-slow intrinsic brain activity reorganizes across wake and slow wave sleep. Elife, 4.

Palanca, B. J., Mitra, A., Larson-Prior, L., Snyder, A. Z., Avidan, M. S., & Raichle, M. E. (2015). Resting-state Functional Magnetic Resonance Imaging Correlates of Sevoflurane-induced Unconsciousness. Anesthesiology, 123(2), 346-356.

Penn, A. A., & Shatz, C. J. (1999). Brain waves and brain wiring: the role of endogenous and sensory-driven neural activity in development. Pediatr Res, 45(4 Pt 1), 447-458.

Poldrack, R. A., Laumann, T. O., Koyejo, O., Gregory, B., Hover, A., Chen, M. Y., Luci, J., Huk, A., Joo, S. J., Boyd, R., et al. (2015). Long-term neural and physiological phenotyping of a single human. Nature Communications.

Power, J. D., Barnes, K. A., Snyder, A. Z., Schlaggar, B. L., & Petersen, S. E. (2012). Spurious but systematic correlations in functional connectivity MRI networks arise from subject motion. Neuroimage, 59(3), 2142-2154.

Power, J. D., Cohen, A. L., Nelson, S. M., Wig, G. S., Barnes, K. A., Church, J. A., Vogel, A. C., Laumann, T. O., Miezin, F. M., Schlaggar, B. L., et al. (2011). Functional network organization of the human brain. Neuron, 72(4), 665-678.

Power, J. D., Mitra, A., Laumann, T. O., Snyder, A. Z., Schlaggar, B. L., & Petersen, S. E. (2014). Methods to detect, characterize, and remove motion artifact in resting state fMRI. Neuroimage, 84, 320-341.

Raichle, M. E., & Mintun, M. A. (2006). Brain work and brain imaging. Annu Rev Neurosci, 29, 449-476.

Raichle, M. E., & Snyder, A. Z. (2007). A default mode of brain function: a brief history of an evolving idea. Neuroimage, 37(4), 1083-1090; discussion 1097-1089.

Rosvall, M., & Bergstrom, C. T. (2008). Maps of random walks on complex networks reveal community structure. Proc Natl Acad Sci U S A, 105(4), 1118-1123.

Sadaghiani, S., Scheeringa, R., Lehongre, K., Morillon, B., Giraud, A. L., & Kleinschmidt, A. (2010). Intrinsic connectivity networks, alpha oscillations, and tonic alertness: a simultaneous electroencephalography/functional magnetic resonance imaging study. J Neurosci, 30(30), 10243-10250.

Samann, P. G., Wehrle, R., Hoehn, D., Spoormaker, V. I., Peters, H., Tully, C., Holsboer, F., & Czisch, M. (2011). Development of the brain's default mode network from wakefulness to slow wave sleep. Cereb Cortex, 21(9), 2082-2093.

Satterthwaite, T. D., Wolf, D. H., Loughead, J., Ruparel, K., Elliott, M. A., Hakonarson, H., Gur, R. C., & Gur, R. E. (2012). Impact of in-scanner head motion on multiple measures of functional connectivity: relevance for studies of neurodevelopment in youth. Neuroimage, 60(1), 623-632.

Segonne, F., Dale, A. M., Busa, E., Glessner, M., Salat, D., Hahn, H. K., & Fischl, B. (2004). A hybrid approach to the skull stripping problem in MRI. Neuroimage, 22(3), 1060-1075.

Shehzad, Z., Kelly, A. M., Reiss, P. T., Gee, D. G., Gotimer, K., Uddin, L. Q., Lee, S. H., Margulies, D. S., Roy, A. K., Biswal, B. B., et al. (2009). The resting brain: unconstrained yet reliable. Cereb Cortex, 19(10), 2209-2229.

Smith, S. M., Fox, P. T., Miller, K. L., Glahn, D. C., Fox, P. M., Mackay, C. E., Filippini, N., Watkins, K. E., Toro, R., Laird, A. R., et al. (2009). Correspondence of the brain's functional architecture during activation and rest. Proc Natl Acad Sci U S A, 106(31), 13040-13045.

Smith, S. M., Jenkinson, M., Woolrich, M. W., Beckmann, C. F., Behrens, T. E., Johansen-Berg, H., Bannister, P. R., De Luca, M., Drobnjak, I., Flitney, D. E., et al. (2004). Advances in functional and structural MR image analysis and implementation as FSL. Neuroimage, 23 Suppl 1, S208-219.

Tagliazucchi, E., Balenzuela, P., Fraiman, D., & Chialvo, D. R. (2012). Criticality in large-scale brain FMRI dynamics unveiled by a novel point process analysis. Front Physiol, 3, 15.

Tagliazucchi, E., & Laufs, H. (2014). Decoding wakefulness levels from typical fMRI resting-state data reveals reliable drifts between wakefulness and sleep. Neuron, 82(3), 695-708.

Van Dijk, K. R., Sabuncu, M. R., & Buckner, R. L. (2012). The influence of head motion on intrinsic functional connectivity MRI. Neuroimage, 59(1), 431-438.

Van Essen, D. C., Drury, H. A., Dickson, J., Harwell, J., Hanlon, D., & Anderson, C. H. (2001). An integrated software suite for surface-based analyses of cerebral cortex. J Am Med Inform Assoc, 8(5), 443-459.

Van Essen, D. C., Glasser, M. F., Dierker, D. L., Harwell, J., & Coalson, T. (2012a). Parcellations and hemispheric asymmetries of human cerebral cortex analyzed on surface-based atlases. Cereb Cortex, 22(10), 2241-2262.

Vincent, J. L., Patel, G. H., Fox, M. D., Snyder, A. Z., Baker, J. T., Van Essen, D. C., Zempel, J. M., Snyder, L. H., Corbetta, M., & Raichle, M. E. (2007a). Intrinsic functional architecture in the anaesthetized monkey brain. Nature, 447(7140), 83-86.

Weatherburn, C. E. (1961). *A First Course in Mathematical Statistics* (3rd ed.). London: Cambridge University Press.

Wilson, M. A., & McNaughton, B. L. (1994). Reactivation of hippocampal ensemble memories during sleep. Science*,* 265(5172), 676-679.

Wong, K. F., Galka, A., Yamashita, O., & Ozaki, T. (2006). Modelling non-stationary variance in EEG time series by state space GARCH model. Computers in biology and medicine*,* 36(12), 1327-1335.

Yeo, B. T., Krienen, F. M., Sepulcre, J., Sabuncu, M. R., Lashkari, D., Hollinshead, M., Roffman, J. L., Smoller, J. W., Zollei, L., Polimeni, J. R., et al. (2011). The organization of the human cerebral cortex estimated by intrinsic functional connectivity. J Neurophysiol*,* 106(3), 1125-1165.

Zalesky, A., & Breakspear, M. (2015). Towards a statistical test for functional connectivity dynamics. Neuroimage*,* 114, 466-470.

Zalesky, A., Fornito, A., Cocchi, L., Gollo, L. L., & Breakspear, M. (2014). Time-resolved resting-state brain networks. Proc Natl Acad Sci U S A*,* 111(28), 10341-10346.

Chapter 6: Discussion

6.1 Summary of Results

In Chapter 2, we presented an approach for non-invasive cortex-wide parcellation of the human brain into putative functional areas. By analogy with classical tracer-based or architectonic investigations, this technique is based on the idea that transitions in patterns of resting-state correlations represent boundaries between cortical areas. Cortical areas identified in this way were found, in part, to correspond with architectonic divisions, task-based functional localization, and resting state-based systems-level cortical divisions.

Chapter 3 refined and consolidated the approach presented in Chapter 2 with technical enhancements and a null model-based evaluation procedure for demonstrating internal and external validity of identified cortical areas. Our RSFC gradient-based parcellation was found to be superior by this evaluation to several popular RSFC-based or anatomic parcellations.

In Chapter 4, we applied techniques for RSFC-based areal and system definition to a highly sampled individual. This analysis revealed that even as they generally share most properties of functional organization with group-averaged data, an individual can exhibit idiosyncratic features of functional organization. Critically, we also developed a model (and related empirical observations) of resting state BOLD variability that allows for computation of the quantity of data needed to generate precise estimates of correlation. According to this model, sampling error explained most of the observed variability in BOLD correlations from day to day, although other sources of variability

(e.g. caffeine state) likely contributed to the distinct topographic pattern of within-subject variability observed in somatomotor and visual regions.

The analyses in the highly sampled individuals point to the stability of resting state BOLD correlations over relatively long time scales (i.e. day to day or over a year). In Chapter 5, however, we studied shorter time-scale variability in resting-state BOLD data. In particular, we evaluated the presence of non-stationary properties within individual resting state BOLD sessions. We found, first, that sampling variability can generate fluctuations in BOLD correlation that are frequently misconstrued as non-stationary dynamics, and, second, that bona fide non-stationarity in signals can largely be explained by head motion and sleep state. We concluded that resting state BOLD fluctuations are essentially stationary to second-order (i.e., stable covariance structure) over timescales (minutes) that are most often measured in practice.

In the following section, we will elaborate on some of the themes of this work with a particular focus on potential future directions.

6.2 Comments on using resting-state to study spatial functional organization

Our results suggest that resting state BOLD activity can be used to describe area and system-level spatial organization of the human brain. The utility of such descriptions is manifest in several domains. Firstly, accurate parcellation of the brain into discrete functional areas that does not duplicate or omit constituent elements of the system allows for analysis in a lower dimensional space than the physiologically meaningless voxel space in which BOLD data is collected (and often analyzed). Further, any sensible network-based analysis of information processing in the brain requires that the nodes of

the network be meaningfully defined to reflect relevant units of information processing (Power et al., 2011; Wig et al., 2011b). We hope that the reported parcellation will be productive in this regard. In particular, the present parcellation may form a more accurate basis than has previously been available (e.g. the sphere-based nodes of (Power et al., 2011) in which to compute and interpret important node properties underlying functional network organization, such as within module degree and participation coefficient.

Second, the whole-brain approaches for delineating patterns of spontaneous BOLD activity outlined here (and in previous work) potentially expose previously unknown functional organization. Presumably, divisions observed in the spontaneous BOLD data reflect real distinct functional systems or areas that may not yet have known functional roles. For example, functional system delineation through resting state fMRI has recently helped to define a previously unrecognized system of regions in the parietal cortex hypothesized to be involved in memory processes (Gilmore 2015; Power 2015). This same system was observed in the highly sampled subject reported in Chapter 4, adding further evidence for its discrete existence in individuals. At the level of areas, the parcellation reflects a large number of spontaneous BOLD activity-based distinctions with often-unknown functional significance. Annotation of the functional role(s) of each of the identified areas represents a substantial future undertaking, ultimately requiring a compilation of the universe of tasks eliciting discrete functional processes. A first step in this direction may be to link databases of extant functional activation locations (e.g. Brainmap (P. T. Fox et al., 2002) or SumsDB (Dickson et al., 2001)) to the resting-state defined cortical areas, as has been demonstrated at the

systems-level (e.g. (Smith et al., 2009; Yeo et al., 2014)). It would be of considerable interest to note which areas have at least some well-defined processing roles dissociable from adjacent regions, and which have not yet been meaningfully distinguished by extant tasks, despite being distinguishable by spontaneous BOLD activity. Such an analysis might expose the gaps in our current repertoire of functional tasks and the limitations of the cognitive ontologies that underlie them (Poldrack, 2010).

Finally, individual-level identification of the spatial topology of functional organization using spontaneous BOLD activity presents several exciting avenues for exploring cross-subject functional localization. In particular, in Chapter 4 we observed individual-specific topological features in functional organization distinct from group average patterns of organization. In this case, these differences could not be easily explained away by insufficient data or sampling error. A key next step in understanding this observation is to characterize the nature and extent of RSFC variability across many individuals. Ideally, we would acquire sufficient data to have precise and accurate description of functional organization in each subject, but even with less robust datasets we can begin to describe the characteristic patterns of RSFC variability. Figure 6.1 illustrates the variability of system identification across subjects based on RSFC (approximately 12 minutes of data per subject; (Gordon et al., 2015).

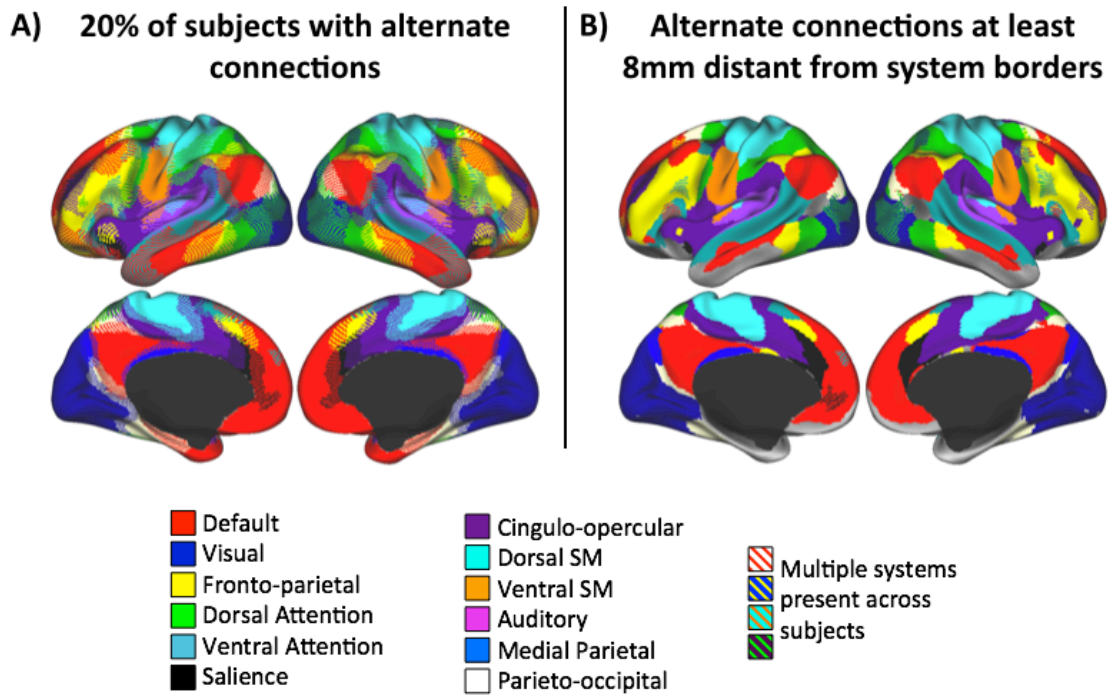

Figure 6-1. Most regions with consistent non-modal system identities in at least 20% of subjects are primarily near group average system borders, but some are far from those borders. A) Striped colors indicate all vertices where at least 20% of subjects (n=228) had the same non-modal system identity, with one color in the stripes representing the modal identity and the others representing alternate identities. B) Striped colors indicate regions of at least 100mm^2 that had consistent non-modal system identities in at least 20% of subjects (as in the left panel) and that were also at least 8mm from the group average system borders. Fourteen such regions can be observed (modified from Gordon et al 2015).

Most of the RSFC variability is localized near system borders, but there are several regions far from system borders that also exhibited variable system identity across subjects. These results confirm the need for further evaluation of functional organization of highly sampled individual subjects, but already expose the possibility that there may be characteristic alternate patterns of cortical organization that exist in different subsets of subjects.

The presence of these topological distinctions gives rise to several intriguing questions. Do these topological differences correspond to behavioral attributes of a

given subject or do they represent degenerate and equally viable configurations of functional organization? Relatedly, what causes individuals to differ in their topological functional organization? Are these differences genetically determined or experience driven? Studying the topological similarities in functional organization between identical and fraternal twins could help determine the extent to which different functional topologies relate to genetic variants. On the other hand, analysis of individuals with anatomical deficits (e.g. perinatal strokes) or individuals with radically altered inputs (e.g. congenitally blind) could be used to evaluate the impact of environmental context on observed cortical functional organization.

These observations of system variability across subjects also present important methodological consequences. Specifically, appropriate comparison of functional organization across subjects may require forms of cortical alignment beyond the traditional anatomical registrations that are typically applied (e.g. structural volume-based (Lancaster et al., 1995b) or cortical folding on the surface (A. M. Dale et al., 1999; Fischl et al., 1999). New approaches using functional, and other, measurements of brain properties have been proposed and may usefully improve cortical alignment across subjects (Robinson et al., 2014). However, if there are true topological differences in functional organization, i.e. a region of cortex functionally connects with one system in one person and a different system in the next, comparison between subjects may require techniques that align data in a functional space that may not necessarily respect anatomical contiguity (Haxby et al., 2011; Sabuncu et al., 2010). Such a registration may usefully occur at the voxel-level, but may particularly benefit from cross-subject assignment at the areal or systems-level.

One final note of caution is warranted when considering the meaning of RSFC-based descriptions of cortical organization. While it is incredibly valuable to confirm and explore where RSFC-based areal or system definition aligns with other brain properties such as architectonics, myelin content, or axonal connectivity, it is important to recognize that RSFC may not perfectly align with these modalities for biologically meaningful reasons. For example, we found RSFC gradients within early visual areas that appear to divide foveal and peripheral representations of the visual field (Chapter 4, Figure 2). Further, these effects varied by resting state condition at the systems-level. Eyes-closed rest demonstrated clear separation of striate and extrastriate visual cortex, while eyes-open rest generated foveal and peripheral systems that cut across early visual areas (Chapter 4, Figure S4). Thus, spontaneous BOLD activity can reflect organization that may be distinct from traditional cortical areas but may be functionally explicable. Indeed, spontaneous BOLD may reflect different aspects of underlying organization depending on the context in which it is observed. Interpretation of functional areas defined by RSFC must be constrained by this observation.

6.3 Comments on using resting-state to study temporal functional organization

The results reported in the latter chapters of this thesis speak to the stability of RSFC patterns at several temporal scales. We have shown that much of the observed variance at both long and short scales is accounted for by sampling error. Taken together, these observations generally support the view that spontaneous BOLD activity primarily supports off-line processes as opposed to moment-to-moment cognition (Raichle et al., 2007). However, there are sources of variability in RSFC within a subject

that are not attributable to sampling error. We will discuss the challenges involved in separating the layers of overlapping functional processes that together form the measured BOLD signal and propose future experiments to explore how RSFC may reflect underlying changes in physiology.

As we have seen, while RSFC variability is largely accounted for by sampling variability, small but true changes in correlation relationships between cortical areas can be observed from day to day (Chapter 4) or within a single scanning session (Chapter 5). Setting aside motion (which has the most disruptive effect on correlation relationships), we have suggested that, in each case, sleep state may be a significant contributing factor to fluctuations in RSFC, as Tagliazucchi et al have found (Tagliazucchi et al., 2014). We speculate that changes in functional connectivity related to shifts in sleep state may represent changes in off-line neural activity as a result of changes in the neuromodulatory regime affecting cortical excitability (Steriade et al., 1976).

Beyond sleep, there are likely other reasons one may observe changes in correlated BOLD activity. One obvious possibility is a change in neural activity associated with changing cognitive demands. Indeed, using the kurtosis measured introduced in Chapter 5, we have found that mixed block/event-related task runs (which include inter-block intervals of resting fixation) show increased multivariate kurtosis relative to pure resting sessions of the same length (Figure 6.2). We first note that the relatively lower kurtosis of the resting scans suggests that the resting state does not contain correlation changes consistent with meaningful changes in cognitive state. This

result reaffirms the notion that spontaneous BOLD activity during rest does not reflect moment-to-moment changes in cognition.

On the other hand, the relative increase in kurtosis during task runs indicates that there are changes in correlation structure from rest to a goal-directed task state. As opposed to the sleep state related correlation changes discussed above, the task-related changes may represent a fundamentally different online process that superimposes on spontaneous activity-dependent correlation. In fact, it has been proposed (Al-Aidroos et al., 2012) that focal transient attention-related changes in functional connectivity measured by BOLD may relate to transient coupling of local field potentials with neuron-level activity (Lee et al., 2005). Together, these observations suggest that measured BOLD activity may reflect a complex combination of state-dependent offline and online processes.

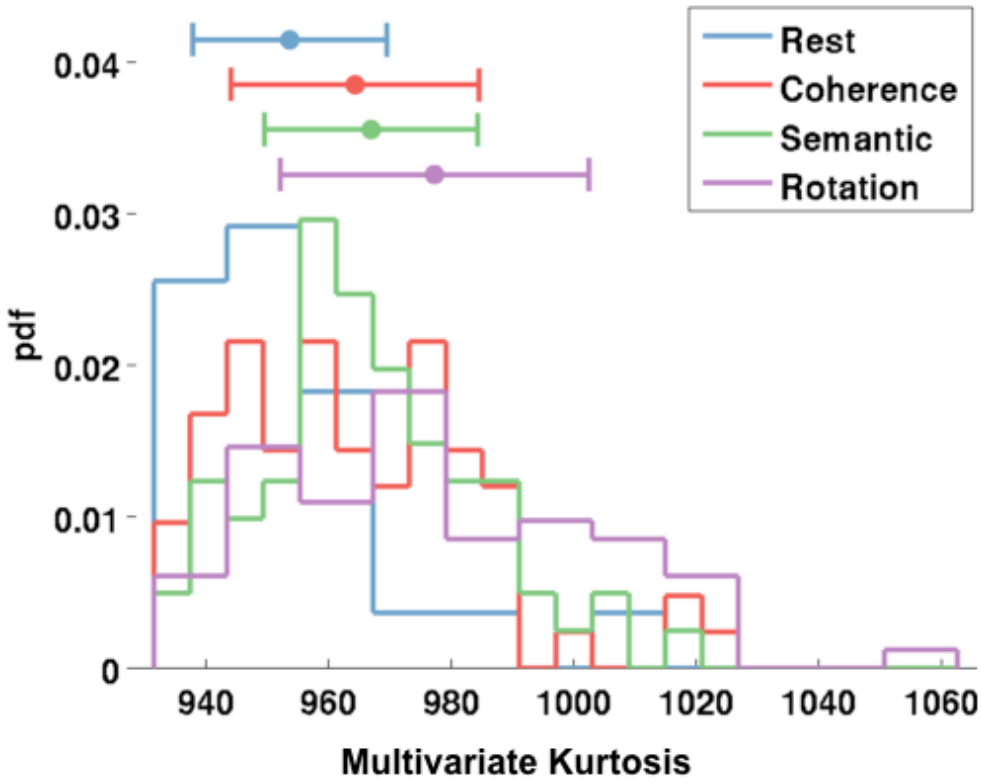

Figure 6-2. Relative distributions from 23 subjects of measured multivariate kurtosis computed on equal lengths of resting state, a Glass pattern coherence discrimination task, a noun vs. verb semantic judgment task, and a mental rotation task. Sessions were each 188 frames (TR = 2.5 seconds).

Future analyses of task-dependent changes in functional correlation that carefully account for trial and block-related evoked effects may help to elucidate the separable properties that contribute to dynamic functional network organization during task processing. For example, which regions are likely to change most during a task, those that are most involved in the task-specific processing or those that are important connector nodes (i.e.. high participation coefficient hubs; Power et al., 2013) in the core network structure reflected in the resting state? The context-dependent behavior of different nodes may reflect the contributions of distinct underlying processes.

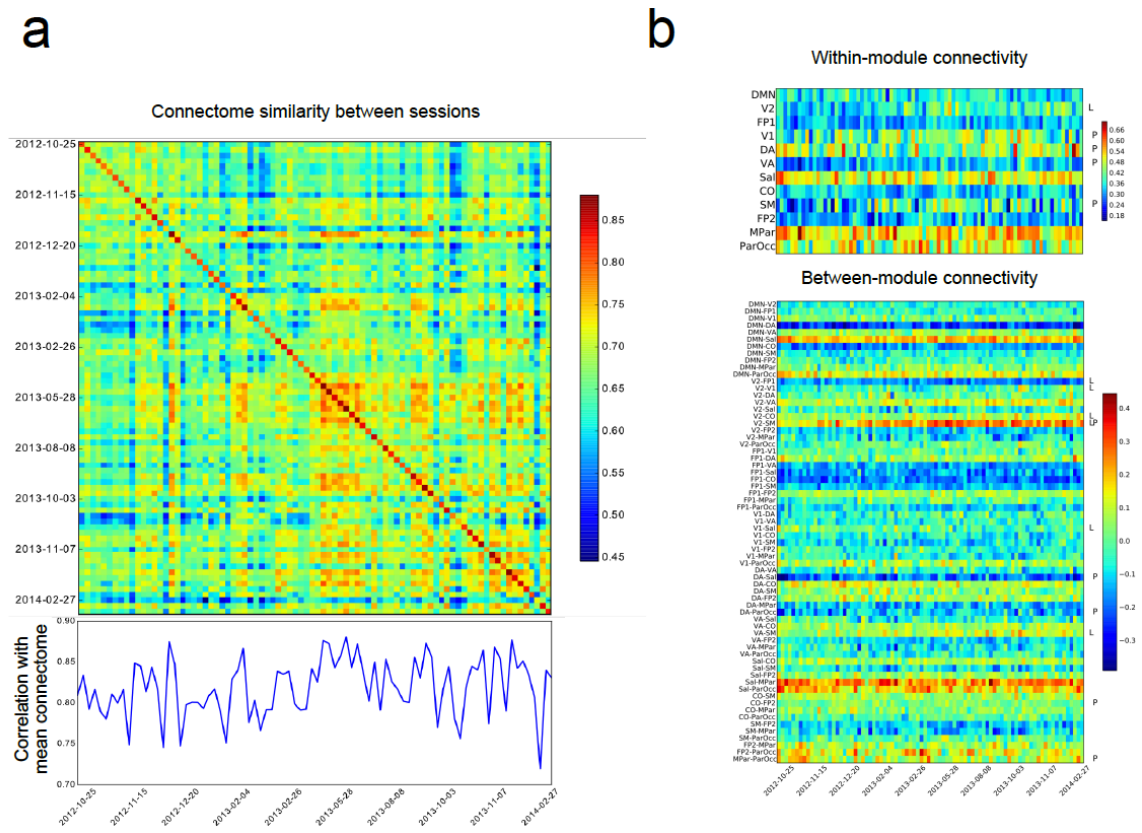

Figure 6-3. Longitudinal variability in brain connectivity. (a) Similarity between connectome-wide connectivity patterns across sessions, computed as the Pearson correlation between connectivity values across the parcellated connectivity matrix. Values on the diagonal as wells as the lower plot represent the similarity between each session and the mean across sessions; off-diagonal elements reflect the similarity between each pair of sessions. (b) Time series of connectivity within modules (upper panel) and between modules (lower panel). Notations to the right of each row mark the presence of significant linear (L) and polynomial (P) trends. Adapted from Poldrack, et al 2015.

While short-term changes in BOLD correlations may be inducible by brief task demands, true changes in the core functional architecture reflected in spontaneous BOLD activity during rest likely require much longer sustained interventions. In Chapter 5, we argued that spontaneous BOLD activity reflects preferred synaptic pathways, as many others have (Dosenbach et al., 2007; Nelson et al., 2010a). Thus, “core” RSFC will not be expected to change without long-term synaptic modification. Interestingly, such changes do not appear to be commonplace or widespread over a typical year of a person’s life, as measured in the highly sampled subject described in Chapter 4. While

there were a few significant trends in within-module connectivity (striate and extrastriate visual, somatomotor, dorsal and ventral attention modules), most modules were fairly stable over the course of the 18-month study and the network as a whole did not change significantly (Figure 6.3; Poldrack et al., 2015). With this general stability in adult RSFC as a set point, we are quite interested to know whether RSFC can be permanently altered by drastic behavioral modification such as constraining a limb or covering an eye. In particular, how long does it take for RSFC to change and settle on a new organization? Further, will the presence of ongoing neural plasticity be reflected in relatively greater instability in measured spontaneous BOLD activity? Experiments of experience-dependent plasticity have been attempted before (Lewis et al., 2009; Mackey et al., 2013; Sami et al., 2014), but none have established a timecourse of RSFC change or demonstrated long-term persistent changes. Such an experiment would require extensive repeated measurements over many days, but may reveal important principles of systems-level neural plasticity.

6.4 References

Al-Aidroos, N., Said, C. P., & Turk-Browne, N. B. (2012). Top-down attention switches coupling between low-level and high-level areas of human visual cortex. Proc Natl Acad Sci U S A, 109(36), 14675-14680.

Dale, A. M., Fischl, B., & Sereno, M. I. (1999). Cortical surface-based analysis. I. Segmentation and surface reconstruction. Neuroimage, 9(2), 179-194.

Dickson, J., Drury, H., & Van Essen, D. C. (2001). 'The surface management system' (SuMS) database: a surface-based database to aid cortical surface reconstruction, visualization and analysis. Philos Trans R Soc Lond B Biol Sci, 356(1412), 1277-1292.

Dosenbach, N. U., Fair, D. A., Miezin, F. M., Cohen, A. L., Wenger, K. K., Dosenbach, R. A., Fox, M. D., Snyder, A. Z., Vincent, J. L., Raichle, M. E., et al. (2007). Distinct brain networks for adaptive and stable task control in humans. Proc Natl Acad Sci U S A, 104(26), 11073-11078.

Fischl, B., Sereno, M. I., & Dale, A. M. (1999). Cortical surface-based analysis. II: Inflation, flattening, and a surface-based coordinate system. Neuroimage, 9(2), 195-207.

Fox, P. T., & Lancaster, J. L. (2002). Opinion: Mapping context and content: the BrainMap model. Nat Rev Neurosci, 3(4), 319-321.

Gordon, E. M., Laumann, T. O., Adeyemo, B., & Petersen, S. E. (2015). Individual Variability of the System-Level Organization of the Human Brain. Cereb Cortex.

Haxby, J. V., Guntupalli, J. S., Connolly, A. C., Halchenko, Y. O., Conroy, B. R., Gobbini, M. I., Hanke, M., & Ramadge, P. J. (2011). A common, high-dimensional model

of the representational space in human ventral temporal cortex. Neuron, 72(2), 404-416.

Lancaster, J. L., Glass, T. G., Lankipalli, B. R., Downs, H., Mayberg, H. S., & Fox, P. T. (1995b). A modality-independent approach to spatial normalization of tomographic images of the human brain. Hum Brain Mapp, 3(3), 209-223.

Lee, H., Simpson, G. V., Logothetis, N. K., & Rainer, G. (2005). Phase locking of single neuron activity to theta oscillations during working memory in monkey extrastriate visual cortex. Neuron, 45(1), 147-156.

Lewis, C. M., Baldassarre, A., Committeri, G., Romani, G. L., & Corbetta, M. (2009). Learning sculpts the spontaneous activity of the resting human brain. Proc Natl Acad Sci U S A, 106(41), 17558-17563.

Mackey, A. P., Miller Singley, A. T., & Bunge, S. A. (2013). Intensive reasoning training alters patterns of brain connectivity at rest. J Neurosci, 33(11), 4796-4803.

Nelson, S. M., Cohen, A. L., Power, J. D., Wig, G. S., Miezin, F. M., Wheeler, M. E., Velanova, K., Donaldson, D. I., Phillips, J. S., Schlaggar, B. L., et al. (2010a). A parcellation scheme for human left lateral parietal cortex. Neuron, 67(1), 156-170.

Poldrack, R. A. (2010). Mapping Mental Function to Brain Structure: How Can Cognitive Neuroimaging Succeed? Perspect Psychol Sci, 5(6), 753-761.

Poldrack, R. A., Laumann, T. O., Koyejo, O., Gregory, B., Hover, A., Chen, M. Y., Luci, J., Huk, A., Joo, S. J., Boyd, R., et al. (2015). Long-term neural and physiological phenotyping of a single human. Nature Communications.

Power, J. D., Cohen, A. L., Nelson, S. M., Wig, G. S., Barnes, K. A., Church, J. A., Vogel, A. C., Laumann, T. O., Miezin, F. M., Schlaggar, B. L., et al. (2011). Functional network organization of the human brain. Neuron, 72(4), 665-678.

Power, J. D., Schlaggar, B. L., Lessov-Schlaggar, C. N., & Petersen, S. E. (2013). Evidence for hubs in human functional brain networks. Neuron, 79(4), 798-813.

Raichle, M. E., & Snyder, A. Z. (2007). A default mode of brain function: a brief history of an evolving idea. Neuroimage, 37(4), 1083-1090; discussion 1097-1089.

Robinson, E. C., Jbabdi, S., Glasser, M. F., Andersson, J., Burgess, G. C., Harms, M. P., Smith, S. M., Van Essen, D. C., & Jenkinson, M. (2014). MSM: a new flexible framework for Multimodal Surface Matching. Neuroimage, 100, 414-426.

Sabuncu, M. R., Singer, B. D., Conroy, B., Bryan, R. E., Ramadge, P. J., & Haxby, J. V. (2010). Function-based intersubject alignment of human cortical anatomy. Cereb Cortex, 20(1), 130-140.

Sami, S., Robertson, E. M., & Miall, R. C. (2014). The time course of task-specific memory consolidation effects in resting state networks. J Neurosci, 34(11), 3982-3992.

Smith, S. M., Fox, P. T., Miller, K. L., Glahn, D. C., Fox, P. M., Mackay, C. E., Filippini, N., Watkins, K. E., Toro, R., Laird, A. R., et al. (2009). Correspondence of the brain's functional architecture during activation and rest. Proc Natl Acad Sci U S A, 106(31), 13040-13045.

Steriade, M., & Hobson, J. (1976). Neuronal activity during the sleep-waking cycle. Prog Neurobiol, 6(3-4), 155-376.

Tagliazucchi, E., & Laufs, H. (2014). Decoding wakefulness levels from typical fMRI resting-state data reveals reliable drifts between wakefulness and sleep. Neuron, 82(3), 695-708.

Wig, G. S., Schlaggar, B. L., & Petersen, S. E. (2011b). Concepts and principles in the analysis of brain networks. Ann N Y Acad Sci, 1224, 126-146.

Yeo, B. T., Krienen, F. M., Eickhoff, S. B., Yaakub, S. N., Fox, P. T., Buckner, R. L., Asplund, C. L., & Chee, M. W. (2014). Functional Specialization and Flexibility in Human Association Cortex. Cereb Cortex.